

AN ABSTRACT OF THE DISSERTATION OF

Kai Tao for the degree of Doctor of Philosophy in Molecular and Cellular Biology presented on June 7, 2018.

Title: Investigating Protein-lipid-membrane Interactions in Plant Cells using Bimolecular Fluorescence Complementation

Abstract approved: _____
Brett M. Tyler

The overall focus of this thesis is on the distribution of specific lipids and membrane proteins of the external and internal membranes of plant cells, in the context of the roles that those lipids and proteins may play in microbe-plant interactions. The work includes the development of several new tools, the refinement of some existing tools, and the highlighting of several poorly appreciated artifacts that are common to such studies.

This thesis is comprised of five chapters. In Chapter 1, I would like to step back to have a general overview, including initial questions we asked, the way we interpreted unexpected results. In Chapter 2 “Manipulating Endoplasmic Reticulum-Plasma Membrane Tethering through BiFC interactions in plants”, I demonstrated that the heterogeneous network of patches produced in FLS2-StRem1.3 BiFC complexes corresponded to ER-PM tethering, which resulted from the non-specific dimerization between FLS2-VenusN and VenusC-StRem1.3. This work confirmed that membrane targeting of integral membrane proteins (IMPs) such as FLS2 requires either co-translational or post-translational integration into the ER membrane before trafficking to their membrane destination. These observations suggest a re-visit of several previous studies which have reported heterogeneous patch-like distributions when using IMPs and PMPs in BiFC experiments.

In Chapter 3 “Manipulating Tethering of Multivesicular Bodies and the Tonoplast to the Plasma Membrane Through BiFC Interactions in Plants”, I strengthened the evidence that the patch-like distributions observed when combining PtdIns(3)P biosensors with StREM1.3, resulted from tethering of MVBs and the tonoplast to the PM. I also observed that the membrane binding domains of the E3 ubiquitin-ligases SAUL1 (AtPUB44) and AtPUB43, could tether MVBs and the tonoplast to the PM, suggesting a possible functional role for these proteins in MVB-PM tethering, such as the secretion of exosomes.

Although my observations reported in Chapter 2 and Chapter 3 led to new insights into membrane organization in plant cells, they also highlighted the risk of using BiFC assays to study membrane protein interactions in plants, which without proper controls could lead to misinterpretation, or cause unrecognized alterations in cellular structure and membrane organization. In chapter 4 “Fluorescent Protein mEos3.2 Shows Low Self-Association in Bimolecular Fluorescence Complementation Assays in Plants”, I show that the mEOS3.2 BiFC probe, split at residue 164E, also produced minimal non-specific detectable BiFC signals when transiently expressed in *Nicotiana benthamiana* leaf cortical cells, but produced excellent signals with interacting protein partners. I also demonstrated that the re-assembled mEos3.2 could still photo-convert from green to red, which aided in distinguishing specific BiFC signals from background, and could allow the visualization of BiFC complexes at nanometer spatial resolution using photo-activated localization microscopy (PALM) imaging.

In chapter 5 “In vivo Super-Resolution Imaging of the Dynamics of PtdIns(4)P in the Plasma Membrane Of Plant Cells”, I successfully extended the application of mEos3.2 to study the spatiotemporal dynamics of a lipid species, PtdIns(4)P, in the plasma membrane of plant cells at single-molecule resolution using Single Particle Tracking PALM imaging (sptPALM). This work demonstrated the advantages of sptPALM compared to traditional imaging methods, such as Fluorescence Recovery After Photobleaching (FRAP), for studying the molecular dynamics of the plasma membrane. In addition, my work refined the specificity of the PtdIns(4)P biosensor FAPP1.

©Copyright by Kai Tao
June 7, 2018
All Rights Reserved

Investigating Protein-lipid-membrane Interactions in Plant Cells
using Bimolecular Fluorescence Complementation

By

Kai Tao

A DISSERTATION

submitted to

Oregon State University

in partial fulfillment of
the requirements for the
degree of

Doctor of Philosophy

Presented June 7, 2018
Commencement June 2019

Doctor of Philosophy dissertation of Kai Tao presented on June 7, 2018

APPROVED:

Major Professor, representing Molecular and Cellular Biology

Director of the Molecular and Cellular Biology Program

Dean of the Graduate School

I understand that my dissertation will become part of the permanent collection of Oregon State University libraries. My signature below authorizes release of my dissertation to any reader upon request.

Kai Tao, Author

ACKNOWLEDGEMENTS

First of all, I would like to thank my advisor, Prof. Brett Tyler for letting me join in his lab, giving me this life-changing chance to study in the United States, and providing almost everything needed for my success. His open mind and great patience allowed me to touch those state of art technologies building fundament for my future career. His wise guidance gave me great support during the researches. Importantly, his attitude to works encouraged me to become a successful scientist. He is my mentor, my friend, and my family member. I also want to thank my committee members, Xiaolin Nan, John Fowler, Colin Johnson, Richard Coopley, and previous members Julie Greenwood, Lary Malcome for their great guidance and thoughtful suggestions. I am ever grateful to my lab members, Felipe Arredondon, Sam Tylor, Hua wise, Emily, Justin, Missy, Ana, Jordan, Heather. Especially I would like to thank Justin, allowing me to learn how to be a good mentor. I also want to acknowledge our visiting scholars in labs, Wei Zhao, Danyu Shen, Linkai Cui, Meng Cai, Biao Gu, Jianqiang Miao, Tingquan Wu. I also wish to thank people in CGRB, Anne-Marie Girard, Jeannine Cropley, Jessica Nixon, Aaron Trippe, Brent Kronmiller, Matthew Peterson, Chris Sullivan, Shawn O'Neil, Mark Dasenko, Keith Foster. I want to give my special thanks to Rosa Hill, who was always willing to solve difficulties I encountered here, and taught me the real American's life and culture. Xiaolin's lab in OHSU provided me a great chance to learn superresolution imaging, and his lab member Tao Huang, Jing Wang, Linli Jun, Carey, Ying Zhang, Yerim lee gave great instructions and help. I also want to thank Siva lab and his member Jiang Hysang for teaching me to conduct human cells transformation. I also want to thank Weihong Qiu and his lab member Guofu Tseng for guiding me to use TIRFM imaging on campus. At last, I want to thank my previous mentor (Master degree) Prof. Yuanchao Wang at NJAU in China, always giving me great encouragements.

Lastly, I want to thank my family members. Although I'm thousands of miles away from them, they are still like being around me for supports and encouragements.

Thank you very much, everyone! Without you, this dissertation would not have been possible.

CONTRIBUTION OF AUTHORS

This thesis was guided by Prof. Brett M. Tyler, including providing research funding, conceiving experimental designs, analyzing data, editing this manuscript. Justin R. Waletich assisted in conducting several experiments in this thesis. Felipe Arredondo contributed some of experiments in this thesis. Dr. Hua Wise conducted *Arabidopsis thaliana* stable transformation assay.

Chapter 4 and 5 were co-authored with Dr. Xiaolin Nan, who provided important advices for experimental design and the critical equipment of PALM microscopy. Dr. Huang Tao, Yerim Lee assisted the PALM imaging and analyzed the data.

TABLE OF CONTENTS

	Page
Chapter 1: Overview	1
Overview	2
Bibliography	10
Chapter 2: Manipulating Endoplasmic Reticulum-Plasma Membrane Tethering through BiFC interactions in plants.....	15
Abstract	16
Introduction.....	17
Results	20
Heterogeneous patch-like distribution of FLS2-StRem1.3 BiFC complexes	20
The FLS2-StRem1.3 complexes localize to ER-PM contact sites.....	21
StREM1.3 and other Peripheral Membrane Proteins can replace the C-terminus of SYT1 in ER-PM tethering	25
Integral membrane proteins can contribute ER anchoring to produce ER-PM tethering	27
PtdIns(4)P- and PtdIns(4,5)P ₂ -binding proteins could replace peripheral membrane- binding proteins in BiFC complexes to produce ER-PM tethering	29
Discussion.....	32
Materials and Methods	36
Plant Materials.....	36
Cloning and Construction	36
Transient expression in <i>N. benthamiana</i> leaves and <i>A. thaliana</i> mesophyll protoplasts	37
Live-cell imaging by confocal microscopy and image analysis	41
Supplementary Figures.....	42
Bibliography	53
Appendix Figures	64
Chapter 3: Manipulating Endosomal membrane-Plasma Membrane Tethering through BiFC interactions	65
Abstract	66
Introduction.....	67
Results	70

TABLE OF CONTENTS (Continued)

	Page
Localization of PtdIns(3)P biosensors VAM7-PX, Hrs-2xFYVE, and plasma membrane remorin StRem1.3.	70
BiFC complexes containing PtdIns(3)P biosensors and StRem1.3 display large unexpected patches of plasma membrane fluorescence	71
Formation of membrane patches requires a PM-binding partner	76
Membrane patches may correspond to tethering of the tonoplast and MVBs to the PM	78
Both the tonoplast and MVBs can be tethered to the PM.....	80
TP/MVB-PM tethering also modifies the distribution of PM-localized proteins.....	83
TP/MVB-PM tethering is limited by the cytoskeleton and ER network	86
TP/MVB-PM tethering is associated with two plant U-box (PUB) armadillo (ARM) repeat E3 ubiquitin ligases	86
Discussion.....	91
Materials and Methods	94
Plant Material	94
Cloning and Construction	94
Transient expression in <i>N. benthamiana</i> leaves and <i>A. thaliana</i> protoplasts	95
Live-cell imaging by confocal microscopy and image analysis	100
Supplementary Figures	101
Bibliography	109
Appendix Figures	122
Chapter 4: Fluorescent protein mEOS3.2 shows low self-association in bimolecular fluorescence complementation assays in plants.....	123
Abstract	124
Introduction.....	124
Results	126
Assessment of self-assembly in traditional BiFC systems in <i>N. benthamiana</i>	126
Assessment of photo-convertible fluorescent protein mEOS3.2 for BiFC assays in plants	127
mEOS3.2 retains photo-convertibility after BiFC complementation.....	131

TABLE OF CONTENTS (Continued)

	Page
BiFC mEOS3.2 provides sub-diffraction resolution of StRem1.3 localization in PALM imaging	134
Discussion.....	136
Materials and Methods	138
Plant Material	138
Cloning and Construction	139
Transient expression in <i>N. benthamiana</i> leaves	139
Confocal laser scanning microscopy(CLSM) and analysis	144
Protein extraction and western blots	144
Fixation of agroinfiltrated <i>N. benthamiana</i> leaves.....	145
PALM Microscopy	146
Supplementary Figures:.....	147
Bibliography	150
Chapter 5: <i>In vivo</i> super-resolution imaging of the dynamics of PtdIns(4)P in the plasma membrane of plant cells.....	155
Abstract	156
Introduction.....	157
Results	160
Different binding locations of FAPP1 are determined by its PtdIns(4)P and ARF1 binding regions.	160
Refining the subcellular localization of the three FAPP1 mutants <i>in vivo</i>	162
PALM single-particle tracking of FAPP1a on the PM <i>in vivo</i>	164
Discussion.....	168
Materials and Methods	171
Plant Material	171
Cloning and Construction	171
Transient expression in <i>N. benthamiana</i> leaves and <i>A. thaliana</i> protoplasts	174
Laser confocal scanning microscopy (LCSM) and image analysis	174
sptPALM imaging.....	175
Supplementary Figures.....	176

TABLE OF CONTENTS (Continued)

	Page
Bibliography	179

LIST OF FIGURES

Figure	Page
Figure 1.1 Conventional co-localization assay could not discriminate whether PtdIns(3)P biosensors targeting the PM in <i>N. benthamiana</i> leaf cortical cells.....	5
Figure 1.2. Two different distribution patterns of discrete microdomains observed in <i>N. benthamiana</i> leaf cortical cells.....	7
Figure 2.1 The FLS2-StRem1.3 BiFC complexes produced heterogeneous distribution patterns in <i>N. benthamiana</i> leaf cortical cells.	22
Figure 2.2 FLS2-StRem1.3 BiFC complexes co-localize with <i>Arabidopsis</i> ER-PM contact site tethering protein Synaptogamin 1 (SYT1) fused to tagRFP in <i>N. benthamiana</i> leaf cortical cells.	24
Figure 2.3 A C-terminal peripheral PM-binding domain is required for ER-PM tethering by <i>Arabidopsis</i> SYT1 in <i>N. benthamiana</i> leaf cortical cells.	26
Figure 2.4 Integral membrane proteins co-expressed with StRem1.3 in Venus BiFC complexes produce EM-PM tethering in <i>N. benthamiana</i> leaf cortical cells.	28
Figure 2.5 Lipid binding proteins co-expressed with SYT1 N-terminal domain in BiFC complexes produce EM-PM tethering in <i>N. benthamiana</i> leaf cortical cells....	31
Figure 2.6 Model for the production of ER-PM tethering complexes via BiFC.	33
Figure S2.1. Efficiently spontaneous reassembly of the two fragments of Venus into BiFC complexes with membrane proteins in <i>N. benthamiana</i> leaf cortical cells.	42
Figure S2.2 Heterogeneous distribution patterns observed for BiFC complexes produced in <i>N. benthamiana</i> leaf cortical cells or <i>Arabidopsis</i> mesophyll protoplasts.	43
Figure S2.3 Orthogonal imaging of SYT1 and FLS2-StRem1.3 BiFC complexes in <i>N. benthamiana</i> leaf cortical cells.	44
Figure S2.4 Orthogonal imaging of FLS2-StRem1.3 BiFC complexes relative to the cytoskeleton of <i>N. benthamiana</i> leaf cortical cells.	45
Figure S2.5 Distribution and kymograph analysis of SYT1, SYT1n and SYT1-StRem1.3 BiFC complexes co-expressed with ER marker tagRFP-HDEL in <i>N. benthamiana</i> leaf cortical cells.	46
Figure S2.6 Distribution of peripheral membrane proteins fused to YFP in <i>N. benthamiana</i> leaf cortical cells.	47

LIST OF FIGURES (Continued)

Figure	Page
Figure S2.7 Co-expression of peripheral membrane proteins and SYTn in BiFC complexes in <i>N. benthamiana</i> leaf cortical cells results in ER-PM tethering.	48
Figure S2.8 Membrane distributions of integral membrane proteins fused to YFP and transiently expressed in <i>N. benthamiana</i> leaf cortical cells.....	49
Figure S2.9 Co-expression of peripheral membrane proteins and StRem1.3 in <i>N. benthamiana</i> leaf cortical cells does not result in ER-PM tethering by BiFC complexes.	50
Figure S2.10 Co-expression of PtdIns(3)P binding proteins with the SYT1 N-terminal domain in BiFC complexes in <i>N. benthamiana</i> leaf cortical cells does not result in ER-PM tethering.	51
Figure S2.11 Subcellular localization of cytoplasm, PM, and tonoplast in <i>N. benthamiana</i> leaf cortical cells.	52
Figure 3.1 Subcellular localization of PtdIns(3)P relative to the plasma membrane in <i>N. benthamiana</i> leaf cortical cells.....	72
Figure 3.2 Co-expression of PtdIns(3)P-binding proteins and StRem1.3 produces BiFC complexes distributed in large patches on the PM of <i>N. benthamiana</i> leaf cortical cells.	74
Figure 3.3 BiFC complexes containing PM-targeted peripheral membrane proteins and PtdIns(3)P biosensors form membrane patches in <i>N. benthamiana</i> leaf cortical cells.	77
Figure 3.4 BiFC complexes containing peripheral membrane proteins targeted to both the PM and to MVBs or the tonoplast can form membrane patches in <i>N. benthamiana</i> leaf cortical cells.	79
Figure 3.5 Membrane patches can involve PM-tethering of either MVBs or the tonoplast.....	82
Figure 3.6 Distribution of cytoplasm-targeted free fluorescent proteins in the presence of membrane patches.	84
Figure 3.7 Distribution of fluorescently tagged PM-localized proteins in the presence of membrane patches in <i>N. benthamiana</i> leaf cortical cells.	85
Figure 3.8 Relationship of membrane patches with the cytoskeleton in <i>N. benthamiana</i> leaf cortical cells.	87

LIST OF FIGURES (Continued)

Figure	Page
Figure 3.9 Relationship of membrane patches to cortical ER networks in <i>N. benthamiana</i> leaf cortical cells.	88
Figure 3.10 Association of membrane patches with plant U-box (PUB) armadillo (ARM) repeat E3 ubiquitin ligases in <i>N. benthamiana</i> leaf cortical cells.	90
Figure S3.1 Subcellular localizations of PtdIns(3)P biosensors and non-binding mutants in <i>N. benthamiana</i> leaf cortical cells.	101
Figure S3.2 Co-expression of PtdIns(3)P biosensors and StRem1.3 produces large membrane patches on the PM of <i>A. thaliana</i> mesophyll protoplasts.	102
Figure S3.3 Subcellular localization of trifunctional fusion proteins in <i>N. benthamiana</i> leaf cortical cells.	103
Figure S3.4 Subcellular localizations of wildtype and mutant plasma membrane proteins and PtdIns(4) biosensors in <i>N. benthamiana</i> leaf cortical cells.	104
Figure S3.5 Subcellular localizations of proteins associated with MVBs and the tonoplast in <i>N. benthamiana</i> leaf cortical cells.	105
Figure S3.6 Exclusion of PM proteins by membrane patches in <i>N. benthamiana</i> leaf cortical cells is not an artifact of confocal microscopic image analysis.	106
Figure S3.7 Membrane patches produced by YFP-AtPUB43 and YFP-SAUL1 in <i>N. benthamiana</i> leaf cortical cells.	107
Figure S3.8 Relationship of membrane patches produced by SAUL1(ARM ⁷⁻¹¹) to MVB-, tonoplast- and PM-targeted proteins.	108
Figure 4.1 Spontaneous assembly of BiFC complexes from free fluorescent protein fragments.	128
Figure 4.2 Fluorescent protein mEOS3.2 expressed in <i>N. benthamiana</i> leaf cortical cells remains photo-convertible and displays minimal BiFC self-assembly.	130
Figure 4.3 Fluorescence of mEOS3.2 BiFC complexes formed with remorin StRem1.3 in <i>N. benthamiana</i> leaf cortical cells.	132
Figure 4.4 Photo-convertibility of mEOS3.2 BiFC complexes in <i>N. benthamiana</i> leaf cortical cells.	133
Figure 4.5 Use of mEOS3.2 BiFC complexes for PALM imaging in <i>N. benthamiana</i> leaf cortical cells.	135

LIST OF FIGURES (Continued)

Figure	Page
Figure S4.1 Localization of various StRem1.3 with YFP fusions expressed in <i>N. benthamiana</i> leaf cortical cells.	147
Figure S4.2 Validation of BiFC fusion protein expression in <i>N. benthamiana</i> leaves.	148
Figure S4.3 Self-assembly of BiFC mEOS3.2 complexes expressed in <i>N. benthamiana</i> leaf cortical cells.	149
Figure 5.1 Fluorescence distribution of YFP fused to wild-type and mutant FAPP1 PH domains, transiently expressed in <i>N. benthamiana</i> leaf cortical cells.	161
Figure 5.2 Subcellular co-localization analysis of three FAPP1 mutants in <i>N. benthamiana</i> leaf cortical cells.	163
Figure 5.3 Confocal and PALM single-particle tracking imaging of mEOS3.2 fusions in the PM of <i>N. benthamiana</i> leaf cortical cells.....	165
Figure 5.4 FRAP analysis of the mobility of FAPP1a and 2xFAPP1a in the PM of <i>N. benthamiana</i> leaf cortical cells.	167
Figure S5.1 YFP tagged PtdIns(4)P-bound biosensors and mutants transiently expressed in <i>A. thaliana</i> mesophyll protoplasts.....	176
Figure S5.2 Subcellular co-localization analysis of three FAPP1 mutants in <i>A. thaliana</i> mesophyll protoplasts.....	177
Figure S5.3 Specific formation of mEOS3.2 BiFC complexes on the PM through binding of FAPP1a biosensors, compared to controls.	178

LIST OF TABLES

Table	Page
Table 2.1 Primer designed and used in chapter 2.	38
Table 3.1 Primer designed and used in chapter 3.	96
Table 4.1 Primer designed and used in chapter 4.	140
Table 5.1 Primer designed and used in chapter 5.	172

LIST OF APPENDIX FIGURES

Figure	Page
Figure 2.1 Subcellular localization of all proteins tested in chapter 2 when transiently expressed in plant cells.	64
Figure 3.1 Subcellular localization of all proteins tested in chapter 3 when transiently expressed in plant cells.	122

Chapter 1: Overview

Overview

The overall focus of this thesis is on the distribution of specific lipids and membrane proteins of the external and internal membranes of plant cells, in the context of the roles that those lipids and proteins may play in microbe-plant interactions. The work includes the development of several new tools, the refinement of some existing tools, and the highlighting of several poorly appreciated artifacts that are common to such studies.

Plant-associated microbes secrete effectors to modulate the physiology and immune systems of hosts through several mechanisms during colonization, e.g. bacterial pathogens of plants utilize the Type III secretion system to deliver their effectors directly into host cells, while oomycete and fungal pathogens secrete effectors into the apoplast where then they are taken into the host cells (Ellis et al., 2006, Jones and Dangl, 2006). The mechanisms for translocation of oomycete and fungal effectors into host cells still remain elusive. One hypothesis is that effectors may enter into host cells through binding to phospholipids or other receptors in the plasma membrane (PM), leading to entry into the endocytic pathway (Gan et al., 2010, Kale et al., 2010, Gu et al., 2011, Plett et al., 2011). Evidence has been presented that effectors from fungal and oomycete effectors may bind to phosphatidylinositol 3-phosphate (PtdIns(3)P) for the purpose of host cell entry (Kale et al., 2010, Plett et al., 2011, Yaeno et al., 2011). PtdIns(3)P is highly enriched in endosomal membranes and could be generated in the PM under certain conditions (Falasca and Maffucci, 2009); thus it is plausible that effector entry might be mediated by PtdIns(3)P-binding. However, the clear visualization of PtdIns(3)P on the plant PM has proven difficult due to the close proximity of the cell wall and the PtdIns(3)P-rich vacuolar membrane.

More recently, small membrane-bound vesicles referred to as exosomes that are secreted into the apoplast for cell-to-cell and inter-organismal communication have attracted considerable attention. One mechanism for the formation of exosomes involves vesicles formed inside the endosomal multivesicular bodies (MVBs); membrane fusion between the MVBs and the PM can result in exocytic release of the internal vesicles as exosomes (Simons and Raposo, 2009, Angélique et al., 2011). Notably, exosomes have been found to be involved in transport of a variety of

metabolites and proteins (Perez-Gonzalez et al., 2012). Moreover, exosomes are also found to be able to incorporate mRNAs, microRNAs (miRNAs), and other non-coding RNAs (ncRNA), which subsequently can be taken up by recipient cells resulting in the regulation of targeted genes (Zhang et al., 2015). Since exosomes can be released by most cell types, they have been implicated in various cellular functions. In the battle between plants and pathogens, exosomes produced by microbial pathogens have been hypothesized as a more efficient delivery mechanism for virulence effectors than simple diffusion (Maxwell and E., 2011, Samuel et al., 2015). On the plant side, exosomes produced by plant hosts also play a key role in the innate immune system, including secretion of antimicrobial proteins, defense molecules, as well as small RNAs which could be shuttled into pathogens, suppressing virulence gene expression (Regente et al., 2012, Weiberg et al., 2013, Cai et al., 2018).

In addition to the fusion of exosomes with the PM of recipient cells, the uptake of proteins and other molecules into cells can be mediated by several endocytic mechanisms, including phagocytosis, macropinocytosis, clathrin-dependent endocytosis, caveolin-dependent endocytosis, and clathrin and caveolin independent pathways (Kruth et al., 2005, Mayor and Pagano, 2007). Membrane rafts have been widely described as possible entry point at the PM (Urbanus and Ott, 2012, Fan et al., 2015). Membrane rafts, more recently termed lipid micro-domains or nano-domains, denote a lateral compartmentalization of proteins and lipids in the PM, providing functional platforms for a variety of cellular processes such as signal transduction, and regulation of endocytosis and exocytosis (Cheng et al., 2006, Malinsky et al., 2013). In plants, two major protein families, flotillins and remorins, have been identified to be enriched in membrane microdomains, and both have been shown to participate in endocytic events (Lefebvre et al., 2010, Bandmann and Homann, 2012, Wang et al., 2013). Typically, Plant-specific remorins have been found in almost all land plants, where they are encoded by large multi-gene families which can be subdivided into six groups (Raffaele et al., 2007). Their structure is characterized by an intrinsically disordered N-terminus, and a highly conserved C-terminal coiled-coil domain (Marín and Ott, 2012, Perraki et al., 2012). An amphipathic loop at the very C-terminus is necessary and sufficient for PM binding (Perraki et al., 2012). Several remorins have

been reported to be associated with colonization of plant tissues by microbes. For example, a legume *Medicago truncatula* remorin protein MtSYMREM1 acts as a scaffolding protein interacting with the core set of symbiotic receptors for symbiotic responses to rhizobia bacterial *Sinorhizobium meliloti* (Lefebvre et al., 2010). Furthermore, remorin protein StRem1.3 from *Solanum tuberosum* can interfere with cell-to-cell movement of the plant virus, Potato Virus X (Raffaele et al., 2009). Moreover, StRem1.3 has also been implicated as a susceptibility factor for infection of plants by an oomycete pathogen, *Phytophthora infestans* (Bozkurt et al., 2014).

In this thesis, initially, I set out to investigate whether PtdIns(3)P could be detected on the plasma membrane in plant cells, and if so, whether it was associated with specific lipid microdomains involved in endocytosis. For this purpose I used a variety of specific PtdIns(3)P-binding proteins as biosensors, and as controls, mutants of those proteins which abolished PtdIns(3)P-binding. I genetically fused these PtdIns(3)P biosensors with fluorescent proteins, and transiently expressed them in *N. benthamiana* leaf cortical cells using *Agrobacterium tumefaciens*-mediated transformation. Using confocal laser scanning microscopy, all of the biosensors were found predominantly on a variety of dynamic vesicles, and on the vacuolar membrane (tonoplast) (Figure 1.1a). To visualize the PM, I co-expressed the biosensors with PM associated protein StRem1.3 (Perraki et al., 2012). However, the presence of PtdIns(3)P on the PM still could not be confirmed, particularly as the PtdIns(3)P-rich tonoplast was often found in very close proximity to the PM (Figure 1.1b).

To more unambiguously test for the presence of PtdIns(3)P in association with PM lipid microdomains, I co-expressed the PtdIns(3)P-specific biosensors together with StRem1.3, in a bimolecular fluorescence complementation (BiFC) assay. BiFC has commonly been used as a live-cell imaging approach to study protein-protein interactions (Kerppola, 2008). The assay is based on two non-fluorescing fragments split from a fluorescent protein, each of which is translationally fused with a different protein of interest; the interaction between the two proteins of interest can bring the two non-fluorescing fragments into proximity with each other resulting in assembly of a functional fluorescent protein. Moreover, the fluorescence produced by the reconstituted protein could enable subcellular localization of the protein complex

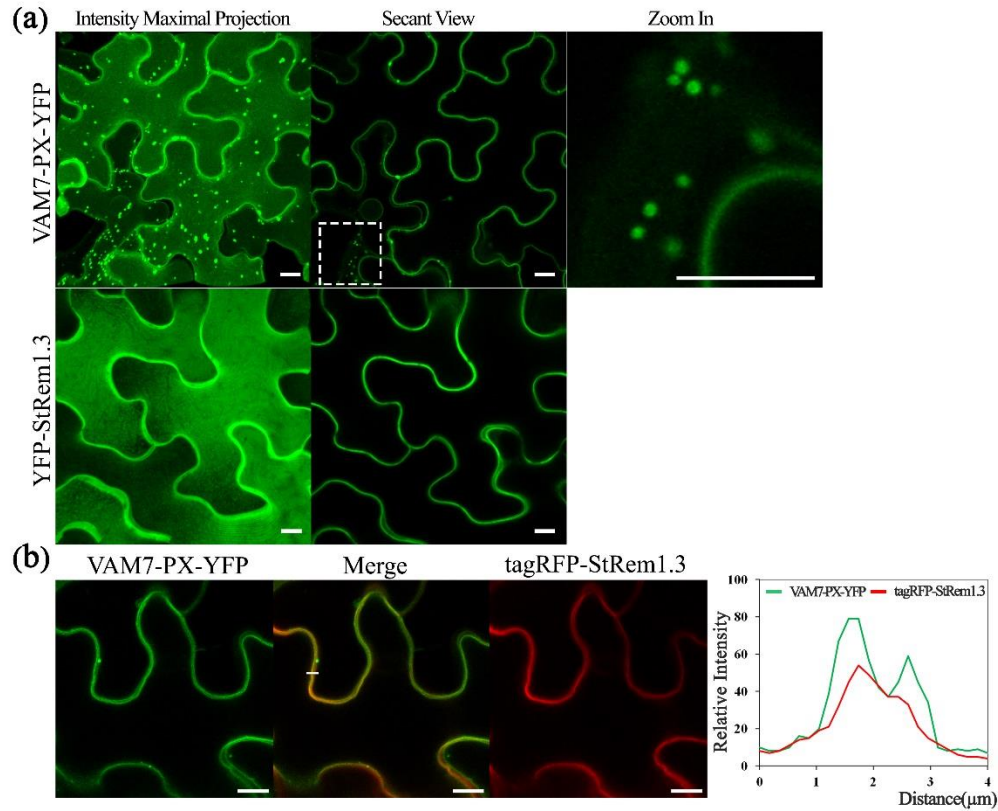


Figure 1.1 Confocal imaging of PtdIns(3)P biosensor VAM7-PX and plasma membrane-associated protein StRem1.3 in *N. benthamiana* leaf cortical cells.

(a) subcellular localizations of PtdIns(3)P biosensor phox homology (PX) of the *Saccharomyces cerevisiae* Qc-SNARE protein VAM7 (VAM7-PX) and *Solanum tuberosum* PM-associated remorin protein StRem1.3 fused with YFP. (b) the co-localization assay of co-expressed VAM7-PX-YFP and StRem1.3-tagRFP using the fluorescence plot as shown in the right panel that the fluorescence intensity profiles show relative fluorescence from white line scan in the overlaid image. The white scale bar represents 10 μm.

(Kerppola, 2006). BiFC can also detect proteins in close proximity, for example co-localized in a lipid microdomain. Thus I aimed to determine if PtdIns(3)P was enriched in StREM1.3-containing membrane microdomains; such proximity between PtdIns(3)P-bound biosensors and StRem1.3 might be sufficient for the assembly of a fluorescent BiFC complex. BiFC complexes can also form spontaneously, without close association of their fused proteins, especially if the fluorescent protein matures very rapidly. As became evident as my study progressed, Venus FP matures very rapidly, and efficiently forms spontaneous BiFC complexes – a property that led to new insights into membrane organization.

I fused the selected PtdIns(3)P-specific biosensors and StRem1.3 with either an N-terminal fragment of Venus (VenusN) or a C-terminal fragment (VenusC). By confocal microscopy live-cell imaging, I observed strong fluorescent signals in all BiFC complexes that included a PtdIns(3)P biosensor and StREM1.3. Surprisingly however, the BiFC fluorescent signals were distributed in large heterogeneous patches on the PM throughout the cortical cells (Figure 1.2a), suggesting perhaps that microdomains or aggregations of them were being visualized. (Demir et al., 2013, Jarsch et al., 2014). BiFC experiments using the mutant PtdIns(3)P-non-binding biosensors or a functional PtdIns(4)P biosensor also produced strong Venus fluorescence, but this was distributed uniformly on the PM. These results indicated that PtdIns(3)P binding was required for formation of the patches, but also indicated that PtdIns(3)P binding was not required for formation of the BiFC complexes by the two fragments of Venus. The ability of Venus to efficiently reassemble spontaneously was confirmed by expression of the two fragments alone, with no other proteins attached, which resulted in cytoplasmic localization. When the PtdIns(3)P biosensors were replaced in the BiFC complexes with PM-localized transmembrane proteins such as FLS2, a different, network-like, pattern of membrane patches, resembling PM-ER tethering sites (Zhang et al., 2012), was observed (Figure 1.2b). This led me to question whether the patches formed with the PtdIns(3)P biosensors might involve tethering of MVBs to the PM. Resolving these questions, and developing improved tools for BiFC in plant cells, formed the basis for this thesis.

In Chapter 2 “**Manipulating Endoplasmic Reticulum-Plasma Membrane**

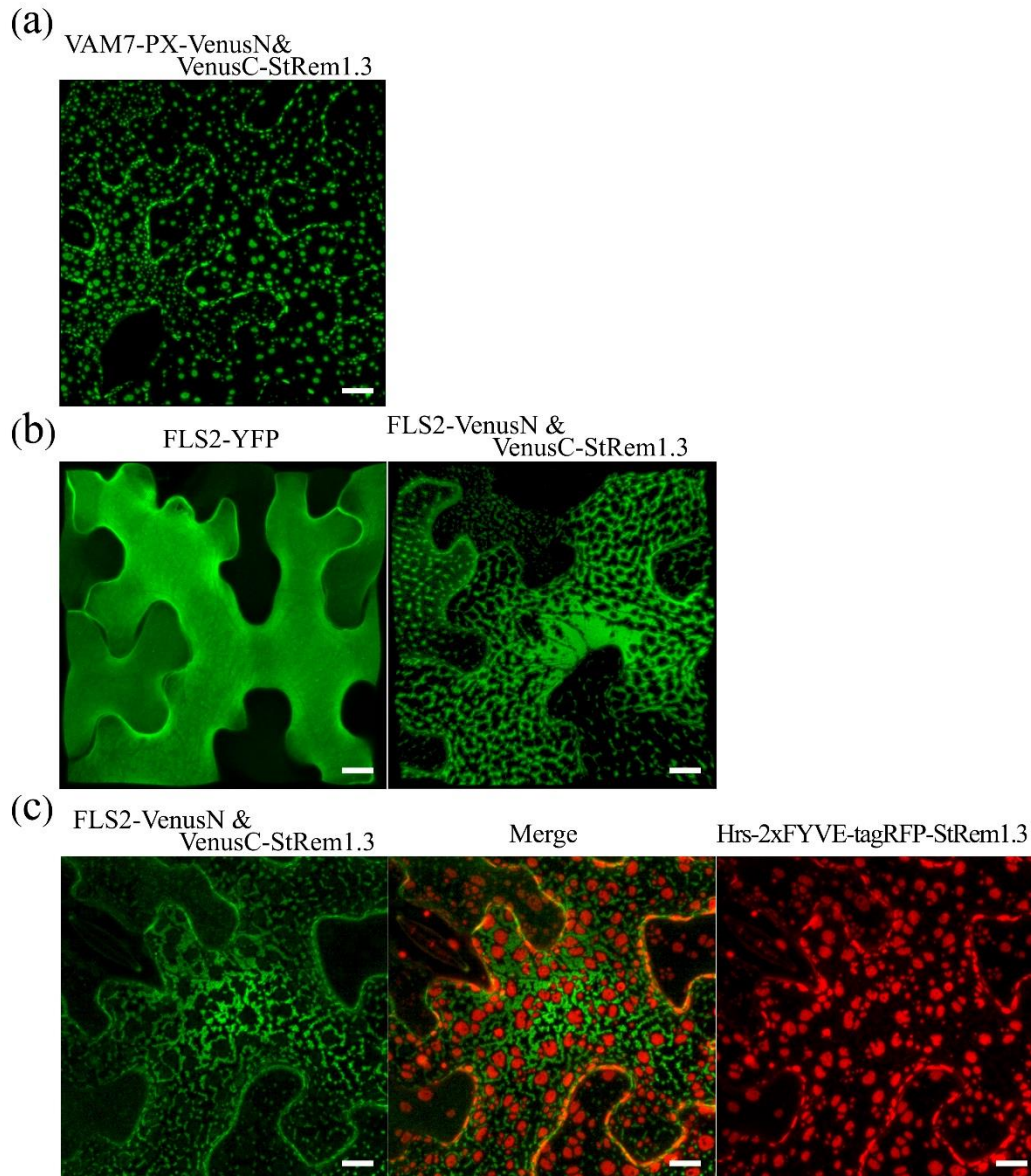


Figure 1.2. Two different distribution patterns of discrete microdomains observed in *N. benthamiana* leaf cortical cells.

(a) co-expressing PtdIns(3)P-bound biosensors VAM7-PX and plant-specific membrane microdomain maker StRem1.3 in BiFC complexes resulted in fluorescent patch distribution. (b) The prominent RLK receptor FLS2 co-expressed with StRem1.3 in BiFC complexes produced heterogeneous distribution along the PM. (c) These two discrete patterns mutually excluded each other, as shown by co-expressing FLS2-StRem1.3 BiFC complexes and Hrs-2xFYVE-tagRFP-StRem1.3. The white scale bar represents 10 μm .

Tethering through BiFC interactions in plants”, by using domain swap experiments with the native ER-PM tether protein Synaptotagmin1 (SYT1), I demonstrated that the heterogeneous network of patches produced in FLS2-StRem1.3 BiFC complexes corresponded to ER-PM tethering, that resulted from the dimerization between VenusN and VenusC in FLS2-VenusN and VenusC-StRem1.3. This work confirmed that membrane targeting of integral membrane proteins (IMPs) such as FLS2 requires either co-translational or post-translational integration into the ER membrane before trafficking to their membrane destination. Moreover, this work also confirmed that peripheral membrane proteins (PMPs) such as StRem1.3 are directly recruited to the cytoplasmic leaflet of the plasma membrane, for example via signals such as a membrane-insertion or lipid-binding domain, or lipid modifications. These observations suggest a re-visit of several previous studies (Demir *et al.*, 2013, Jarsch *et al.*, 2014, Bücherl *et al.*, 2017) which have reported heterogeneous patch-like distributions when using IMPs and PMPs in BiFC experiments.

In Chapter 3 “**Manipulating Tethering of Multivesicular Bodies and the Tonoplast to the Plasma Membrane Through BiFC Interactions in Plants**”, I strengthened the evidence that the patch-like distributions observed when combining PtdIns(3)P biosensors with StREM1.3, resulted from tethering of MVBs and the tonoplast to the PM. For example, I observed the membrane patches when I replaced PtdIns(3)P biosensors with several MVB-associated proteins, including *Arabidopsis* Rab5-type GTPases (Bonifacino and Glick, 2004, Ebine *et al.*, 2011, Bottanelli *et al.*, 2012), a Rab7-type GTPase (Nahm *et al.*, 2003), and endosomal SNARE proteins (Niihama *et al.*, 2005, Foresti *et al.*, 2006, Sanderfoot, 2007, Hachez *et al.*, 2014). I also observed that the membrane binding domains of the E3 ubiquitin-ligases SAUL1 (AtPUB44) and AtPUB43, could tether MVBs and the tonoplast to the PM, suggesting a possible functional role for these proteins in MVB-PM tethering, such as the secretion of exosomes.

Although my observations reported in Chapter 2 and Chapter 3 led to new insights into membrane organization in plant cells, they also highlighted the risk of using BiFC assays to study membrane protein interactions in plants, which without proper controls could lead to misinterpretation, or cause unrecognized alterations in cellular

structure and membrane organization. The problem that two non-fluorescing fragments spontaneously could re-assemble in the absence of associating protein partners has been recognized for some time as a major drawback of BiFC experiments (Miller et al., 2015). Recently however, Liu et al. (Liu et al., 2014) successfully performed BiFC assays in *Escherichia coli* cells using a newly developed photo-convertible fluorescent protein mEos3.2. In these assays the residue 164E was identified as the split site that could result in the least non-specific BiFC signals. In chapter 4 “**Fluorescent Protein mEos3.2 Shows Low Self-Association in Bimolecular Fluorescence Complementation Assays in Plants**”, I show that the mEOS3.2 BiFC probe, split at residue 164E, also produced minimal non-specific detectable BiFC signals when transiently expressed in *Nicotiana benthamiana* leaf cortical cells, but produced excellent signals with interacting protein partners. I also demonstrated that the re-assembled mEos3.2 could still photo-convert from green to red, which aided in distinguishing specific BiFC signals from background, and could allow the visualization of BiFC complexes at nanometer spatial resolution using photo-activated localization microscopy (PALM) imaging.

In chapter 5 “**In vivo Super-Resolution Imaging of the Dynamics of PtdIns(4)P in the Plasma Membrane Of Plant Cells**”, I successfully extended the application of mEos3.2 to study the spatiotemporal dynamics of a lipid species, PtdIns(4)P, in the plasma membrane of plant cells at single-molecule resolution using Single Particle Tracking PALM imaging (sptPALM). This work demonstrated the advantages of sptPALM compared to traditional imaging methods, such as Fluorescence Recovery After Photobleaching (FRAP), for studying the molecular dynamics of the plasma membrane. In addition, my work refined the specificity of the PtdIns(4)P biosensor FAPP1.

Bibliography

- Angélique, B., Marina, C., Graça, R. and Clotilde, T.** (2011) Exosome Secretion: Molecular Mechanisms and Roles in Immune Responses. *Traffic*, **12**, 1659-1668.
- Bandmann, V. and Homann, U.** (2012) Clathrin - independent endocytosis contributes to uptake of glucose into BY - 2 protoplasts. *The Plant Journal*, **70**, 578-584.
- Bonifacino, J.S. and Glick, B.S.** (2004) The Mechanisms of Vesicle Budding and Fusion. *Cell*, **116**, 153-166.
- Bottanelli, F., Gershlick, D.C. and Denecke, J.** (2012) Evidence for Sequential Action of Rab5 and Rab7 GTPases in Prevacuolar Organelle Partitioning. *Traffic*, **13**, 338-354.
- Bozkurt, T.O., Richardson, A., Dagdas, Y.F., Mongrand, S., Kamoun, S. and Raffaele, S.** (2014) The plant membrane-associated REM1.3 remorin accumulates in discrete perahaustorial domains and enhances susceptibility to *Phytophthora infestans*. *Plant physiology*.
- Bücherl, C.A., Jarsch, I.K., Schudoma, C., Segonzac, C., Mbengue, M., Robatzek, S., MacLean, D., Ott, T. and Zipfel, C.** (2017) Plant immune and growth receptors share common signalling components but localise to distinct plasma membrane nanodomains. *eLife*, **6**, e25114.
- Cai, Q., Qiao, L., Wang, M., He, B., Lin, F.M., Palmquist, J., Huang, H.D. and Jin, H.** (2018) Plants send small RNAs in extracellular vesicles to fungal pathogen to silence virulence genes. *Science*.
- Cheng, Z.-J., Deep Singh, R., Marks, D.L. and Pagano, R.E.** (2006) Membrane microdomains, caveolae, and caveolar endocytosis of sphingolipids (Review). *Molecular Membrane Biology*, **23**, 101-110.
- Demir, F., Horntrich, C., Blachutzik, J.O., Scherzer, S., Reinders, Y., Kierszniowska, S., Schulze, W.X., Harms, G.S., Hedrich, R., Geiger, D. and Kreuzer, I.** (2013) Arabidopsis nanodomain-delimited ABA signaling pathway regulates the anion channel SLAH3. *Proceedings of the National Academy of Sciences*, **110**, 8296-8301.

- Ebine, K., Fujimoto, M., Okatani, Y., Nishiyama, T., Goh, T., Ito, E., Dainobu, T., Nishitani, A., Uemura, T., Sato, M.H., Thordal-Christensen, H., Tsutsumi, N., Nakano, A. and Ueda, T.** (2011) A membrane trafficking pathway regulated by the plant-specific RAB GTPase ARA6. *Nature Cell Biology*, **13**, 853.
- Ellis, J., Catanzariti, A.-M. and Dodds, P.** (2006) The problem of how fungal and oomycete avirulence proteins enter plant cells. *Trends in plant science*, **11**, 61-63.
- Falasca, M. and Maffucci, T.** (2009) Rethinking phosphatidylinositol 3-monophosphate. *Biochimica et Biophysica Acta (BBA) - Molecular Cell Research*, **1793**, 1795-1803.
- Fan, L., Li, R., Pan, J., Ding, Z. and Lin, J.** (2015) Endocytosis and its regulation in plants. *Trends in Plant Science*, **20**, 388-397.
- Foresti, O., daSilva, L.L.P. and Denecke, J.** (2006) Overexpression of the Arabidopsis Syntaxin PEP12/SYP21 Inhibits Transport from the Prevacuolar Compartment to the Lytic Vacuole in Vivo. *The Plant cell*, **18**, 2275-2293.
- Gan, P.H., Rafiqi, M., Ellis, J.G., Jones, D.A., Hardham, A.R. and Dodds, P.N.** (2010) Lipid binding activities of flax rust AvrM and AvrL567 effectors. *Plant signaling & behavior*, **5**, 1272-1275.
- Gu, B., Kale, S.D., Wang, Q., Wang, D., Pan, Q., Cao, H., Meng, Y., Kang, Z., Tyler, B.M. and Shan, W.** (2011) Rust Secreted Protein Ps87 Is Conserved in Diverse Fungal Pathogens and Contains a RXLR-like Motif Sufficient for Translocation into Plant Cells. *PLOS ONE*, **6**, e27217.
- Hachez, C., Laloux, T., Reinhardt, H., Cavez, D., Degand, H., Grefen, C., De Rycke, R., Inzé, D., Blatt, M.R., Russinova, E. and Chaumont, F.** (2014) Arabidopsis SNAREs SYP61 and SYP121 Coordinate the Trafficking of Plasma Membrane Aquaporin PIP2;7 to Modulate the Cell Membrane Water Permeability. *The Plant cell*, **26**, 3132-3147.
- Jarsch, I.K., Konrad, S.S.A., Stratil, T.F., Urbanus, S.L., Szymanski, W., Braun, P., Braun, K.-H. and Ott, T.** (2014) Plasma Membranes Are Subcompartmentalized into a Plethora of Coexisting and Diverse Microdomains in Arabidopsis and Nicotiana benthamiana. *The Plant Cell Online*.
- Jones, J.D. and Dangl, J.L.** (2006) The plant immune system. *Nature*, **444**, 323-329.

- Kale, S.D., Gu, B., Capelluto, D.G., Dou, D., Feldman, E., Rumore, A., Arredondo, F.D., Hanlon, R., Fudal, I., Rouxel, T., Lawrence, C.B., Shan, W. and Tyler, B.M.** (2010) External lipid PI3P mediates entry of eukaryotic pathogen effectors into plant and animal host cells. *Cell*, **142**, 284-295.
- Kerppola, T.K.** (2006) Visualization of molecular interactions by fluorescence complementation. *Nature Reviews Molecular Cell Biology*, **7**, 449.
- Kerppola, T.K.** (2008) Bimolecular Fluorescence Complementation (BiFC) Analysis as a Probe of Protein Interactions in Living Cells. *Annual Review of Biophysics*, **37**, 465-487.
- Kruth, H.S., Jones, N.L., Huang, W., Zhao, B., Ishii, I., Chang, J., Combs, C.A., Malide, D. and Zhang, W.-Y.** (2005) Macropinocytosis Is the Endocytic Pathway That Mediates Macrophage Foam Cell Formation with Native Low Density Lipoprotein. *Journal of Biological Chemistry*, **280**, 2352-2360.
- Lefebvre, B., Timmers, T., Mbengue, M., Moreau, S., Hervé, C., Tóth, K., Bittencourt-Silvestre, J., Klaus, D., Deslandes, L., Godiard, L., Murray, J.D., Udvardi, M.K., Raffaele, S., Mongrand, S., Cullimore, J., Gamas, P., Niebel, A. and Ott, T.** (2010) A remorin protein interacts with symbiotic receptors and regulates bacterial infection. *Proceedings of the National Academy of Sciences*, **107**, 2343-2348.
- Liu, Z., Xing, D., Su, Q.P., Zhu, Y., Zhang, J., Kong, X., Xue, B., Wang, S., Sun, H., Tao, Y. and Sun, Y.** (2014) Super-resolution imaging and tracking of protein-protein interactions in sub-diffraction cellular space. *Nat Commun*, **5**.
- Malinsky, J., Opekarová, M., Grossmann, G. and Tanner, W.** (2013) Membrane Microdomains, Rafts, and Detergent-Resistant Membranes in Plants and Fungi. *Annual Review of Plant Biology*, **64**, 501-529.
- Marín, M. and Ott, T.** (2012) Phosphorylation of Intrinsically Disordered Regions in Remorin Proteins. *Frontiers in Plant Science*, **3**.
- Maxwell, S.J. and E., R.N.** (2011) Exosomes and other microvesicles in infection biology: organelles with unanticipated phenotypes. *Cellular Microbiology*, **13**, 1-9.
- Mayor, S. and Pagano, R.E.** (2007) Pathways of clathrin-independent endocytosis. *Nature Reviews Molecular Cell Biology*, **8**, 603.

- Miller, K.E., Kim, Y., Huh, W.-K. and Park, H.-O.** (2015) Bimolecular fluorescence complementation (BiFC) analysis: advances and recent applications for genome-wide interaction studies. *Journal of molecular biology*, **427**, 2039-2055.
- Nahm, M.Y., Kim, S.W., Yun, D., Lee, S.Y., Cho, M.J. and Bahk, J.D.** (2003) Molecular and biochemical analyses of OsRab7, a rice Rab7 homolog. *Plant Cell Physiol*, **44**, 1341-1349.
- Niihama, M., Uemura, T., Saito, C., Nakano, A., Sato, M.H., Tasaka, M. and Morita, M.T.** (2005) Conversion of Functional Specificity in Qb-SNARE VTI1 Homologues of *Arabidopsis*. *Current Biology*, **15**, 555-560.
- Perez-Gonzalez, R., Gauthier, S.A., Kumar, A. and Levy, E.** (2012) The Exosome Secretory Pathway Transports Amyloid Precursor Protein Carboxyl-terminal Fragments from the Cell into the Brain Extracellular Space. *Journal of Biological Chemistry*, **287**, 43108-43115.
- Perraki, A., Cacas, J.L., Crowet, J.M., Lins, L., Castroviejo, M., German-Retana, S., Mongrand, S. and Raffaele, S.** (2012) Plasma membrane localization of *Solanum tuberosum* remorin from group 1, homolog 3 is mediated by conformational changes in a novel C-terminal anchor and required for the restriction of potato virus X movement]. *Plant physiology*, **160**, 624-637.
- Plett, J.M., Kemppainen, M., Kale, S.D., Kohler, A., Legue, V., Brun, A., Tyler, B.M., Pardo, A.G. and Martin, F.** (2011) A secreted effector protein of *Laccaria bicolor* is required for symbiosis development. *Current biology : CB*, **21**, 1197-1203.
- Raffaele, S., Bayer, E., Lafarge, D., Cluzet, S., German Retana, S., Boubekeur, T., Leborgne-Castel, N., Carde, J.P., Lherminier, J., Noiro, E., Satiat-Jeunemaitre, B., Laroche-Traineau, J., Moreau, P., Ott, T., Maule, A.J., Reymond, P., Simon-Plas, F., Farmer, E.E., Bessoule, J.J. and Mongrand, S.** (2009) Remorin, a solanaceae protein resident in membrane rafts and plasmodesmata, impairs potato virus X movement. *The Plant cell*, **21**, 1541-1555.
- Raffaele, S., Mongrand, S., Gamas, P., Niebel, A. and Ott, T.** (2007) Genome-wide annotation of remorins, a plant-specific protein family: evolutionary and functional perspectives. *Plant physiology*, **145**, 593-600.

- Regente, M., Pinedo, M., Elizalde, M. and de la Canal, L.** (2012) Apoplastic exosome-like vesicles: A new way of protein secretion in plants? *Plant signaling & behavior*, **7**, 544-546.
- Samuel, M., Bleackley, M., Anderson, M. and Mathivanan, S.** (2015) Extracellular vesicles including exosomes in cross kingdom regulation: a viewpoint from plant-fungal interactions. *Frontiers in Plant Science*, **6**, 766.
- Sanderfoot, A.** (2007) Increases in the Number of SNARE Genes Parallels the Rise of Multicellularity among the Green Plants. *Plant physiology*, **144**, 6-17.
- Simons, M. and Raposo, G.** (2009) Exosomes – vesicular carriers for intercellular communication. *Current Opinion in Cell Biology*, **21**, 575-581.
- Urbanus, S. and Ott, T.** (2012) Plasticity of plasma membrane compartmentalization during plant immune responses. *Frontiers in Plant Science*, **3**.
- Wang, Q., Zhao, Y., Luo, W., Li, R., He, Q., Fang, X., Michele, R.D., Ast, C., von Wirén, N. and Lin, J.** (2013) Single-particle analysis reveals shutoff control of the *Arabidopsis* ammonium transporter AMT1;3 by clustering and internalization. *Proceedings of the National Academy of Sciences*, **110**, 13204-13209.
- Weiberg, A., Wang, M., Lin, F.M., Zhao, H., Zhang, Z., Kaloshian, I., Huang, H.D. and Jin, H.** (2013) Fungal small RNAs suppress plant immunity by hijacking host RNA interference pathways. *Science*, **342**, 118-123.
- Yaeno, T., Li, H., Chaparro-Garcia, A., Schornack, S., Koshiba, S., Watanabe, S., Kigawa, T., Kamoun, S. and Shirasu, K.** (2011) Phosphatidylinositol monophosphate-binding interface in the oomycete RXLR effector AVR3a is required for its stability in host cells to modulate plant immunity. *Proceedings of the National Academy of Sciences of the United States of America*, **108**, 14682-14687.
- Zhang, D., Vjestica, A. and Oliferenko, S.** (2012) Plasma Membrane Tethering of the Cortical ER Necessitates Its Finely Reticulated Architecture. *Current Biology*, **22**, 2048-2052.
- Zhang, J., Li, S., Li, L., Li, M., Guo, C., Yao, J. and Mi, S.** (2015) Exosome and Exosomal MicroRNA: Trafficking, Sorting, and Function. *Genomics, Proteomics & Bioinformatics*, **13**, 17-24.

Chapter 2: Manipulating Endoplasmic Reticulum-Plasma Membrane Tethering through BiFC interactions in plants

Manipulating Endoplasmic Reticulum-Plasma Membrane Tethering through BiFC interactions in plants

Kai Tao^{1,2}, Justin R. Waletich³, Felipe Arredondo², Brett M. Tyler^{2,4}.

1. Molecular and Cellular Biology Program, Oregon State University, Corvallis, OR 97331

2. Department of Botany and Plant Pathology, Oregon State University, Corvallis, OR 97331

3. Department of Microbiology, Oregon State University, Corvallis, OR 97331

4. Center for Genome Research and Biotechnology, Oregon State University, Corvallis, OR 97331

Abstract

Proteins in the plasma membrane are laterally organized into distinct functional platforms referred to as micro- or nano-domains. In plants, micro-domain proteins include remorins and a variety of plasma membrane (PM) targeted receptor-like kinase (RLKs) receptors, such as FLS2 and BRI1. We investigated the distribution of RLKs and remorins using the bimolecular fluorescence complementation (BiFC) assay, which detects co-localization of proteins, but is also subject to non-specific dimerization under certain circumstances. We observed heterogeneous distribution patterns of fluorescent signals ranging from distinct patch-like domains to nearly continuous networks when RLKs such as FLS2 were fused to VenusN and co-expressed with VenusC-StRem1.3 in *Nicotiana benthamiana* cortical cells. These patterns co-localized with the endoplasmic reticulum (ER) and ER-PM contact sites, and closely resembled patterns caused by over-expression of the ER-PM tether protein Synaptotagmin1 (SYT1). Using domain swap experiments with SYT1, we inferred that non-specific dimerization between FLS2-VenusN and VenusC-StRem1.3 could create artificial ER-PM tether proteins analogous to SYT1. The same phenomenon occurred with a representative set of integral membrane proteins and PM-targeted peripheral membrane proteins. This study highlights the risk of using the BiFC assay to study membrane protein interactions in plants which could lead to the misinterpretation of protein-protein interactions, or cause alterations in cellular structures and membrane

organization. At the same time, this phenomenon could be used to deliberately manipulate ER-PM tethering or to test protein membrane localization.

Introduction

The plasma membrane is comprised of phospholipid bilayers with various consortia of proteins embedded or peripherally attached. Most of these membrane proteins carry out critical functions such as detecting and transducing signals from the environment, transporting molecules in and out of the cell, and supporting the structure of the membrane and the cell. Growing evidence has revealed that different phospholipid species and membrane proteins may be hierarchically organized into coalescences with diameters ranging from 2.0 to 300 nm, referred to as “lipid or membrane rafts” or more recently as “micro- or nano-domains” (Kusumi et al., 2011, Lillemeier and Klammt, 2012, Varshney et al., 2016). For the rest of this chapter I will use the term “microdomains” These microdomains are the result of lipid-lipid, protein-lipid, and protein-protein interactions in the plasma membrane, potentially providing functional platforms to orchestrate a multitude of signaling pathways (Kusumi et al., 2012). To date, two major protein families, called flotillins and remorins, both of which are detected in detergent-resistant membrane fractions, have been identified as specific proteins associated with plasma membrane microdomains (Raffaele et al., 2009). Flotillins are widely present in all kingdoms of life, and their membrane targeting is mediated by either myristoylation, palmitoylation, or both (Jarsch et al., 2014). In contrast, remorins are plant-specific proteins, which have been well-characterized and contain a highly conserved C-terminal coiled-coil domain for plasma membrane anchoring (Perraki et al., 2012).

In plants, a spectrum of PM-bound receptor-like kinases (RLKs) are employed to coordinate signaling pathways in growth, development, and innate immunity (He et al., 2018). Several RLKs have been found to be functionally associated with remorins or flotillins (Jarsch et al., 2014). For example, the remorin protein MtSYMREM1 from the legume *Medicago truncatula*, was reported to mediate spatial distribution of RLKs NFP (Arrighi et al., 2006), LYK3 (Smit et al., 2007), and DMI2 (Limpens et al., 2005) during symbiotic plant-microbe interactions (Lefebvre et al., 2010). MtSYMREM1

was reported to mediate spatial regulation of symbiotic RLKs (Nakagawa et al.). Likewise, the *Lotus japonicus* MtSYMREM1 ortholog, LjSYMREM1 (Tóth et al., 2012), was shown to interact with the *L. japonicus* RLKs, NFR5 (Madsen et al., 2003), NFR1 (Radutoiu et al., 2003), and SYMRK (Stracke et al., 2002). The *Arabidopsis* flotillin protein, AtFlotillin1 (Borner et al., 2005), was shown to be critically involved in the activation of the RLK growth regulator, BRI1 (Russeinova et al., 2004); the two proteins showed increased co-localization in response to the brassinosteroid ligand (Wang et al., 2015). More recently, Bücherl et al. (Bücherl et al., 2017) observed that in *Arabidopsis*, BRI1 and the RLK immune receptor FLS2 (Gómez-Gómez and Boller, 2000) are heterogeneously but differently distributed in the membrane and that each receptor was associated with distinct remorin proteins. Despite these advances, the underlying mechanisms of compartmentalization of cell surface receptors into plasma membrane microdomains is still incompletely understood.

A variety of internal organelles and structures are closely associated with the PM, especially in plant cells where the large central vacuole compresses the cytoplasm into a thin layer against the PM. These include endosomes, multi-vesicular bodies (MVBs), cortical microtubules, actin filaments, and the cortical layers of the endoplasmic reticulum (ER). The ER is the largest membrane-bound organelle comprising an expansive network throughout the cell, functioning in protein synthesis and modification, lipid biosynthesis, metabolism, and Ca^{2+} and other intracellular signaling (Burgoyne et al., 2015). In order to coordinate its specialized functions with other membrane-bound organelles or the PM, the ER is functionally connected through vesicular trafficking, which involves the fusion of the membranes of interacting organelles (Saheki and Camilli, 2017). Alternatively, the existence of junctional appositions between the ER and other organelles including the PM, known as membrane contact sites (MCSs), provides a mechanism for direct inter-membrane contact. These contact sites are mediated by tethering proteins which simultaneously bind the two membranes together and bridge the nanometer-scale interface without membrane fusion taking place (Helle et al., 2013). Since it was first discovered in larval muscle cells (Porter and Palade, 1957), the ER-PM contact site has become the best characterized MCS. A number of tethering proteins mediating ER-PM contact have

been identified. These mainly belong to four protein groups, namely Extended-synaptotagmins (E-SYTs) or tricalbins, Vesicle-associated membrane protein-associated proteins (VAPs), Junctophilins, and Ist2 (Prinz, 2014). Though it has been suggested that each of these tethering proteins is independently associated with different cellular functions, all of them carry an ER-anchored region, which could be either a hydrophobic hairpin inserted into the ER membrane or a transmembrane domain integrated into the ER. Each also carries a cytosolic domain which contains motifs for binding lipids or proteins in the PM (Henne et al., 2015, Saheki and De Camilli, 2017). In *Arabidopsis* plants, Synaptogamin 1 (SYT1) is a well characterized ER-PM contact site protein. SYT1 contains a transmembrane domain at the N terminus, a synaptotagmin-like-mitochondria-lipid binding domain (SMP) close to C terminus of the transmembrane domain, and a cytoplasmic domain containing two conserved calcium-binding domains C2A and C2B at the C terminus which are responsible for binding negatively charged lipids on the plasma membrane such as phosphatidylserine (Shapire et al., 2008) and phosphoinositides (Yamazaki et al., 2010, Pérez-Sancho et al., 2015). The binding of calcium to the C2 domains regulates the binding of SYT1 to the PM, and hence regulates the tethering of the PM to the ER that is required to establish a contact site.

The bimolecular fluorescence complementation (BiFC) assay (Kerppola, 2008) is a commonly used experimental approach to study protein-protein interactions in various model organisms (Kerppola, 2008). The BiFC assay is based on two non-fluorescing fragments split from a fluorescent protein, each of which is translationally fused with a different protein of interest; interaction between the proteins of interest will bring the two non-fluorescing fragments into proximity with each other resulting in the re-assembly of a functional fluorescent protein (Kerppola, 2006). Thus, the BiFC assay not only enables identification of a potential protein-protein interaction, but also allows direct visualization of the protein complex *in vivo*. Due to these useful characteristics, the BiFC assay has also been successfully applied as a high-throughput approach in several large-scale studies to map potential protein-protein interactions (Remy and Michnick, 2004, Boruc et al., 2010, Snider et al., 2013). Venus, a variant of enhanced yellow fluorescence protein (EYFP) with a higher efficiency of maturation

and better adaptability in acid and high temperature environments, has become a widely used fluorescent protein for BiFC assays (Saka et al., 2007, Kodama and Hu, 2010, Miller et al., 2015). Moreover, a residue at position 155 located within a loop between the seventh and eighth β -sheets is the most commonly-used split site for Venus in BiFC assays (Wong and O'Bryan, 2011, Kodama and Hu, 2012). However, a challenge for this strategy is the spontaneous reassembly of the two fragments in the absence of associating protein partners can result in false positive BiFC signals (Shyu et al., 2006, Saka et al., 2007).

In this study, we set out to investigate pairwise associations between a set of representative membrane receptors and remorins using the BiFC assay. When RLKs such as FLS2 were ectopically co-expressed with *Solanum tuberosum* remorin StRem1.3 in *N. benthamiana* cortical cells, the BiFC fluorescent signal was heterogeneously distributed in distinct patch-like domains or nearly continuous networks across the PM. Co-localization assays indicated these patterns were associated with ER-PM contact sites, suggesting that the BiFC complexes might unexpectedly be acting as artificial ER-PM tethering proteins. Here, using domain swap experiments involving SYT1, we have demonstrated that this hypothesis is correct, and that any BiFC complex that involves one integral membrane protein and one peripheral membrane protein has the potential to act as an artificial ER-PM tethering protein. This artifact has been overlooked in previous studies of membrane organization using BiFC assay.

Results

Heterogeneous patch-like distribution of FLS2-StRem1.3 BiFC complexes

To provide a positive control for our studies of protein-lipid organization in the PM, we first chose FLS2 and StRem1.3, which have been found co-localizing to each other at the haustorial interface when activated by flg22 (Bozkurt et al., 2015), to create BiFC constructs and observe the subcellular localization when co-expressed in cells. To do this, we fused the N-terminal fragment of Venus (VenusN) to the C terminus of FLS2, and the C-terminal fragment of Venus (VenusC) to the N terminus of StRem1.3.

We also made complementary FLS2-VenusC and VenusN-StREM1.3 constructs. The pairs of BiFC constructs were ectopically co-expressed under the control the Cauliflower Mosaic Virus (CaMV) 35S promoter in *N. benthamiana* leaf cortical cells using *Agrobacterium tumefaciens*-mediated transient transformations. By confocal microscopy live-cell imaging, we observed strong BiFC fluorescence signals with both BiFC configuration pairs: FLS2-VenusN + VenusC-StRem1.3 and FLS2-VenusC + VenusN-StRem1.3 (Figure 2.1a). In both configurations, the BiFC fluorescence signal was heterogeneously distributed in distinct patterns ranging from discrete patches with diameters varying from ~0.5 μm to over 100 μm , through to continuous networks spanning the cortical surface. As a control, we co-expressed the FLS2 and StREM1.3 fusions with complementary Venus fragments that were not fused to another protein. In each case, we observed appreciable BiFC fluorescent signals (Figure S2.1), indicating that non-specific interactions between the two fragments of Venus could occur in the absence of FLS2-StREM1.3 associations (Kodama and Hu, 2010, Gookin and Assmann, 2014). However, the BiFC fluorescence signals produced by each of these control pairs were homogeneously distributed on the plasma membrane, especially in the case of FLS2. In each case, the subcellular localization closely matched that of fusions of FLS2 or StREM1.3 with full-length YFP (Figure S2.1), indicating that the subcellular localization of each control BiFC complex was determined by the respective FLS2 or StRem1.3 component. It also indicated that the heterogeneous distribution patterns observed with the FLS2-StREM1.3 BiFC complexes required both FLS2 and StREM1.3 to be present. Similar results were obtained when using YFP as the BiFC fluorophore, or when the constructs were expressed in *Arabidopsis* mesophyll protoplasts (Figure S2.2).

The FLS2-StRem1.3 complexes localize to ER-PM contact sites

Since the net-like distribution of the FLS2-StREM1.3 BiFC complexes resembled the distribution of the cortical ER, we performed co-localization assays using the ER marker tagRFP-HDEL (Boulaflous et al., 2009). The cellular distribution of FLS2-StRem1.3 BiFC fluorescence closely followed the distribution patterns of tagRFP-HDEL, namely net-like and sheet-like patterns of fluorescence (Figure 2.1b).

The dynamic movement of the ER network has been considered to provide propelling forces for cytoplasmic streaming in plant cells (Stefano et al., 2014). Thus, we also

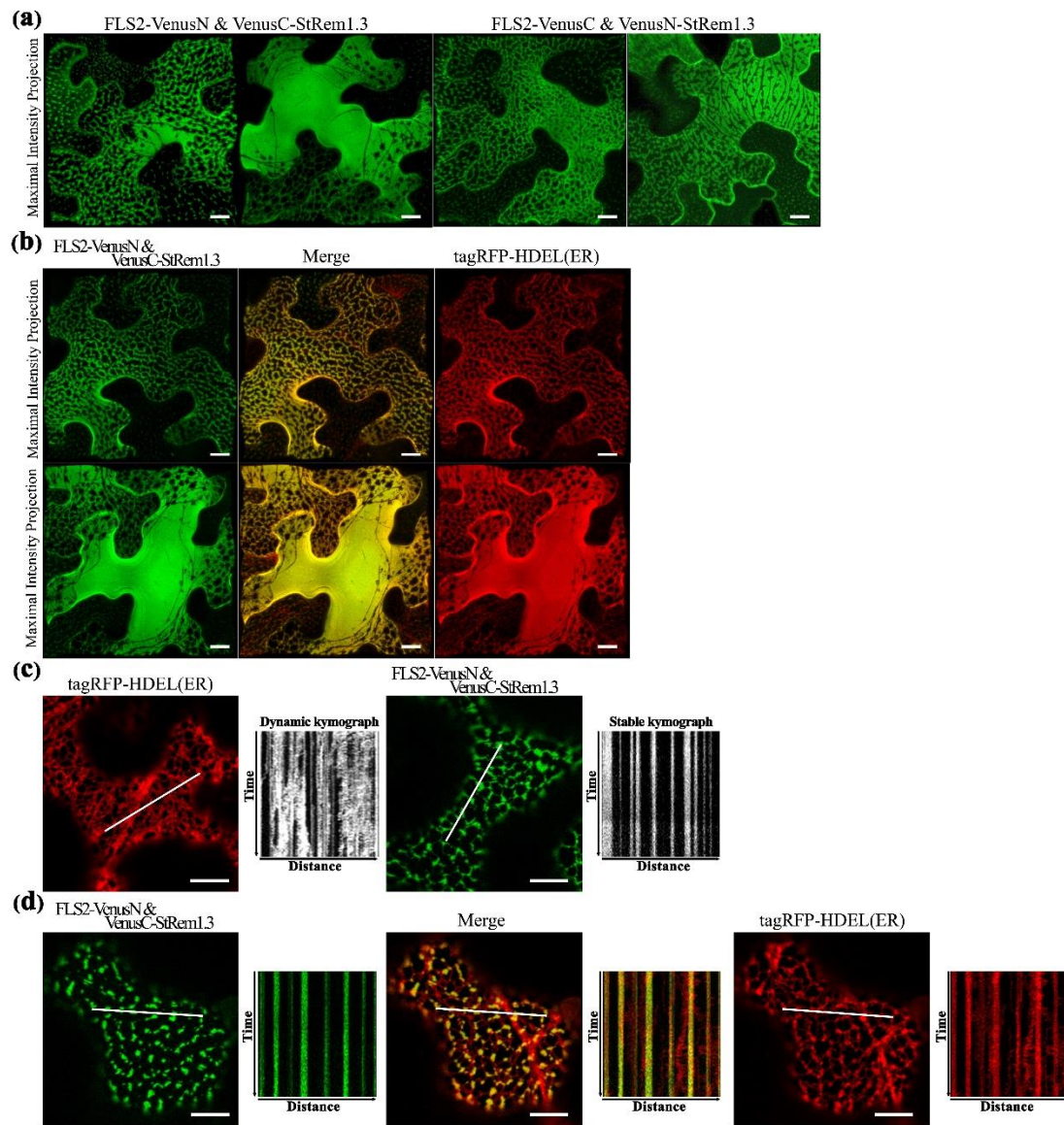


Figure 2.1 The FLS2-StRem1.3 BiFC complexes produced heterogeneous distribution patterns in *N. benthamiana* leaf cortical cells.

(a) BiFC fluorescence signal observed after co-expression of the following pairs of constructs: FLS2-VenusN and VenusC-StRem1.3; FLS2-VenusC and VenusN-StRem1.3. (b) FLS2-StRem1.3 BiFC complexes co-localized with endoplasmic reticulum maker tagRFP-HDEL. (c) Dynamic motion of the ER network labeled by ER tagRFP-HDEL and stable localization of puncta of FLS2-StRem1.3 BiFC complexes revealed by kymograph analysis. (d) Kymograph analysis of FLS2-StRem1.3 BiFC complexes co-expressed with tagRFP-HDEL. Kymographs were created from a short

time-lapse series (80 s) across a transect line which is $\sim 30\mu\text{m}$ in length. Scale bars represent $10\mu\text{m}$.

commonly observed dynamic movements of the ER network when tagRFP-HDEL was expressed alone (Figure 2.1c, Video S2.1). We documented the dynamic movements of the labeled organelles by using kymographs, in which the fluorescent signal along a transect is imaged over time. As shown in Figure 1c, the dynamic movements of the ER network labeled by tagRFP-HDEL produced a chaotic kymograph (Figure 2.1c). In contrast, we observed that the puncta of the FLS2-StRem1.3 BiFC complexes were relatively static, producing straight lines on the kymograph (Figure 2.1c, Video S2.2). Moreover, in cells co-expressing both FLS2-StRem1.3 BiFC complexes and tagRFP-HDEL, the puncta of the FLS2-StRem1.3 BiFC complexes co-localized with tagRFP-HDEL at junctions in the ER network where the tagRFP-HDEL signal showed increased stability (Figure 2.1d). However, small portions of the ER networks that were not co-localized with FLS2-StRem1.3 complexes still showed dynamic movements (Figure 2.1d). Since ER-PM contact sites are sites of reduced mobility of the ER (Henne et al., 2015), we hypothesized that the FLS2-StRem1.3 puncta may correspond to ER-PM contact sites.

To confirm whether the FLS2-StRem1.3 puncta corresponded to ER-PM contact sites, we co-expressed tagRFP-tagged SYT1 protein from *Arabidopsis*, which has been well-characterized as a tethering protein for ER-PM contact sites (Pérez-Sancho et al., 2015). As shown in Fig. 2, FLS2-StRem1.3 BiFC signals were clearly co-localized with SYT1. Moreover, a characteristic property of ER-PM junctions is that they restrict the distribution of other membrane proteins (Carrasco and Meyer, 2011). Thus the distribution of membrane-associated protein AtFlotillin1 was reduced in regions of the membrane displaying either SYT1-YFP or the FLS2-StRem1.3 complexes, as revealed by both maximum intensity projection and orthogonal projection (Figure S2.3) whereas the general membrane labeled by FM4-64 was not excluded.

In membrane locations where the FLS2-StRem1.3 BiFC signal was present in a near-confluent sheet, negatively-stained filament-like structures were apparent

(Figure 2.1a-b). Co-expression of the microtubule binding domain of *Arabidopsis* Casein Kinase 1-Like 6 (ACK6) (Ben-Nissan et al., 2008) fused with tagRFP, revealed

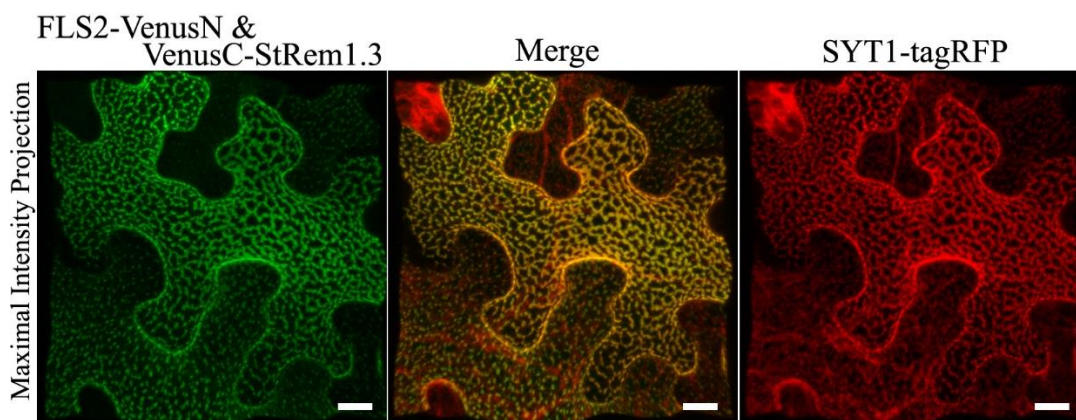


Figure 2.2 FLS2-StRem1.3 BiFC complexes co-localize with *Arabidopsis* ER-PM contact site tethering protein Synaptogamin 1 (SYT1) fused to tagRFP in *N. benthamiana* leaf cortical cells.

Scale bars represent 10 μm .

that the filament-like structures corresponded to microtubules (Figure S2.4). Orthogonal projection revealed that the cortical microtubules and the BiFC complexes mutually exclusively occupied the same layer (Figure S2.4). On the other hand, co-expression of the actin-binding protein AtFimbrin1 fused with tagRFP (Yuh-Shuh et al., 2004), confirmed that the filament-like structures did not correspond to actin filaments, which were revealed by orthogonal imaging to accumulate underneath the membrane instead, forming a mesh (Figure S2.4). These observations match previous studies that negative staining of microtubules was also observed with labeled ER-PM contact site proteins VAP27-1/NET3C (Wang et al., 2016) and synaptotagmin 1 (SYT1) (Pérez-Sancho et al., 2015).

StREM1.3 and other Peripheral Membrane Proteins can replace the C-terminus of SYT1 in ER-PM tethering

The PM-ER tethering protein SYT1 contains an N-terminal ER transmembrane domain (SYT1n) and a C-terminal peripheral PM-binding C2AC2B domain (Prinz, 2014) (Figure 2.3a). As shown in Figure 3b, formation of a Venus BiFC complex was sufficient to reconstitute the membrane tethering function of the separated SYT1 N- and C-terminal domains. The complex showed the same distribution and stability as intact SYT1 (Figure 2.3c). Removal of the C-terminal C2AC2B domain of SYT1 resulted in a dynamic net-like distribution, whether the SYT1 N-terminus was labeled with full length YFP (Figure 2.3d) or a Venus BiFC complex (Figure 2.3e). This dynamic distribution co-localized with the ER marker tagRFP-HDEL (Figure S2.5). However, adding StREM1.3 to the C-terminus of SYT1n via a BiFC complex was sufficient to restore the stable ER-PM contact site distribution (Figure 2.3f) and could also partially stabilize the distribution of co-expressed tagRFP-HDEL (Figure S2.5). Mutation of the C-terminal membrane insertion helix of StREM1.3 abolished its PM localization (Figure S2.6) as previously described (Perraki et al., 2012), and abolished its ability to reconstitute ER-PM tethering with SYT1n (Figure 2.3g).

To test if other peripheral membrane proteins could also participate in ER-PM tethering, we replaced the C2AC2B domain of SYT1 with the well-studied receptor-like cytoplasmic kinases (RLCKs), BIK1 (Lu et al., 2010), PBS1 (Qi et al., 2014), and

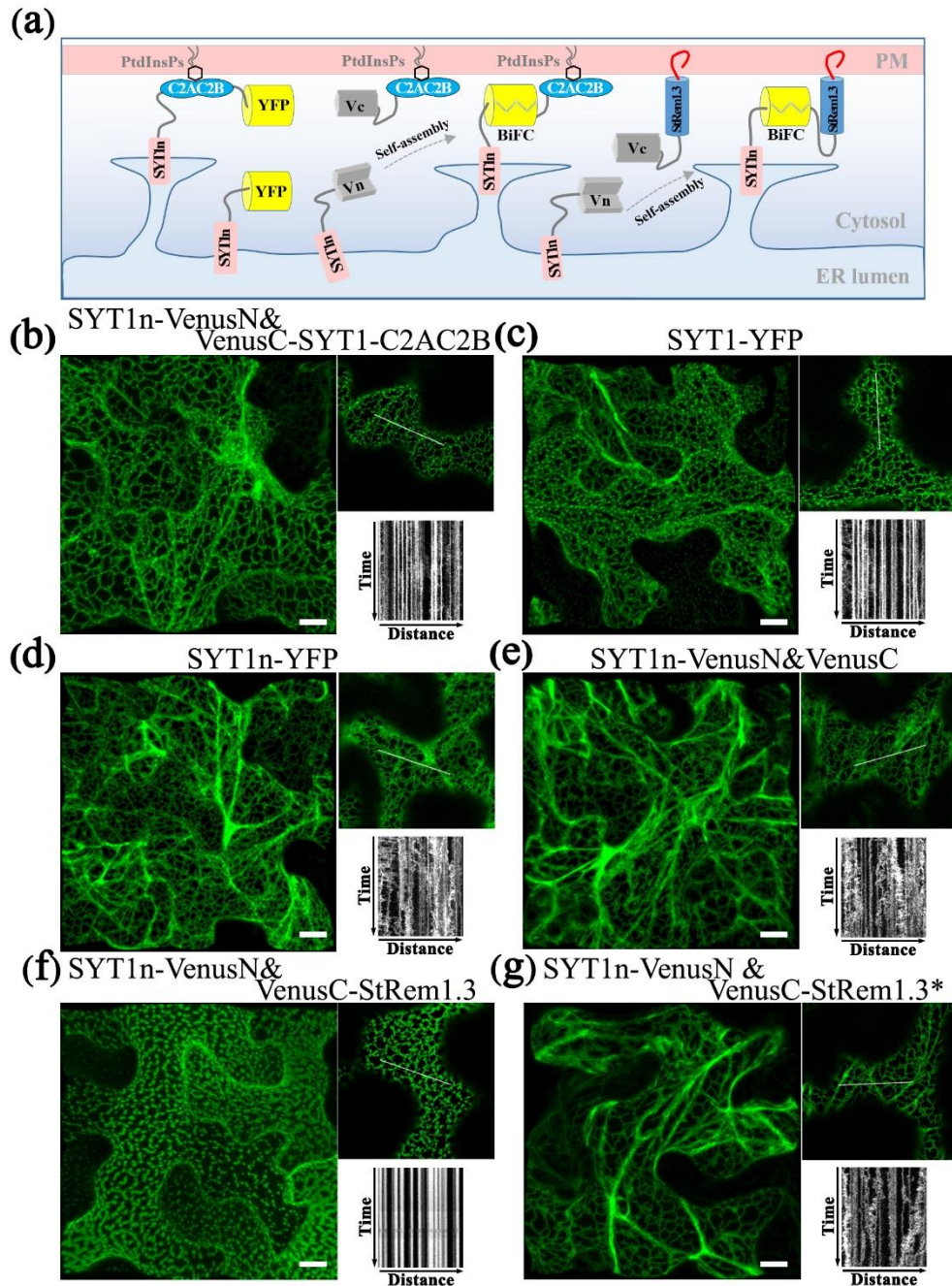


Figure 2.3 A C-terminal peripheral PM-binding domain is required for ER-PM tethering by *Arabidopsis* SYT1 in *N. benthamiana* leaf cortical cells.

(a) Explanatory schematic of reconstitution of SYT1 ER-PM tethering using BiFC complexes. (b-c) Distribution and kymograph analysis of full length SYT1 or SYT1 reconstituted using Venus BiFC complexes (d-e) SYT1 lacking the C-terminal peripheral PM-binding domain C2AC2B labeled by either full-length YFP or a free Venus BiFC complex. (f-g). Fusion of SYT1n to WT-type StRem1.3 or StRem1.3* PM-non-binding mutant via Venus BiFC complexes. All kymographs were created as described in Figure 2.1. Scale bars represent 10 μm.

CPK21 (Asai et al., 2013); these three proteins are targeted to the PM by either by N-terminal myristoylation, palmitoylation or both (Figure S2.6). Co-expression of BIK1-VenusN + SYT1n-VenusC, PBS1-VenusN + SYT1n-VenusC, and CPK21-VenusN + SYT1n-VenusC all produced stable puncta-like distributions resembling ER-PM tethering (Figure S2.7), which was further confirmed by co-localization analysis using SYT1 fused with tagRFP (Figure S2.7).

Integral membrane proteins can contribute ER anchoring to produce ER-PM tethering

Integral membrane proteins (IMPs) such as FLS2 are synthesized on the ER, with the N-terminal domain in the lumen of the ER and the C-terminal domain in the cytoplasm (Walter and Johnson, 1994, Goder and Spiess, 2001). We hypothesized that the reason that FLS2 could participate in tethering was because the formation of the FLS2-StREM1.3 complex trapped FLS2 in the ER, with its C-terminal-attached VenusN or VenusC fragment in the cytoplasm, bound to the StREM1.3 component. As demonstrated above, StREM1.3 can contribute the PM-binding required for ER-PM tethering. Thus it is likely that binding of the StREM1.3 component to the PM acts to trap the FLS component in the ER.

To address whether other IMPs could also form this ER-PM tethering structure with StRem1.3 through BiFC self-assembly, we selected several well-studied plasma membrane RLKs which share similar structural characteristics with FLS2 and also have similar localization patterns (Figure S2.8). RLKs are integrated into ER through the co-translational translocation machinery. We selected EF-Tu receptor (EFR) (Zipfel et al., 2006), brassinosteroid-associated kinase (BAK1) (Heese et al., 2007), and the BRI1 (Rusinova et al., 2004) and ERECTA receptors (ERec) (Bemis et al., 2013). When co-expressed with StREM1.3 in BiFC complexes, all these RLKs produced stable distribution patterns consistent with ER-PM tethering (Figure 2.4).

Next we tested IMPs that insert into the ER membrane post-translationally. For this purpose we selected tail-anchored (TA) proteins. These proteins lack an N-terminal signal peptide but contain a solo transmembrane domain (TMD) which resides so close to the C terminus that it cannot be recognized by the signal recognition particle (SRP) (Rapoport, 2007, Hegde and Keenan, 2011). We selected a set of *Arabidopsis* TA

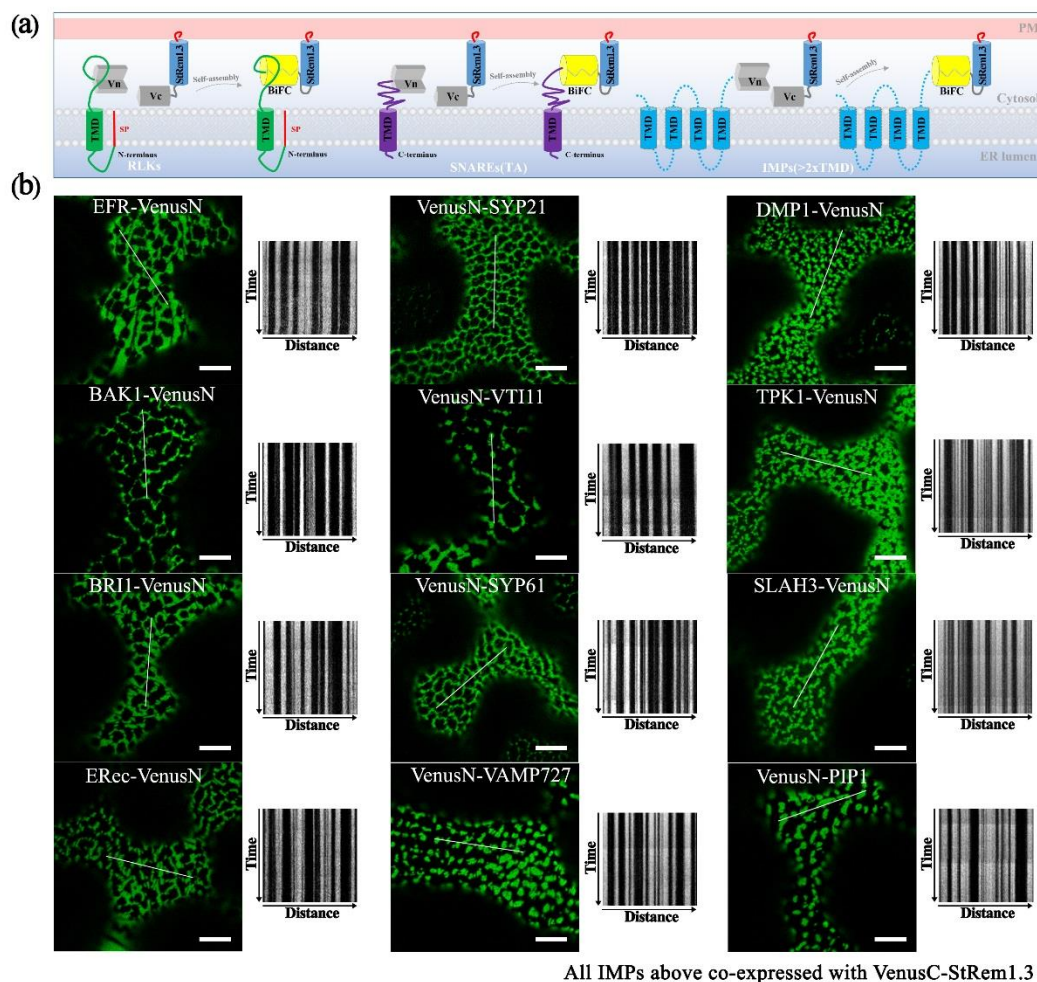


Figure 2.4 Integral membrane proteins co-expressed with StRem1.3 in Venus BiFC complexes produce EM-PM tethering in *N. benthamiana* leaf cortical cells.

(a) Explanatory schematic of representative classes of IMPs tested: IMPs with a cleavable N-terminal signal peptide and single-pass TMD; C-terminally anchored IMPs with single-pass TMD (tail-anchored SNARE proteins); IMPs with multi-pass TMDs. (b) Localization and kymograph analysis of Venus BiFC complexes formed with each IMP and StREM1.3. All kymographs were created as described in Figure 2.1. Scale bars represent 10 μm .

SNARE proteins, namely SYP21 (Qa-SNARE) (Foresti et al., 2006), VTI11 (Qb-SNARE) (Niihama et al., 2005), SYP61 (Qc-SNARE) (Hachez et al., 2014), and VAMP727 (R-SNARE) (Sanderfoot, 2007). In these proteins, the C-terminal TMD determines their localization in vesicles of the secretory and endocytic pathways (Figure S8). In each case, co-expression of these TA SNARE proteins with StRem1.3 in BiFC complexes resulted in a stable distribution consistent with ER-PM tethering (Figure 2.4).

We also tested several IMPs which span the membrane bilayer more than once, that reside on the PM, endosomal membranes, and vacuolar membrane (Figure S2.8). We tested *Arabidopsis* DUF679 membrane protein (DMP1) (Kasaras et al., 2012), tonoplast potassium channel protein TPK1 (Maîtrejean et al., 2011), slow anion channel 1 (SLAC) homolog SLAH3 (Demir et al., 2013), and intracellular aquaporin PIP1 (Wudick et al., 2009). As shown in Figure 2.4, a pattern consistent with ER-PM tethering was observed when each of the multi-pass IMPs was co-expressed with StRem1.3 in BiFC complexes. Together, the above results demonstrate that patterns consistent with ER-PM tethering were produced with multiple types of IMPs.

In contrast to the IMPs, we did not observe distributions consistent with ER-PM tethering when peripheral membrane proteins were paired with StREM1.3 in BiFC complexes. BIK1-VenusN, PBS1-VenusN, CPK21-VenusN co-expressed with VenusC-StRem1.3, produced only homogeneously distributed BiFC signals on the PM (Figure S2.9). Similar results were also obtained with *Arabidopsis* SNAP33 (Kargul et al., 2001, Jahn and Scheller, 2006) which has been recognized as a membrane targeted Qbc-SNARE protein lacking a TMD (Figure S9). Collectively, these results imply at least one IMP is required in the BiFC complex to produce ER-PM tethering.

PtdIns(4)P- and PtdIns(4,5)P₂-binding proteins could replace peripheral membrane-binding proteins in BiFC complexes to produce ER-PM tethering

SYT1 normally binds acidic lipids in the PM via a C2 domain (Pérez-Sancho et al., 2015) (Figure 2.3). C2 domains are large family of phospholipid binding proteins with a broad range of selectivity and affinity characteristics. Pleckstrin homology (PH) domains are another large family of phosphoinositide-binding proteins with a broad

range of specificities (Lemmon, 2008). Fluorescent protein-tagged PH domain proteins have been used in plants and other organisms to detect PtdIns(4)P and PtdIns(4,5)P₂. In plants, the PM has been identified as a pool for both PtdIns(4)P and PtdIns(4,5)P₂ (Van Leeuwen et al., 2007, Vermeer et al., 2009). We therefore tested whether PtdIns(4)P and PtdIns(4,5)P₂ binding PH domain proteins could replace the C2 domains of SYT1 for ER-PM tethering. We used the PH domains of the PtdIns(4)P-binding protein FAPP1 (Dowler et al., 2000), and of the PtdIns(4,5)P₂ binding protein PLC-delta 1 (Yagisawa et al., 1998); both have been well characterized in animal cell systems and have been used in plants previously (Van Leeuwen et al., 2007, Vermeer et al., 2009, Simon et al., 2016). In the case of FAPP1, we used a mutant of FAPP1 (FAPP1a) that no longer binds the golgi protein ARF1 (See Chapter 5). As a negative binding control, we designed site-directed mutants of each biosensor lacking lipid binding based on previous reports (Yagisawa et al., 1998, He et al., 2011). To begin with, we performed subcellular localization assays on YFP-tagged SYT1-C2AC2B, FAPP1a, FAPP1am (See Chapter 5), PLC δ 1-PH, PLC δ 1-PH*. Similar to the results previously observed for C2AC2B-GFP (Pérez-Sancho et al., 2015), YFP-FAPP1a (Simon et al., 2016), and YFP-PH_{PLC δ 1} (Van Leeuwen et al., 2007), we observed that FAPP1a-PH-YFP was more strictly localized at the PM than YFP-SYT1-C2AC2B and PLC δ 1-PH-YFP, in which cytosolic and nuclear localizations were also evident (Figure 2.5a). In contrast, both the FAPP1a-PH* and PLC δ 1-PH* mutants showed strongly diffuse patterns of cytosolic localization (Figure 2.5a). When co-expressed with SYT1n-VenusN, all three of VenusC-SYT1-C2AC2B, VenusC-FAPP1a-PH, and PLC δ 1-PH-VenusC each showed patterns consistent with ER-PM tethering (Figure 2.5b), but the PH mutant proteins produced only dynamic patterns associated with ER localization (Figure 2.5b). In contrast, when the PtdIns(3)P-binding protein domains, VAM7-PX (Cheever et al., 2001) and Hrs-2xFYVE (Vermeer et al., 2006), were provided as potential PM-binding proteins, only dynamic ER localization patterns were observed, comparable to the FAPP1a-PH* and PLC δ 1-PH* mutants (Figure S2.10). Furthermore, PtdIns(3)P-non-binding mutants of VAM7-PX and Hrs-2xFYVE, which were designed according to previously identified binding sites (Hayakawa et al., 2004, Lee et al., 2006), produced distribution patterns comparable to their wild type

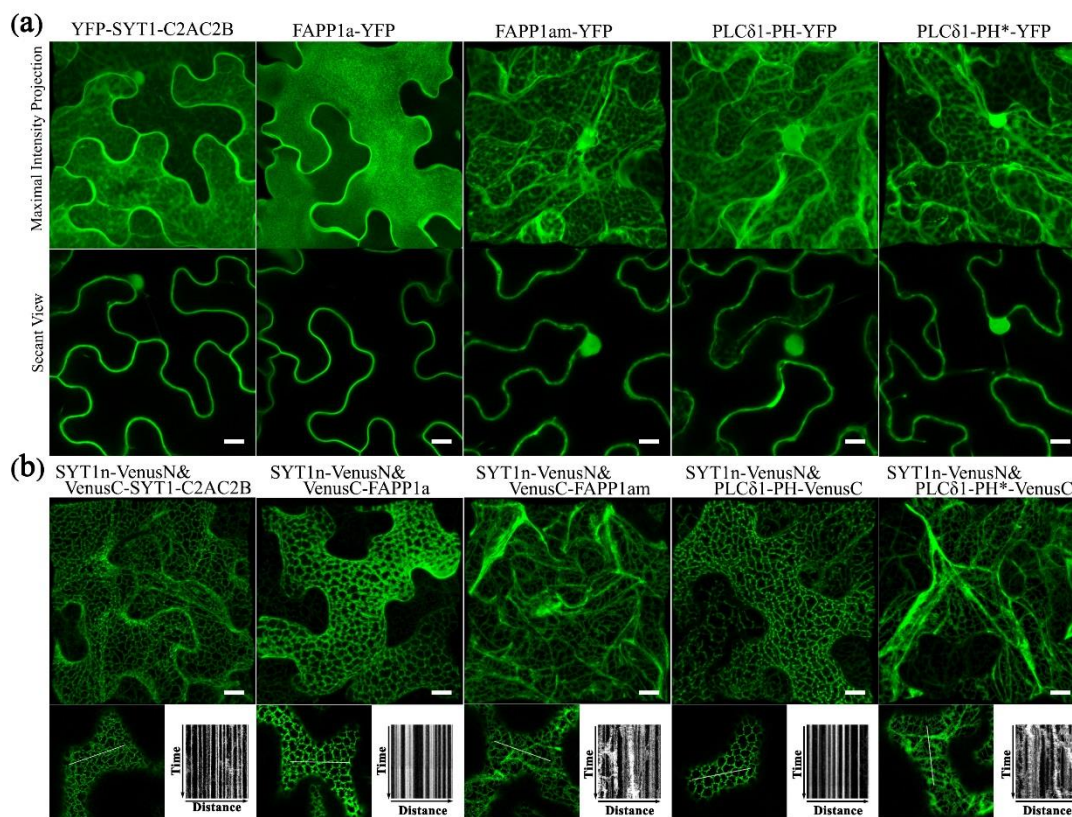


Figure 2.5 Lipid binding proteins co-expressed with SYT1 N-terminal domain in BiFC complexes produce EM-PM tethering in *N. benthamiana* leaf cortical cells.

(A) Subcellular localization of YFP-fused lipid-binding domains SYT1-C2AC2B, FAPP1a, and PLCδ1-PH, together with lipid-non-binding mutants FAPP1am and PLCδ1-PH*. (B) Localization and kymograph analysis of BiFC complexes formed from lipid binding domains and mutants fused with VenusC and co-expressed with SYT1n-VenusN. All kymographs were created as described in Figure 2.1. Scale bars represent 10 μm.

counterparts (Figure S2.10). Interestingly, the SYTn-PLC δ 1-PH BiFC complexes produced a very fine network distribution, with well defined puncta, that was closely similar to the pattern produced by SYTn-SYT1-C2AC2B BiFC complexes. In contrast, the SYTn-FAPP1a-PH BiFC complexes exhibited a thicker network with very abundant puncta, comparable to the patterns exhibited SYT1n-StRem1.3 BiFC complexes. We speculate that this difference may be correlated with the more defined PM localization exhibited by FAPP-PH and StRem1.3 (Figure 2.5a). In conclusion, our data suggest that PtdIns(4)P- and PtdIns(4,5)P₂-binding proteins, but not PtdIns(3)P-binding proteins, could contribute the PM-targeting needed for ER-PM tethering in plants.

Discussion

In this study, we observed that BiFC complexes containing both the RLK FLS2 and the membrane-associated remorin protein StRem1.3 exhibited a range of heterogeneous distribution patterns closely resembling those produced by over-expression of the *Arabidopsis* ER-PM tether protein SYT1 (Figures 2.1 and 2.2). Indeed co-expression of the FLS2-StREM1.3 BiFC complexes with SYT1 produced fully overlapping distributions (Figure 2.2). We therefore tested the hypothesis that the FLS2-StREM1.3 BiFC complexes acted as artificial ER-PM tethering proteins (Figure 2.6). We showed that StREM1.3 and also the lipid-conjugated peripheral membrane proteins BIK1, PBS1, and CPK21, could replace the PM-binding C2 domain of SYT1 (Figures 2.3 & S2.4) to produce ER-PM tethering. We showed that the phosphoinositide-binding PH domains from FAPP1 and PLC δ 1 could also functionally replace the C2 domain of SYT1 (Figure 2.5). Finally, we showed that a wide variety of IMPs that transit the ER, including 5 RLKs, 4 tail-anchored proteins, and 4 multi-transmembrane domain proteins, could provide the EM-anchoring function when paired with StREM1.3 as the PM-anchoring protein (Figure 2.4). On the other hand, peripheral membrane proteins that do not transit the ER could not provide the ER-anchoring function (Figure S2.5). On the basis of these observations, we have concluded that FLS2-StREM1.3 BiFC complexes do in fact act as artificial ER-PM tethering proteins. More generally, our model is that any ER-transiting IMP paired with a peripheral membrane protein, either in a BiFC complex or through a direct linkage,

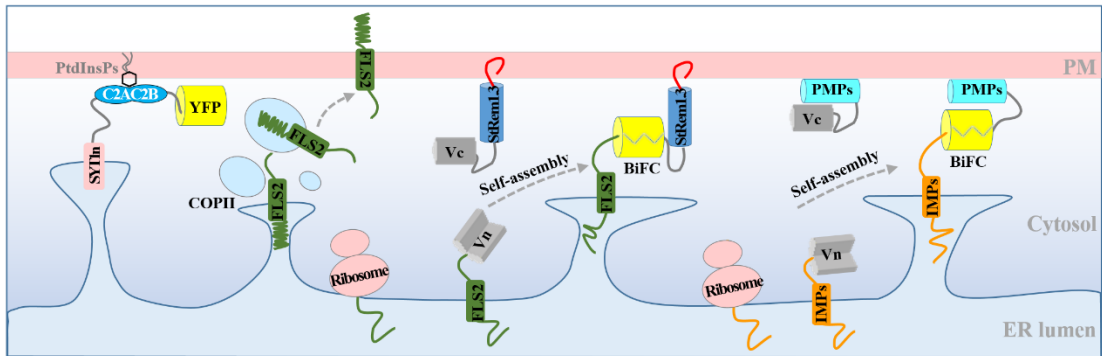


Figure 2.6 Model for the production of ER-PM tethering complexes via BiFC.

Normally, newly synthesized RLK protein FLS2 is targeted to the PM through the ER and transported to the PM via the coat protein complex II (COPII) system. Co-expression of FLS2 and StRem1.3 in BiFC constructs results in rapid spontaneous formation of Venus BiFC complexes tethered to the PM. PM tethering blocks ER-anchored FLS2 from delivery to the PM, resulting in artificial PM-ER complexes. Artificial ER-PM tethering could be created by pairing any ER-transiting integral membrane protein (IMP) with any peripheral membrane protein (PMP) in a BiFC complexes.

could act as an artificial ER-PM tethering protein (Figure 2.6). In this model, the IMP must transit through the ER, either co-translationally or post-translationally (Walter and Johnson, 1994, Goder and Spiess, 2001). Furthermore, the binding of the peripheral membrane protein to the PM should be sufficiently strong to trap the IMP in the ER, and prevent the completion of the IMP's transit to its final membrane destination. Conversely, the peripheral membrane protein should be synthesized in the cytoplasm and then be targeted to the PM post-translationally, without entering the ER, either via conjugation to a lipid, binding to a PM lipid, or via insertion of a hydrophobic loop or helix (Vögler et al., 2008, Pu et al., 2010, Resh, 2013, Stillwell, 2016).

In plants, several studies have reported observing heterogeneous distributions of BiFC complexes that combine IMPs with peripheral membrane proteins. However, none of these studies have considered the possibility that the distribution patterns observed may have arisen as a result of the formation of artificial ER-PM tethering proteins. For example, Jarsch et al (2014) showed that whereas FP-tagged RLK NFR1 and remorin MtSYMREM1 were uniformly distributed across the PM when individually expressed in *N. benthamiana* leaf epidermal cells, when the two were co-expressed in a BiFC complex, the fluorescent signal was exclusively observed in distinct, immobile puncta. Similarly, Demir et al (2013) observed that BiFC complexes comprised of *Arabidopsis* SLAH3 (an IMP) and CPK21 (a PMP) localized to distinct PM puncta. Likewise, Bücherl et al. (2017) expressed the following RLK-PMP proteins pairs in BiFC complexes and observed the formation of distinct puncta on the PM: FLS2-BSK1, BRI1-BSK1, FLS2-BIK1, and BRI1-BIK1. Our data suggest that it is necessary to re-evaluate the applicability of BiFC assays for plant membrane studies, and the validity of published studies (as mentioned above) using this approach should be re-visited.

Unambiguously determining PM localization in plant cells is challenging. In comparison to mammalian cells, plants cells contain a large central vacuole that takes up most of the cell volume resulting in the cytoplasm and organelles being constrained into the periphery of the cell, as well as appressed to the PM. As shown in Figure S2.11, except for the presence of nuclear staining, the comparison of free YFP with that of either a plasma membrane targeted YFP-StRem1.3 or a tonoplast marker TPK1-YFP

reveals that the cytosolic localization pattern of free YFP in the secant view is quite similar to that of the plasma membrane or tonoplast. Even by plotting the fluorescence intensity profiles of different co-expressed FPs, e.g. CFP, YFP-StRem1.3, and TPK1-tagRFP (Figure S2.11), the plasma membrane and tonoplast may be subtly distinguished as non-overlapping fluorescent peaks (YFP-StRem1.3 and TPK1-tagRFP in Figure S2.11) but the fluorescence of the cytoplasmic protein often overlaps either the membrane or tonoplast signals (Figure S2.11). Several methods have been commonly used to distinguish it, including plasmolysis (Speth et al., 2009) and osmolysis (Serna, 2005). However, these methods may be confounded by the presence of the tonoplast or of overexpression artifacts. For example, we observed that some weakly binding PMPs, e.g. SNAP33 (Figure S2.6), SYT1-C2AC2B (Figure 2.5), and PLC δ 1-PH (Figure 2.5), show substantial cytoplasmic localization when they are over-expressed as FP fusions. The ability of PMPs to form ER-PM tethering complexes may in some circumstances aid in distinguishing between cytosolic and membrane proteins. For example, there is currently not a strong consensus as to the localization of PtdIns(4,5)P₂ in plant cells (Delage et al., 2012). Although PtdIns(4,5)P₂ has been well established as a PM lipid in animal cells (Hammond et al., 2012), evidence for the same localization in plant cells has been ambiguous (Van Leeuwen et al., 2007). Our observations that PLC δ 1-PH is effective in forming ER-PM tethering complexes with SYT1n suggests that PtdIns(4,5)P₂ is indeed located in the plant PM (but does not rule out other locations as well). In contrast, our negative tethering results with PtdIns(3)P-binding proteins suggest that this lipid does not reside on the cytoplasmic face of the PM.

Zamyatnin et al. (2006) suggested that BiFC-based reporter systems can be used as a high-throughput strategy to study the topology of proteins integrated into the ER in *N. benthamiana* epidermal cells. Similarly, artificial ER-PM tethering could also be used to investigate whether a protein may be an IMP or not, and if so, what is its domain topology relative to the membrane. In the absence of x-ray crystallography and NMR spectroscopy data, (Arora et al., 2001, Topiol and Sabio, 2009), which are labor intensive and time consuming to obtain, bioinformatic analysis has been increasingly used to predict the identity and topology of IMPs. However these algorithms are not

fully accurate. For example, two commonly used programs TMHMM (Krogh et al., 2001) and Protter (Omasits et al., 2014) can differ in their predictions. In our study, Protter and TMHMM predicted the presence of TMDs in CPK21; whereas no members of the CDPK family have TMDs and their PM targeting is mediated by myristoylation and palmitoylation (Speth et al., 2009, Asai et al., 2013, Schulz et al., 2013). Consistent with this fact, we observed that CPK21-StRem1.3 BiFC complexes did not exhibit tethering. For confirmed IMPs, fusing a PMP at different positions in the IMP, either directly or via BiFC, could be used to probe of which domains faced the cytoplasm, thus gathering information about their topology in vivo.

In yeasts and mammalian cells, several genetically designed chimeric proteins have been successfully developed as tools to manipulate tethering of the ER to the PM or to other organelles, and to study cellular processes involving tethering. For example, the yeast Ist2p protein, which tethers the ER to the Golgi coat protein complex I (COPI) coatomer, was used to demonstrate how coatomer regulates the formation of cortical ER in animal cells (Lavieu et al., 2010). Chang et al. (2013) and Poteser et al. (2016) used a modified version of the human ER-PM tether protein STIM1, called MAPPER, in order to measure the formation and tightness of ER-PM contact sites in conjunction with TIRF microscopy. Therefore, it is plausible that artificial tethers could serve as a tools to gain insights into organelle interactions in plants including formation of ER-PM contact sites in plants. One can imagine, for example, tethering complexes in which dimerization of the two components is regulated by small molecules and/or light as reported previously (Karginov et al., 2011, Guntas et al., 2015).

Materials and Methods

Plant Materials

N. benthamiana and *A. thaliana* were grown in soil (Fafard® 4M Mix). *N. benthamiana* plants were grown in a growth chamber with a 14 hr photoperiod at 25°C for 5 weeks before *A. tumefaciens* infiltration assays. *A. thaliana* seeds were sown in soil and left at 4°C for 3 day of cold stratification. Then the seedlings were grown in a growth chamber with a 12-hr photoperiod at 20°C for 4 weeks before protoplast isolation.

Cloning and Construction

FLS2, BAK1, BRI1, ER, BIK1, PBS1, ACK6, FAPP1-PH, Hrs-2xFYVE, VAM7-PX were sub-cloned from constructs as reported previously (Ben-Nissan et al., 2008, Kale et al., 2010, Lu et al., 2010, Meng et al., 2015). The SYT1 (AT2G20990.1), AtDMP1 (AT3G21520.1), TPK1 (AT5G55630.1), AtPIP1 (AT3G61430.1), SLAH3 (AT5G24030.1), CPK21 (AT4G04720.1), SNAP33 (AT5G61210.1), AtSYP21 (AT5G16830.1), AtVTI11 (AT5G39510.1), AtVAMP727 (AT3G54300.1), AtSYP61 (AT1G28490.1), AtFlotillin1 (AT5G25250), AtFimbrin1 (At4g26700.1) coding regions were amplified from *Arabidopsis* Col-0 cDNA. StRem1.3 (U72489.1), and PLC δ 1-PH (BC050382.1) were synthesized by GenScript Corporation. All PCR amplifications were performed by High-Fidelity DNA polymerase (CloneAmpTM HiFi PCR Premix, TaKaRa Bio) using oligonucleotides as listed in Table 2.1. All PCR products were individually recombined by In-Fusion[®] HD Cloning (TaKaRa Bio) into the Gateway vector pDONR207 into which VenusN, YFPn, VenusC, YFPc, or full length FPs had previously been inserted. The ER marker was generated by PCR mutagenesis to add a carboxyl-terminal HDEL peptide to tagRFP. The site-specific mutations of PLC δ 1-PH*, StRem1.3*, FAPP1-PH*, VAM7-PX* and Hrs-2xFYVE* were introduced into their respective pDONR207 constructs using appropriate oligonucleotides in a PCR reaction that amplified the entire vector. By using the Gateway[®] LR reaction (Thermoscientificbio), all constructs were transferred from their pDONR207 vectors into the destination expression binary vectors, pmAEV (for cytoplasmic expression) or psAEV (for ER targeting), both of which are derived from binary vectors pCAMBIA (Dou *et al.*, 2008) and driven by the Cauliflower Mosaic Virus (CaMV) 35S promoter conferring constitutive high level expression in plant cells. All these plasmid constructs were confirmed by DNA sequencing at the Center for Genome Research and Biocomputing (Oregon State University).

Transient expression in *N. benthamiana* leaves and *A. thaliana* mesophyll protoplasts

The procedures to introduce expression vectors into *A. tumefaciens* strain GV3101, and to infiltrate transformed *A. tumefaciens* cells into 5-week-old *N. benthamiana* leaves were carried out as described previously (Lu et al., 2013). *A. tumefaciens* cells were infiltrated at OD₆₀₀ of 0.1 for the expression of the full-length fluorescent protein

Table 2.1 Primer designed and used in chapter 2.

Oligo Name	Forward primer(5'-3')	Reverse primer(5'-3')	Application notes
StRem1.3	GGCGGTAGCGCTAGCGCAGAA TTGGAAGCTAAG	AAGCTGGGTGATATCTTAAAAT ATTCCAAGGATTTTC	FP-StRem1.3
FLS2-FP	AGCAGGCTCCTCGCGAATGAAG TACTCTCAAAG	CTCCTCCACCTCTAGAACTTC TCGATCCTCGTT	FLS2-FP
BIK1	AGCAGGCTCCTCGCGAATGGGT TCTTGCTTCAGTTCTCGAG	CTCCTCCACCTCTAGACACAAG GTGCCTGCCAAAAGGTT	BIK1-FP
PBS1	AGCAGGCTCCTCGCGAATGGGT TGTTTCTCGTGTTTTGATTC	CTCCTCCACCTCTAGACCCGGT ACTGTTGCTCTCTGAAGTAC	PBS1-FP
FAPP1	AGCAGGCTCCTCGCGAATGGAA GGTGTCTGTGA	CTCCTCCACCTCTAGAGCGAGT ATCGGTCAGACACG	FAPP1-FP
SYT1	AGCAGGCTCCTCGCGAATGGGC TTTTTCAGTACGATACTAG	CTCCTCCACCTCTAGAAGAGGC AGTTCGCCACTCGAGCT	SYT1-FP
tagRFP-HDEL	CATGATGAACTGTAAGTTTAAA CCCACCCAGCTTC	CAGTTCATCATGTCTAGAGTTC AATTTGTGACC	psAEV as destination
AtFlotillin1	AGCAGGCTCCTCGCGAATGTTC AAAGTTGCAAGAGCGTCAC	CTCCTCCACCTCTAGAGCTGCG AGTCACTTGCTTCGGTTCC	AtFlotillin1-FP
ACK6	GGCGGTAGCGCTAGCAGTAGTG CCAGGTCCCATTCC	AAGCTGGGTGATATCTCATTG CGGATCGAAAGAAG	FP-ACK6
AtFimbrin1	GGCGGTAGCGCTAGCGAGATC GTTGAAGGATCTTCAAC	AAGCTGGGTGATATCTTACTCT GAGACCGTGGTGATTTTCAGAAA C	FP-AtFimbrin1
SYT1n		CTCCTCCACCTCTAGAGGTCTT AGGCCAGAGATACATG	SYT1n (1-729 bp)
SYT1-C2AC2B	AGCAGGCTCCTCGCGAATGCTT GTAGTTCCAATCCTTGAC		SYT1-C2AC2B (732-1626 bp)

StRem1.3*-1	CATCATCATAAATCTCGTTCTA CTGTGACTAGTCCA	AGATTTATGATGATGCTCCTCT GCCTTGAGAAGATC	L179H, A180H, A181H, Y184S, A185S, G187V, A189A, L194S, G195Q, I196Q, F197Q
StRem1.3*-2	CAACAGCAATCTAGATGAGATA TCACCCAG	TTGCTGTTGAGAGATTTTCTTTG GACTAGTC	L179H, A180H, A181H, Y184S, A185S, G187V, A189A, L194S, G195Q, I196Q, F197Q
CPK21	AGCAGGCTCCTCGCGAATGGGT TGCTTCAGCAGTAAACAC	CTCCTCCACCTCTAGAATGGAA TGGAAGCAGTTTCCCCTG	CPK21-FP
AtDMP1	AGCAGGCTCCTCGCGAATGTCC GAAACTTCTTTGCTCATACC	CTCCTCCACCTCTAGAGGCAGA GACCGAGGCTTTCTTGGTC	AtDMP1-FP
AtTPK1	AGCAGGCTCCTCGCGAATGTCCG AGTGATGCAGCTCGTACGCCAT TG	CTGCCTCCTCCACCTCTAGACC TTTGAATCTGAGACGTGGTCTG AGC	AtTPK1-FP
SNAP33	AGCAGGCTCCTCGCGAATGTTT GGTTTAAGGAAATCACCGGCA	CTGCCTCCTCCACCTCTAGACTT TCCAAGCAAACGGCGACC	SNAP33-FP
BAK1	AGCAGGCTCCTCGCGAATGGAA CGAAGATTAATGATC	CTCCTCCACCTCTAGATCTTGG ACCCGAGGGGTATTC	BAK1-FP
BRI1	AGCAGGCTCCTCGCGAATGAAG ACTTTTTCAAGCTTCTTTC	CTCCTCCACCTCTAGATAATTTT CCTTCAGGAACTTCTTTTATAC	BRI1-FP
ERec	AGCAGGCTCCTCGCGAATGGCT CTGTTTAGAGATATTGTTT	CTCCTCCACCTCTAGACTCACT GTTCTGAGAAATAACTTG	ERec-FP
SYP21	GGCGGTAGCGCTAGCAGTTTCC AAGATCTCGAAGCTGGTAC	AAGCTGGGTGATATCTTAGACC AAGACAACGATGATGACAATG	FP-SYP21
VTI11	GGCGGTAGCGCTAGCAGTGAC GTGTTTGATGGATATGAGC	AAGCTGGGTGATATCTTACTTG GTGAGTTTGAAGTACAAG	FP-VTI11
SYP61	GGCGGTAGCGCTAGCTCTTCAG CTCAAGATCCATTCTACATTG	AAGCTGGGTGATATCTTAGGTC AAGAAGACAAGAACGAATAGG	YFP-SYP61

VAMP727	GGCGGTAGCGCTAGCAGTCAA AAGGGTTTGATATATAGCTTTG	AAGCTGGGTGATATCTCATGAT GAGCATTTGAAACCTCCACAAG C	FP-VAMP727
SLAH3	AGCAGGCTCCTCGCGAATGGAG GAGAAACCAAACCTATGTG	CTCCTCCACCTCTAGATGATGA ATCACTCTCTTGAGTTTTGC	SLAH3-FP
AtPIP1	GCAGGCTCCTCGCGAATGGAAG GCAAGGAAGAAGACGTTAGAG	TCCTCCACCTCTAGAGCTTCTG GACTTGAAGGGGATGGC	AtPIP1-FP
PLCδ1-PH	GCAGGCTCCTCGCGAATGGACT CGGGCCGGGACTTCCTGAC	TCCTCCACCTCTAGAGATGTTG AGCTCCTTCAGGAAGTTC	PLCδ1-PH-FP
Hrs-2xFYVE	GGCGGTAGCGCTAGCGAATTTG AAAGCGATGCGATGTTTG	AAGCTGGGTGATATCTTACTTC GGTTGCAGGTCCACGGCC	FP-Hrs-2xFYVE
VAM7-PX	GGCGGTAGCGCTAGCGCAGCTA ATTCTGTAGGGAAAATG	AAGCTGGGTGATATCTTATAGA TGCTGCTGTGACTTTTC	FP-VAM7-PX
VAM7-PX*	AAAGAGTATGCCGAGTTTTGGA AACTGAAGACACG	GGCATACTCTTTGTAAAGGCGC TTGTTTG	R40E, S42A
Hrs-2xFYVE* 1	TCTTCAAGCAGTTGTTCCGCCT GCGGACAGATTTTCTGTGG	GGAACAACCTGCTTGAAGAGGTC ACAACACCAAACCTGAACAC	R34S, K35S, H36S, H37S, R39S, R116S, K117S, H118S, H119S, R121S
Hrs-2xFYVE* 2	TCAAGCAGTTCCTGTTTCAGCAT GCGGCCAAATCTTTTGTGG	TGAACAGGAACTGCTTGATGTA ACGACTCCGAACTGCACG	R34S, K35S, H36S, H37S, R39S, R116S, K117S, H118S, H119S, R121S
FAPP1	AGCAGGCTCCTCGCGAATGGAA GGTGTCTGTGTA	CTCCTCCACCTCTAGAGCGAGT ATCGGTCAGACACG	FAPP1-FP
FAPP1-2	GGCGGTAGCGCTAGCATGGAA GGTGTCTGTGTA	AAGCTGGGTGATATCTTAGCGA GTATCGGTCAGACACG	FP-FAPP1

tagged proteins; for co-expression of BiFC constructs, two *A. tumefaciens* cultures with OD₆₀₀ of 0.2 respectively, were equally mixed together to reach the final OD₆₀₀ at 0.1. All infiltrated *A. tumefaciens* cells were suspended in MES buffer (10 mM MgCl₂, 10mM MES PH5.7, and 100uM acetosyringone). *N. benthamiana* leaves were imaged at 3 days post infiltration. *A. thaliana* mesophyll protoplasts were extracted from 4-week-old seedlings, and 10 µg of plasmid DNA were used for each transformation which was performed same as described (Yoo et al., 2007). Following transformation, protoplasts were suspended overnight in W5 buffer at 25°C before observation.

Live-cell imaging by confocal microscopy and image analysis

FM 4-64 (Thermoscientificbio) staining employed a concentration of 10 µM, and was performed as previously described (Günl et al., 2011). All microscopy images were obtained using a ZEISS LSM 780 NLO confocal microscope system equipped with a 458-nm argon laser for CFP (emission wavelength 560-509 nm), a 514-nm argon laser for YFP/Venus (emission wavelength 518-553 nm), and a 561-nm Diode Pumped Solid State (DPSS) laser for tagRFP and FM4-64 (emission wavelength 562-640 nm). For time-lapse imaging, 100 consecutive frames without time intervals (combined speed of about 0.78 fps) were acquired sequentially. The kymograph plots were generated using ImageJ (Version 1.51n, NIH) and the plug-in “KymographBuilder” with a 30 µm segmented line for this measurement. The spectral imaging and linear unmixing were conducted using 32 channel spectral array GaAsP detectors in a Lambda model. The width of fluorescence spectra was chosen from 460~640 at a resolution of 3 nm. All microscopy images were processed using the Zeiss ZEN2 (Blue edition) program.

Supplementary Figures

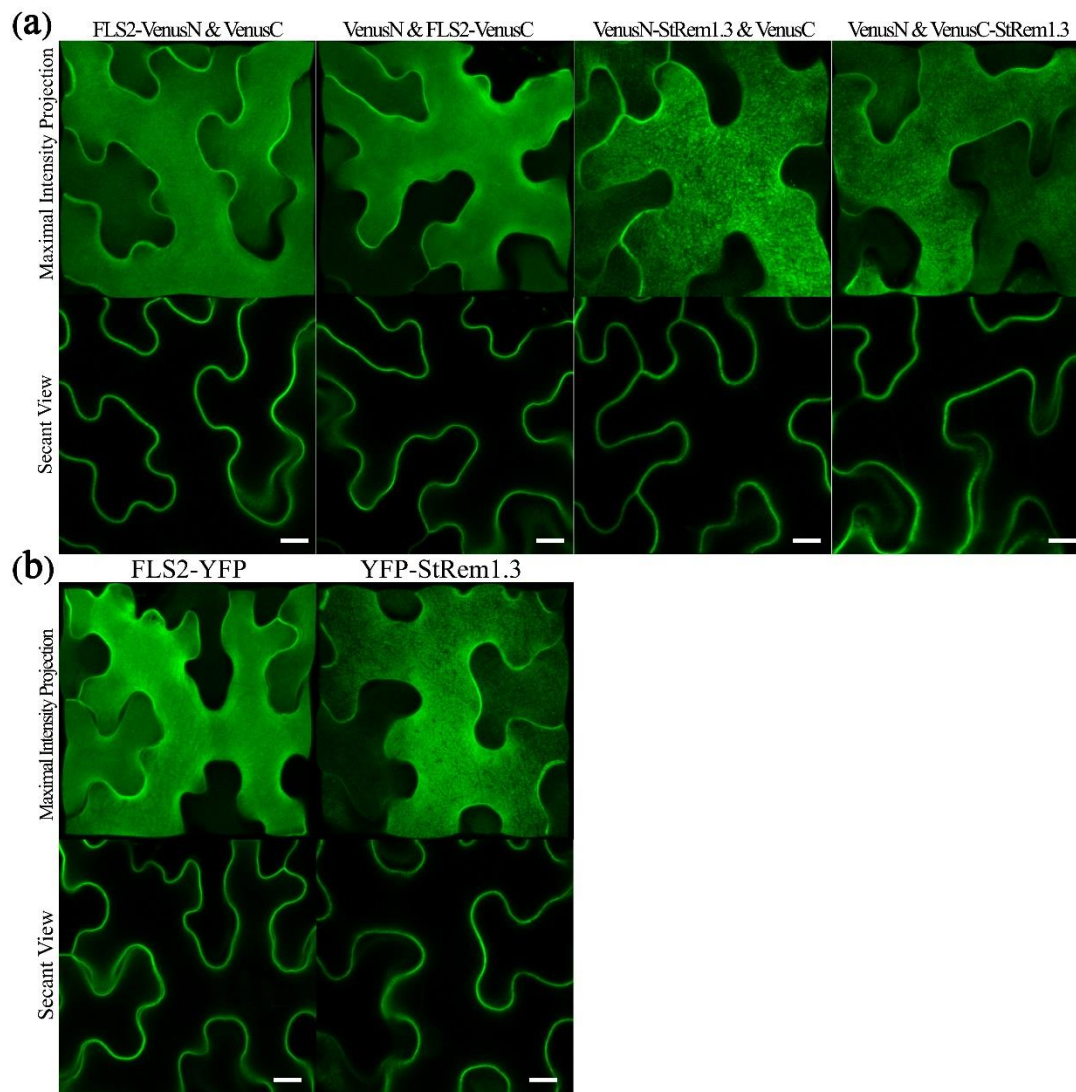


Figure S2.1. Efficiently spontaneous reassembly of the two fragments of Venus into BiFC complexes with membrane proteins in *N. benthamiana* leaf cortical cells.

(a) PM-localized FLS2 and StRem1.3 BiFC complexes formed with free Venus fragments (b) FLS2 and StRem1.3 individually fused with full-length YFP and expressed in *N. benthamiana* cells. Scale bars represent 10 μm .

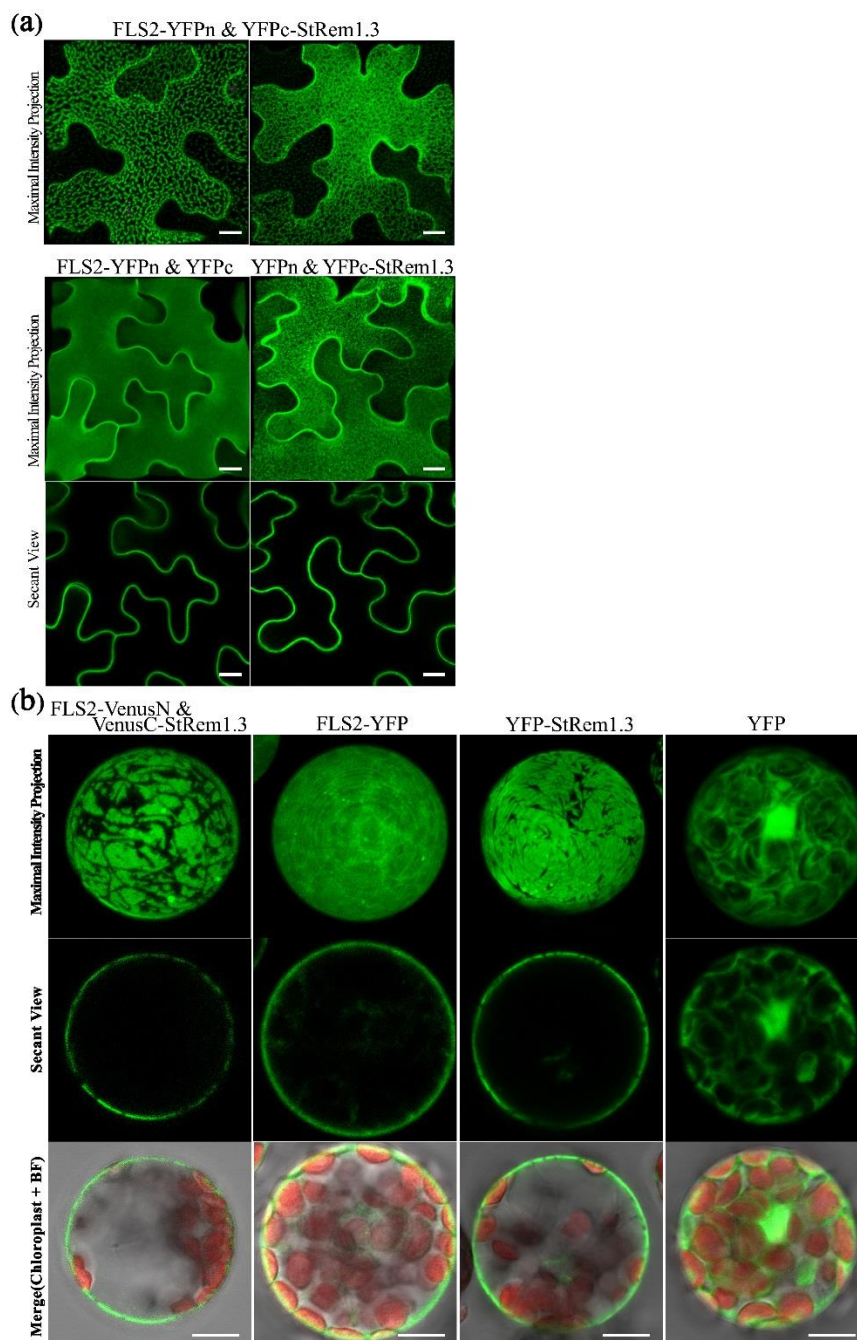


Figure S2.2 Heterogeneous distribution patterns observed for BiFC complexes produced in *N. benthamiana* leaf cortical cells or *Arabidopsis* mesophyll protoplasts.

(a) Co-expression of FLS2-YFPn and YFPc-StRem1.3 produced a heterogeneous distribution of the BiFC signal to that for Venus BiFC shown in Figure 1A. (b) PM-localized FLS2 and StRem1.3 BiFC complexes formed with free YFP fragments (c) Transiently expressed in *Arabidopsis* mesophyll protoplasts, FLS2-StRem1.3 BiFC complexes exhibited heterogeneous discrete patches, different from either plasma membrane-localized FLS2-YFP or YFP-StRem1.3, or cytoplasm-localized YFP. Red fluorescence represents chloroplast autofluorescence. Scale bars represent 10 μm .

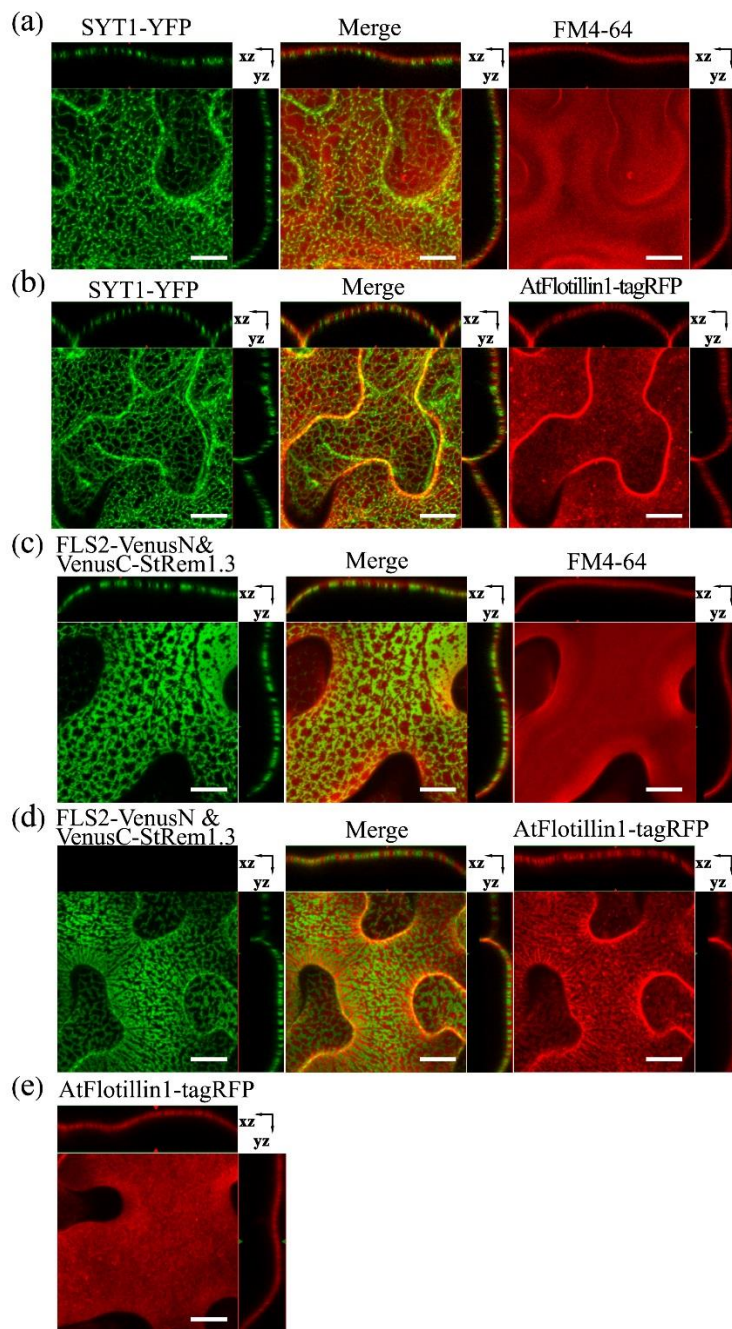


Figure S2.3 Orthogonal imaging of SYT1 and FLS2-StRem1.3 BiFC complexes in *N. benthamiana* leaf cortical cells.

(a) The *Arabidopsis* tethering protein SYT1 tightly associates with the plasma membrane visualized by FM4-64. (b) Regions of the plasma membrane associated with SYT1 show reduced presence of membrane protein AtFlotillin1 fused to tagRFP. (c) FLS2-StRem1.3 BiFC complexes also tightly associate with the plasma membrane, visualized by FM4-64. (d) Regions of the plasma membrane associated with FLS2-StRem1.3 BiFC complexes show reduced presence of AtFlotillin1-tagRFP. Scale bars represent 10 μ m.

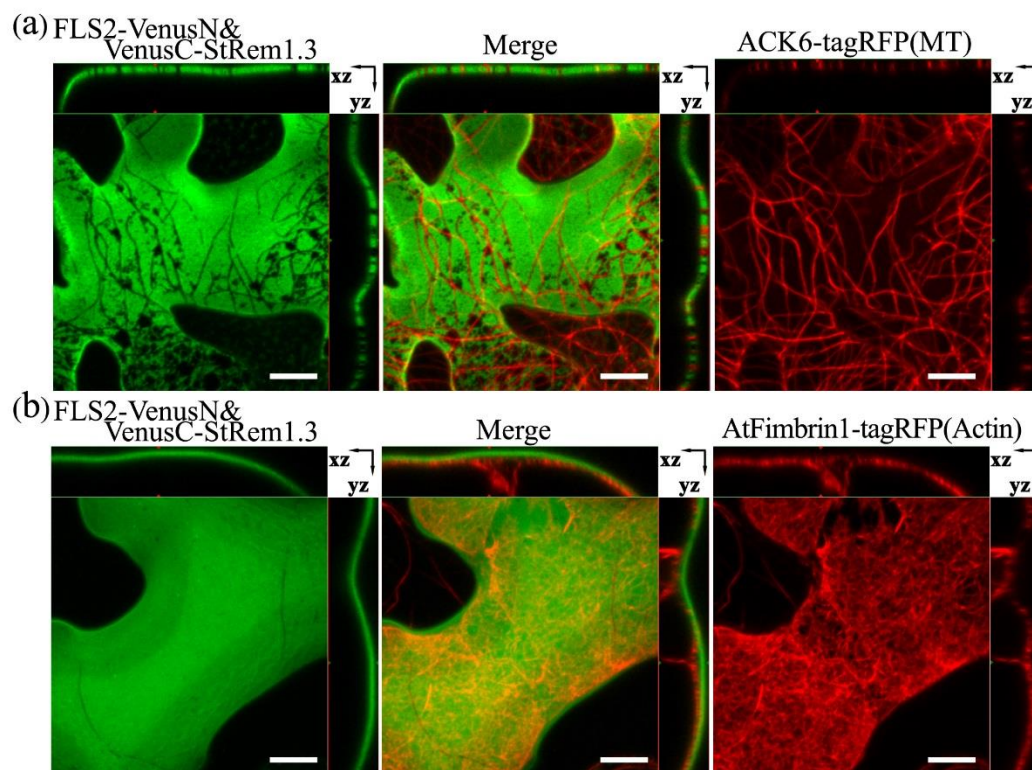


Figure S2.4 Orthogonal imaging of FLS2-StRem1.3 BiFC complexes relative to the cytoskeleton of *N. benthamiana* leaf cortical cells.

(a) Cortical microtubules labeled by *Arabidopsis* Casein Kinase 1-Like 6 (ACK6) fused with tagRFP imaged relative to filament-like structures negatively-stained by near-confluent sheets of FLS2-StRem1.3 BiFC complexes. (b) Actin filaments labeled by *Arabidopsis* actin-binding protein AtFimbrin1 fused with tagRFP imaged relative to confluent sheets of FLS2-StRem1.3 BiFC complexes. Scale bars represent 10 μm .

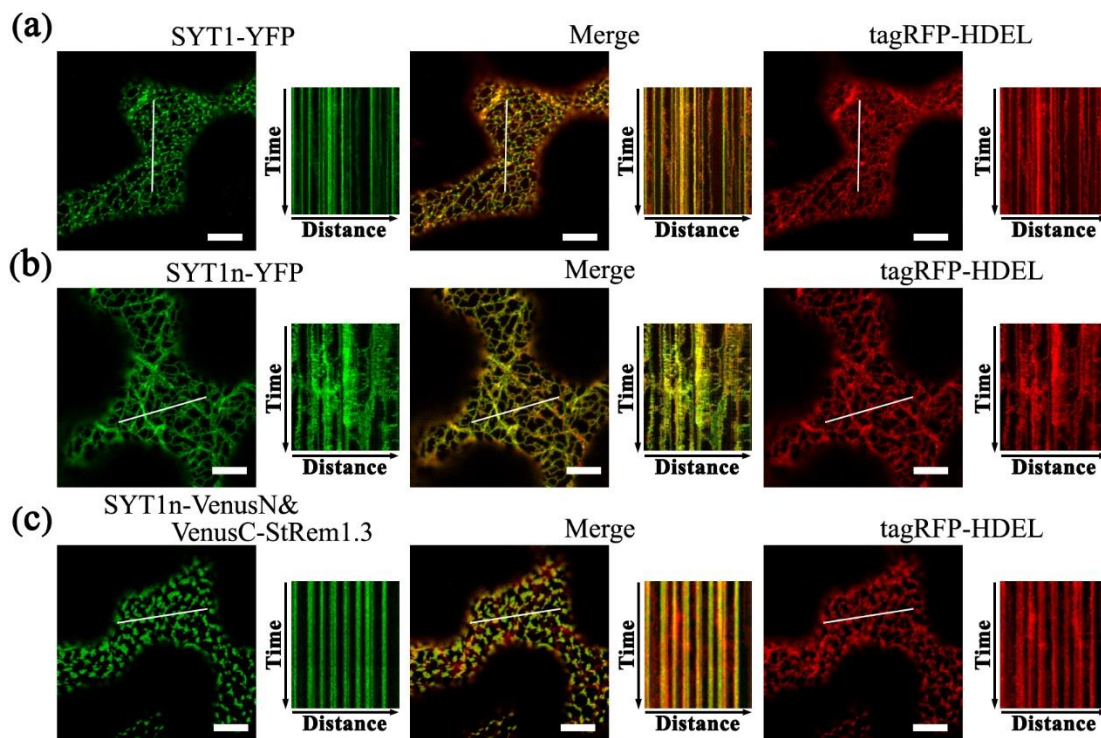


Figure S2.5 Distribution and kymograph analysis of SYT1, SYT1n and SYT1-StRem1.3 BiFC complexes co-expressed with ER marker tagRFP-HDEL in *N. benthamiana* leaf cortical cells.

(a) SYT1-YFP co-expressed with tagRFP-HDEL. Arrowheads highlight bright puncta corresponding to ER-PM contact sites that stabilize the dynamic ER. (b) SYT1n-YFP co-expressed with tagRFP-HDEL, showing coordinated dynamic mobility. (c) FLS2-StRem1.3 BiFC complexes were co-expressed with tagRFP-HDEL showing stabilization of dynamic mobility. Kymographs produced as in Figure 1. Scale bars represent 10 μm .

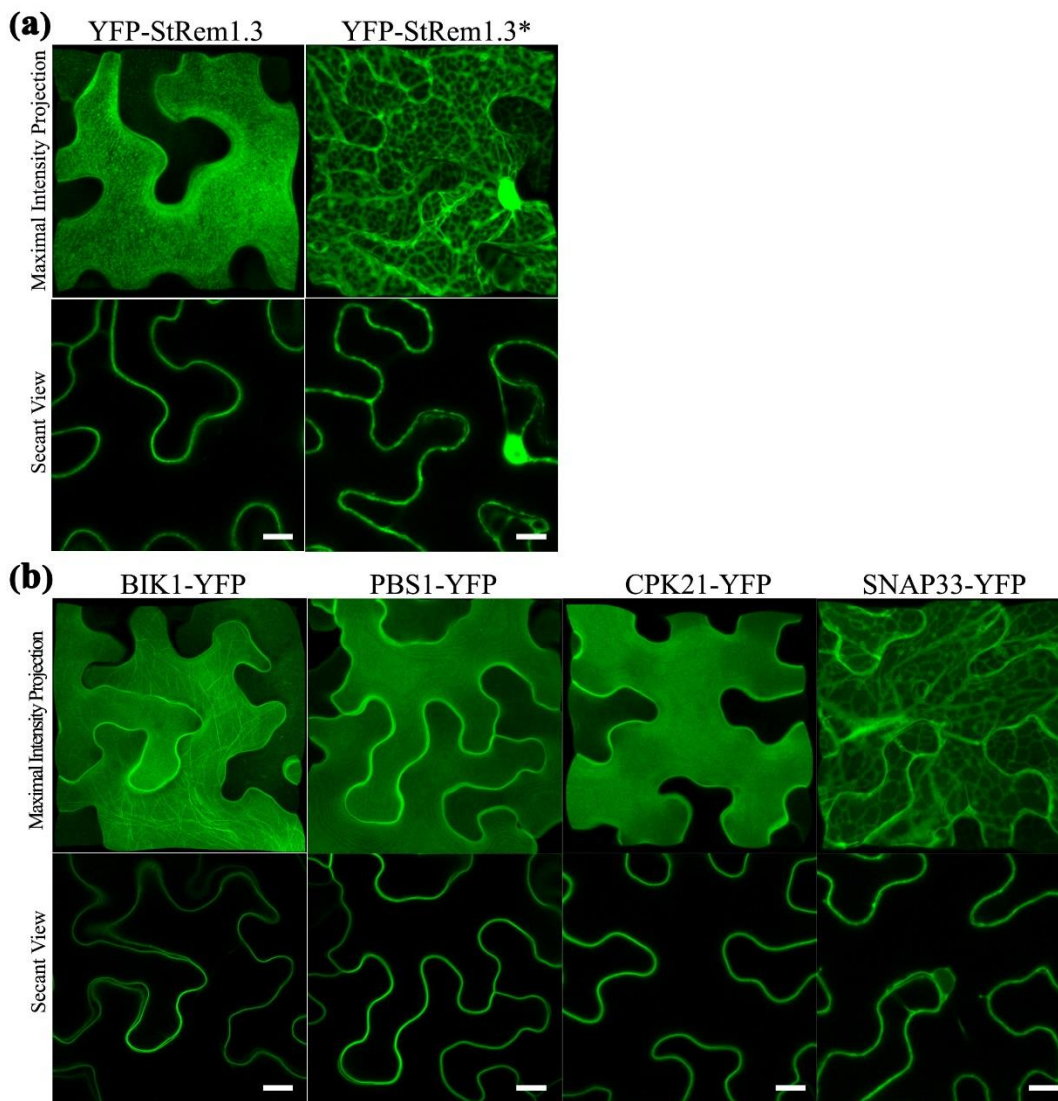


Figure S2.6 Distribution of peripheral membrane proteins fused to YFP in *N. benthamiana* leaf cortical cells.

(a) YFP-StRem1.3 wild type and YFP-StRem1.3* mutant with PM-targeting residues altered by site-directed mutagenesis. (b) Peripheral membrane proteins BIK1, PBS1, CPK21 and SNAP33 fused with YFP. Scale bars represent 10 μm .

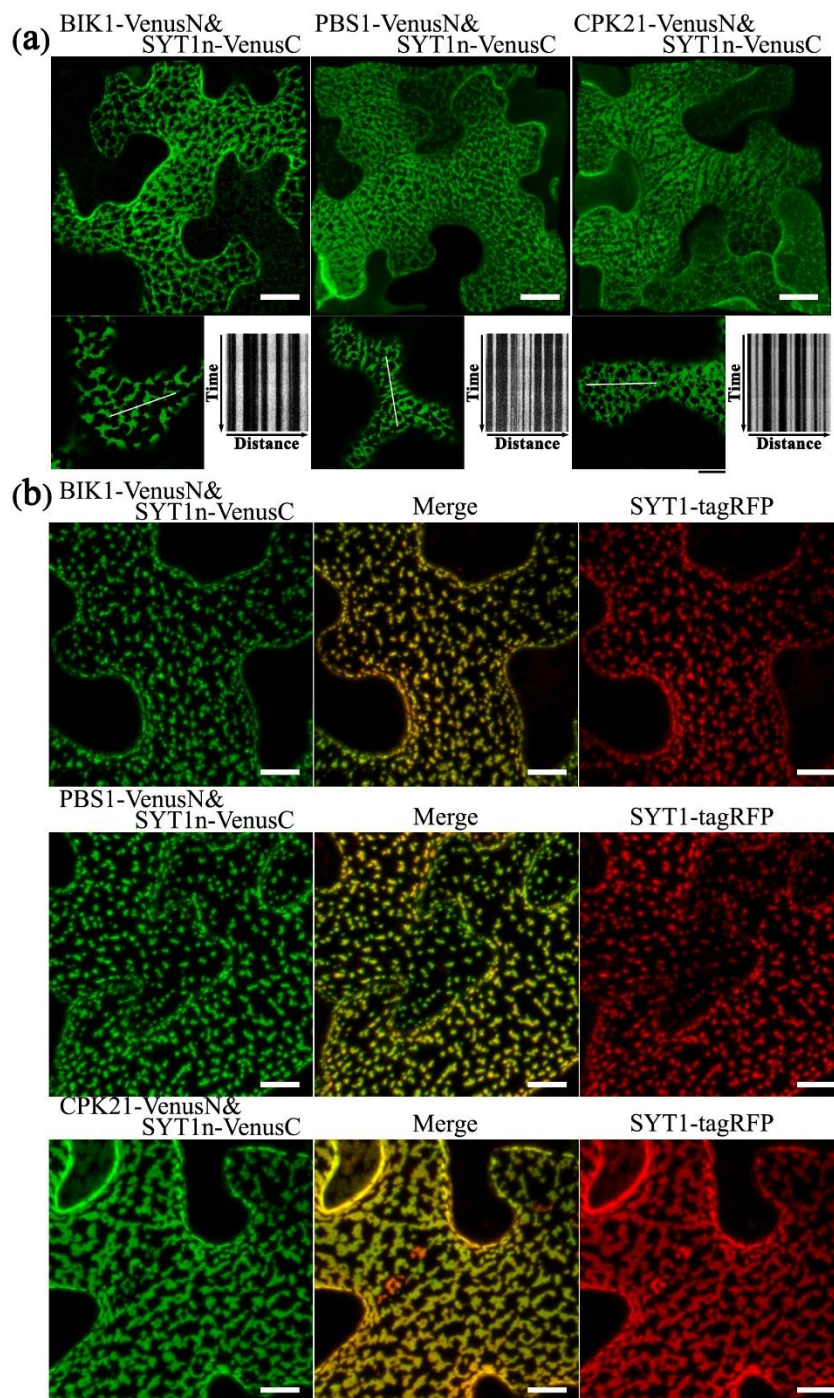


Figure S2.7 Co-expression of peripheral membrane proteins and SYTn in BiFC complexes in *N. benthamiana* leaf cortical cells results in ER-PM tethering.

(a) Distribution and kymograph analysis of BiFC complexes produced by SYT1n-VenusC co-expressed with BIK1-VenusN, PBS1-VenusN, or CPK21-VenusN. (b) Puncta observed in BiFC complexes produced by BIK1 & SYT1n, PBS1 & SYT1n and CPK21 & SYT1n were co-localized with wild type SYT1-tagRFP. Scale bars represent 10 μ m.

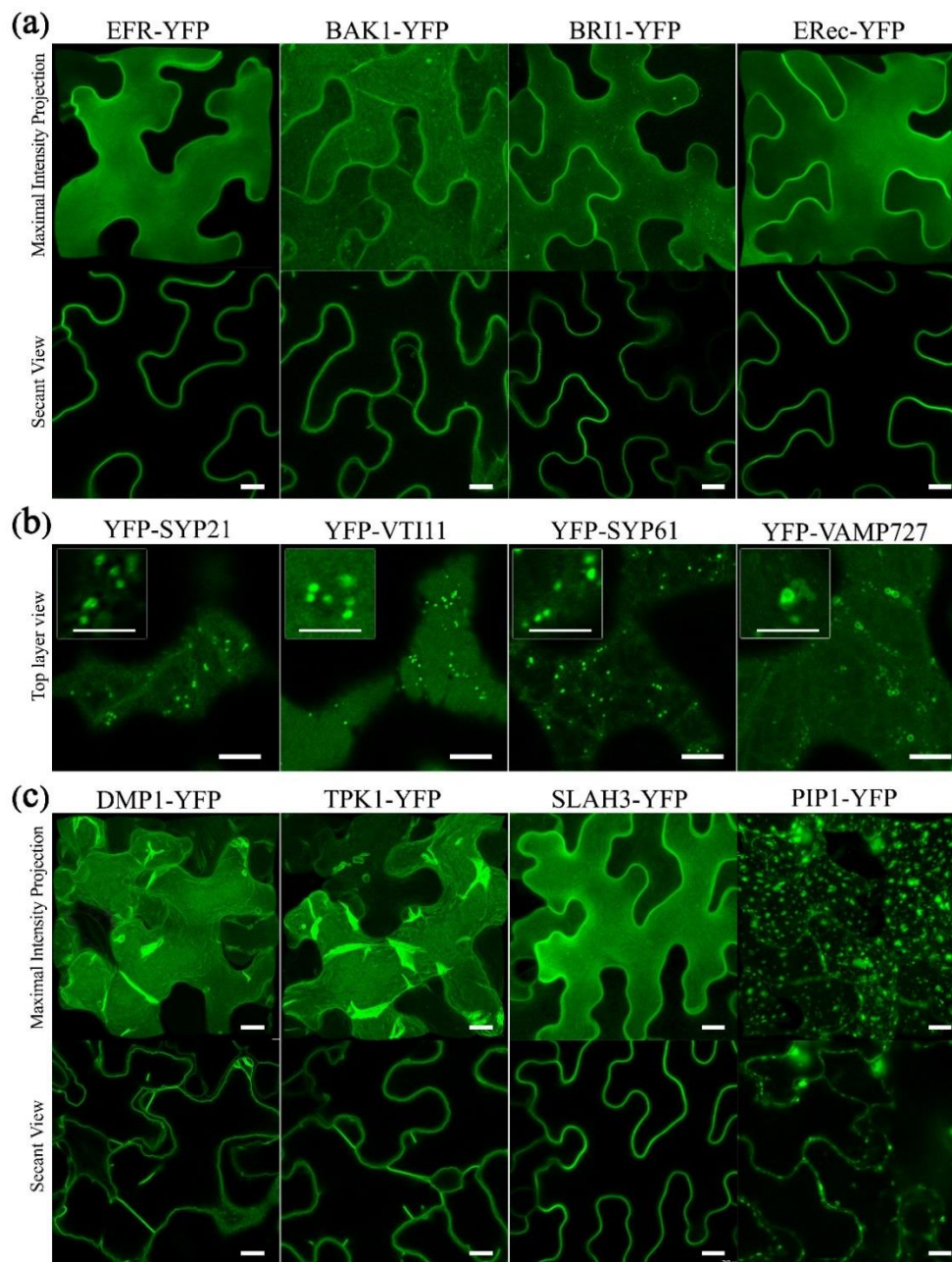


Figure S2.8 Membrane distributions of integral membrane proteins fused to YFP and transiently expressed in *N. benthamiana* leaf cortical cells.

(a) Subcellular localization of PM IMPs with a cleavable N-terminal signal peptide and single-pass TMD. (b) Subcellular localization of tail-anchored SNARE proteins. Qa-SNARE SYP21 and R-SNARE VAMP727 are localized to endosomal vesicles; Qb-SNARE VTI11 and Qc-SNARE SYP61 are localized to the Golgi. (c) Subcellular localization of IMPs with multi-pass TMDs. DMP1 and TPK1 are localized to the vacuolar membrane (tonoplast); SLAH3 is localized on the PM; PIP1 is localized on endosomal membranes. Thick and thin white scale bars respectively represent 10 μm and 5 μm.

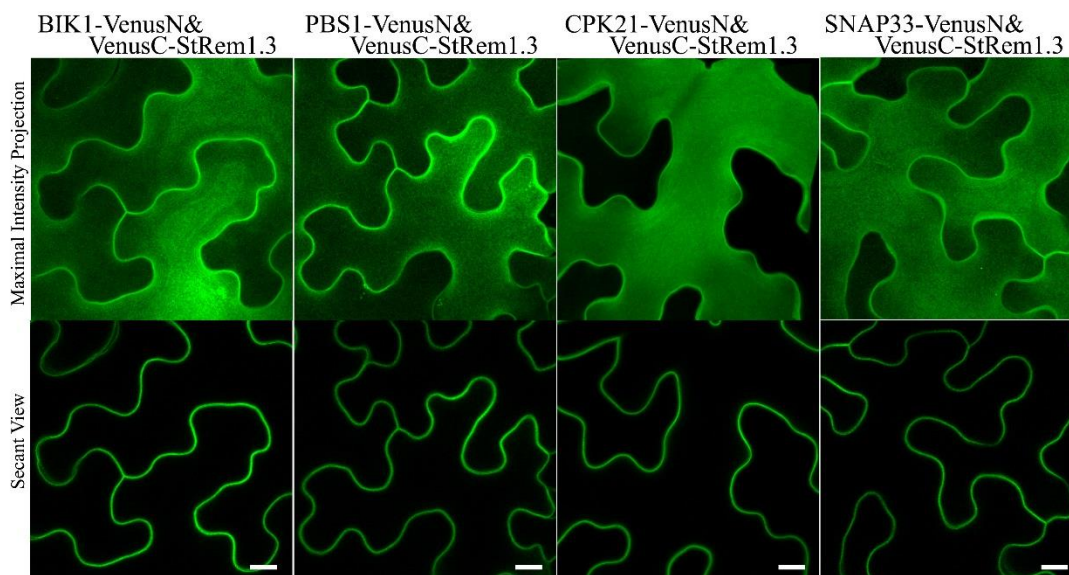


Figure S2.9 Co-expression of peripheral membrane proteins and StRem1.3 in *N. benthamiana* leaf cortical cells does not result in ER-PM tethering by BiFC complexes. Scale bars represent 10 μm.

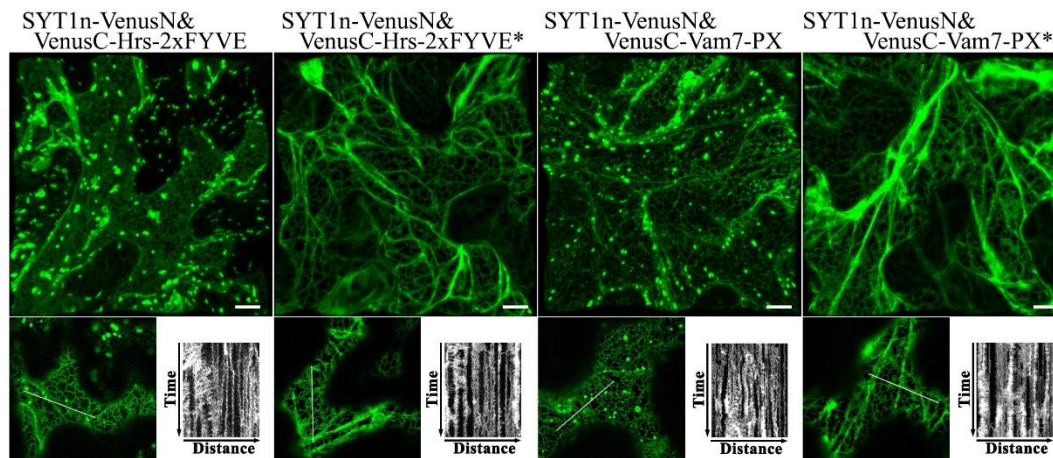


Figure S2.10 Co-expression of PtdIns(3)P binding proteins with the SYT1 N-terminal domain in BiFC complexes in *N. benthamiana* leaf cortical cells does not result in ER-PM tethering.

Hrs-2xFYVE, and Vam7P-PX proteins are PtdIns(3)P binding proteins while Hrs-2xFYVE* and Vam7-PX* are PtdIns(3)P-non-binding mutants. Kymographs produced as in Figure 1. Scale bars represent 10 μm .

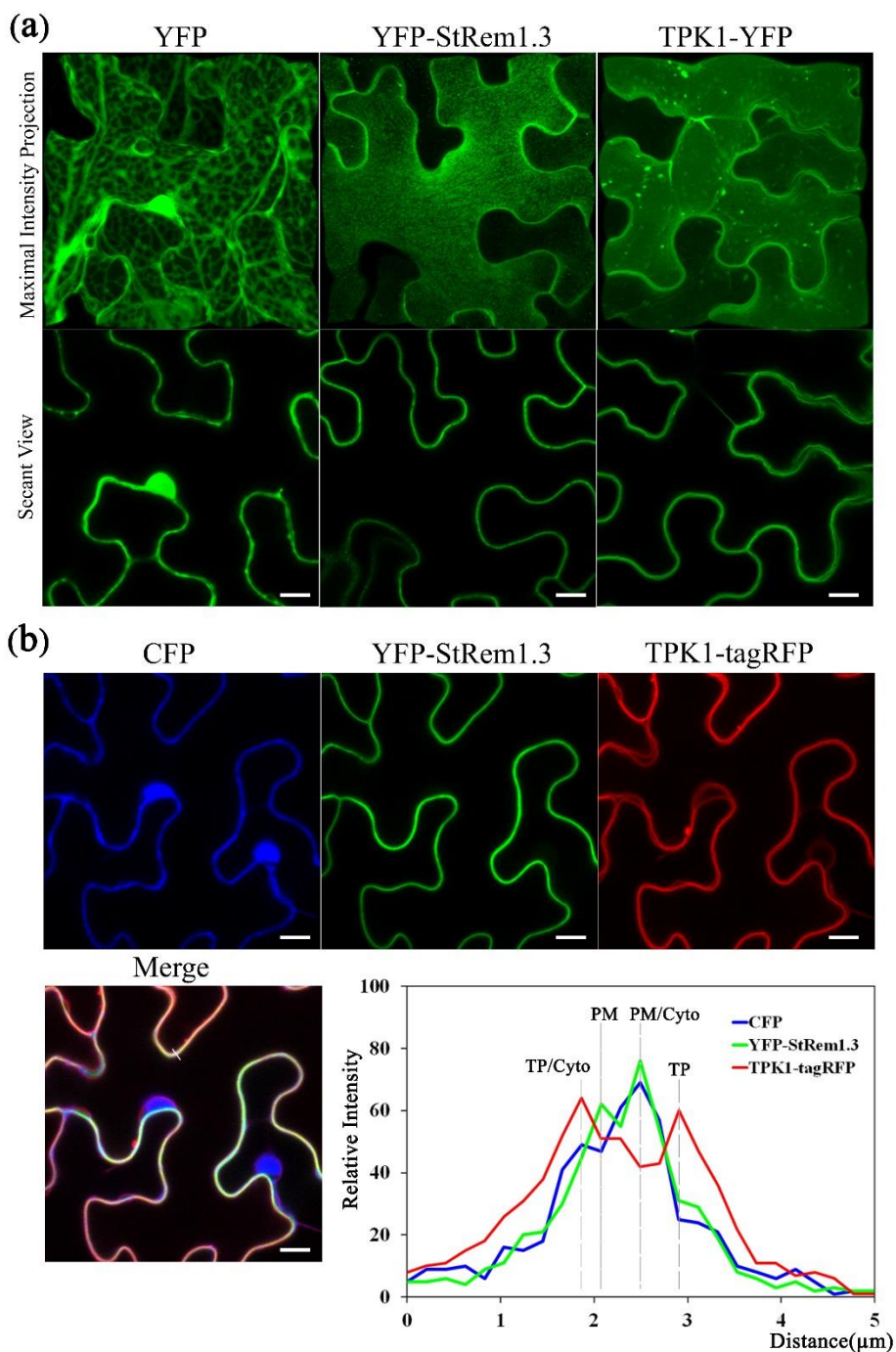


Figure S2.11 Subcellular localization of cytoplasm, PM, and tonoplast in *N. benthamiana* leaf cortical cells.

(a) Confocal images of free full-length YFP, YFP-tagged PM-associated protein StRem1.3 and tonoplast-localized protein TPK1. **(b)** Co-localization assay of CFP, YFP-StRem1.3, TPK-tagRFP when co-expressed together. The fluorescence intensity profiles in the bottom panel show relative fluorescence levels along the transect marked in white in the merged image panel. Scale bars represent 10 μm .

Bibliography

Arrighi, J.-F., Barre, A., Ben Amor, B., Bersoult, A., Soriano, L.C., Mirabella, R., de Carvalho-Niebel, F., Journet, E.-P., Ghérardi, M., Huguet, T., Geurts, R., Dénarié, J., Rougé, P. and Gough, C. (2006) The *Medicago truncatula* Lysine Motif-Receptor-Like Kinase Gene Family Includes *NFP* and New Nodule-Expressed Genes. *Plant Physiology*, **142**, 265-279.

Asai, S., Ichikawa, T., Nomura, H., Kobayashi, M., Kamiyoshihara, Y., Mori, H., Kadota, Y., Zipfel, C., Jones, J.D.G. and Yoshioka, H. (2013) The Variable Domain of a Plant Calcium-dependent Protein Kinase (CDPK) Confers Subcellular Localization and Substrate Recognition for NADPH Oxidase. *Journal of Biological Chemistry*, **288**, 14332-14340.

Bemis, S.M., Lee, J.S., Shpak, E.D. and Torii, K.U. (2013) Regulation of floral patterning and organ identity by Arabidopsis ERECTA-family receptor kinase genes. *Journal of Experimental Botany*, **64**, 5323-5333.

Ben-Nissan, G., Cui, W., Kim, D.-J., Yang, Y., Yoo, B.-C. and Lee, J.-Y. (2008) Arabidopsis Casein Kinase 1-Like 6 Contains a Microtubule-Binding Domain and Affects the Organization of Cortical Microtubules. *Plant Physiology*, **148**, 1897-1907.

Borner, G.H.H., Sherrier, D.J., Weimar, T., Michaelson, L.V., Hawkins, N.D., MacAskill, A., Napier, J.A., Beale, M.H., Lilley, K.S. and Dupree, P. (2005) Analysis of Detergent-Resistant Membranes in Arabidopsis. Evidence for Plasma Membrane Lipid Rafts. *Plant Physiology*, **137**, 104-116.

Boruc, J., Van den Daele, H., Hollunder, J., Rombauts, S., Mylle, E., Hilson, P., Inzé, D., De Veylder, L. and Russinova, E. (2010) Functional Modules in the Arabidopsis Core Cell Cycle Binary Protein-Protein Interaction Network. *The Plant Cell*, **22**, 1264-1280.

Boulaflous, A., Saint-Jore-Dupas, C., Herranz-Gordo, M.-C., Pagny-Salehabadi, S., Plasson, C., Garidou, F., Kiefer-Meyer, M.-C., Ritzenthaler, C., Faye, L. and Gomord, V. (2009) Cytosolic N-terminal arginine-based signals together with a luminal signal target a type II membrane protein to the plant ER. *BMC Plant Biology*, **9**, 144.

- Bozkurt, T.O., Belhaj, K., Dagdas, Y.F., Chaparro-Garcia, A., Wu, C.-H., Cano, L.M. and Kamoun, S.** (2015) Rerouting of Plant Late Endocytic Trafficking Toward a Pathogen Interface. *Traffic*, **16**, 204-226.
- Bücherl, C.A., Jarsch, I.K., Schudoma, C., Segonzac, C., Mbengue, M., Robatzek, S., MacLean, D., Ott, T. and Zipfel, C.** (2017) Plant immune and growth receptors share common signalling components but localise to distinct plasma membrane nanodomains. *eLife*, **6**, e25114.
- Burgoyne, T., Patel, S. and Eden, E.R.** (2015) Calcium signaling at ER membrane contact sites. *Biochimica et Biophysica Acta (BBA) - Molecular Cell Research*, **1853**, 2012-2017.
- Carrasco, S. and Meyer, T.** (2011) STIM Proteins and the Endoplasmic Reticulum-Plasma Membrane Junctions. *Annual review of biochemistry*, **80**, 973-1000.
- Chang, C.-L., Hsieh, T.-S., Yang, T.T., Rothberg, Karen G., Azizoglu, D.B., Volk, E., Liao, J.-C. and Liou, J.** (2013) Feedback Regulation of Receptor-Induced Ca²⁺ Signaling Mediated by E-Syt1 and Nir2 at Endoplasmic Reticulum-Plasma Membrane Junctions. *Cell Reports*, **5**, 813-825.
- Cheever, M.L., Sato, T.K., de Beer, T., Kutateladze, T.G., Emr, S.D. and Overduin, M.** (2001) Phox domain interaction with PtdIns(3)P targets the Vam7 t-SNARE to vacuole membranes. *Nature Cell Biology*, **3**, 613.
- Chinchilla, D., Boller, T. and Robatzek, S.** (2007) Flagellin signalling in plant immunity. *Advances in experimental medicine and biology*, **598**.
- Delage, E., Ruelland, E., Guillas, I., Zachowski, A. and Puyaubert, J.** (2012) Arabidopsis Type-III Phosphatidylinositol 4-Kinases β 1 and β 2 are Upstream of the Phospholipase C Pathway Triggered by Cold Exposure. *Plant and Cell Physiology*, **53**, 565-576.
- Demir, F., Horntrich, C., Blachutzik, J.O., Scherzer, S., Reinders, Y., Kierszniowska, S., Schulze, W.X., Harms, G.S., Hedrich, R., Geiger, D. and Kreuzer, I.** (2013) Arabidopsis nanodomain-delimited ABA signaling pathway regulates the anion channel SLAH3. *Proceedings of the National Academy of Sciences*, **110**, 8296-8301.

- Dou, D., Kale, S.D., Wang, X., Jiang, R.H., Bruce, N.A., Arredondo, F.D., Zhang, X. and Tyler, B.M.** (2008) RXLR-mediated entry of *Phytophthora sojae* effector Avr1b into soybean cells does not require pathogen-encoded machinery. *The Plant cell*, **20**, 1930-1947.
- Dowler, S., Currie, R.A., Campbell, D.G., Deak, M., Kular, G., Downes, C.P. and Alessi, D.R.** (2000) Identification of pleckstrin-homology-domain-containing proteins with novel phosphoinositide-binding specificities. *Biochem J*, **351**, 19-31.
- Foresti, O., daSilva, L.L.P. and Denecke, J.** (2006) Overexpression of the Arabidopsis Syntaxin PEP12/SYP21 Inhibits Transport from the Prevacuolar Compartment to the Lytic Vacuole in Vivo. *The Plant Cell*, **18**, 2275-2293.
- Goder, V. and Spiess, M.** (2001) Topogenesis of membrane proteins: determinants and dynamics. *FEBS Letters*, **504**, 87-93.
- Gómez-Gómez, L. and Boller, T.** (2000) FLS2: An LRR Receptor-like Kinase Involved in the Perception of the Bacterial Elicitor Flagellin in Arabidopsis. *Molecular Cell*, **5**, 1003-1011.
- Gookin, T.E. and Assmann, S.M.** (2014) Significant reduction of BiFC non-specific assembly facilitates in planta assessment of heterotrimeric G-protein interactors. *The Plant Journal*, **80**, 553-567.
- Günl, M., Neumetzler, L., Kraemer, F., de Souza, A., Schultink, A., Pena, M., York, W.S. and Pauly, M.** (2011) AXY8 Encodes an α -Fucosidase, Underscoring the Importance of Apoplastic Metabolism on the Fine Structure of *Arabidopsis* Cell Wall Polysaccharides. *The Plant Cell*, **23**, 4025-4040.
- Haas, B., Kamoun, S., Zody, M., Jiang, R., Handsaker, R., Cano, L., Grabherr, M., Kodira, C., Raffaele, S. and Torto-Alalibo, T.** (2009) Genome sequence and analysis of the Irish potato famine pathogen *Phytophthora infestans*. *Nature*, **461**, 393 - 398.
- Hachez, C., Laloux, T., Reinhardt, H., Cavez, D., Degand, H., Grefen, C., De Rycke, R., Inzé, D., Blatt, M.R., Russinova, E. and Chaumont, F.** (2014) Arabidopsis SNAREs SYP61 and SYP121 Coordinate the Trafficking of Plasma Membrane Aquaporin PIP2;7 to Modulate the Cell Membrane Water Permeability. *The Plant Cell*, **26**, 3132-3147.

- Hammond, G.R.V., Fischer, M.J., Anderson, K.E., Holdich, J., Koteci, A., Balla, T. and Irvine, R.F.** (2012) PI4P and PI(4,5)P2 Are Essential But Independent Lipid Determinants of Membrane Identity. *Science*, **337**, 727-730.
- Hayakawa, A., Hayes, S.J., Lawe, D.C., Sudharshan, E., Tuft, R., Fogarty, K., Lambright, D. and Corvera, S.** (2004) Structural basis for endosomal targeting by FYVE domains. *J Biol Chem*, **279**, 5958-5966.
- He, J., Scott, J.L., Heroux, A., Roy, S., Lenoir, M., Overduin, M., Stahelin, R.V. and Kutateladze, T.G.** (2011) Molecular Basis of Phosphatidylinositol 4-Phosphate and ARF1 GTPase Recognition by the FAPP1 Pleckstrin Homology (PH) Domain. *Journal of Biological Chemistry*, **286**, 18650-18657.
- He, Y., Zhou, J., Shan, L. and Meng, X.** (2018) Plant cell surface receptor-mediated signaling - a common theme amid diversity. *J Cell Sci*, **131**.
- Heese, A., Hann, D.R., Gimenez-Ibanez, S., Jones, A.M.E., He, K., Li, J., Schroeder, J.I., Peck, S.C. and Rathjen, J.P.** (2007) The receptor-like kinase SERK3/BAK1 is a central regulator of innate immunity in plants. *Proceedings of the National Academy of Sciences*, **104**, 12217-12222.
- Hegde, R.S. and Keenan, R.J.** (2011) Tail-anchored membrane protein insertion into the endoplasmic reticulum. *Nature reviews. Molecular cell biology*, **12**, 787-798.
- Helle, S.C.J., Kanfer, G., Kolar, K., Lang, A., Michel, A.H. and Kornmann, B.** (2013) Organization and function of membrane contact sites. *Biochimica et Biophysica Acta (BBA) - Molecular Cell Research*, **1833**, 2526-2541.
- Henne, W.M., Liou, J. and Emr, S.D.** (2015) Molecular mechanisms of inter-organelle ER–PM contact sites. *Current Opinion in Cell Biology*, **35**, 123-130.
- Jahn, R. and Scheller, R.H.** (2006) SNAREs — engines for membrane fusion. *Nature Reviews Molecular Cell Biology*, **7**, 631.
- Jarsch, I.K., Konrad, S.S.A., Stratil, T.F., Urbanus, S.L., Szymanski, W., Braun, P., Braun, K.-H. and Ott, T.** (2014) Plasma Membranes Are Subcompartmentalized into a Plethora of Coexisting and Diverse Microdomains in Arabidopsis and Nicotiana benthamiana. *The Plant Cell Online*.
- Kale, S.D., Gu, B., Capelluto, D.G., Dou, D., Feldman, E., Rumore, A., Arredondo, F.D., Hanlon, R., Fudal, I., Rouxel, T., Lawrence, C.B., Shan, W. and Tyler, B.M.**

(2010) External lipid PI3P mediates entry of eukaryotic pathogen effectors into plant and animal host cells. *Cell*, **142**, 284-295.

Kargul, J., Gansel, X., Tyrrell, M., Sticher, L. and Blatt, M.R. (2001) Protein-binding partners of the tobacco syntaxin NtSyr1. *FEBS Letters*, **508**, 253-258.

Kasaras, A., Melzer, M. and Kunze, R. (2012) Arabidopsis senescence-associated protein DMP1 is involved in membrane remodeling of the ER and tonoplast. *BMC Plant Biology*, **12**, 54.

Kerppola, T.K. (2006) Design and implementation of bimolecular fluorescence complementation (BiFC) assays for the visualization of protein interactions in living cells. *Nature Protocols*, **1**, 1278.

Kerppola, T.K. (2008) Bimolecular Fluorescence Complementation (BiFC) Analysis as a Probe of Protein Interactions in Living Cells. *Annual Review of Biophysics*, **37**, 465-487.

Kodama, Y. and Hu, C.-D. (2012) Bimolecular fluorescence complementation (BiFC): A 5-year update and future perspectives. *BioTechniques*, **53**, 285-298.

Kodama, Y. and Hu, C.D. (2010) An improved bimolecular fluorescence complementation assay with a high signal-to-noise ratio. *BioTechniques*, **49**, 793-805.

Krogh, A., Larsson, B., von Heijne, G. and Sonnhammer, E.L.L. (2001) Predicting transmembrane protein topology with a hidden markov model: application to complete genomes¹¹ Edited by F. Cohen. *Journal of Molecular Biology*, **305**, 567-580.

Kusumi, A., Fujiwara, T.K., Chadda, R., Xie, M., Tsunoyama, T.A., Kalay, Z., Kasai, R.S. and Suzuki, K.G. (2012) Dynamic organizing principles of the plasma membrane that regulate signal transduction: commemorating the fortieth anniversary of Singer and Nicolson's fluid-mosaic model. *Annual review of cell and developmental biology*, **28**, 215-250.

Kusumi, A., Suzuki, K.G.N., Kasai, R.S., Ritchie, K. and Fujiwara, T.K. (2011) Hierarchical mesoscale domain organization of the plasma membrane. *Trends in Biochemical Sciences*, **36**, 604-615.

Lavieu, G., Orci, L., Shi, L., Geiling, M., Ravazzola, M., Wieland, F., Cosson, P. and Rothman, J.E. (2010) Induction of cortical endoplasmic reticulum by dimerization of a coatamer-binding peptide anchored to endoplasmic reticulum

membranes. *Proceedings of the National Academy of Sciences of the United States of America*, **107**, 6876-6881.

Lee, S.A., Kovacs, J., Stahelin, R.V., Cheever, M.L., Overduin, M., Setty, T.G., Burd, C.G., Cho, W. and Kutateladze, T.G. (2006) Molecular mechanism of membrane docking by the Vam7p PX domain. *J Biol Chem*, **281**, 37091-37101.

Lefebvre, B., Timmers, T., Mbengue, M., Moreau, S., Hervé, C., Tóth, K., Bittencourt-Silvestre, J., Klaus, D., Deslandes, L., Godiard, L., Murray, J.D., Udvardi, M.K., Raffaele, S., Mongrand, S., Cullimore, J., Gamas, P., Niebel, A. and Ott, T. (2010) A remorin protein interacts with symbiotic receptors and regulates bacterial infection. *Proceedings of the National Academy of Sciences*, **107**, 2343-2348.

Lemmon, M.A. (2008) Membrane recognition by phospholipid-binding domains. *Nat Rev Mol Cell Biol*, **9**, 99-111.

Lillemeier, B.F. and Klammt, C. (2012) How membrane structures control T cell signaling. *Frontiers in Immunology*, **3**.

Limpens, E., Mirabella, R., Fedorova, E., Franken, C., Franssen, H., Bisseling, T. and Geurts, R. (2005) Formation of organelle-like N₂-fixing symbiosomes in legume root nodules is controlled by *DMI2*. *Proceedings of the National Academy of Sciences of the United States of America*, **102**, 10375-10380.

Lu, D., Wu, S., Gao, X., Zhang, Y., Shan, L. and He, P. (2010) A receptor-like cytoplasmic kinase, BIK1, associates with a flagellin receptor complex to initiate plant innate immunity. *Proceedings of the National Academy of Sciences*, **107**, 496-501.

Lu, S., Chen, L., Tao, K., Sun, N., Wu, Y., Lu, X., Wang, Y. and Dou, D. Intracellular and Extracellular Phosphatidylinositol 3-Phosphate Produced by *Phytophthora* Species Is Important for Infection. *Molecular Plant*, **6**, 1592-1604.

Madsen, E.B., Madsen, L.H., Radutoiu, S., Olbryt, M., Rakwalska, M., Szczyglowski, K., Sato, S., Kaneko, T., Tabata, S., Sandal, N. and Stougaard, J. (2003) A receptor kinase gene of the LysM type is involved in legume perception of rhizobial signals. *Nature*, **425**, 637.

Maîtrejean, M., Wudick, M.M., Voelker, C., Prinsi, B., Mueller-Roeber, B., Czempinski, K., Pedrazzini, E. and Vitale, A. (2011) Assembly and Sorting of the

Tonoplast Potassium Channel AtTPK1 and Its Turnover by Internalization into the Vacuole. *Plant Physiology*, **156**, 1783-1796.

Meng, X., Chen, X., Mang, H., Liu, C., Yu, X., Gao, X., Torii, K.U., He, P. and Shan, L. (2015) Differential function of Arabidopsis SERK family receptor-like kinases in stomatal patterning. *Current biology : CB*, **25**, 2361-2372.

Miller, K.E., Kim, Y., Huh, W.-K. and Park, H.-O. (2015) Bimolecular fluorescence complementation (BiFC) analysis: advances and recent applications for genome-wide interaction studies. *Journal of molecular biology*, **427**, 2039-2055.

Niihama, M., Uemura, T., Saito, C., Nakano, A., Sato, M.H., Tasaka, M. and Morita, M.T. (2005) Conversion of Functional Specificity in Qb-SNARE VTI1 Homologues of Arabidopsis. *Current Biology*, **15**, 555-560.

Omasits, U., Ahrens, C.H., Müller, S. and Wollscheid, B. (2014) Protter: interactive protein feature visualization and integration with experimental proteomic data. *Bioinformatics*, **30**, 884-886.

Pérez-Sancho, J., Vanneste, S., Lee, E., McFarlane, H.E., Esteban del Valle, A., Valpuesta, V., Friml, J., Botella, M.A. and Rosado, A. (2015) The Arabidopsis Synaptotagmin1 Is Enriched in Endoplasmic Reticulum-Plasma Membrane Contact Sites and Confers Cellular Resistance to Mechanical Stresses. *Plant Physiology*, **168**, 132-143.

Perraki, A., Cacas, J.L., Crowet, J.M., Lins, L., Castroviejo, M., German-Retana, S., Mongrand, S. and Raffaele, S. (2012) Plasma membrane localization of Solanum tuberosum remorin from group 1, homolog 3 is mediated by conformational changes in a novel C-terminal anchor and required for the restriction of potato virus X movement]. *Plant Physiol*, **160**, 624-637.

Poteser, M., Leitinger, G., Pritz, E., Platzer, D., Frischauf, I., Romanin, C. and Groschner, K. (2016) Live-cell imaging of ER-PM contact architecture by a novel TIRFM approach reveals extension of junctions in response to store-operated Ca²⁺-entry. **6**, 35656.

Prinz, W.A. (2014) Bridging the gap: Membrane contact sites in signaling, metabolism, and organelle dynamics. *The Journal of Cell Biology*, **205**, 759-769.

- Pu, M., Orr, A., Redfield, A.G. and Roberts, M.F.** (2010) Defining Specific Lipid Binding Sites for a Peripheral Membrane Protein in Situ Using Subtesla Field-cycling NMR. *Journal of Biological Chemistry*, **285**, 26916-26922.
- Qi, D., Dubiella, U., Kim, S.H., Sloss, D.I., Downen, R.H., Dixon, J.E. and Innes, R.W.** (2014) Recognition of the Protein Kinase AVRPPHB SUSCEPTIBLE1 by the Disease Resistance Protein RESISTANCE TO PSEUDOMONAS SYRINGAE5 Is Dependent on S-Acylation and an Exposed Loop in AVRPPHB SUSCEPTIBLE1. *Plant Physiology*, **164**, 340-351.
- Radutoiu, S., Madsen, L.H., Madsen, E.B., Felle, H.H., Umehara, Y., Grønlund, M., Sato, S., Nakamura, Y., Tabata, S., Sandal, N. and Stougaard, J.** (2003) Plant recognition of symbiotic bacteria requires two LysM receptor-like kinases. *Nature*, **425**, 585.
- Raffaele, S., Bayer, E., Lafarge, D., Cluzet, S., German Retana, S., Boubekeur, T., Leborgne-Castel, N., Carde, J.P., Lherminier, J., Noirot, E., Satiat-Jeunemaitre, B., Laroche-Traineau, J., Moreau, P., Ott, T., Maule, A.J., Reymond, P., Simon-Plas, F., Farmer, E.E., Bessoule, J.J. and Mongrand, S.** (2009) Remorin, a solanaceae protein resident in membrane rafts and plasmodesmata, impairs potato virus X movement. *The Plant cell*, **21**, 1541-1555.
- Rapoport, T.A.** (2007) Protein translocation across the eukaryotic endoplasmic reticulum and bacterial plasma membranes. *Nature*, **450**, 663.
- Remy, I. and Michnick, S.W.** (2004) Regulation of apoptosis by the Ft1 protein, a new modulator of protein kinase B/Akt. *Mol Cell Biol*, **24**, 1493-1504.
- Resh, M.D.** (2013) Covalent lipid modifications of proteins. *Current Biology*, **23**, R431-R435.
- Rusinova, E., Borst, J.W., Kwaaitaal, M., Cano-Delgado, A., Yin, Y., Chory, J. and de Vries, S.C.** (2004) Heterodimerization and endocytosis of Arabidopsis brassinosteroid receptors BRI1 and AtSERK3 (BAK1). *The Plant cell*, **16**, 3216-3229.
- Saheki, Y. and Camilli, P.D.** (2017) Endoplasmic Reticulum–Plasma Membrane Contact Sites. *Annual Review of Biochemistry*, **86**, 659-684.
- Saheki, Y. and De Camilli, P.** (2017) The Extended-Synaptotagmins. *Biochimica et Biophysica Acta (BBA) - Molecular Cell Research*, **1864**, 1490-1493.

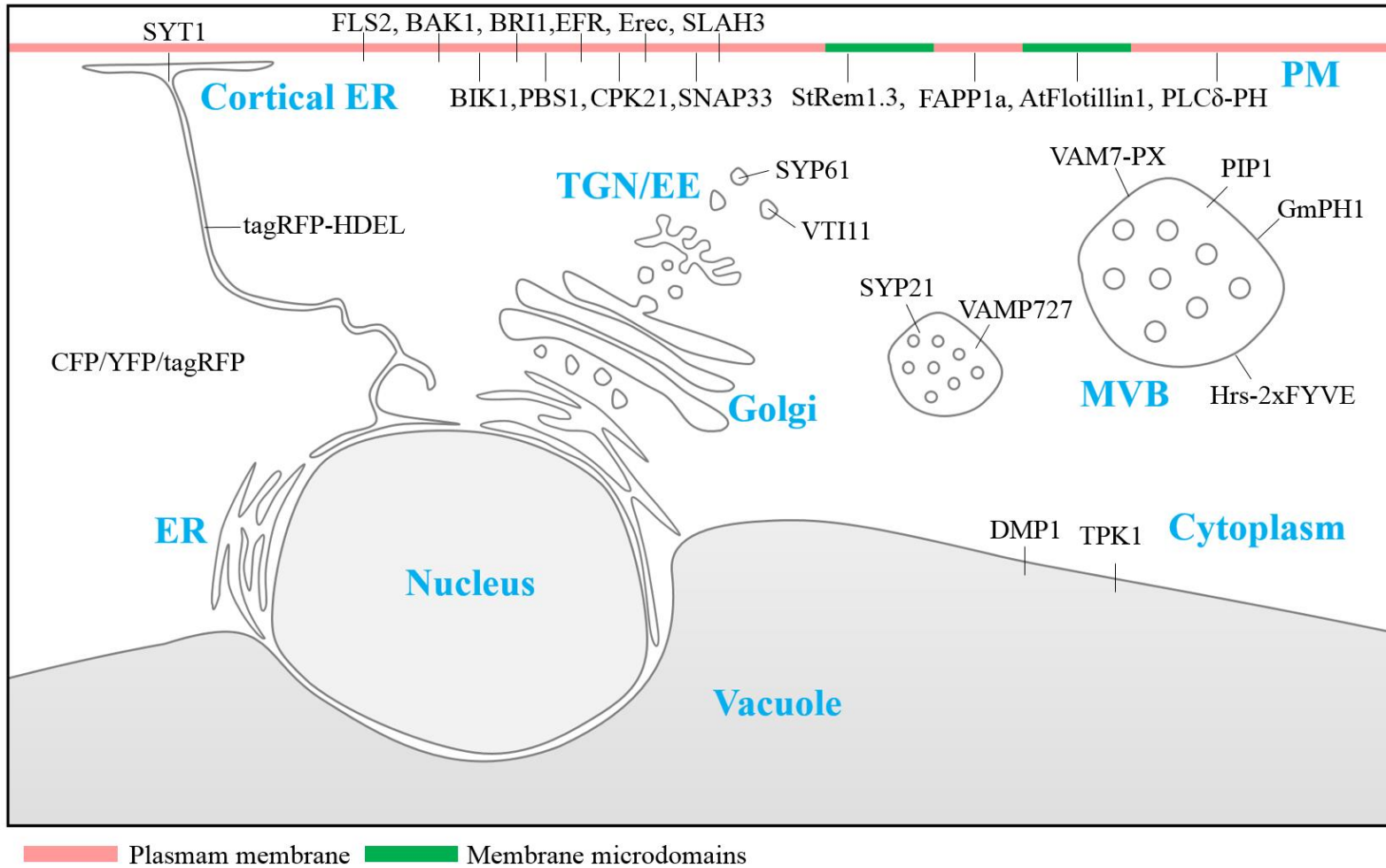
- Saka, Y., Hagemann, A., Piepenburg, O. and Smith, J.C.** (2007) Nuclear accumulation of Smad complexes occurs only after the midblastula transition in *Xenopus*. *Development (Cambridge, England)*, **134**, 4209-4218.
- Sanderfoot, A.** (2007) Increases in the Number of SNARE Genes Parallels the Rise of Multicellularity among the Green Plants. *Plant Physiology*, **144**, 6-17.
- Schulz, P., Herde, M. and Romeis, T.** (2013) Calcium-Dependent Protein Kinases: Hubs in Plant Stress Signaling and Development. *Plant physiology*, **163**, 523-530.
- Serna, L.** (2005) A simple method for discriminating between cell membrane and cytosolic proteins. *New Phytologist*, **165**, 947-952.
- Shyu, Y.J., Liu, H., Deng, X. and Hu, C.D.** (2006) Identification of new fluorescent protein fragments for bimolecular fluorescence complementation analysis under physiological conditions. *BioTechniques*, **40**, 61-66.
- Simon, M.L.A., Platre, M.P., Marquès-Bueno, M.M., Armengot, L., Stanislas, T., Bayle, V., Caillaud, M.-C. and Jaillais, Y.** (2016) A PtdIns(4)P-driven electrostatic field controls cell membrane identity and signalling in plants. *Nature Plants*, **2**, 16089.
- Smit, P., Limpens, E., Geurts, R., Fedorova, E., Dolgikh, E., Gough, C. and Bisseling, T.** (2007) Medicago LYK3, an Entry Receptor in Rhizobial Nodulation Factor Signaling. *Plant Physiology*, **145**, 183-191.
- Snider, J., Hanif, A., Lee, M.E., Jin, K., Yu, A.R., Graham, C., Chuk, M., Damjanovic, D., Wierzbicka, M., Tang, P., Balderes, D., Wong, V., Jessulat, M., Darowski, K.D., San Luis, B.-J., Shevelev, I., Sturley, S.L., Boone, C., Greenblatt, J.F., Zhang, Z., Paumi, C.M., Babu, M., Park, H.-O., Michaelis, S. and Stagljar, I.** (2013) Mapping the functional yeast ABC transporter interactome. *Nature Chemical Biology*, **9**, 565.
- Speth, E.B., Imboden, L., Hauck, P. and He, S.Y.** (2009) Subcellular Localization and Functional Analysis of the Arabidopsis GTPase RabE. *Plant Physiology*, **149**, 1824-1837.
- Stefano, G., Renna, L. and Brandizzi, F.** (2014) The endoplasmic reticulum exerts control over organelle streaming during cell expansion. *Journal of Cell Science*, **127**, 947-953.

- Stillwell, W.** (2016) Chapter 6 - Membrane Proteins. In *An Introduction to Biological Membranes (Second Edition)*: Elsevier, pp. 89-110.
- Stracke, S., Kistner, C., Yoshida, S., Mulder, L., Sato, S., Kaneko, T., Tabata, S., Sandal, N., Stougaard, J., Szczyglowski, K. and Parniske, M.** (2002) A plant receptor-like kinase required for both bacterial and fungal symbiosis. *Nature*, **417**, 959.
- Tóth, K., Stratil, T.F., Madsen, E.B., Ye, J., Popp, C., Antolín-Llovera, M., Grossmann, C., Jensen, O.N., Schübler, A., Parniske, M. and Ott, T.** (2012) Functional Domain Analysis of the Remorin Protein LjSYMREM1 in *Lotus japonicus*. *PLOS ONE*, **7**, e30817.
- Van Leeuwen, W., Vermeer, J.E.M., Gadella, T.W.J. and Munnik, T.** (2007) Visualization of phosphatidylinositol 4,5-bisphosphate in the plasma membrane of suspension-cultured tobacco BY-2 cells and whole *Arabidopsis* seedlings. *The Plant Journal*, **52**, 1014-1026.
- Varshney, P., Yadav, V. and Saini, N.** (2016) Lipid rafts in immune signalling: current progress and future perspective. *Immunology*, **149**, 13-24.
- Vermeer, J.E., Thole, J.M., Goedhart, J., Nielsen, E., Munnik, T. and Gadella, T.W., Jr.** (2009) Imaging phosphatidylinositol 4-phosphate dynamics in living plant cells. *The Plant journal : for cell and molecular biology*, **57**, 356-372.
- Vermeer, J.E., van Leeuwen, W., Tobena-Santamaria, R., Laxalt, A.M., Jones, D.R., Divecha, N., Gadella, T.W., Jr. and Munnik, T.** (2006) Visualization of PtdIns3P dynamics in living plant cells. *Plant J*, **47**, 687-700.
- Vögler, O., Barceló, J.M., Ribas, C. and Escribá, P.V.** (2008) Membrane interactions of G proteins and other related proteins. *Biochimica et Biophysica Acta (BBA) - Biomembranes*, **1778**, 1640-1652.
- Walter, P. and Johnson, A.E.** (1994) Signal Sequence Recognition and Protein Targeting to the Endoplasmic Reticulum Membrane. *Annual Review of Cell Biology*, **10**, 87-119.
- Wang, L., Li, H., Lv, X., Chen, T., Li, R., Xue, Y., Jiang, J., Jin, B., Baluška, F., Šamaj, J., Wang, X. and Lin, J.** (2015) Spatiotemporal Dynamics of the BRI1 Receptor and its Regulation by Membrane Microdomains in Living *Arabidopsis* Cells. *Molecular Plant*, **8**, 1334-1349.

- Wang, P., Richardson, C., Hawkins, T.J., Sparkes, I., Hawes, C. and Hussey, P.J.** (2016) Plant VAP27 proteins: domain characterization, intracellular localization and role in plant development. *New Phytologist*, **210**, 1311-1326.
- Wong, K.A. and O'Bryan, J.P.** (2011) Bimolecular Fluorescence Complementation. *Journal of Visualized Experiments : JoVE*, 2643.
- Wudick, M.M., Luu, D.-T. and Maurel, C.** (2009) A look inside: localization patterns and functions of intracellular plant aquaporins. *New Phytologist*, **184**, 289-302.
- Yagisawa, H., Sakuma, K., Paterson, H.F., Cheung, R., Allen, V., Hirata, H., Watanabe, Y., Hirata, M., Williams, R.L. and Katan, M.** (1998) Replacements of Single Basic Amino Acids in the Pleckstrin Homology Domain of Phospholipase C- δ 1 Alter the Ligand Binding, Phospholipase Activity, and Interaction with the Plasma Membrane. *Journal of Biological Chemistry*, **273**, 417-424.
- Yamazaki, T., Kawamura, Y., Minami, A. and Uemura, M.** (2008) Calcium-Dependent Freezing Tolerance in Arabidopsis Involves Membrane Resealing via Synaptotagmin SYT1. *The Plant Cell*, **20**, 3389-3404.
- Yamazaki, T., Takata, N., Uemura, M. and Kawamura, Y.** (2010) Arabidopsis Synaptotagmin SYT1, a Type I Signal-anchor Protein, Requires Tandem C2 Domains for Delivery to the Plasma Membrane. *Journal of Biological Chemistry*, **285**, 23165-23176.
- Yoo, S.-D., Cho, Y.-H. and Sheen, J.** (2007) Arabidopsis mesophyll protoplasts: a versatile cell system for transient gene expression analysis. *Nat. Protocols*, **2**, 1565-1572.
- Yuh - Shuh, W., M., M.C., R., M.D. and B., B.E.** (2004) Green fluorescent protein fusions to Arabidopsis fimbrin 1 for spatio - temporal imaging of F - actin dynamics in roots. *Cell Motility*, **59**, 79-93.
- Zipfel, C., Kunze, G., Chinchilla, D., Caniard, A., Jones, J.D.G., Boller, T. and Felix, G.** (2006) Perception of the Bacterial PAMP EF-Tu by the Receptor EFR Restricts Agrobacterium-Mediated Transformation. *Cell*, **125**, 749-760.

Appendix Figures

Figure 2.1 Subcellular localization of all proteins tested in chapter 2 when transiently expressed in plant cells.



Chapter 3: Manipulating Endosomal membrane-Plasma Membrane Tethering through BiFC interactions

Manipulating Endosomal membrane-Plasma Membrane Tethering through BiFC interactions

Kai Tao^{1,2}, Justin R. Waletich³, Hua Wise², Felipe Arredondo², Brett M. Tyler^{1,2,4}.

1. Molecular and Cellular Biology Program, Oregon State University, Corvallis, OR 97331
2. Department of Botany and Plant Pathology, Oregon State University, Corvallis, OR 97331
3. Department of Microbiology, Oregon State University, Corvallis, OR 97331
4. Center for Genome Research and Biotechnology, Oregon State University, Corvallis, OR 97331

Abstract

Phosphatidylinositol 3-phosphate (PtdIns(3)P) is considered a hallmark of endosomal membranes and has been predominantly found on those membranes. However, in plant cells, it remains unclear whether PtdIns(3)P occurs in other locations such as the plasma membrane (PM). We used specific PtdIns(3)P-binding proteins and their mutants, in conjunction with the bimolecular fluorescence complementation (BiFC) assay, to map the distribution of PtdIns(3)P relative to a set of membrane proteins specific for a variety of cellular membranes. When the PtdIns(3)P-binding proteins, VAM7-PX and Hrs-2xFYVE, were co-expressed in *Nicotiana benthamiana* cortical cells together with the PM lipid microdomain protein, StREM1.3, using VenusN and VenusC BiFC constructs, the BiFC fluorescence signal was surprisingly distributed into large well defined patches on the PM. The same distribution was also observed when a representative set of multivesicular body (MVB)-targeted proteins were paired with PM-targeted peripheral membrane proteins. Based on our recent work showing that BiFC complexes can act as artificial ER-PM tethers, we inferred that BiFC complexes could also act to tether MVBs, and also the tonoplast, to the PM. Our results suggest new tools for manipulating organellar localization in plant cells, but also highlight the risk of unexpected artifacts when using BiFC assays to study protein–protein and protein membrane associations in plant cells. We also observed that the *Arabidopsis* U-box (PUB) E3 ubiquitin ligases SAUL1 (AtPUB44) and AtPUB43 could tether MVBs and the tonoplast to the PM under certain circumstances, suggesting a possible new function of these two E3 ligases.

Introduction

In eukaryotic cells, the uptake of extracellular materials (including ligands, proteins and lipids) is processed through a system of endosomes. Signaling receptors and other plasma membrane (PM) integral membrane proteins internalized into cells are processed through the same system. This system is composed of a series of highly dynamic membrane-bound vesicular organelles performing the intermediate functions of cargo storage, sorting and delivery to destinations within the cells (Mellman, 1996, Bonifacino and Traub, 2003). Based on their different functions, these membrane-bound organelles have been generally classified in animal cells as early endosomes (EE), recycling endosomes (REs), and late endosomes (LEs) (also known as multivesicular bodies; MVBs) (Singh et al., Hu et al., 2015). As the portal of entry into this endocytic network, EEs receive cargos which are initially internalized at the PM into endocytic vesicles via either clathrin-coated endocytosis (Merrifield et al., 2002), caveolae-mediated endocytosis (Doherty and McMahon, 2009), or lipid microdomain-associated endocytosis (Ewers and Helenius, 2011). Subsequent heterotypic fusion between endocytic vesicles and the EE is regulated by a small GTPase referred to as Rab5. The GTP-bound conformation of Rab5 also carries out the key roles of recruiting various specialized effectors to the EEs, and promoting homotypic fusion between EEs (Jovic et al., 2010, Zeigerer et al., 2012). EEs function as the major sorting hub for membrane and soluble cargos. Most membrane cargos are sorted for recycling back to the PM via recycling endosomes (REs), which have also been recently characterized as another major route for retrograde transport to the trans-Golgi networks (TGN), resulting in access to the exocytic pathway (Ang et al., 2004, van IJzendoorn, 2006, Hsu and Prekeris, 2010). On the other hand, cargos destined for degradation in lysosomes are targeted to regions of the EEs destined to mature into LEs (Huotari and Helenius, 2011). The hallmark of the maturation of EEs to LEs is loss of Rab5 from endosomal membrane with the concomitant acquisition of Rab7 (Poteryaev et al., 2010). LEs move unidirectionally towards, and then fuse with, the lysosomes which contain a variety of hydrolytic enzymes for the turnover of the endocytic cargos (Xu and Ren, 2015).

The endosomal system in plant cells shares major similarities with mammalian systems. However, it has been suggested that plant cells lack distinct EEs and instead that the TGN takes on the function of EEs in receiving endocytic cargos (Dettmer et al., 2006, Chow et al., 2008, Viotti et al., 2010). This suggestion was based on the use of the fluorescent styryl dye FM4-64 which binds to the outer leaflet of the PM, and is quickly internalized by endocytosis, labeling the earliest endosome compartments. Furthermore, it was reported that in plants, subdomains of the TGN could either function as REs, or could gradually mature into MVBs which correspond to LEs in mammalian cells (Scheuring et al., 2011, Singh et al., 2014). MVBs in plants have been generally identified as an intermediate hub, where endocytic cargo can either undergo retrograde trafficking to the TGN or be targeted to the lytic compartments for degradation (Cui et al., 2016). Moreover, MVBs also appear to function in the sorting of biosynthetic endosomes destined for the vacuole, and therefore are often termed prevacuolar compartments (PVCs) (Tse et al., 2004, Shen et al., 2011, Contento and Bassham, 2012). For simplicity, for the remainder of this chapter, I will use the term MVBs. Consistent with this model, vacuolar sorting receptor (VSR) proteins, which are responsible for recognizing the vacuolar sorting determinants (VSDs) on cargos destined for degradation, are found to be predominantly enriched in MVBs (Tse et al., 2004, Miao et al., 2006, Luo et al., 2014).

A further major difference in plant cells is that lysosomes are replaced by vacuoles as the end-point of the endocytic pathway for degradation. In contrast to lysosomes however, the vacuole is the largest membrane-enclosed compartment in many but not all plant cells, occupying more than 90% of the total cell volume (Festa et al., 2016). The vacuole also carries out several important functions such as maintaining cellular homeostasis (e.g., pH, redox, osmolarity) (Zhu, 2001, Hurth et al., 2005, Andreev, 2012), serving as a reservoir for nutrient ions, sugars, proteins, metabolites and pigments (Andreev, 2001, Pourcel et al., 2010, Zhang et al., 2015), contributing to the immune response against pathogens via programmed cell death or discharge of anti-microbial vacuolar contents (Hatsugai and Hara-Nishimura, 2010, Hatsugai et al., 2015), and regulating cell volume in support of the structural integrity of plants (Reisen et al., 2005). To enable these diverse functions, the vacuolar

membrane, also called the tonoplast, harbors a variety of transporters, channel proteins, and other membrane proteins. The tonoplast is also the location for the fusion of TGN-derived MVBs with vacuoles (Scheuring et al., 2011).

In the endocytic pathway, the lipid composition of the endosomal membranes dramatically influences the differentiation, identity and function of the various vesicular components of the system. The lipids not only influence the biophysical properties of the membrane bilayers, but they also recruit specific endosomal effector proteins that mediate vesicle targeting, sorting, fusion, and docking. In animal endosomal systems, phosphatidylinositol 3-phosphate (PtdIns(3)P) is a defining characteristic of the EEs (Di Paolo and De Camilli, 2006). GTP-bound Rab5 on the endosomal membrane can interact with the effector protein phosphoinositide 3-kinase (PI3K) resulting in local synthesis of PtdIns(3)P (Murray et al., 2002, Jovic et al., 2010). The presence of PtdIns(3)P establishes the identity of EEs by recruiting a variety of effector proteins that contain PtdIns(3)P-binding modules such as the FYVE domain of early endosomal antigen-1 (EEA1) of human cells (Gaullier et al., 1998), and the Phox (PX) domain in Qc-SNARE (soluble NSF attachment protein receptor) Vam7 of yeast cells (Sato et al., 2001). These effectors further coordinate endosomal trafficking, fusion, intraluminal vesicle formation, and maturation (Jaber et al., 2016, Wallroth and Haucke, 2017). Similarly, MVBs/LEs also contain PtdIns(3)P. The displacement of Rab5 for Rab7 requires PtdIns(3)P binding and Rab7 is able to recruit PI3K (Poteryaev et al., 2010, Raiborg et al., 2013).

In plant cells, as mentioned above, the TGN appears to functionally replace the role of EEs. Nevertheless, it is usually devoid of PtdIns(3)P (Paez Valencia et al., 2016). Instead, PtdIns(3)P is highly enriched on the MVBs (Otegui and Spitzer, 2008, Simon et al., 2014). A pair of functionally redundant canonical Rab5-type GTPases, RABF2a/RHA1 (Sohn et al., 2003) and RABF2b/ARA7 (Bottanelli et al., 2012), together with a plant-specific Rab5-like GTPase RABF1/ARA6 (Ebine et al., 2011) are found on multivesicular endosomes. In addition, a Rab7-type GTPase, RABG3f, is localized on MVBs and the tonoplast, mediating vesicular trafficking to the vacuoles (Nahm et al., 2003, Cui et al., 2014). Thus in plants, PtdIns(3)P is characteristic of the system of vesicles and membranes that functionally replaces the LEs of animal cells.

During plant-microbe interactions, effector proteins are secreted from microbial pathogens and enter host cells to manipulate host immune signaling response to promote successful infection. However questions about how effectors from fungi and oomycetes are translocated into host cells have not been fully resolved yet. Several studies have reported that pathogen effectors have the capability to bind PtdIns(3)P *in vitro* (Gan et al., 2010, Kale et al., 2010, Gu et al., 2011, Plett et al., 2011, Weigele et al., 2017). Furthermore it has been proposed that PtdIns(3)P-binding may be involved in host entry by effectors, possibly via lipid microdomain-mediated endocytosis (Kale et al., 2010, Gu et al., 2011, Plett et al., 2011). Furthermore, it has been reported that, in animal cells, synthesis of PtdIns(3)P on the PM could be stimulated under certain conditions (Falasca and Maffucci, 2009). Given the role of PtdIns(3)P in endocytic trafficking, and the potential presence of PtdIns(3)P on the plasma membrane of host cells, we set out to map the distribution of PtdIns(3)P in the plant cells, and particularly to examine the plant PM for the presence of PtdIns(3)P. We found no evidence for PtdIns(3)P on the cytoplasmic face of the plasma membrane. However, we observed that the tonoplast and a variety of MVBs and endosomes carrying PtdIns(3)P could closely dock with the PM under certain circumstances, especially when tethering proteins carrying PM and MVB binding domains were over-expressed.

Results

Localization of PtdIns(3)P biosensors VAM7-PX, Hrs2xFYVE, and plasma membrane remorin StRem1.3.

To create a biosensor that could localize PtdIns(3)P, we fused YFP to the C terminus of the phox homology (PX) domain of the *Saccharomyces cerevisiae* Qc-SNARE protein, VAM7. This ~130 residue domain specifically recognizes PtdIns(3)P (Cheever et al., 2001, Lee et al., 2006). To use as a PM marker, we fused tagRFP or YFP to the *Solanum tuberosum* remorin protein, StRem1.3, a well characterized member of the remorin protein family, which has been widely used as a PM microdomain marker in plants (Perraki et al., 2012, Jarsch et al., 2014). We used *Agrobacterium tumefaciens*-mediated transient transformation to ectopically express VAM7-PX and StRem1.3 fluorescent protein fusions in *Nicotiana benthamiana* leaf cortical cells. Then the leaf tissue was examined by confocal fluorescence microscopy.

To obtain a comprehensive view of the plasma membrane, Z-axis scanning imaging was utilized to build 3D visualizations via maximal intensity projection. As shown in Fig. 3.1a, the fluorescence of VAM7-PX-YFP was observed on motile vesicular organelles, and also at or near the PM. YFP-StRem1.3 showed the localization pattern expected for uniform localization to the plasma membrane (Figure 3.1a). These results aligned with a previous study using the PtdIns(3)P-specific biosensor Hrs-2xFYVE that showed PtdIns(3)P localization on endosomes and the vacuolar membrane in tobacco BY-2 cells (Vermeer et al., 2006). Though VAM7-PX-YFP predominantly resided on the vacuolar membrane as well as endosomes, co-expressing VAM7-PX-YFP and tagRFP-StRem1.3 could not unambiguously rule out that PtdIns(3)P is also distributed on the plasma membrane as well as the tonoplast (Figure 3.1b).

To further characterize the distribution of PtdIns(3)P, we utilized additional PtdIns(3)P-specific binding proteins as biosensors, namely the tandem repeat of the FYVE domain from the rat hepatocyte growth factor-regulated tyrosine kinase substrate (Hrs-2xFYVE)(Komada and Kitamura, 1995, Vermeer et al., 2006), and a soybean homolog of the *Arabidopsis* AtPH1 protein (Dowler et al., 2000), GmPH1 (Helliwell et al., 2016). Both of these biosensors showed a subcellular localization closely similar to VAM7-PX (Figure S3.1), supporting that PtdIns(3)P-binding was required for their respective subcellular localization.

To confirm that PtdIns(3)P-binding was required for their observed subcellular localization, we designed mutations in the PtdIns(3)P binding sites of the biosensor proteins through site-directed mutagenesis as previously described (Dowler et al., 2000, Kutateladze and Overduin, 2001, Lee et al., 2006, Pankiv et al., 2010). Each of these mutants, VAM7-PX*, Hrs-2xFYVE* and GmPH1*, lost targeting to any membrane, including the vacuolar membrane and the MVBs; instead they accumulated in the cytoplasm (Figure S3.1). These results further supported that PtdIns(3)P-binding was required for the respective subcellular localization of each biosensor.

BiFC complexes containing PtdIns(3)P biosensors and StRem1.3 display large unexpected patches of plasma membrane fluorescence

To more unambiguously address whether PtdIns(3)P was located only on the vacuolar membrane and not on the PM, we used the bimolecular fluorescence

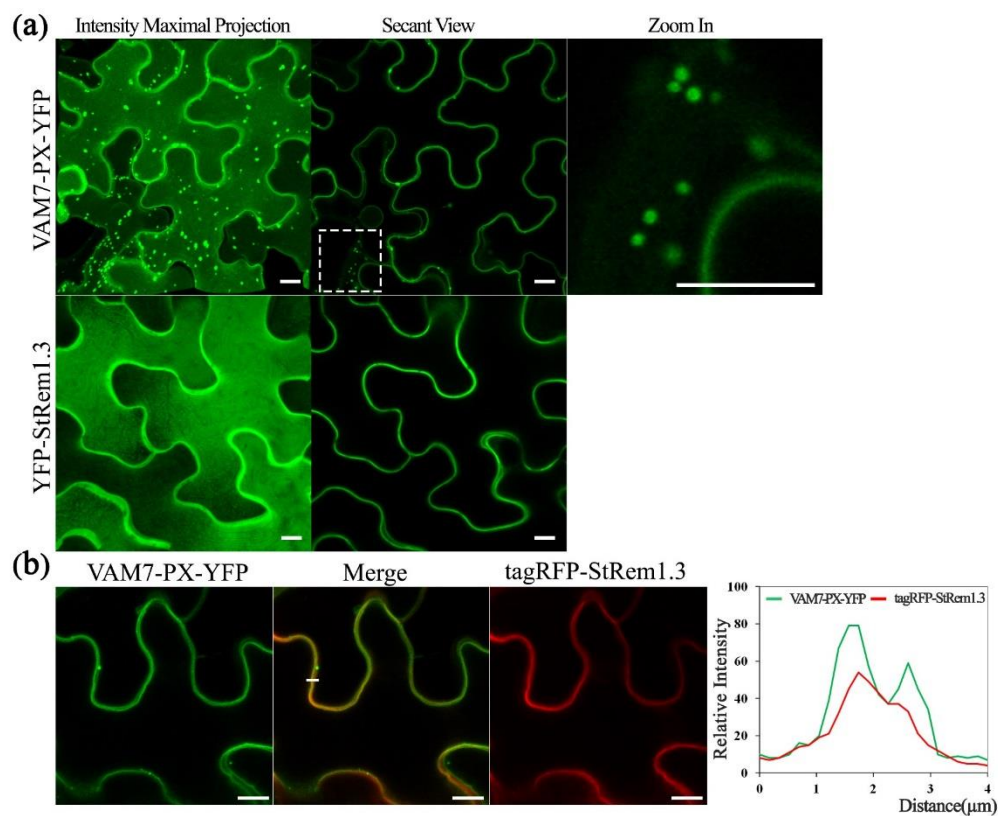


Figure 3.1 Subcellular localization of PtdIns(3)P relative to the plasma membrane in *N. benthamiana* leaf cortical cells.

(a) Subcellular localization of PtdIns(3)P biosensor VAM7-PX-YFP and PM-associated remorin StRem1.3 fused with YFP. The dotted box indicates the zoomed-in region. (b) Localization of VAM7-PX-YFP relative to co-expressed StRem1.3-tagRFP. Right panel: fluorescence intensity plot along a transect shown by the white line on the merged image. White scale bars represent 10 μ m.

complementation (BiFC) assay. Normally in this technique, two non-fluorescing fragments of a fluorescent protein are translationally fused with proteins of interest. If the proteins of interest bind to each other, the two non-fluorescing fragments are brought into proximity resulting in the re-assembly of a functional fluorescent protein (Kerppola, 2006). However, actual physical interaction between the proteins of interest is not always required, and it may be sufficient to bring the proteins into near proximity, e.g. by binding to the same membrane domain. Furthermore, if the fluorescent protein used in the BiFC assays matures quickly, and is highly expressed, the two non-fluorescing fragments may associate into a functional protein as a result of random transient contacts, and association of the proteins of interest may not be required. As reported in earlier chapters, Venus FP can self-assemble efficiently in this manner.

To examine the sub-cellular proximity of PtdIns(3)P and StRem1.3, we fused VAM7-PX to an N-terminal fragment of Venus FP (1-155; VenusN) and StRem1.3 was fused to a C-terminal fragment (156-239; VenusC). We expected that if VAM7-PX-VenusN targeted PM PtdIns(3)P, then its co-expression with PM-localized VenusC-StRem1.3 might result in a fluorescent signal from re-assembled Venus, especially if PtdIns(3)P was localized in the same microdomains as StRem1.3. In fact, we did observe significant BiFC fluorescent signals from this experiment. Surprisingly however, the BiFC fluorescent signal was distributed into large patches of various sizes across most of the surfaces of the cortical cells (Figure 3.2a). These patches typically had a variety of small, round, non-fluorescent inclusions (Supplementary Video 3.1). To further characterize the observed membrane patches, we paired StRem1.3 with additional PtdIns(3)P biosensors, Hrs-2xFYVE and GmPH1. BiFC complexes composed of both pairs displayed large membrane patches similar to those produced using VAM7-PX (Figure 3.2a), suggesting that PtdIns(3)P-binding was required for formation of the patches. Additionally, we also observed this characteristic pattern when the constructs were co-expressed in *Arabidopsis* mesophyll protoplasts (Figure S3.2). To confirm the requirement for PtdIns(3)P binding, we paired StRem1.3 with the mutant biosensors VAM7-PX*, Hrs-2xFYVE* and GmPH1* that can no longer

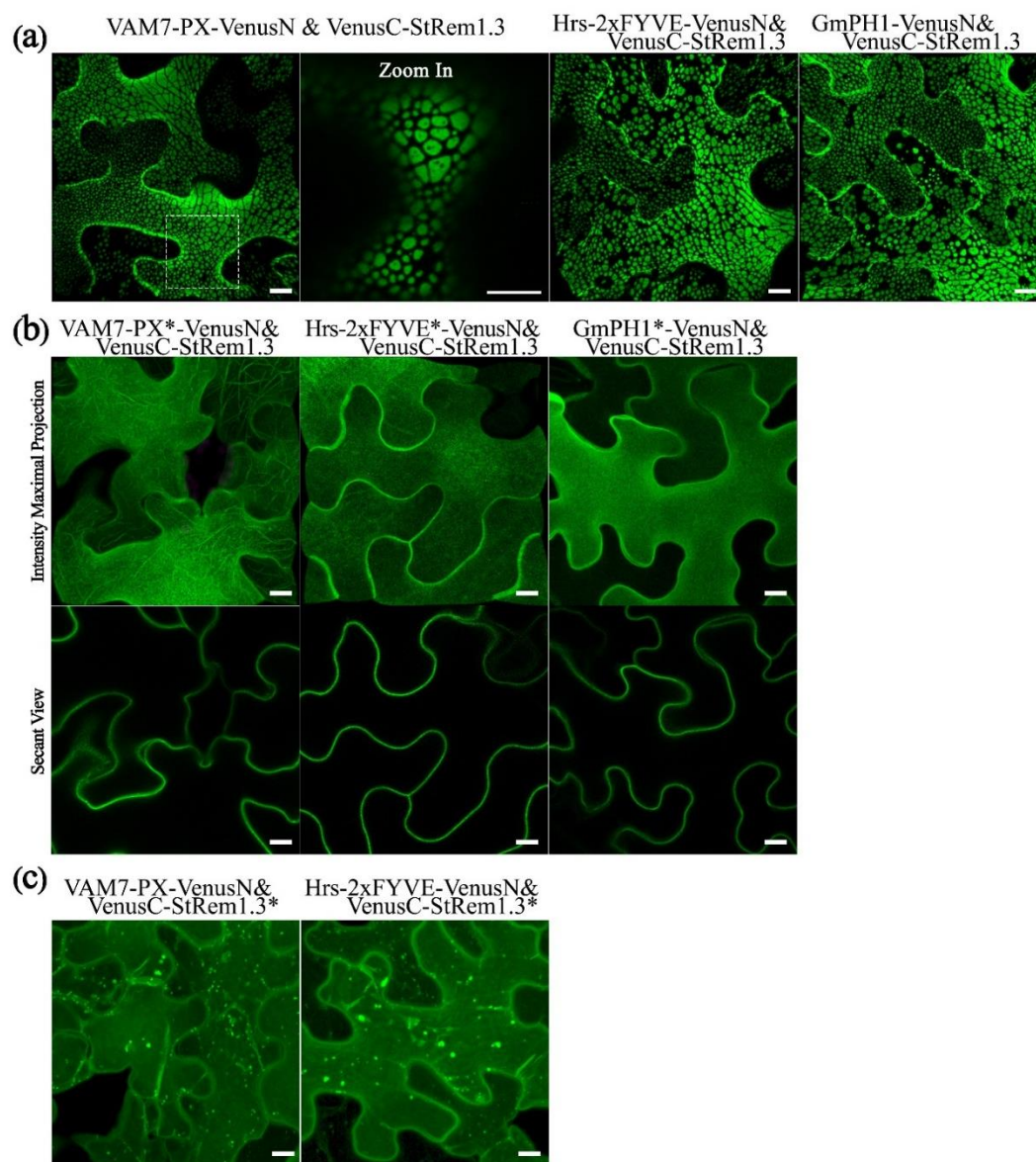


Figure 3.2 Co-expression of PtdIns(3)P-binding proteins and StRem1.3 produces BiFC complexes distributed in large patches on the PM of *N. benthamiana* leaf cortical cells. (a) BiFC fluorescence in cells co-expressing VAM7-PX-VenusN, Hrs-2xFYVE-VenusN and GmPH1-VenusN with VenusC-StRem1.3 individually. The dotted box indicates the zoomed-in region. (b) BiFC fluorescence in cells co-expressing VenusC-StRem1.3 with VenusN fusions to the PtdIns(3)P-non-binding mutants, VAM7-PX*, Hrs-2xFYVE*, and GmPH1*. (c) Mutations of the PM-targeting motif of StRem1.3 abolished the formation of membrane patches when co-expressed with VAM7-PX or Hrs-2xFYVE in BiFC complexes. White scale bars represent 10 μ m.

bind PtdIns(3)P (Figure S1). In each case, the fluorescent BiFC complexes were homogeneously distributed on the plasma membrane (Figure 3.2b), closely matching the localization of fusions of StRem1.3 with full-length YFP (Figure 3.1a). Furthermore, since fluorescent Venus BiFC complexes were formed by the mutant biosensors as efficiently as the non-mutant ones, we concluded that, under the conditions of our assays, the VenusN and VenusC fragments could spontaneously re-assemble without the need for close association of the fused proteins of interest. Efficient spontaneous re-assembly by Venus BiFC fragments has been noted by others (Gookin and Assmann, 2014).

We also designed chimeric fusion proteins consisting of a PtdIns(3)P biosensor at the N terminus, full length YFP or tagRFP in the middle, and StRem1.3 at the C terminus, that are structurally equivalent to the BiFC complexes used above. Both the YFP and tagRFP versions of the chimeric fusion proteins displayed the characteristic pattern of patches observed above (Supplementary Figure S3.3). Thus the formation of the patches is not restricted to BiFC experiments.

The sizes of the membrane patches are highly variable among different cells, or even within the same cells (Figures 3.2, Supplementary Figure S3.2 and S3.3). To test the hypothesis that the differences in sizes resulted from differences in levels of transgene expression, we compared the patterns produced by constructs driven by the strong cauliflower mosaic virus 35S promoter (CaMV35S) (Sunilkumar et al., 2002) (used for all experiments described above), with those driven by the native promoter of *Arabidopsis* AtRem1.4 (At5g23750.1), the closest *Arabidopsis* homolog of StRem1.3 (Raffaele et al., 2007). For these experiments, VAM7-PX was paired with AtRem1.4, and the two were joined by full length YFP. Membrane patches were observed upon expression of VAM7-PX-YFP-AtRem1.4 under the control of either the CaMV35S promoter and or the AtRem1.4 promoter. Constructs containing the AtRem1.4 promoter produced patches that were much smaller in size than those produced with the CaMV35S promoter (Figure S3.3). Patches produced by VAM7-PX-YFP-AtRem1.4 under the control of either promoter were abolished when the VAM7-PX* mutant was used; uniform PM binding characteristic of AtREM1.4 (Figure 3.7) (and

StREM1.3 in Figure 3.1) was observed with the mutant constructs. These results supported that the sizes of the patches were influenced by transgene expression levels.

Formation of membrane patches requires a PM-binding partner

StRem1.3 is exclusively targeted to the PM through a short C-terminal anchor which has been identified as an amphipathic α -helix (Perraki et al., 2012), and also as an unconventional lipid-binding motif (Gronnier et al., 2017). Therefore, StRem1.3 is a typical peripheral membrane protein. To test if this membrane binding motif is required for formation of lipid patches, mutations were introduced into this domain of StRem1.3. The mutant, StREM1.3*, showed only cytoplasmic localization (Figure S3.4). When paired with the VAM7-PX or Hrs2xFYVE PtdIns(3)P biosensors, the BiFC complexes showed only localization characteristic of those biosensors (Figure 3.2d). Thus membrane binding by StRem1.3 was required for formation of the large patches.

To test if other peripheral membrane proteins could also produce large membrane patches when paired with PtdIns(3) biosensors, we replaced StRem1.3 with the well-characterized receptor-like cytoplasmic kinases (RLCKs), BIK (Lu et al., 2010), PBS1 (Qi et al., 2014), and CPK21 (Asai et al., 2013); those proteins are targeted to the PM via N-terminal myristoylation, palmitoylation or both (Figure S3.4). Consistent with the pattern observed with StRem1.3, when each of them was co-expressed with either VAM7-PX or Hrs-2xFYVE fluorescent BiFC complexes distributed in large membrane patches were produced (Figure 3.3). When the myristoylation and palmitoylation sites of BIK1 were eliminated by mutation, the resultant BIK1* mutant was not membrane localized and did not produce patches when paired with VAM7-PX or Hrs-2xFYVE (Figure S3.4).

PtdIns(4)P accumulates on the PM of plant cells (Vermeer et al., 2009, Simon et al., 2016). Consistent with these reports, we observed that biosensors containing the PtdIns(4)P-binding PH domain of FAPP1 (Dowler et al., 2000) and Osh2 (Roy and Levine, 2004) were targeted to the PM (see Chapter 5; Figure S3.4); our experiments used a mutant of FAPP1-PH, FAPP1a-PH, that no longer binds the Golgi protein ARF1 (see Chapter 5). When we paired these two PM-targeted lipid binding proteins with either VAM7-PX or Hrs-2xFYVE, the resultant fluorescent BiFC complexes appeared

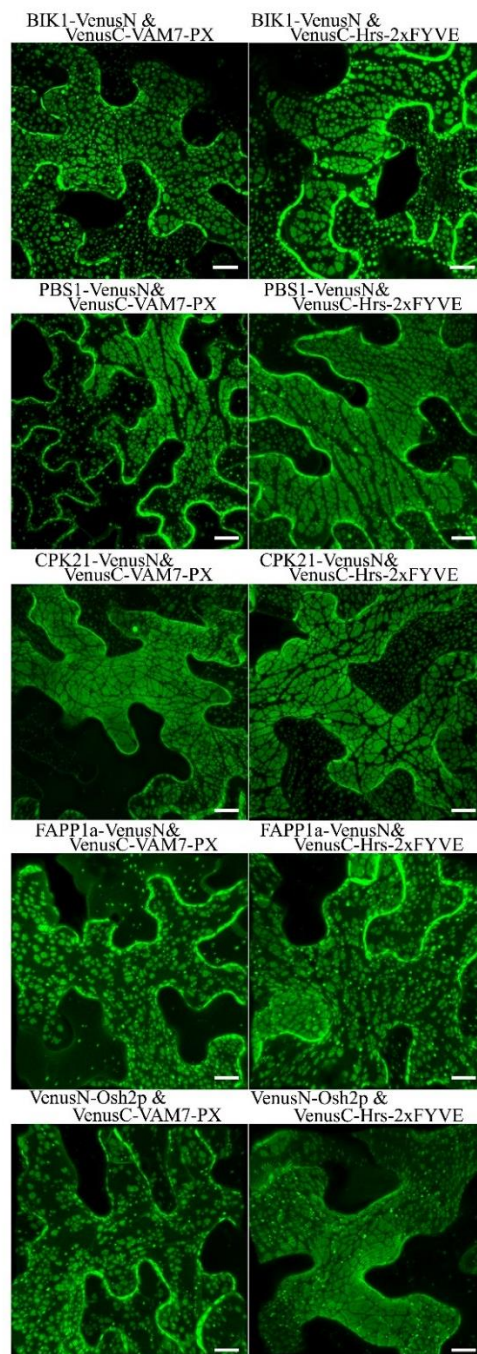


Figure 3.3 BiFC complexes containing PM-targeted peripheral membrane proteins and PtdIns(3)P biosensors form membrane patches in *N. benthamiana* leaf cortical cells. Peripheral membrane proteins BIK1, PBS1, CPK21, and PtdIns(4)P binding proteins FAPP1a and Osh2p, fused to VenusN could produce membrane patches when co-expressed with VenusC-VAM7-PX or VenusC-Hrs-2xFYVE in BiFC complexes. Scale bars represent 10 μ m.

as large membrane patches similar to those produced with StRem1.3 (Figure 3.3). As a control, we used a FAPP1a-PH mutant, FAPP1am (see chapter 3.5), in which the PtdIns(4)P binding site was abolished via site-directed mutagenesis. This mutant biosensor showed only cytoplasmic localization, resulting in an entire loss of PM localization (Figure S3.4). When paired with VAM7-PX and Hrs-2xFYVE, the FAPP1a-PH* BiFC complexes displayed only organellar localization characteristic of the two PtdIns(3)P biosensors (Figure S3.4). Together the above observations indicated that formation of membrane patches by PtdIns(3)P biosensors requires a peripheral membrane protein as a PM-binding partner.

Membrane patches may correspond to tethering of the tonoplast and MVBs to the PM

Based on the evidence presented above, we formulated two alternative hypotheses regarding the origin of the membrane patches. The first hypothesis was that the patches resulted from aggregation of lipid microdomains, triggered by cross-linking of proteins or lipids enriched in those microdomains. The second hypothesis was that the patches were produced by the tethering to the PM of organelles such as endosomes, multi-vesicular bodies or the tonoplast that carried PtdIns(3)P in their membranes. The possibility that organellar tethering might be responsible for formation of the patches was suggested by our observation (see Chapter 2) that ER-PM tethering, analogous to that produced by *Arabidopsis* synaptotagmin1 (SYT1) (Yamazaki et al., 2010), could be produced by BiFC complexes carrying a PM-specific peripheral membrane protein and an ER-trafficked integral membrane protein.

To test the hypothesis that BiFC complexes triggered aggregation of lipid microdomains, we paired StRem1.3 with peripheral membrane proteins or PtdIns(4)P binding proteins to examine whether they could trigger the formation of patches. All co-expressed BiFC complexes involving two peripheral membrane proteins, namely BIK1-VenusN plus VenusC-StRem1.3, PBS1-VenusN plus VenusC-StRem1.3, CPK21-VenusN plus VenusC-StRem1.3, and FAPP1a-PH-VenusN plus VenusC-StRem1.3, were found to be homogeneously distributed on the PM (Figure 3.4), closely similar to distribution characteristics of each of them fused with full-length FPs (Figure

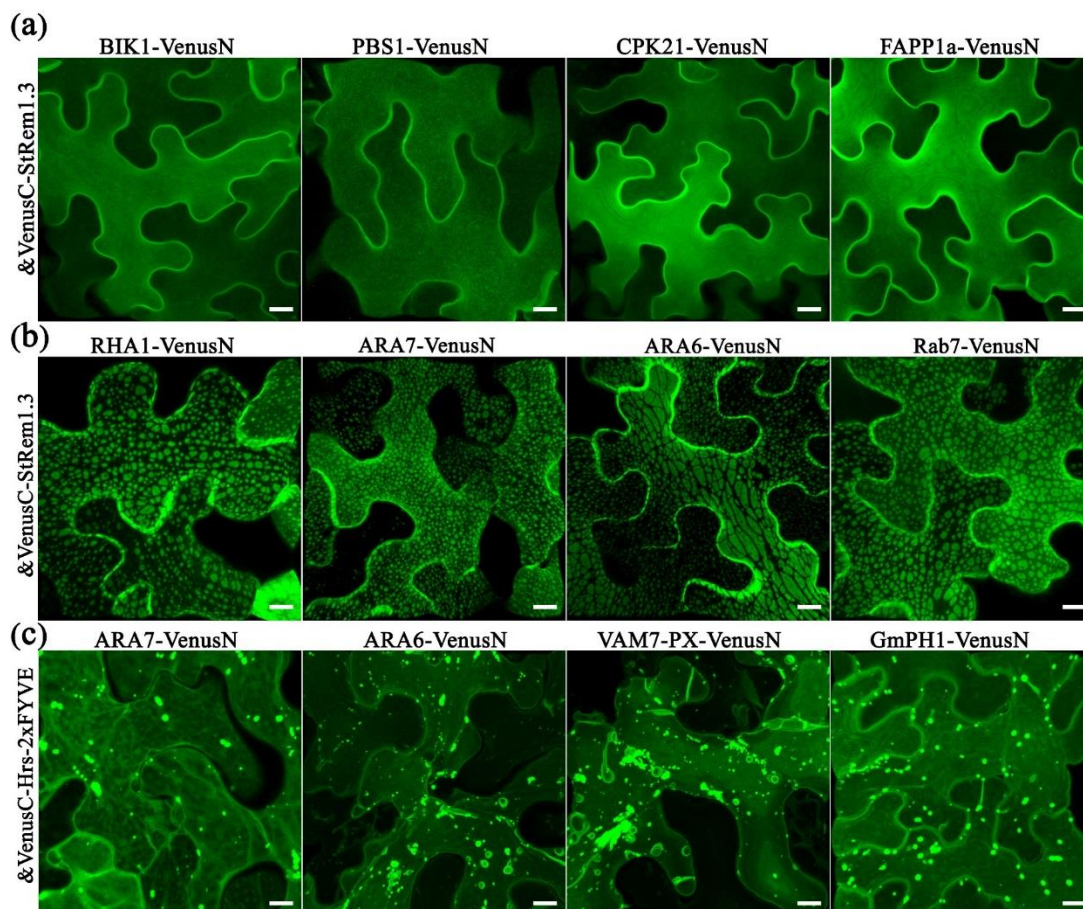


Figure 3.4 BiFC complexes containing peripheral membrane proteins targeted to both the PM and to MVBs or the tonoplast can form membrane patches in *N. benthamiana* leaf cortical cells.

(a) Fluorescence distribution of BiFC complexes containing only PM-targeted peripheral membrane proteins (PMPs). VenusN-fused BIK1, PBS1, CPK21, FAPP1a and Osh2 were paired with VenusC-StRem1.3. (b) Fluorescence distribution of BiFC complexes containing one PM-targeted PMP and one PMP targeted to MVBs and the tonoplast. VenusN-fused RHA1, ARA7, ARA6, or RABG3f were paired with VenusC-StRem1.3 or FAPP1a-PH-VenusC, as indicated. (c) Fluorescence distribution of BiFC complexes containing only tonoplast- or MVB-targeted peripheral membrane proteins and PtdIns(3)P biosensors. VenusC-Hrs-2xFYVE was paired with VenusN-fused ARA7, ARA6, VAM7-PX, or GmPH1. Scales are identical in all panels, white bars represent 10 μm .

S3.4). Thus there was no evidence that cross-linking different PM-targeted PMPs in BiFC complexes could trigger the formation of patches.

To test the hypothesis that the BiFC complexes triggered tethering of PtdIns(3)P-containing membranes to the PM, we paired StRem1.3 with proteins that have been well characterized as associating with MVBs and the tonoplast in *Arabidopsis*, namely the Rab5-type GTPase RHA1 (Sohn et al., 2003), ARA7 (Bottanelli et al., 2012), ARA6 (Ebine et al., 2011), and the Rab7-type GTPase RABG3f (Cui et al., 2014) (Figure S3.5). Co-expressing each of them with StRem1.3 in Venus BiFC complexes produced the characteristic membrane patches in every case, (Figure 3.4b), supporting the hypothesis that this characteristic structure may correspond to the tethering of MVBs and/or the tonoplast to the PM.

As mentioned above, the BiFC complexes may also connect the PtdIns(3)P-containing tonoplast to the PM. To examine this question, we used two well-identified tonoplast-localized proteins namely DUF679 membrane protein (AtDMP1) (Kasaras et al., 2012) and tonoplast potassium channel protein AtTPK1 (Maîtrejean et al., 2011), which are integral membrane proteins. When we co-expressed the two proteins with StRem1.3 however, the BiFC complexes produced ER-PM tethering, due to trapping of the two integral membrane proteins in the ER, as described in Chapter 2 (Figure 2.4).

When we paired a PtdIns(3)P biosensor with an MVB-associated protein, specifically ARA7-VenusN plus VenusC-Hrs-2xFYVE or ARA6-VenusN plus VenusC-Hrs-2xFYVE, the BiFC complexes did not produce membrane patches (Figure 3.4c). BiFC complexes containing two different PtdIns(3)P biosensors, specifically VAM7-PX-VenusN plus VenusC-Hrs-2xFYVE or GmPH1-VenusN plus VenusC-Hrs-2xFYVE, no patches were produced (Figure 3.4c). From this observation we concluded that, unlike PtdIns(4)P, PtdIns(3)P did not reside on the cytoplasmic face of the PM, and thus was not available to tether the tonoplast or MVBs to the PM.

Both the tonoplast and MVBs can be tethered to the PM

Since many marker proteins are shared between MVBs and the tonoplast, it was initially ambiguous whether tethering of the tonoplast, MVBs, or both were responsible for the formation of membrane patches. To examine the relationship of the patches to

the MVBs and the tonoplast, we fused full length YFP to the MVB markers RHA1, ARA7, ARA6, and RABG3f, then co-expressed the fusions with Hrs-2xFYVE-tagRFP-StREM1.3. We also co-expressed Hrs2xFYVE-tagRFP-StRem1.3 with GFP fused to the tonoplast-markers AtDMP1 (Kasaras et al., 2012) and AtTPK1 (Maîtrejean et al., 2011). With the both MVB and tonoplast markers, we observed two patterns of interaction between the patches produced by Hrs-2xFYVE-tagRFP-StRem1.3 and the membranes stained with the respective GFP fusions. The GFP fusions labeled two sets of membranes (Figure 3.5b-d and Supplementary Videos 3.2-3.6). One membrane, which we identified as the tonoplast, was moderately stained by the GFP markers and was spread over the entire width of the cell with wrinkling patterns in the 3D visualizations corresponding to furrows and ridges in the tonoplast (Figure 3.5a) as described previously (Marty, 1999, Reisen et al., 2005). The second set of membranes, which we identified as MVBs, appeared as brightly stained, highly dynamic networks of tubes or vesicles. In the regions displaying just the tonoplast, the patches produced by Hrs-2xFYVE-tagRFP-StRem1.3 excluded the YFP-tagged membrane proteins such as AtDMP1 and AtTPK1 (highlighted by open arrows in Figures 3.5b-d). We inferred that in these regions, the tonoplast was tethered directly to the PM through aggregations of Hrs-2xFYVE-tagRFP-StREM1.3. In the regions displaying MVBs, the MVBs appeared focused on the patches, but the YFP-tagged membrane proteins were not excluded (highlighted by filled arrows in Figures 3.5b-d). Instead, the patches appeared ringed by brightly stained MVB membranes. We inferred that in these regions, the MVBs were tethered to the PM through the aggregations of Hrs-2xFYVE-tagRFP-StRem1.3 proteins.

To test these inferences further, we co-expressed soluble GFP with Hrs-2xFYVE-tagRFP-StRem1.3, to determine if the cytoplasm was displaced, as expected if the tonoplast was tethered to the PM. As shown in Figure 3.6a, 3.6b and Supplementary Video 3.7, the GFP fluorescence was clearly excluded by the patches. To further examine the inferred tethering of the MVBs, we co-expressed soluble tagRFP and AtDMP1-GFP together with VAM7-PX-YFP*-StRem1.3. VAM7-PX-YFP*-StRem1.3 contains a colorless mutant of YFP (Stepanenko et al., 2011) and thus produces colorless patches that can be visualized by negative staining with proteins that

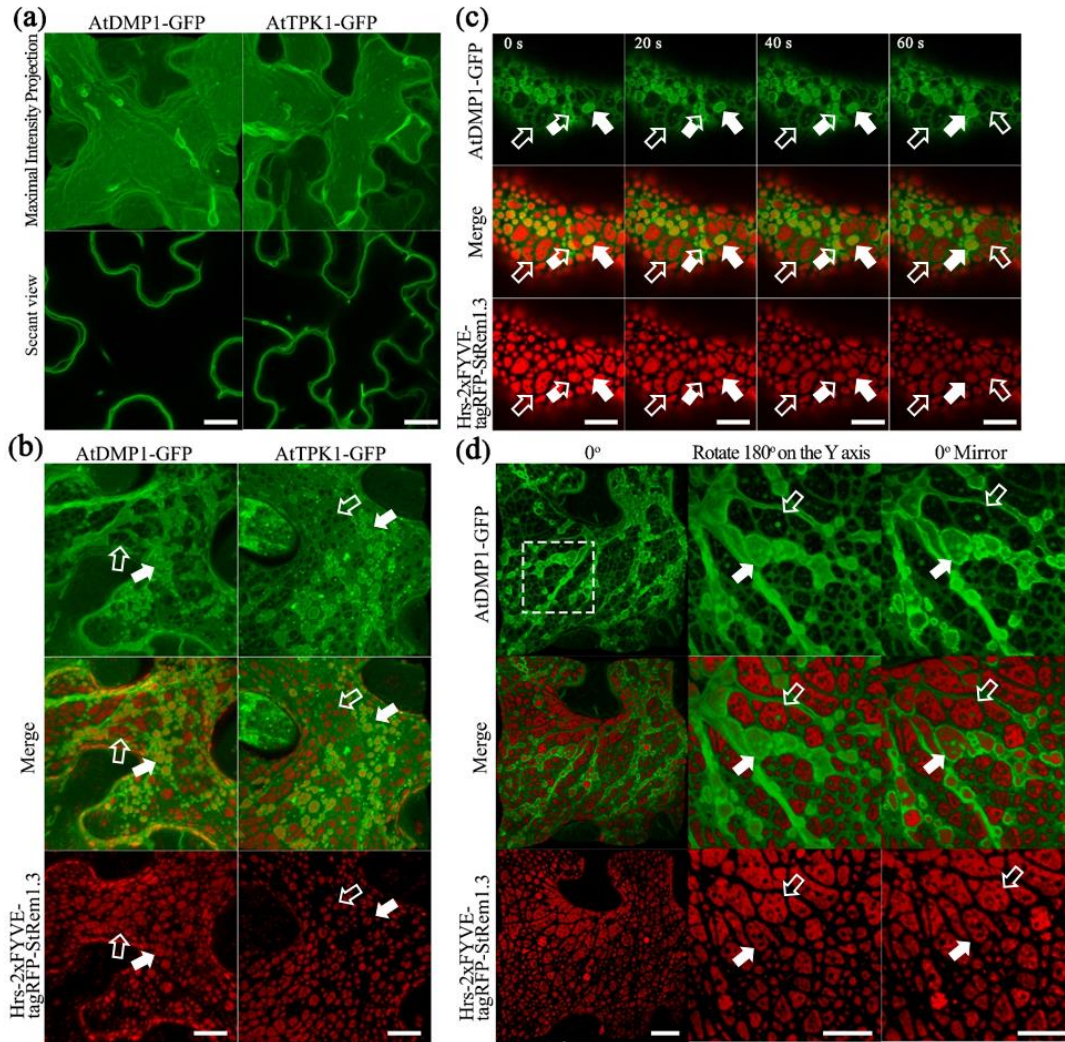


Figure 3.5 Membrane patches can involve PM-tethering of either MVBs or the tonoplast.

(a) Subcellular localizations of tonoplast-targeted proteins AtDMP1 and AtTPK1 fused to GFP. (b), Distinct tonoplast- and MVB-associated patches revealed by co-expression of GFP-fused AtDMP1 or AtTPK1 when with Hrs-2xFYVE-tagRFP-StRem1.3. Examples of tonoplast- and MVB-associated patches are highlighted with open and filled arrows, respectively. (c) Dynamic nature of interactions with MVBs and tonoplast revealed by time-lapse imaging of BiFC fluorescence produced by AtDMP1-GFP co-expressed with Hrs-2xFYVE-tagRFP-StRem1.3. Examples of patches that are tonoplast-associated, MVB-associated, or dynamically associated are highlighted with open, fully-filled and partially filled arrows, respectively. (d) 3D reconstruction of a cell co-expressing AtDMP1-GFP and Hrs-2xFYVE-tagRFP-StRem1.3, rendered by transparency mode. Both sides of the PM are visualized, revealing MVBs overlaying some, but not all, patches. Dotted square indicates region enlarged and rotated on the y-axis (center panels) or mirrored (right panels). Examples of tonoplast- and MVB-associated patches are highlighted with open and filled arrows, respectively. White scale bars represent 10 μ m.

they exclude such as tagRFP and AtDMP1-GFP. As shown in Fig. 3.6c, 3.6d and supplementary videos 8-9, the tagRFP fluorescence was fully excluded by the patches in regions lacking MVBs (highlighted with open arrows). However, in the regions containing MVBs, tagRFP fluorescence was excluded in some z-sections, but not in other z-sections of the same region (highlighted by filled arrows), indicating that the tonoplast was not closely appressed to the PM and that a layer of cytoplasm covered the MVBs associated with the patches. We also note that the exclusion of AtDMP1-GFP and tagRFP by the colorless VAM7-PX-YFP*-StRem1.3 rules out that the exclusion phenomenon is an artifact of confocal microscopy in regions expressing two different fluorescent proteins.

TP/MVB-PM tethering also modifies the distribution of PM-localized proteins.

We previously showed (in chapter 2) that the peripheral membrane protein, AtFlotillin1, is spatially excluded from the region of the PM involved in ER-PM tethering produced by BiFC complexes. To determine whether TP/MVB-PM junctions could also modify the distribution of PM proteins, we co-expressed Hrs-2xFYVE-tagRFP-StRem1.3 fusion proteins with a variety of PM-associated proteins including BIK1, PBS1, AtFlotillin1, and the integral membrane protein FLS2 (Gómez-Gómez and Boller, 2000). In each case, the patches corresponding to the TP/MVB-PM contact regions significantly excluded the co-expressed membrane protein (Figure 3.7). Similar exclusion was observed when the PtdIns(4)P biosensor FAPP1a-PH was co-expressed (Figure 3.7), though we could not determine if PtdIns(4)P was excluded from the patches or whether access to PtdIns(4)P by FAPP1a was blocked. As a control, we stained the PM using the lipophilic styryl dye FM4-64 which intercalates into outer leaflet of the PM (Vitko et al., 2007, Dupont et al., 2010, Song et al., 2012, Nonejuie et al., 2013). No exclusion of FM4-64-stained was observed (Figure 3.7). Interestingly, in contrast to the exclusion patterns observed for PM-associated proteins noted above, AtRem1.4-YFP, was enriched at the TP/MVB-PM contact sites (Figure 3.7).

The colorless fusion protein, VAM7-PX-YFP*-StRem1.3 also could produce colorless patches that excluded the PM-associated proteins FLS2-YFP and FAPP1a-YFP (Figure S3.6), confirming that the regions of exclusion were not a microscopy artifact. Moreover, to test if the fluorescing patches could suppress fluorescence of the

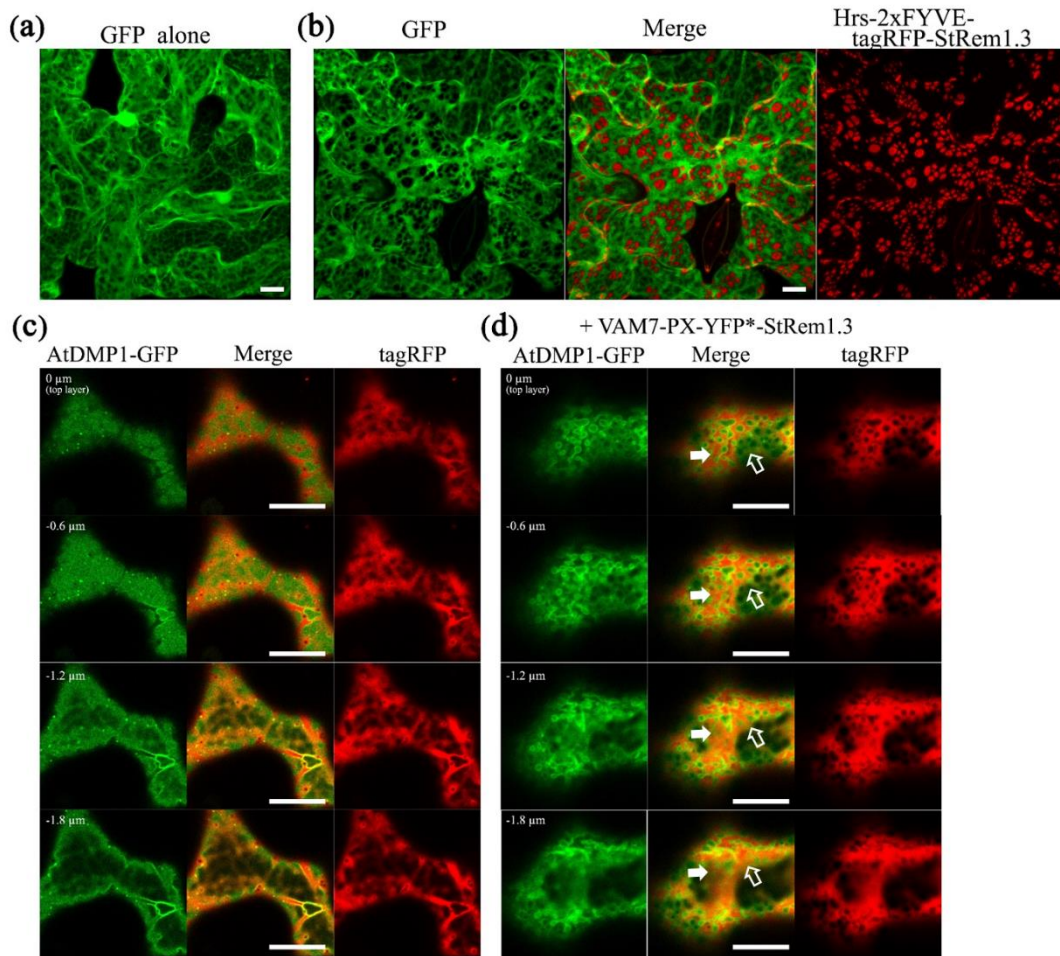


Figure 3.6 Distribution of cytoplasm-targeted free fluorescent proteins in the presence of membrane patches.

(a) Soluble GFP alone. (b) Soluble GFP showing exclusion by membrane patches produced by Hrs-2xFYVE-tagRFP-StRem1.3 (dark holes in GFP panel). (c) Serial z-axis sections of control cells co-expressing tagRFP and AtDMP1-GFP. (d) Serial z-axis sections of cells co-expressing tagRFP and AtDMP1-GFP together with the fusion protein VAM7-PX-YFP*-StRem1.3 that produces colorless, negatively-stained patches. The sections reveal that cytoplasm overlaps patches associated with MVBs, but not patches associated with the tonoplast. Examples of tonoplast- and MVB-associated patches are highlighted with open and filled arrows, respectively. In both (c) and (d) the Z-axis image scanning interval was 0.6 μm. Scale was identical in all panels of (a) and (b), and in all panels of (c) and (d). White scale bar represents 10 μm in each case.

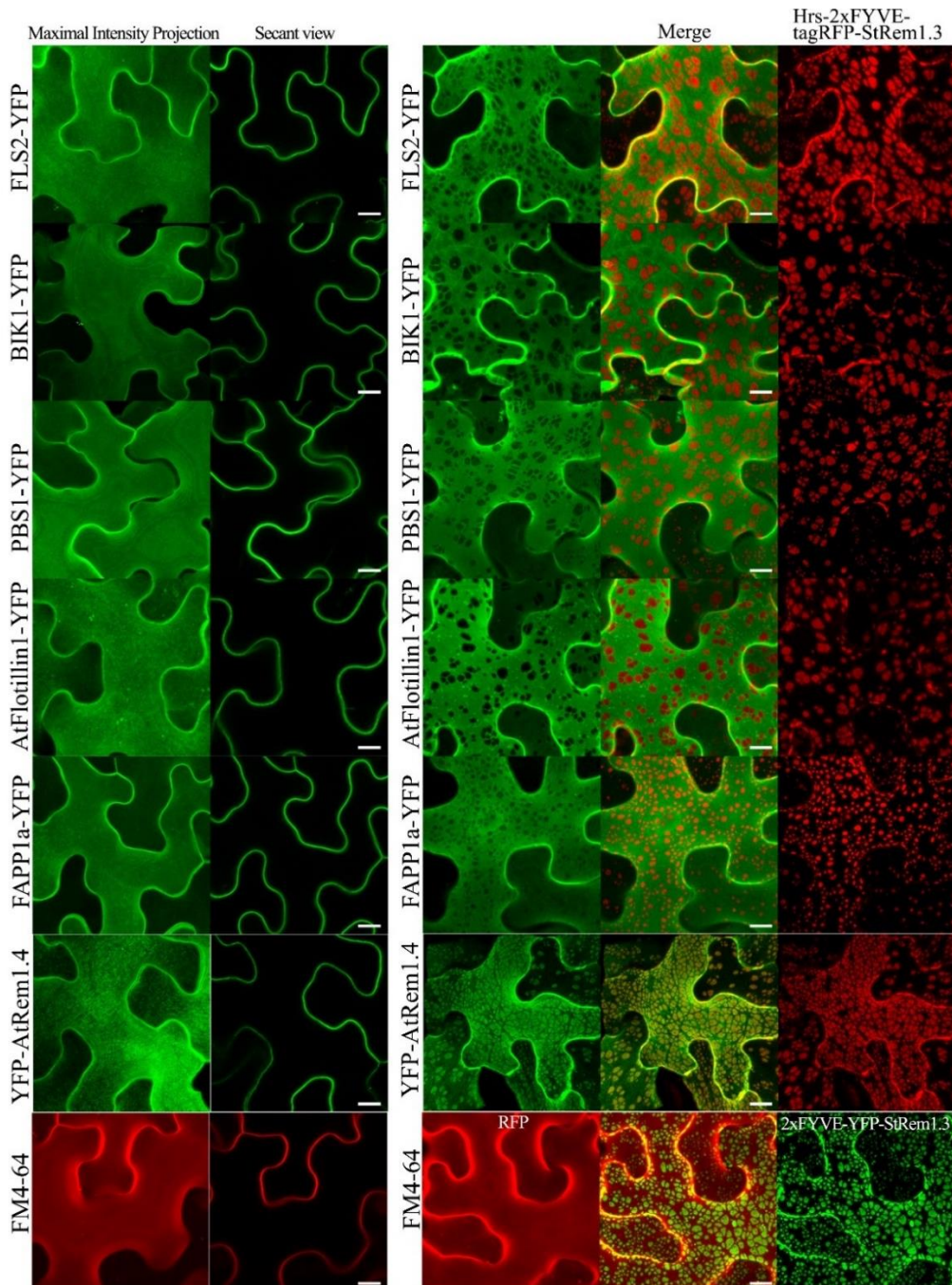


Figure 3.7 Distribution of fluorescently tagged PM-localized proteins in the presence of membrane patches in *N. benthamiana* leaf cortical cells.

Left panels: distribution of fluorescently tagged PM proteins expressed alone. Right panels: distribution of fluorescently tagged PM proteins co-expressed with Hrs-2xFYVE-tagRFP-StRem1.3. Bottom panels: FM4-64 staining in the presence or absence of expressed Hrs-2xFYVE-YFP-StRem1.3. YFP-tagged PM proteins were integral membrane protein FLS2, peripheral membrane proteins BIK1, PBS1, AtFlotillin1, and AtRem1.4, and PtdIns(4)P-binding protein FAPP1a-PH. White scale bar represents 10 μ m.

layer immediately below (Poteser et al., 2016), we co-expressed Hrs-2xFYVE-YFP-StRem1.3 with the vacuolar lumen marker SP-tagRFP-AFVY (Hunter et al., 2007). No depletion of SP-tagRFP-AFVY fluorescence was observed (Figure S3.6).

TP/MVB-PM tethering is limited by the cytoskeleton and ER network

The TP/MVB-PM tethering produced by the self-assembly of the BiFC complexes displayed a degree of order. For example, the observed patches often appeared to negatively stain long tracks. To test the hypothesis that these tracks corresponded to cortical microtubules, we co-expressed the cortical microtubule (MT) marker *Arabidopsis* Casein Kinase 1-Like 6 (ACK6) (Ben-Nissan et al., 2008) together with Hrs-2xFYVE-YFP-StRem1.3. As shown in Figure 3.8a, it was clearly evident that many tethered patches were separated by microtubules. In some cases, growing microtubules could be observed dividing a patch into two smaller patches (arrowed in Figure 3.8a). Similar results were also observed when the actin marker AtFimbrin1 (Wang et al., 2004) was co-expressed with Hrs-2xFYVE-YFP-StRem1.3, except that orthogonal imaging revealed that the actin cytoskeleton also formed a thin layer of meshwork underlying the patches (Figure 3.8b).

The cortical endoplasmic reticulum (ER) is a region of the ER closely juxtaposed to the PM in animal (Zhang et al., 2012) and plant (Sparkes et al., 2010, Stefano et al., 2014) cells. Using the cortical ER-marker SYT1 (Chapter 2)(Yamazaki et al., 2010), we could observe the relationship between the tethered TP/MVB patches and the cortical ER. As shown in Figure 3.9, when the tethered patches (Hrs-2xFYVE-tagRFP-StRem1.3) were small, they appeared localized within the gaps of the cortical ER network labeled by SYT1-YFP (Figure 3.9). When the patches were large, it appeared that the cortical ER was pushed aside, enlarging the gaps in the cortical ER network (Figure 3.9). For the most part the patches and the ER did not overlap.

TP/MVB-PM tethering is associated with two plant U-box (PUB) armadillo (ARM) repeat E3 ubiquitin ligases

Drechsel et al.(Drechsel et al., 2010) observed that *Arabidopsis* PUB (plant U-box) E3 ligase senescence-associated ubiquitin ligase 1 (SAUL1, also called AtPUB44) protein is exclusively targeted to the PM with a homogenous distribution. However,

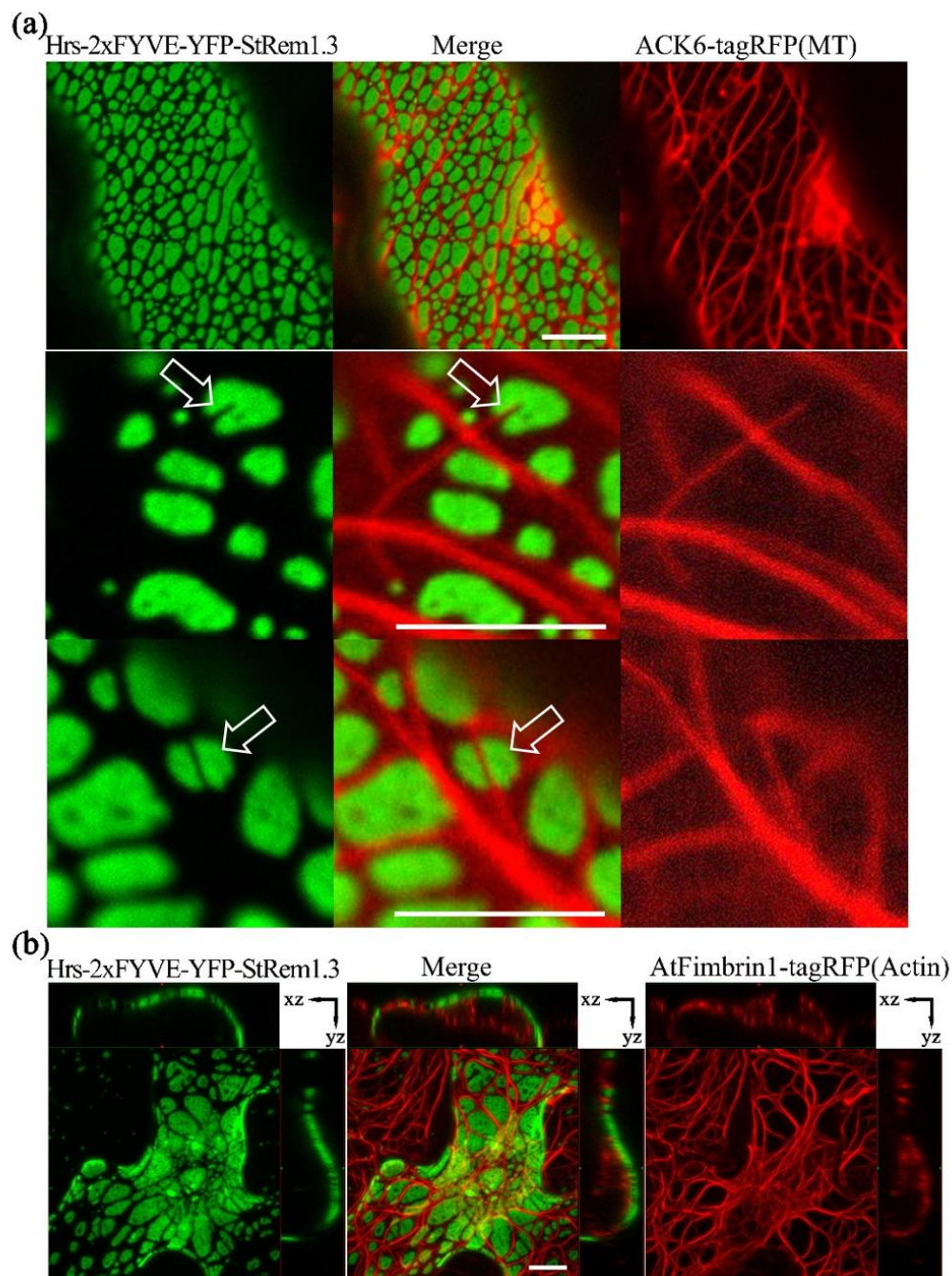


Figure 3.8 Relationship of membrane patches with the cytoskeleton in *N. benthamiana* leaf cortical cells.

(a) Relationship of membrane patches produced by Hrs-2xFYVE-YFP-StRem1.3 to the cortical microtubules labeled with tagRFP fused to *Arabidopsis* Casein Kinase 1-Like 6 (ACK6). Enlarged panels show examples of patches being divided by microtubules (arrowed). (b) Maximum intensity and orthogonal projections of cells exhibiting membrane patches produced by Hrs-2xFYVE-YFP-StRem1.3 and co-expressing the actin filament marker AtFimbrin1-tagRFP. White scale bar represents 10 μm .

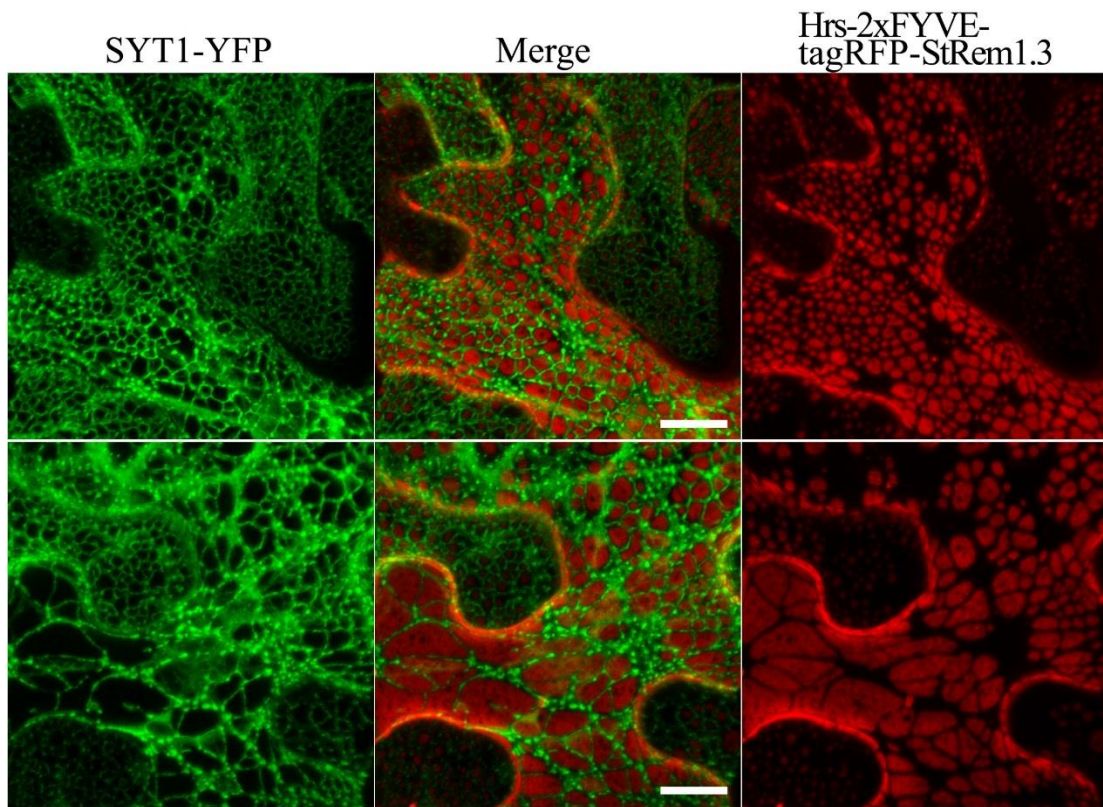


Figure 3.9 Relationship of membrane patches to cortical ER networks in *N. benthamiana* leaf cortical cells.

Patches were produced by expression of Hrs-2xFYVE-YFP-StRem1.3 and the ER was labeled by co-expression of the cortical ER-localized protein, *Arabidopsis* synaptotagmin1 (SYT1) fused with YFP. White scale bar represents 10 μm .

when its C-terminal ARM domain (repeats 7-11), was expressed as a YFP fusion protein, a heterogeneous pattern of large membrane patches was observed, similar to the patches we have described here. A similar result was also reported for its closest paralog AtPUB43 (Vogelmann et al., 2014). To investigate whether TP/MVB-PM tethering is associated with the patches observed with SAUL1 and AtPUB43, we carried subcellular co-localization experiments. When wild type SAUL1 was fused with YFP at the N terminus and transiently expressed in *N. benthamiana* cortical cells, the fluorescence of YFP-SAUL1 was uniformly distributed on the PM (Figure 3.10a) consistent with previous studies (Drechsel et al., 2010, Vogelmann et al., 2014). Furthermore, expressing YFP-tagged ARM repeats 7-11 of SAUL1 produced fluorescent signals distributed into patches (Figure 3.10a), again as previously observed (Drechsel et al., 2010, Vogelmann et al., 2014). Interestingly, when we co-expressed full-length SAUL1 with Hrs-2xFYVE in BiFC complexes, we also observed patches characteristic of TP/MVB-PM tethering, suggesting that SAUL1 could indeed participate in tethering (Figure 3.10a). To test this hypothesis further, we expressed Hrs-2xFYVE-YFP-StRem1.3 to produce MVB tethering and at the same time co-expressed tagRFP-SAUL1(ARM⁷⁻¹¹). As shown in Fig. 3.10b, we observed a full match of green and red fluorescence indicating that the SAUL1(ARM⁷⁻¹¹) patches fully coincided with the TP/MVB tethering produced by Hrs-2xFYVE-YFP-StRem1.3. Similar results were also observed with AtPUB43 (Figure S3.7). Moreover, we also observed complete overlap between patches produced by YFP-SAUL1(ARM⁷⁻¹¹) and tagRFP-AtPUB43(ARM⁷⁻¹¹), and between patches produced by Hrs-2xFYVE-YFP-StRem1.3 and tagRFP-AtPUB43(ARM⁷⁻¹¹) (Figure S3.7), indicating that SAUL1 and AtPUB43 had similar capabilities.

When tagRFP-SAUL1(ARM⁷⁻¹¹) was co-expressed with the MVB and TP markers ARA6, 2xFYVE, AtDMP1, and TPK1 tethering to both the TP and to the MVBs was observed (Figure S3.8). Thus both SAUL1(ARM⁷⁻¹¹) and AtPUB43(ARM⁷⁻¹¹) appear to have the ability to bind both the PM and also the TP or MVBs when expressed by themselves. One difference between the tethered patches produced by StREM1.3 BiFC complexes and those produced by SAUL1(ARM⁷⁻¹¹) and AtPUB43(ARM⁷⁻¹¹) is that the latter patches were commonly observed clustered in

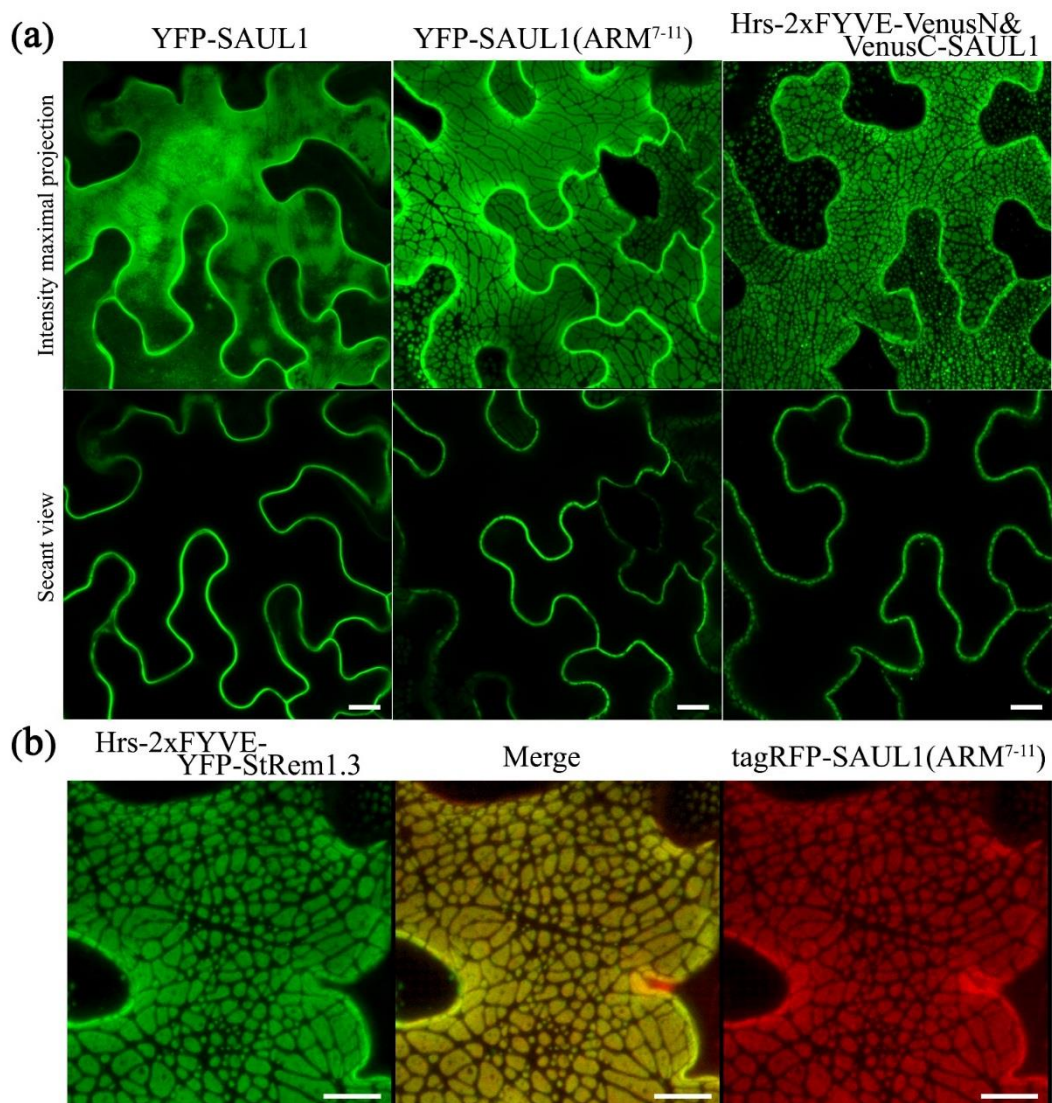


Figure 3.10 Association of membrane patches with plant U-box (PUB) armadillo (ARM) repeat E3 ubiquitin ligases in *N. benthamiana* leaf cortical cells.

(a) Subcellular localization of YFP-tagged full length SAUL1 (left panels) and YFP-tagged SAUL1 C-terminal ARM repeats 7-11 (center panels). Right panels: membrane patches produced by BiFC complexes containing full length VenusC-SAUL1 and Hrs-2xFYVE-VenusN. (b) Co-localization of membrane patches created by expression of Hrs-2xFYVE-YFP-StRem1.3 and by expression of tagRFP-SAUL1(ARM⁷⁻¹¹). White scale bar represents 10 μ m.

sub-regions of the PM, rather than uniformly across the surface (e.g. in Figure S3.8). A further contrast to the tethering produced by StREM1.3 BiFC complexes, was that the PM-associated protein BIK1 and the PtdIns(4)P biosensor FAPP1a were enriched into the patches produced by tagRFP-SAUL1(ARM⁷⁻¹¹) (Figure S3.8), in contrast to the exclusion observed above when these two proteins were co-expressed with Hrs-2xFYVE-tagRFP-StRem1.3 (Figure 3.7), suggesting that the SAUL1 and AtPUB43 patches might aggregate different sub-domains of the PM than the StREM1.3 BiFC complexes. Together these results indicate that the patches produced by ARM repeats 7-11 of SAUL1 (AtPUB44) and AtPUB43 result from TP/MVB-PM tethering, raising the possibility that there may be conditions when full length SAUL1 and AtPUB43 may naturally regulate TP/MVB-PM tethering.

Discussion

In this study, in the process of mapping the distribution of PtdIns(3)P relative to plasma membrane (PM) markers, we observed that BiFC complexes containing both a PtdIns(3)P binding protein, such as VAM7-PX or Hrs-2xFYVE, and a PM-localized peripheral membrane protein such as the remorin protein StRem1.3 or BIK1, were distributed in large but heterogeneous PM patches (Figures 3.2 and 3.3). Proteins that localized to the PM via PtdIns(4)P-binding, such as FAPP1 and Osh2, could also participate in the formation of the patches. Control experiments with mutant proteins confirmed that both PtdIns(3)P-binding and PM-binding by the respective partners were essential for the formation of these patches. By analogy with our recent discovery that BiFC complexes could produce ER-PM tethering, we hypothesized that BiFC complexes that combine PM- and PtdIns(3)P-binding might produce tethering of MVBs and the tonoplast to the PM. We found support for this hypothesis by showing that MVB-associated proteins such as Rab5-type GTPases RHA1, ARA6, and ARA7 as well as Rab7-type GTPase RABG3f could all induce the observed patches when partnered with StRem1.3 in BiFC complexes (Figures 3.4) (We observed that all of these proteins also stained the tonoplast, albeit at lower intensity). An alternative hypothesis, that the BiFC complexes triggered aggregation of lipid micro-domains, was not supported by these observations. In particular, the ability of the observed patches to exclude cytoplasmic markers was consistent with TP/MVB tethering, but not with

aggregation of lipid microdomains. As in the case of ER-PM tethering, TP/MVB-PM tethering could restrict the distribution of PM-associated and tonoplast-associated proteins. Our results raise an interesting question of whether TP/MVB-PM tethering can occur as a natural process.

In eukaryotic cells, membrane-bound organelles are generally segregated to support their individual cellular functions. However functional communications among organelles may occur via vesicular transport most notably in the secretory and endosomal trafficking pathways (Bonifacino and Glick, 2004). Alternatively, appositions between two organelles, often referred to as membrane contact sites (MCSs) may enable inter-organelle communication (Prinz, 2014). MCSs are stabilized by multi-domain tethering proteins which can bridge the membranes of two organelles without promoting their fusion (Helle et al., 2013, Prinz, 2014, Islinger et al., 2015). To date, specific tether proteins have been characterized for MCSs between ER and endosomes/lysosomes/vacuoles/MVBs, ER and mitochondria, ER and peroxisomes, ER and Golgi, ER and chloroplasts, ER and phagosomes, Golgi and Golgi, PM and ER, and PM and mitochondria (Prinz, 2014, Eden, 2016). However, currently there is no evidence for tethering proteins that naturally establish MCSs between the PM and MVBs or the tonoplast. Here, our observations with *Arabidopsis* PUB E3 ubiquitin ligase SAUL1 and its paralog AtPUB43 (Figure 3.10; Figure S3.7) suggest that under some circumstances they might function as tethers mediating docking of MVBs or the tonoplast to the PM. Although full length SAUL1 and AtPUB43 only promoted tethering when joined to a MVB-binding protein, the C-terminal membrane binding domain (ARM7-11) of each protein could promote tethering when expressed alone. Thus we speculate that there may be regulatory events such as phosphorylation or ligand binding that might modify the full length proteins to allow their C-terminal domains to bind to MVBs and the tonoplast to promote tethering.

A member of the PUB family of E3 ubiquitin ligases, SAUL1 has been reported to be involved in the regulation of senescence, cell death, and PAMP-triggered immunity (Drechsel et al., 2010, Disch et al., 2015, Tong et al., 2017). In contrast to other PUB E3 ligases, SAUL1 and its closest paralog, AtPUB43, are exclusively located on the PM (Drechsel et al., 2010, Vogelmann et al., 2014), which we confirmed

in this study. SAUL1 and AtPUB43 carry ARM repeats, which are thought to mainly function as interfaces for protein-protein interactions (Coates, 2003). ARM repeats 7-11 of SAUL1 and AtPUB43 mediate membrane binding by these proteins, and alone can trigger tethering. However, it is unknown whether these processes involve direct membrane interactions or whether contacts with other membrane proteins are involved, or both. It also remains unknown whether protein ubiquitination by E3 ligases such as SAUL1 and AtPUB43 can regulate membrane or vesicle interactions.

Docking of vesicles to the PM is a normal part of the secretion process, releasing cellular molecules and regulating the composition of plasma membrane (Grant and Donaldson, 2009, Hsu and Prekeris, 2010, Donovan and Bretscher, 2015, Wu and Guo, 2015). These vesicles typically originate from the TGN or from recycling endosomes. In plants, TGNs function as early endosomes as well as the sorting hub for secretory vesicles (Scheuring et al., 2011, Paez Valencia et al., 2016). The targeting and tethering of secretory vesicles to the PM involves the octameric exocyst complex (Hála et al., 2008, Žárský et al., 2013). An alternative secretion process that has gained renewed attention recently, especially in the context of plant-microbe interactions, involves membrane-bound vesicles referred to as exosomes that are released into the intercellular environment. Exosomes originate from a variety of sources, particularly MVBs, and appear to be involved in transport of a variety of chemicals and proteins into the extracellular space. They also have the potential to deliver their contents into adjacent cells, including those of invading microbes. The release of exosomes appears to result from membrane fusion between MVBs and the PM (Théry et al., 2002, Hanson and Cashikar, 2012, Colombo et al., 2014). In plants, exosomes are also produced from the MVBs, and in particular are found to be increased in abundance in response to biotic or abiotic stress (An et al., 2007, Samuel et al., 2015, Rutter and Innes, 2017). However, little is known about the machinery of this process. More recently, a membrane protein component of exosomes known as syntaxin PEN1 was reported to be associated with ARA6, possibly to promote membrane fusion between the MVBs and the PMs (Ebine et al., 2011, Nielsen et al., 2012). Notably, here we found that co-expressing PM-associated proteins such as remorin protein StRem1.3 together with ARA6 in BiFC complexes resulted in tethering of MVBs to the PM. It remains to be determined if a

similar process is involved in exosome release. Likewise, it will be of interest to determine if SAUL1 and AtPUB43 may play a tethering role in exosome release.

This study highlights the risks of using the BiFC assay to study protein-protein or protein-membrane interactions in plants, which could lead to alterations in cellular structure and membrane organization. At the same time, our results open the possibility of using tethering as a tool to explore or manipulate the arrangement of membrane proteins and organelles. For example, our observation that the patches of tethering can exclude or include different proteins and lipids on the PM and tonoplast may assist in distinguishing different membrane subdomains.

This study was initiated with the aim of thoroughly documenting the distribution of PtdIns(3)P in plant cells and establishing unambiguously whether PtdIns(3)P occurred on the cytoplasmic face of the PM. The results presented here reveal that PtdIns(3)P is present on a wide variety of vesicles, the MVB, and also the tonoplast. However, based on the inability of PtdIns(3)P-binding proteins to provide the PM attachment required for tethering, in contrast to PtdIns(4)P-binding proteins, we find no evidence for PtdIns(3)P occurring on the cytoplasmic face of the PM. This conclusion is in agreement with the conclusion of chapter 2, where it was shown that PtdIns(3)P-binding proteins could not provide the PM attachment required for ER-PM tethering, whereas proteins that bound PtdIns(4)P and PtdIns(4,5)P₂ could do so.

Materials and Methods

Plant Material

Both *N. benthamiana* and *A. thaliana* plants were grown in soil (Fafard® 4M Mix). *N. benthamiana* plants were provided with a 14 hr photoperiod at 25°C. Fully expanded leaves at 5 weeks were used for *A. tumefaciens* infiltration. *A. thaliana* seeds were sown in soil and stratified at 4°C for 3 days, then the seedlings were grown in a growth chamber with a 12 hr photoperiod at 20°C for 4 weeks before mesophyll protoplast isolation.

Cloning and Construction

DNAs encoding VAM7-PX, Hrs-2xFYVE, GmPH1, FLS2, BIK1, PBS1, ACK6, and FAPP1-PH were sub-cloned from constructs as reported previously (Ben-Nissan et al., 2008, Lu et al., 2010, Meng et al., 2015, Helliwell et al., 2016). DNAs encoding AtRem1.4 (AT5G23750.1), RHA1 (AT5G45130.1), ARA7 (AT4G19640.1), ARA6 (AT3G54840.1), RABG3f (AT3G18820.1), SYT1(AT2G20990.1), AtDMP1(AT3G21520.1), AtTPK1 (AT5G55630.1), CPK21 (AT4G04720.1), AtFlotillin1 (AT5G25250), and AtFimbrin1 (At4g26700.1) were amplified from Col-0 cDNA. Genes encoding StRem1.3 (U72489.1) and Osh2p (NM_001180078) were synthesized by GenScript Corporation. The endogenous promoter proAtRem1.4 was cloned from *A. thaliana* genomic DNA, encompassing 1.6 kb upstream from the start codon of AtRem1.4. All PCR amplifications were performed by High-Fidelity DNA polymerase (CloneAmp™ HiFi PCR Premix, TaKaRa Bio) using oligonucleotides as listed in Table 3.1. All PCR products were recombined into either pDONR207-VenusN, pDONR207-VenusC, or pDON207-xFPs which were derived from Gateway vector pDONR207, by In-Fusion® HD Cloning (TaKaRa Bio). The site-specific mutations of VAM7-PX, Hrs-2xFYVE, GmPH1, StRem1.3*, BIK1*, and FAPP1-PH* were introduced into their pDONR207 vectors using appropriate oligonucleotides in a PCR reaction to amplify the entire vector template. By using the Gateway® LR reaction (Thermo Fisher scientific Inc.), all pDONR207 vectors were subsequently transferred to a destination/expression binary vector, either pmAEV (for cytoplasmic expression), or psAEV (for PM or vacuole targeting), in which the Cauliflower Mosaic Virus (CaMV) 35S promoter confers constitutive expression in plant cells. pCambia3301 was utilized to construct the endogenous-promoter expression vector pCambia3301-ProAtRem1.4 by replacing the 35S promoter with proAtRem1.4 using infusion insertion between the BspEI and NcoI sites. All these plasmid constructs were confirmed by DNA sequencing at Center for Genome Research and Biocomputing (Oregon State University).

Transient expression in *N. benthamiana* leaves and *A. thaliana* protoplasts

The procedures to introduce expression vectors into *A. tumefaciens* strain GV3101, and infiltrate transformed *A. tumefaciens* into 5-week-old *N. benthamiana*

Table 3.1 Primer designed and used in chapter 3.

Oligo Name	Forward primer(5'-3')	Reverse primer(5'-3')	Application notes
Hrs-2xFYVE	GCCGGTAGCGCTAGCGAATTTG AAAGCGATGCGATGTTTG	AAGCTGGGTGATATCTTACTTCGG TTGCAGGTCCACGGCC	FP-Hrs-2xFYVE
Hrs-2xFYVE	AGCAGGCTCCTCGCGAATGGAA ATTTGAAAGCGATGCGATGTTT G	CTCCTCCACCTCTAGACTTCGGTTG CAGGTCCACGGCC	Hrs-2xFYVE-FP
VAM7-PX	GCCGGTAGCGCTAGCGCAGCTA ATTCTGTAGGGAAAATG	AAGCTGGGTGATATCTTATAGATG CTGCTGTGACTTTTC	FP-VAM7-PX
VAM7-PX	AGCAGGCTCCTCGCGAATGGCA GCTAATTCTGTAGGGAAAATG	CTCCTCCACCTCTAGATAGATGCT GCTGTGACTTTTC	VAM7-PX-FP
GmPH1	GCCGGTAGCGCTAGCATGGCG AGCCTGTGGCGCGCG	AAGCTGGGTGATATCTTAGCGCTT GGAGGAGTTGTTATC	FP-GmPH1
GmPH1	AGCAGGCTCCTCGCGAATGGCG AGCCTGTGGCGCGCG	CTCCTCCACCTCTAGAGCGCTTGG AGGAGTTGTTATC	GmPH1-FP
StRem1.3	GCCGGTAGCGCTAGCGCAGAA TTGGAAGCTAAG	AAGCTGGGTGATATCTTAAAATAT TCCAAGGATTTTC	FP-StRem1.3
FLS2-FP	AGCAGGCTCCTCGCGAATGAAG TACTCTCAAAG	CTCCTCCACCTCTAGAACTTCTCG ATCCTCGTT	FLS2-FP
BIK1	AGCAGGCTCCTCGCGAATGGGT TCTTGCTTCAGTTCTCGAG	CTCCTCCACCTCTAGACACAAGGT GCCTGCCAAAAGGTT	BIK1-FP
PBS1	AGCAGGCTCCTCGCGAATGGGT TGTTTCTCGTGTGTTTGATTC	CTCCTCCACCTCTAGACCCGGTACT GTTGCTCTCTGAAGTAC	PBS1-FP
ACK6	GCCGGTAGCGCTAGCAGTAGTG CCAGGTCCCATTCC	AAGCTGGGTGATATCTCATTGCG GATCGAAAGAAG	FP-ACK6
FAPP1	AGCAGGCTCCTCGCGAATGGAA GGTGTCTGTA	CTCCTCCACCTCTAGAGCGAGTAT CGGTCAGACACG	FAPP1-FP

AtRem1.4	GGCGGTAGCGCTAGCATGGCTG AAGAGGAACCGAAG	AAGCTGGGTGATATCTCACATGCA TCCGAAAAGCT	FP-AtRem1.4
RHA1	GGCGGTAGCGCTAGCGCTAGCT CTGGAAACAAGAACATC	AAGCTGGGTGATATCCTAAGCACA ACACGATGAACTCACTGC	FP-RHA1
ARA7	GGCGGTAGCGCTAGCGCTGCAG CTGGAAACAAGAGC	AAGCTGGGTGATATCCTAAGCACA ACAAGATGAGCTCACTGC	FP-ARA7
ARA6	AGCAGGCTCCTCGCGAATGGGA TGTGCTTCTTCTTCCAGATAG	CTCCTCCACCTCTAGATGACGAAG GAGCAGGACGAGGTAG	ARA6-FP
RABG3f	GGCGGTAGCGCTAGCCCGTCCC GTAGACGTACCCTCC	AAGCTGGGTGATATCTTAGCATTC ACACCCTGTAGACCTCTG	FP-RABG3f
SYT1	AGCAGGCTCCTCGCGAATGGGC TTTTTCAGTACGATACTAG	CTCCTCCACCTCTAGAAGAGGCAG TTCGCCACTCGAGCT	SYT1-FP
AtDMP1	AGCAGGCTCCTCGCGAATGTCC GAAACTTCTTTGCTCATAACC	CTCCTCCACCTCTAGAGGCAGAGA CCGAGGCTTTCTTGGTC	AtDMP1-FP
AtTPK1	AGCAGGCTCCTCGCGAATGTCG AGTGATGCAGCTCGTACGCCAT TG	CTGCCTCCTCCACCTCTAGACCTTT GAATCTGAGACGTGGTCTGAGC	AtTPK1-FP
CPK21	AGCAGGCTCCTCGCGAATGGGT TGCTTCAGCAGTAAACAC	CTCCTCCACCTCTAGAATGGAATG GAAGCAGTTTCCCCTG	CPK21-FP
AtFlotillin1	AGCAGGCTCCTCGCGAATGTTC AAAGTTGCAAGAGCGTCAC	CTCCTCCACCTCTAGAGCTGCGAG TCACTTGCTTCGGTTCC	AtFlotillin1-FP
AtFimbrin1	GGCGGTAGCGCTAGCGAGATC GTTGAAGGATCTTCAAC	AAGCTGGGTGATATCTTACTCTGA GACCGTGGTGATTTCAGAAAC	FP-AtFimbrin1
Osh2	GGCGGTAGCGCTAGCCCAAGTA ATAACGTGACACCCGAAATC	AAGCTGGGTGATATCTCATGGGAG GCTACCTTGGGTTTTGCTGTG	FP-Osh2
AtRem1.4	GTACCTAACATCCCATGGCAGC TAATTCTGTAGGGAAAATG	GTCACCTGTAATTCACACATCTCA CATGCATCCGAAAAGCTTTTTG	Chimeric construction
VAM7-PX*	AAAGAGTATGCCGAGTTTTGGA AACTGAAGACACG	GGCATACTCTTTGTAAAGGCGCTT GTTTG	R40E, S42A

Hrs-2xFYVE* 1	TCTTCAAGCAGTTGTTCCGCCT GCGGACAGATTTTCTGTGG	GGAACAACCTGCTTGAAGAGGTCAC AACACCAAACCTGAACAC	R34S, K35S, H36S, H37S, R39S, R116S, K117S, H118S, H119S, R121S
Hrs-2xFYVE* 2	TCAAGCAGTTCCTGTTCAGCAT GCGGCCAAATCTTTTGTGG	TGAACAGGAACTGCTTGATGTAAC GACTCCGAACTGCACG	R34S, K35S, H36S, H37S, R39S, R116S, K117S, H118S, H119S, R121S
GmPH1*	GTACATCAAGACCTGGGAGCGC GAGTGGTTCGTCCTCAAGC	CAGGTCTTGATGTAICTCGCCCTGCT CGGTGAGCCAGC	K34E, R43E, R45E
BIK1*	TCGCGAATGGCTTCTTGCTTCA GT	AGAAGCCATTCGCGAGGAGCCTGC	G1A
StRem1.3*-1	CATCATCATAAATCTCGTTCTA CTGTGACTAGTCCA	AGATTTATGATGATGCTCCTCTGCC TTGAGAAGATC	L179H, A180H, A181H, Y184S, A185S, G187V, A189A, L194S, G195Q, I196Q, F197Q
StRem1.3*-2	CAACAGCAATCTAGATGAGATA TCACCCAG	TTGCTGTTGAGAGATTTTCTTTGGA CTAGTC	L179H, A180H, A181H, Y184S, A185S, G187V, A189A, L194S, G195Q, I196Q, F197Q
AFVY	GGTGCATTTGTTTATTAATCA CCCAGCTTTCTTGACAAAGTT G	ATAAACAATGCACCTCTAGAAGG CGCGCCTGCGGCCGCCTTG	SP-tagRFP-AFVY
AtPUB43	GGCGGTAGCGCTAGCATGGCTG GAAGTGGAAGTTGGGATG	AAGCTGGGTGATATCCTAACCAAT GTTGGTGAATATAACCAGAGAAG	FP-AtPUB43
SAUL1	GGCGGTAGCGCTAGCGTTGGAA GCTCGGATGGTG	AAGCTGGGTGATATCCTATGCGAT GTTTGGGAATATACTTGAG	FP-SAUL1
ARM(AtPUB43)	GGCGGTAGCGCTAGCCCAGTTG GTCCTCATCACCAG		FP-ARM(AtPUB43)
ARM(SAUL1)	GGCGGTAGCGCTAGCGGGTATG ACTTTGACAAAGCCA		FP-ARM(SAUL1)

ProAtRem1.4	CAACAAAGGGTAATATCCGGA ACCAAAGTACCAAGTTACT ATATTAAG	TACCCTCAGATCTACCATGGGATG TTAGGTACAACAACCTAAAGATTAC AAAG	pCambia3301- ProAtRem1.4
-------------	--	---	-----------------------------

leaves were carried out as described previously{Xiong, 2014 #863}. *A. tumefaciens* cells were infiltrated at OD₆₀₀ of 0.1 for the expression of the full-length fluorescent protein tagged proteins; for co-expression of BiFC constructs, two *A. tumefaciens* cultures with OD₆₀₀ of 0.2 respectively, were equally mixed together to reach the final OD₆₀₀ at 0.1. All infiltrated *A. tumefaciens* cells were suspended in MES buffer (10 mM MgCl₂, 10mM MES PH5.7, and 100uM acetosyringone). *N. benthamiana* leaves were imaged at 3 days post infiltration. *A. thaliana* mesophyll protoplasts were extracted from 4-week-old seedlings, and 10 µg of plasmid DNA in total was used for each transformation assay which was performed as described (Yoo et al., 2007). Protoplasts were incubated overnight in W5 buffer at 25°C before observation.

Live-cell imaging by confocal microscopy and image analysis

FM 4-64 (Thermo Fisher scientific Inc.) staining used a concentration of 10 µM and was performed as previously described (Günl et al., 2011). All microscopy images were obtained using a ZEISS LSM 780 NLO confocal microscope system equipped with a 458-nm argon laser for CFP (emission wavelength 560-509 nm), a 514-nm argon laser for YFP and Venus (emission wavelength 518-553 nm), and a 561 nm Diode Pumped Solid State (DPSS) laser for tagRFP and FM4-64 (emission wavelength 562-640 nm). For time-lapse imaging, movies were taken at a combined capture time of 0.97 s per frame. For 3D reconstruction, slice thickness in the z-axis direction of scanning was optimized at 0.6 µm. All microscopy images were processed through ZEN2 (Blue edition) program.

Supplementary Figures

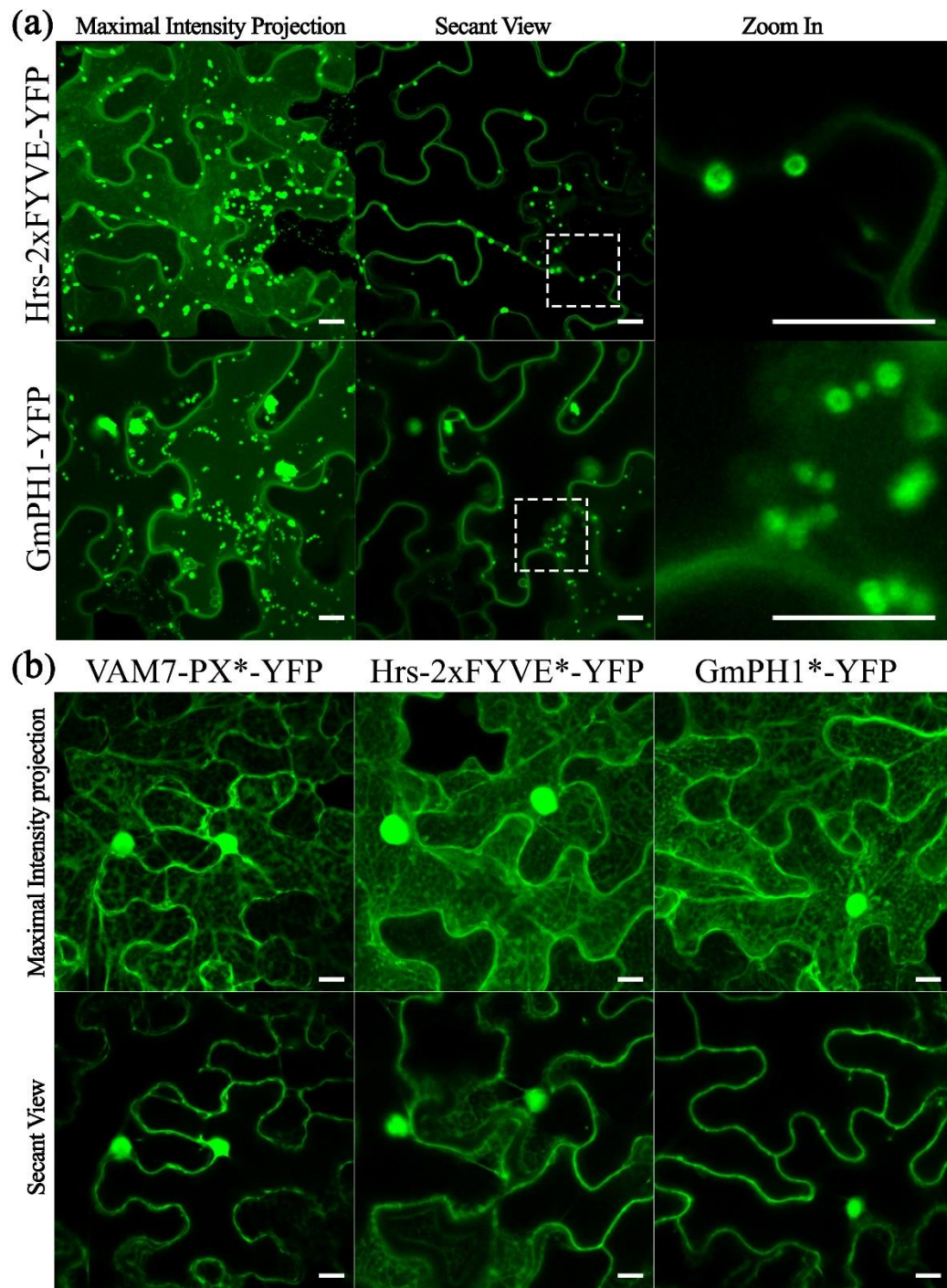


Figure S3.1 Subcellular localizations of PtdIns(3)P biosensors and non-binding mutants in *N. benthamiana* leaf cortical cells.

(a) Localization of Hrs-2xFYVE-YFP and GmPH1-YFP. Dashed boxes showed regions enlarged in the right panels. (b) Localization of biosensor proteins, VAM7-PX*-YFP, and Hrs-2xFYVE*-YFP, and GmPH1*-YFP, carrying point mutations that eliminate their PtdIns(3)P binding. White black bar represents 10 μ m.

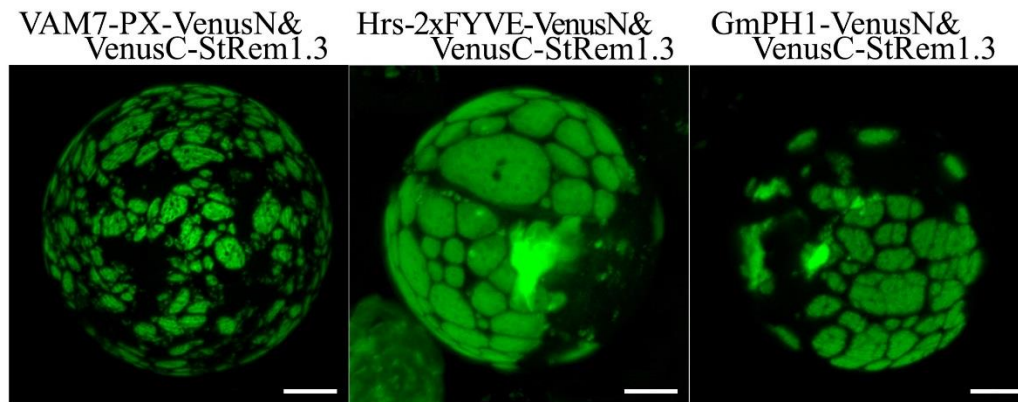


Figure S3.2 Co-expression of PtdIns(3)P biosensors and StRem1.3 produces large membrane patches on the PM of *A. thaliana* mesophyll protoplasts.

VenusC–StRem1.3 was transiently co-expressed with PtdIns(3)P biosensors VAM7-PX-VenusN, Hrs-2xFYVE-VenusN or GmPH1-VenusN. Scale is identical in all panels; white bar represents 10 μ m.

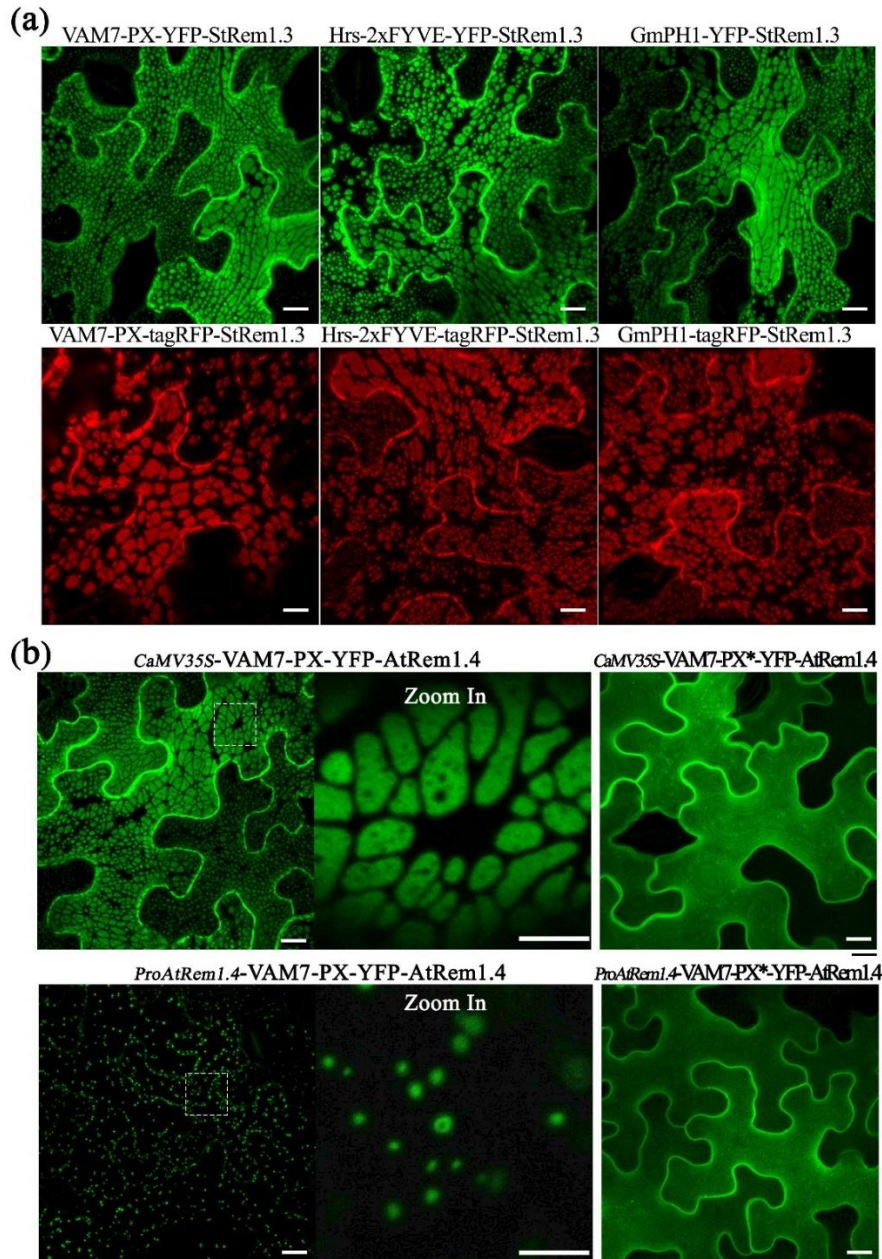


Figure S3.3 Subcellular localization of trifunctional fusion proteins in *N. benthamiana* leaf cortical cells.

(a) Trifunctional fusion proteins contained a PtdIns(3)P biosensor fused to YFP or tagRFP and also to StRem1.3, in that order. Expression of six fusion proteins in *N. benthamiana* cells produced membrane patches without the use of BiFC. (b) Expression level determines the sizes of patches produced by trifunctional fusion protein VAM7-PX-YFP-AtRem1.4. Expression was driven by either the native promoter ProAtRem1.4 or the highly active CaMV35S promoter. Mutations in the PtdIns(3)P binding site of VAM7-PX*-YFP-AtRem1.4 abolishes the formation of patches with either promoter. The white scale bar represents 10 μ m.

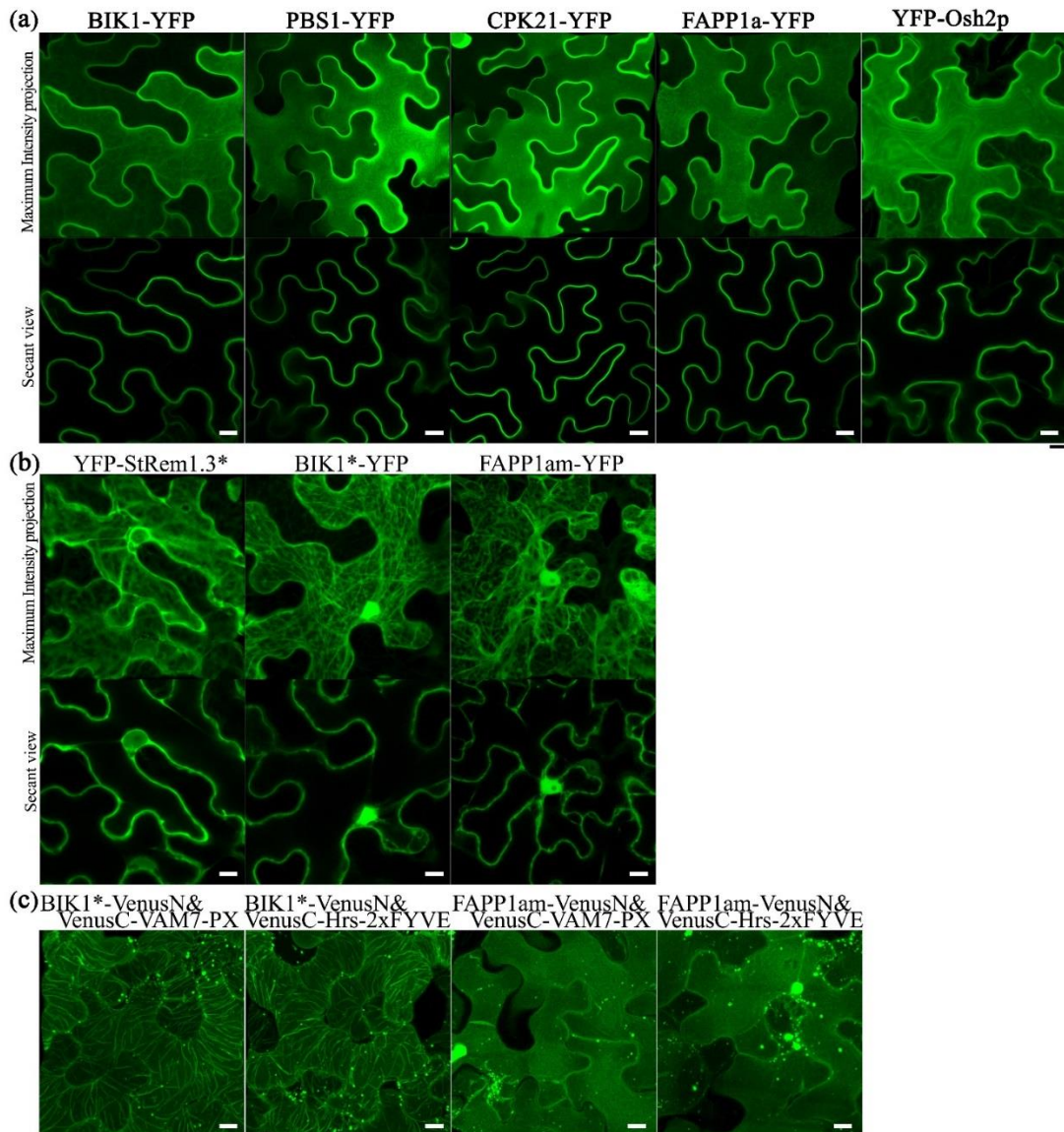


Figure S3.4 Subcellular localizations of wildtype and mutant plasma membrane proteins and PtdIns(4) biosensors in *N. benthamiana* leaf cortical cells.

(a) Localization of YFP-fused peripheral membrane proteins, BIK1, PBS1, and CPK21, and PtdIns(4) biosensors, FAPP1a and Osh2. (b) Localization of YFP-fused mutant versions of PM proteins and PtdIns(4)P biosensors (StRem1.3*, BIK1*, and FAPP1a*) carrying mutations in residues required for binding to the PM or to PtdIns(4)P respectively. (c) Localization of BiFC complexes formed by co-expression of BIK1*-VenusN or FAPP1a-PH*-VenusN with either VenusC-VAM7-PX or VenusC-Hrs-2xFYVE. White scale bar represents 10 μm.

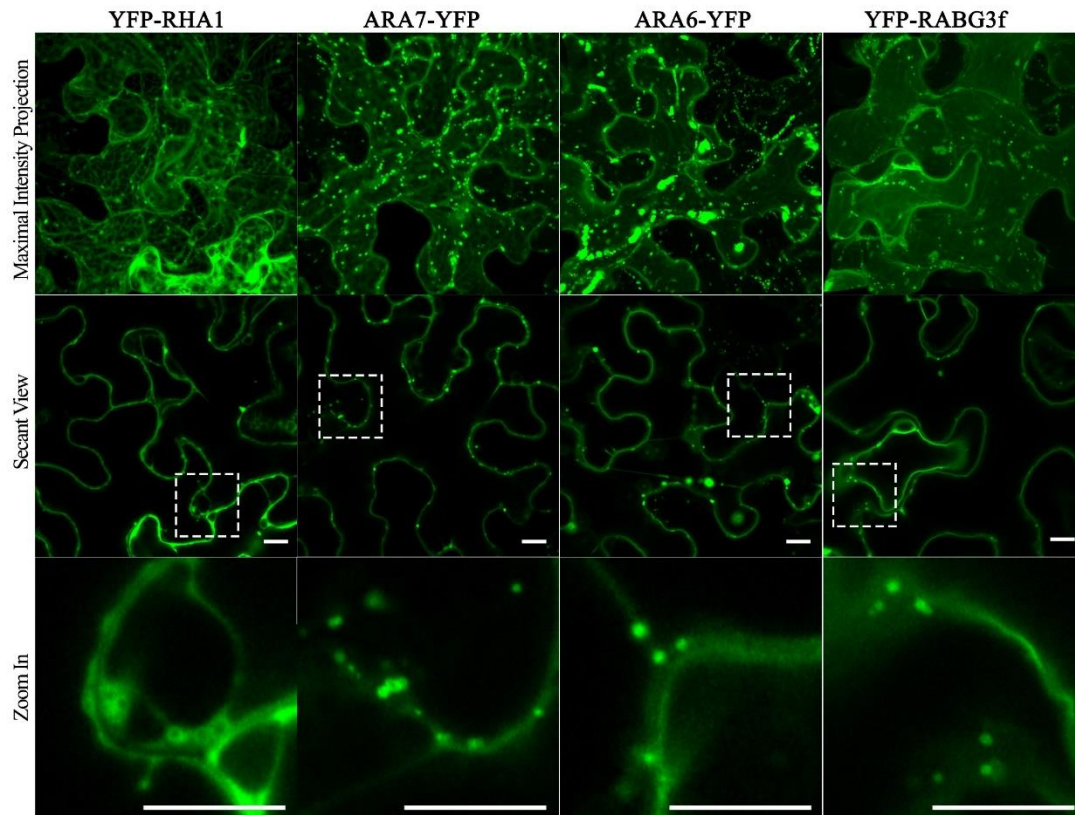


Figure S3.5 Subcellular localizations of proteins associated with MVBs and the tonoplast in *N. benthamiana* leaf cortical cells.

Rab5-type GTPase RHA1, ARA7, ARA6, and Rab7-type GTPase RABG3f were fused with YFP. Dashed boxes indicate regions enlarged in bottom panels. The white scale bar represents 10 μm .

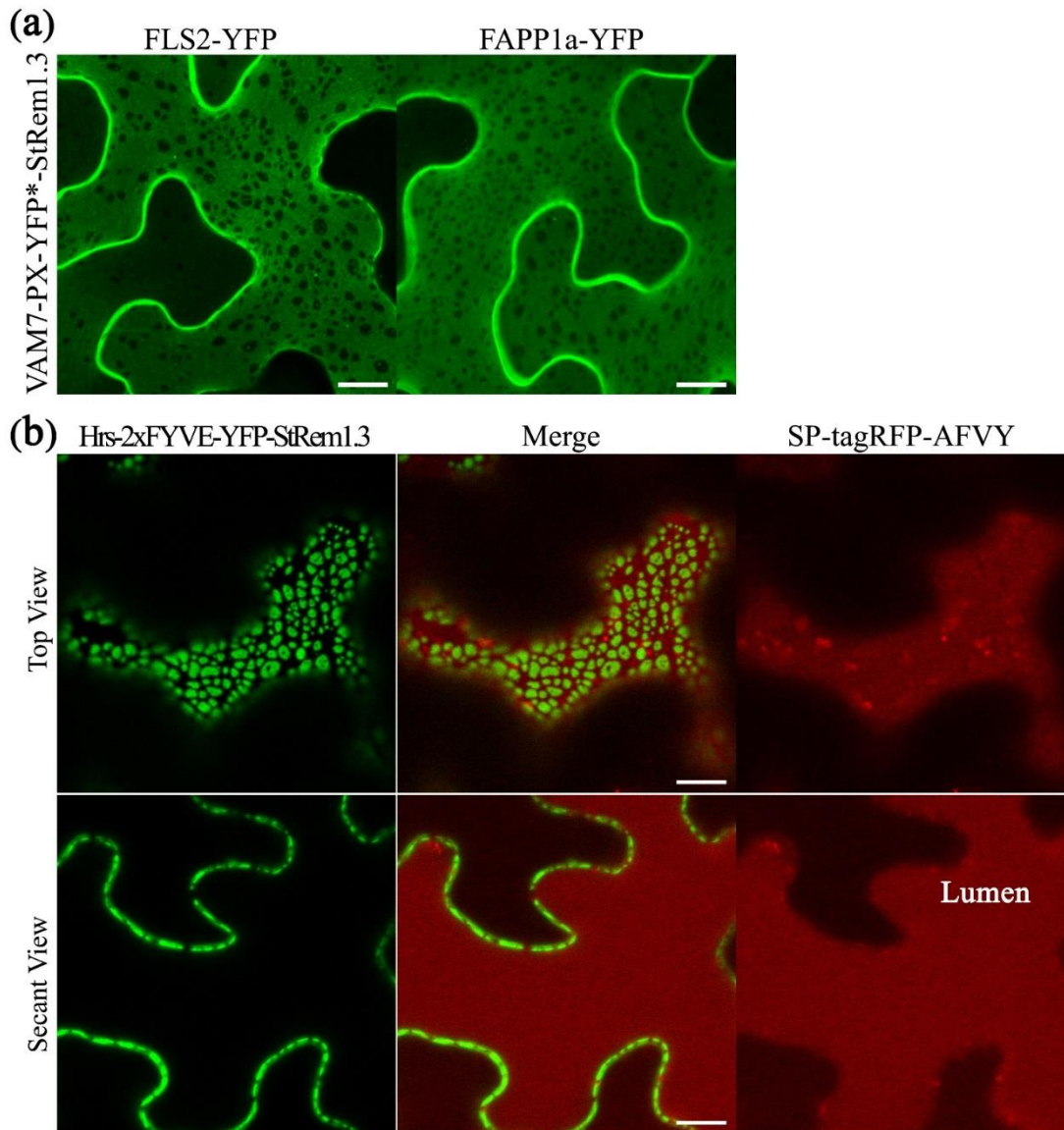


Figure S3.6 Exclusion of PM proteins by membrane patches in *N. benthamiana* leaf cortical cells is not an artifact of confocal microscopic image analysis.

(a) Non-fluorescent membrane patches were produced by expression colorless mutant VAM7-PX-YFP*-StRem1.3. These patches excluded PM-localized FLS2-YFP and FAPP1a-PH-YFP. (b) The presence of fluorescent membrane patches produced by Hrs-2xFYVE-YFP-StRem1.3 did not affect coincident visualization of vacuolar lumen marker SP-tagRFP-AFVY. White scale bar represents 10 μm for all panels.

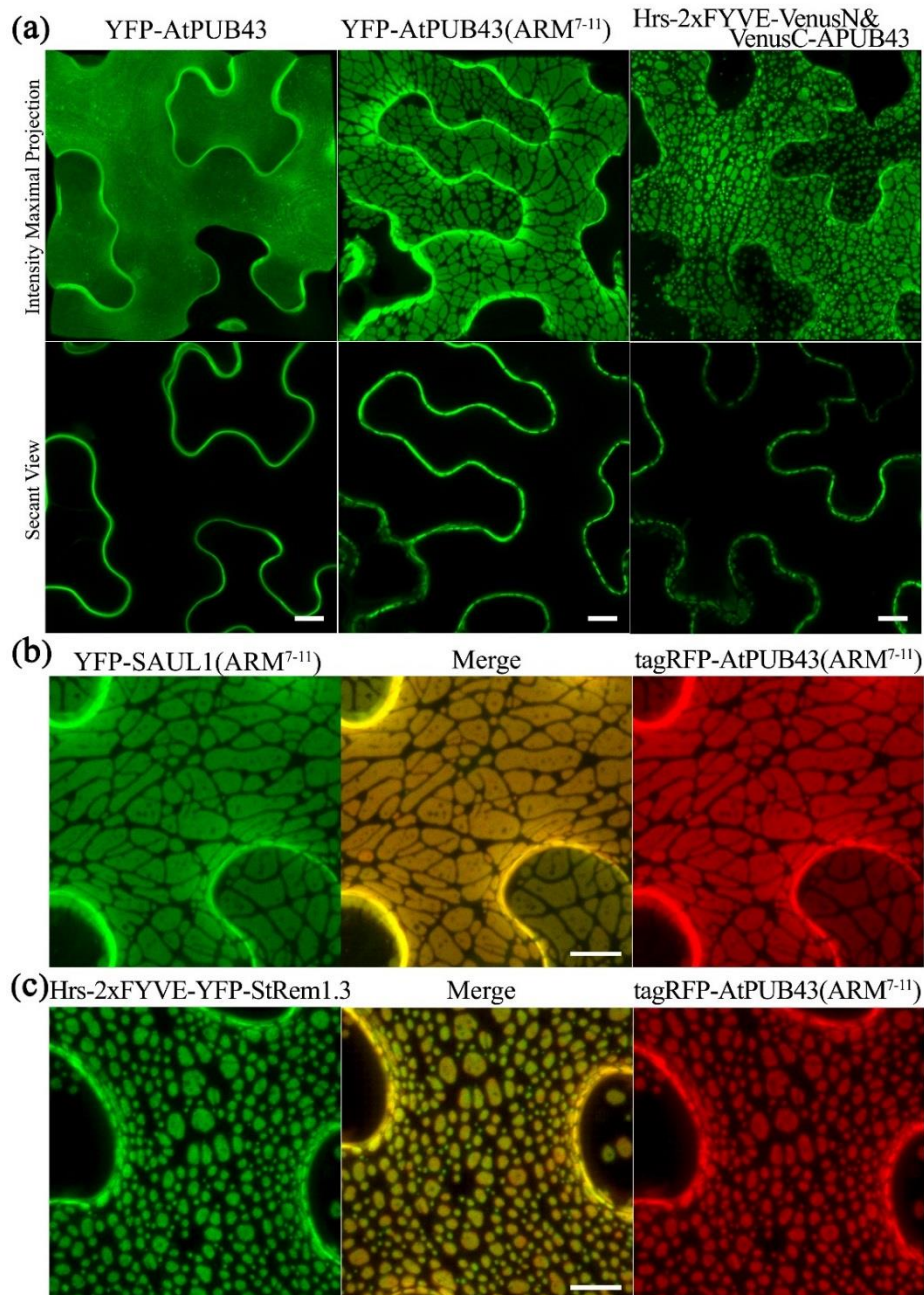


Figure S3.7 Membrane patches produced by YFP-AtPUB43 and YFP-SAUL1 in *N. benthamiana* leaf cortical cells.

(a) Subcellular localization of YFP-tagged full length AtPUB43 (left panels), and YFP-tagged AtPUB43 C-terminal ARM repeats 7-11 (center panels). Right panels: membrane patches produced by BiFC complexes containing full length VenusC-AtPUB43 and Hrs-2xFYVE-VenusN. **(b)** Co-localization of membrane patches produced by expression of YFP-SAUL1(ARM⁷⁻¹¹) and tagRFP-AtPUB43(ARM⁷⁻¹¹). **(c)** Co-localization of membrane patches produced by expression of Hrs-2xFYVE-YFP-StRem1.3 and tagRFP-AtPUB43(ARM⁷⁻¹¹). White scale bar represents 10 μ m in all panels.

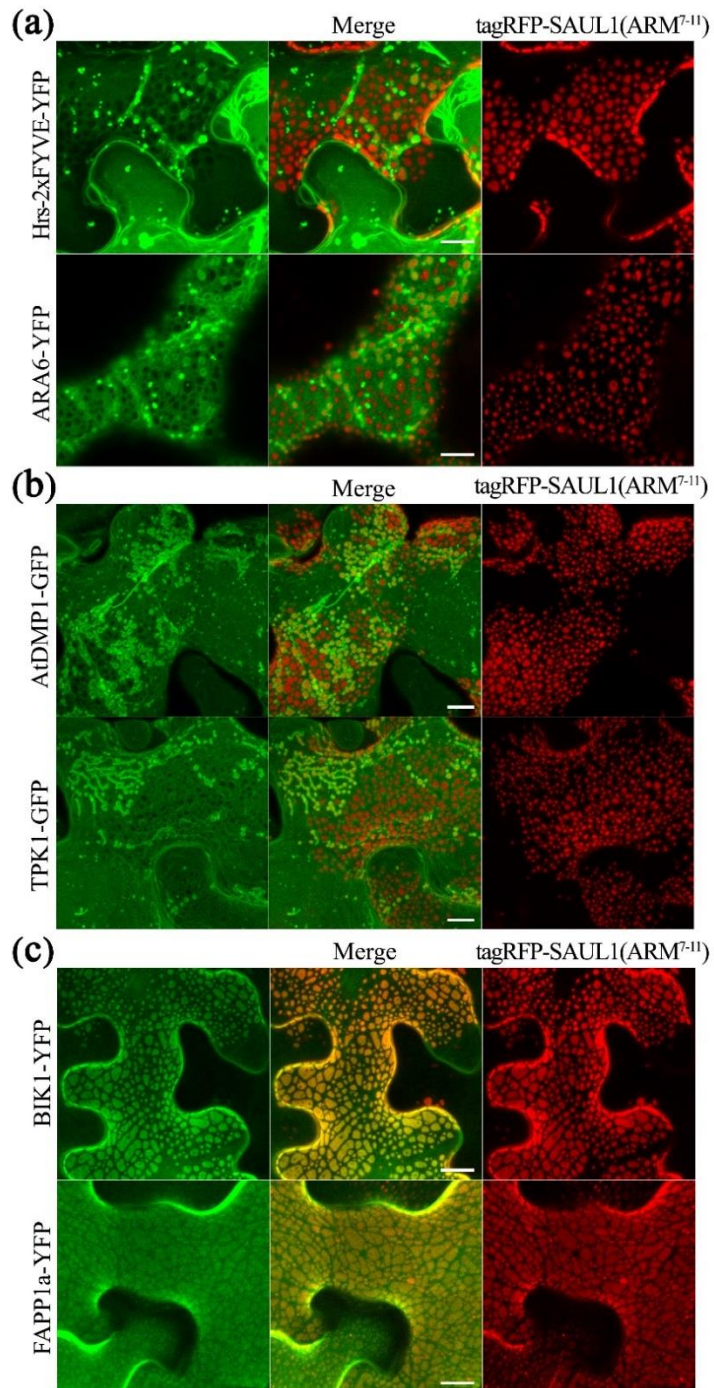


Figure S3.8 Relationship of membrane patches produced by SAUL1(ARM⁷⁻¹¹) to MVB-, tonoplast- and PM-targeted proteins.

(a) Co-expression of tagRFP-SAUL1(ARM⁷⁻¹¹) with MVB-targeted proteins Hrs-2x FYVE-YFP and ARA6-YFP. (b) Co-expression of tagRFP-SAUL1(ARM⁷⁻¹¹) with tonoplast-targeted proteins AtDMP1-GFP and TPK1-GFP. (c) Co-expression of tagRFP-SAUL1(ARM⁷⁻¹¹) with PM-targeted proteins BIK1-YFP and FAPP1a-PH-YFP, revealing enrichment of BIK1 and FAPP1a-PH within the membrane patches produced by SAUL1(ARM⁷⁻¹¹) .. Black scale bar represents 10 μm in all panels.

Bibliography

- An, Q., van Bel, A.J.E. and Hückelhoven, R.** (2007) Do Plant Cells Secrete Exosomes Derived from Multivesicular Bodies? *Plant Signaling & Behavior*, **2**, 4-7.
- Andreev, I.M.** (2001) Functions of the Vacuole in Higher Plant Cells. *Russian Journal of Plant Physiology*, **48**, 672-680.
- Andreev, I.M.** (2012) Role of the vacuole in the redox homeostasis of plant cells. *Russian Journal of Plant Physiology*, **59**, 611-617.
- Ang, A.L., Taguchi, T., Francis, S., Fölsch, H., Murrells, L.J., Pypaert, M., Warren, G. and Mellman, I.** (2004) Recycling endosomes can serve as intermediates during transport from the Golgi to the plasma membrane of MDCK cells. *The Journal of Cell Biology*, **167**, 531-543.
- Asai, S., Ichikawa, T., Nomura, H., Kobayashi, M., Kamiyoshihara, Y., Mori, H., Kadota, Y., Zipfel, C., Jones, J.D.G. and Yoshioka, H.** (2013) The Variable Domain of a Plant Calcium-dependent Protein Kinase (CDPK) Confers Subcellular Localization and Substrate Recognition for NADPH Oxidase. *Journal of Biological Chemistry*, **288**, 14332-14340.
- Ben-Nissan, G., Cui, W., Kim, D.-J., Yang, Y., Yoo, B.-C. and Lee, J.-Y.** (2008) *Arabidopsis* Casein Kinase 1-Like 6 Contains a Microtubule-Binding Domain and Affects the Organization of Cortical Microtubules. *Plant Physiology*, **148**, 1897-1907.
- Bonifacino, J.S. and Glick, B.S.** (2004) The Mechanisms of Vesicle Budding and Fusion. *Cell*, **116**, 153-166.
- Bonifacino, J.S. and Traub, L.M.** (2003) Signals for Sorting of Transmembrane Proteins to Endosomes and Lysosomes. *Annual Review of Biochemistry*, **72**, 395-447.
- Bottanelli, F., Gershlick, D.C. and Denecke, J.** (2012) Evidence for Sequential Action of Rab5 and Rab7 GTPases in Prevacuolar Organelle Partitioning. *Traffic*, **13**, 338-354.
- Cheever, M.L., Sato, T.K., de Beer, T., Kutateladze, T.G., Emr, S.D. and Overduin, M.** (2001) Phox domain interaction with PtdIns(3)P targets the Vam7 t-SNARE to vacuole membranes. *Nature Cell Biology*, **3**, 613.

- Chow, C.-M., Neto, H., Foucart, C. and Moore, I.** (2008) Rab-A2 and Rab-A3 GTPases Define a trans-Golgi Endosomal Membrane Domain in *Arabidopsis* That Contributes Substantially to the Cell Plate. *The Plant Cell*, **20**, 101-123.
- Coates, J.C.** (2003) Armadillo repeat proteins: beyond the animal kingdom. *Trends in cell biology*, **13**, 463-471.
- Colombo, M., Raposo, G. and Théry, C.** (2014) Biogenesis, Secretion, and Intercellular Interactions of Exosomes and Other Extracellular Vesicles. *Annual Review of Cell and Developmental Biology*, **30**, 255-289.
- Contento, A.L. and Bassham, D.C.** (2012) Structure and function of endosomes in plant cells. *Journal of Cell Science*, **125**, 3511-3518.
- Cui, Y., Shen, J., Gao, C., Zhuang, X., Wang, J. and Jiang, L.** (2016) Biogenesis of Plant Prevacuolar Multivesicular Bodies. *Molecular Plant*, **9**, 774-786.
- Cui, Y., Zhao, Q., Gao, C., Ding, Y., Zeng, Y., Ueda, T., Nakano, A. and Jiang, L.** (2014) Activation of the Rab7 GTPase by the MON1-CCZ1 Complex Is Essential for PVC-to-Vacuole Trafficking and Plant Growth in *Arabidopsis*. *The Plant Cell Online*.
- Dettmer, J., Hong-Hermesdorf, A., Stierhof, Y.-D. and Schumacher, K.** (2006) Vacuolar H⁺-ATPase Activity Is Required for Endocytic and Secretory Trafficking in *Arabidopsis*. *The Plant Cell*, **18**, 715-730.
- Di Paolo, G. and De Camilli, P.** (2006) Phosphoinositides in cell regulation and membrane dynamics. *Nature*, **443**, 651-657.
- Disch, E.-M., Tong, M., Kotur, T., Koch, G., Wolf, C.-A., Li, X. and Hoth, S.** (2015) Membrane-Associated Ubiquitin Ligase SAUL1 Suppresses Temperature- and Humidity-Dependent Autoimmunity in *Arabidopsis*. *Molecular Plant-Microbe Interactions*, **29**, 69-80.
- Doherty, G.J. and McMahon, H.T.** (2009) Mechanisms of Endocytosis. *Annual Review of Biochemistry*, **78**, 857-902.
- Donovan, K.W. and Bretscher, A.** (2015) Tracking individual secretory vesicles during exocytosis reveals an ordered and regulated process. *The Journal of Cell Biology*, **210**, 181-189.

- Dowler, S., Currie, R.A., Campbell, D.G., Deak, M., Kular, G., Downes, C.P. and Alessi, D.R.** (2000) Identification of pleckstrin-homology-domain-containing proteins with novel phosphoinositide-binding specificities. *Biochem J*, **351**, 19-31.
- Drechsel, G., Bergler, J., Wippel, K., Sauer, N., Vogelmann, K. and Hoth, S.** (2010) C-terminal armadillo repeats are essential and sufficient for association of the plant U-box armadillo E3 ubiquitin ligase SAUL1 with the plasma membrane. *Journal of Experimental Botany*.
- Dupont, S., Beney, L., Ritt, J.-F., Lherminier, J. and Gervais, P.** (2010) Lateral reorganization of plasma membrane is involved in the yeast resistance to severe dehydration. *Biochimica et Biophysica Acta (BBA) - Biomembranes*, **1798**, 975-985.
- Ebine, K., Fujimoto, M., Okatani, Y., Nishiyama, T., Goh, T., Ito, E., Dainobu, T., Nishitani, A., Uemura, T., Sato, M.H., Thordal-Christensen, H., Tsutsumi, N., Nakano, A. and Ueda, T.** (2011) A membrane trafficking pathway regulated by the plant-specific RAB GTPase ARA6. *Nature Cell Biology*, **13**, 853.
- Eden, E.R.** (2016) The formation and function of ER-endosome membrane contact sites. *Biochimica et Biophysica Acta (BBA) - Molecular and Cell Biology of Lipids*, **1861**, 874-879.
- Ewers, H. and Helenius, A.** (2011) Lipid-mediated endocytosis. *Cold Spring Harb Perspect Biol*, **3**, a004721.
- Falasca, M. and Maffucci, T.** (2009) Rethinking phosphatidylinositol 3-monophosphate. *Biochimica et Biophysica Acta (BBA) - Molecular Cell Research*, **1793**, 1795-1803.
- Festa, M., Lagostena, L. and Carpaneto, A.** (2016) Using the plant vacuole as a biological system to investigate the functional properties of exogenous channels and transporters. *Biochimica et Biophysica Acta (BBA) - Biomembranes*, **1858**, 607-612.
- Gan, P.H.P., Rafiqi, M., Ellis, J.G., Jones, D.A., Hardham, A.R. and Dodds, P.N.** (2010) Lipid binding activities of flax rust AvrM and AvrL567 effectors. *Plant Signaling & Behavior*, **5**, 1272-1275.
- Gaullier, J.-M., Simonsen, A., D'Arrigo, A., Bremnes, B., Stenmark, H. and Aasland, R.** (1998) FYVE fingers bind PtdIns(3)P. *Nature*, **394**, 432.

- Gómez-Gómez, L. and Boller, T.** (2000) FLS2: An LRR Receptor-like Kinase Involved in the Perception of the Bacterial Elicitor Flagellin in *Arabidopsis*. *Molecular Cell*, **5**, 1003-1011.
- Gookin, T.E. and Assmann, S.M.** (2014) Significant reduction of BiFC non-specific assembly facilitates in planta assessment of heterotrimeric G-protein interactors. *The Plant Journal*, **80**, 553-567.
- Grant, B.D. and Donaldson, J.G.** (2009) Pathways and mechanisms of endocytic recycling. *Nature reviews. Molecular cell biology*, **10**, 597-608.
- Gronnier, J., Crowet, J.-M., Habenstein, B., Nasir, M.N., Bayle, V., Hosy, E., Platre, M.P., Gouguet, P., Raffaele, S., Martinez, D., Grelard, A., Loquet, A., Simon-Plas, F., Gerbeau-Pissot, P., Der, C., Bayer, E.M., Jaillais, Y., Deleu, M., Germain, V., Lins, L. and Mongrand, S.** (2017) Structural basis for plant plasma membrane protein dynamics and organization into functional nanodomains. *eLife*, **6**, e26404.
- Gu, B., Kale, S.D., Wang, Q., Wang, D., Pan, Q., Cao, H., Meng, Y., Kang, Z., Tyler, B.M. and Shan, W.** (2011) Rust Secreted Protein Ps87 Is Conserved in Diverse Fungal Pathogens and Contains a RXLR-like Motif Sufficient for Translocation into Plant Cells. *PLOS ONE*, **6**, e27217.
- Günl, M., Neumetzler, L., Kraemer, F., de Souza, A., Schultink, A., Pena, M., York, W.S. and Pauly, M.** (2011) AXY8 Encodes an α -Fucosidase, Underscoring the Importance of Apoplastic Metabolism on the Fine Structure of *Arabidopsis* Cell Wall Polysaccharides. *The Plant Cell*, **23**, 4025-4040.
- Hála, M., Cole, R., Synek, L., Drdová, E., Pečenková, T., Nordheim, A., Lamkemeyer, T., Madlung, J., Hochholdinger, F., Fowler, J.E. and Žárský, V.** (2008) An Exocyst Complex Functions in Plant Cell Growth in *Arabidopsis* and Tobacco. *The Plant Cell*, **20**, 1330-1345.
- Hanson, P.I. and Cashikar, A.** (2012) Multivesicular Body Morphogenesis. *Annual Review of Cell and Developmental Biology*, **28**, 337-362.
- Hatsugai, N. and Hara-Nishimura, I.** (2010) Two vacuole-mediated defense strategies in plants. *Plant Signaling & Behavior*, **5**, 1568-1570.

- Hatsugai, N., Yamada, K., Goto-Yamada, S. and Hara-Nishimura, I.** (2015) Vacuolar processing enzyme in plant programmed cell death. *Frontiers in Plant Science*, **6**, 234.
- Helle, S.C.J., Kanfer, G., Kolar, K., Lang, A., Michel, A.H. and Kornmann, B.** (2013) Organization and function of membrane contact sites. *Biochimica et Biophysica Acta (BBA) - Molecular Cell Research*, **1833**, 2526-2541.
- Helliwell, E.E., Vega-Arreguín, J., Shi, Z., Bailey, B., Xiao, S., Maximova, S.N., Tyler, B.M. and Gultinan, M.J.** (2016) Enhanced resistance in *Theobroma cacao* against oomycete and fungal pathogens by secretion of phosphatidylinositol-3-phosphate-binding proteins. *Plant Biotechnology Journal*, **14**, 875-886.
- Hsu, V.W. and Prekeris, R.** (2010) Transport at the Recycling Endosome. *Current opinion in cell biology*, **22**, 528-534.
- Hu, Y.-B., Dammer, E.B., Ren, R.-J. and Wang, G.** (2015) The endosomal-lysosomal system: from acidification and cargo sorting to neurodegeneration. *Translational Neurodegeneration*, **4**, 18.
- Hunter, P.R., Craddock, C.P., Di Benedetto, S., Roberts, L.M. and Frigerio, L.** (2007) Fluorescent reporter proteins for the tonoplast and the vacuolar lumen identify a single vacuolar compartment in *Arabidopsis* cells. *Plant Physiol*, **145**, 1371-1382.
- Huotari, J. and Helenius, A.** (2011) Endosome maturation. *The EMBO Journal*, **30**, 3481-3500.
- Hurth, M.A., Suh, S.J., Kretzschmar, T., Geis, T., Bregante, M., Gambale, F., Martinoia, E. and Neuhaus, H.E.** (2005) Impaired pH Homeostasis in *Arabidopsis* Lacking the Vacuolar Dicarboxylate Transporter and Analysis of Carboxylic Acid Transport across the Tonoplast. *Plant Physiology*, **137**, 901-910.
- Islinger, M., Godinho, L., Costello, J. and Schrader, M.** (2015) The different facets of organelle interplay—an overview of organelle interactions. *Frontiers in Cell and Developmental Biology*, **3**.
- Jaber, N., Mohd-Naim, N., Wang, Z., DeLeon, J.L., Kim, S., Zhong, H., Sheshadri, N., Dou, Z., Edinger, A.L., Du, G., Braga, V.M.M. and Zong, W.-X.** (2016) Vps34 regulates Rab7 and late endocytic trafficking through recruitment of the GTPase-activating protein Armus. *Journal of Cell Science*, **129**, 4424-4435.

Jarsch, I.K., Konrad, S.S.A., Stratil, T.F., Urbanus, S.L., Szymanski, W., Braun, P., Braun, K.-H. and Ott, T. (2014) Plasma Membranes Are Subcompartmentalized into a Plethora of Coexisting and Diverse Microdomains in *Arabidopsis* and *Nicotiana benthamiana*. The Plant Cell Online.

Jovic, M., Sharma, M., Rahajeng, J. and Caplan, S. (2010) The early endosome: a busy sorting station for proteins at the crossroads. *Histology and histopathology*, **25**, 99-112.

Kale, S.D., Gu, B., Capelluto, D.G., Dou, D., Feldman, E., Rumore, A., Arredondo, F.D., Hanlon, R., Fudal, I., Rouxel, T., Lawrence, C.B., Shan, W. and Tyler, B.M. (2010) External lipid PI3P mediates entry of eukaryotic pathogen effectors into plant and animal host cells. *Cell*, **142**, 284-295.

Kasaras, A., Melzer, M. and Kunze, R. (2012) *Arabidopsis* senescence-associated protein DMP1 is involved in membrane remodeling of the ER and tonoplast. *BMC Plant Biology*, **12**, 54.

Kerppola, T.K. (2006) Design and implementation of bimolecular fluorescence complementation (BiFC) assays for the visualization of protein interactions in living cells. *Nature Protocols*, **1**, 1278.

Komada, M. and Kitamura, N. (1995) Growth factor-induced tyrosine phosphorylation of Hrs, a novel 115-kilodalton protein with a structurally conserved putative zinc finger domain. *Mol Cell Biol*, **15**, 6213-6221.

Kutateladze, T. and Overduin, M. (2001) Structural Mechanism of Endosome Docking by the FYVE Domain. *Science*, **291**, 1793-1796.

Lee, S.A., Kovacs, J., Stahelin, R.V., Cheever, M.L., Overduin, M., Setty, T.G., Burd, C.G., Cho, W. and Kutateladze, T.G. (2006) Molecular Mechanism of Membrane Docking by the Vam7p PX Domain. *Journal of Biological Chemistry*, **281**, 37091-37101.

Lu, D., Wu, S., Gao, X., Zhang, Y., Shan, L. and He, P. (2010) A receptor-like cytoplasmic kinase, BIK1, associates with a flagellin receptor complex to initiate plant innate immunity. *Proceedings of the National Academy of Sciences*, **107**, 496-501.

Luo, F., Fong, Y.H., Zeng, Y., Shen, J., Jiang, L. and Wong, K.-B. (2014) How Vacuolar Sorting Receptor Proteins Interact with Their Cargo Proteins: Crystal

Structures of Apo and Cargo-Bound Forms of the Protease-Associated Domain from an *Arabidopsis* Vacuolar Sorting Receptor. *The Plant Cell*, **26**, 3693-3708.

Maîtrejean, M., Wudick, M.M., Voelker, C., Prinsi, B., Mueller-Roeber, B., Czempinski, K., Pedrazzini, E. and Vitale, A. (2011) Assembly and Sorting of the Tonoplast Potassium Channel AtTPK1 and Its Turnover by Internalization into the Vacuole. *Plant Physiology*, **156**, 1783-1796.

Marty, F. (1999) Plant Vacuoles. *The Plant Cell*, **11**, 587-599.

Mellman, I. (1996) ENDOCYTOSIS AND MOLECULAR SORTING. *Annual Review of Cell and Developmental Biology*, **12**, 575-625.

Meng, X., Chen, X., Mang, H., Liu, C., Yu, X., Gao, X., Torii, K.U., He, P. and Shan, L. (2015) Differential function of *Arabidopsis* SERK family receptor-like kinases in stomatal patterning. *Current biology : CB*, **25**, 2361-2372.

Merrifield, C.J., Feldman, M.E., Wan, L. and Almers, W. (2002) Imaging actin and dynamin recruitment during invagination of single clathrin-coated pits. *Nature Cell Biology*, **4**, 691.

Miao, Y., Yan, P.K., Kim, H., Hwang, I. and Jiang, L. (2006) Localization of Green Fluorescent Protein Fusions with the Seven *Arabidopsis* Vacuolar Sorting Receptors to Prevacuolar Compartments in Tobacco BY-2 Cells. *Plant Physiology*, **142**, 945-962.

Murray, J.T., Panaretou, C., Stenmark, H., Miaczynska, M. and Backer, J.M. (2002) Role of Rab5 in the Recruitment of hVps34/p150 to the Early Endosome. *Traffic*, **3**, 416-427.

Nahm, M.Y., Kim, S.W., Yun, D., Lee, S.Y., Cho, M.J. and Bahk, J.D. (2003) Molecular and biochemical analyses of OsRab7, a rice Rab7 homolog. *Plant Cell Physiol*, **44**, 1341-1349.

Nielsen, M.E., Feechan, A., Böhlenius, H., Ueda, T. and Thordal-Christensen, H. (2012) *Arabidopsis* ARF-GTP exchange factor, GNOM, mediates transport required for innate immunity and focal accumulation of syntaxin PEN1. *Proceedings of the National Academy of Sciences*, **109**, 11443-11448.

Nonejuie, P., Burkart, M., Pogliano, K. and Pogliano, J. (2013) Bacterial cytological profiling rapidly identifies the cellular pathways targeted by antibacterial molecules. *Proceedings of the National Academy of Sciences*, **110**, 16169-16174.

- Otegui, M.S. and Spitzer, C.** (2008) Endosomal Functions in Plants. *Traffic*, **9**, 1589-1598.
- Paez Valencia, J., Goodman, K. and Otegui, M.S.** (2016) Endocytosis and Endosomal Trafficking in Plants. *Annu Rev Plant Biol*, **67**, 309-335.
- Pankiv, S., Alemu, E.A., Brech, A., Bruun, J.-A., Lamark, T., Øvervatn, A., Bjørkøy, G. and Johansen, T.** (2010) FYCO1 is a Rab7 effector that binds to LC3 and PI3P to mediate microtubule plus end-directed vesicle transport. *The Journal of Cell Biology*, **188**, 253-269.
- Perraki, A., Cacas, J.L., Crowet, J.M., Lins, L., Castroviejo, M., German-Retana, S., Mongrand, S. and Raffaele, S.** (2012) Plasma membrane localization of *Solanum tuberosum* remorin from group 1, homolog 3 is mediated by conformational changes in a novel C-terminal anchor and required for the restriction of potato virus X movement]. *Plant Physiol*, **160**, 624-637.
- Plett, Jonathan M., Kemppainen, M., Kale, Shiv D., Kohler, A., Legué, V., Brun, A., Tyler, Brett M., Pardo, Alejandro G. and Martin, F.** (2011) A Secreted Effector Protein of *Laccaria bicolor* Is Required for Symbiosis Development. *Current Biology*, **21**, 1197-1203.
- Poteryaev, D., Datta, S., Ackema, K., Zerial, M. and Spang, A.** (2010) Identification of the Switch in Early-to-Late Endosome Transition. *Cell*, **141**, 497-508.
- Poteser, M., Leitinger, G., Pritz, E., Platzer, D., Frischauf, I., Romanin, C. and Groschner, K.** (2016) Live-cell imaging of ER-PM contact architecture by a novel TIRFM approach reveals extension of junctions in response to store-operated Ca²⁺-entry. **6**, 35656.
- Pourcel, L., Irani, N.G., Lu, Y., Riedl, K., Schwartz, S. and Grotewold, E.** (2010) The Formation of Anthocyanic Vacuolar Inclusions in *Arabidopsis thaliana* and Implications for the Sequestration of Anthocyanin Pigments. *Molecular Plant*, **3**, 78-90.
- Prinz, W.A.** (2014) Bridging the gap: Membrane contact sites in signaling, metabolism, and organelle dynamics. *The Journal of Cell Biology*, **205**, 759-769.
- Qi, D., Dubiella, U., Kim, S.H., Sloss, D.I., Downen, R.H., Dixon, J.E. and Innes, R.W.** (2014) Recognition of the Protein Kinase AVRPPHB SUSCEPTIBLE1 by the

Disease Resistance Protein RESISTANCE TO PSEUDOMONAS SYRINGAE5 Is Dependent on S-Acylation and an Exposed Loop in AVRPPHB SUSCEPTIBLE1. *Plant Physiology*, **164**, 340-351.

Raffaele, S., Mongrand, S., Gamas, P., Niebel, A. and Ott, T. (2007) Genome-wide annotation of remorins, a plant-specific protein family: evolutionary and functional perspectives. *Plant Physiol*, **145**, 593-600.

Raiborg, C., Schink, K.O. and Stenmark, H. (2013) Class III phosphatidylinositol 3-kinase and its catalytic product PtdIns3P in regulation of endocytic membrane traffic. *FEBS J*, **280**, 2730-2742.

Reisen, D., Marty, F. and Leborgne-Castel, N. (2005) New insights into the tonoplast architecture of plant vacuoles and vacuolar dynamics during osmotic stress. *BMC Plant Biology*, **5**, 13.

Roy, A. and Levine, T.P. (2004) Multiple Pools of Phosphatidylinositol 4-Phosphate Detected Using the Pleckstrin Homology Domain of Osh2p. *Journal of Biological Chemistry*, **279**, 44683-44689.

Rutter, B.D. and Innes, R.W. (2017) Extracellular Vesicles Isolated from the Leaf Apoplast Carry Stress-Response Proteins. *Plant Physiology*, **173**, 728-741.

Samuel, M., Bleackley, M., Anderson, M. and Mathivanan, S. (2015) Extracellular vesicles including exosomes in cross kingdom regulation: a viewpoint from plant-fungal interactions. *Frontiers in Plant Science*, **6**.

Sato, T.K., Overduin, M. and Emr, S.D. (2001) Location, Location, Location: Membrane Targeting Directed by PX Domains. *Science*, **294**, 1881-1885.

Scheuring, D., Viotti, C., Krüger, F., Künzl, F., Sturm, S., Bubeck, J., Hillmer, S., Frigerio, L., Robinson, D.G., Pimpl, P. and Schumacher, K. (2011) Multivesicular Bodies Mature from the Trans-Golgi Network/Early Endosome in *Arabidopsis*. *The Plant Cell*, **23**, 3463-3481.

Shen, Y., Wang, J., Ding, Y.u., Lo, S.W., Gouzerh, G., Neuhaus, J.-M. and Jiang, L. (2011) The Rice RMR1 Associates with a Distinct Prevacuolar Compartment for the Protein Storage Vacuole Pathway. *Molecular Plant*, **4**, 854-868.

Simon, M.L., Platre, M.P., Assil, S., van Wijk, R., Chen, W.Y., Chory, J., Dreux, M., Munnik, T. and Jaillais, Y. (2014) A multi-colour/multi-affinity marker set to visualize phosphoinositide dynamics in *Arabidopsis*. *Plant J*, **77**, 322-337.

Simon, M.L.A., Platre, M.P., Marquès-Bueno, M.M., Armengot, L., Stanislas, T., Bayle, V., Caillaud, M.-C. and Jaillais, Y. (2016) A PtdIns(4)P-driven electrostatic field controls cell membrane identity and signalling in plants. *Nature Plants*, **2**, 16089.

Singh, Manoj K., Krüger, F., Beckmann, H., Brumm, S., Vermeer, Joop E.M., Munnik, T., Mayer, U., Stierhof, Y.-D., Grefen, C., Schumacher, K. and Jürgens, G. Protein Delivery to Vacuole Requires SAND Protein-Dependent Rab GTPase Conversion for MVB-Vacuole Fusion. *Current Biology*, **24**, 1383-1389.

Singh, M.K., Kruger, F., Beckmann, H., Brumm, S., Vermeer, J.E.M., Munnik, T., Mayer, U., Stierhof, Y.D., Grefen, C., Schumacher, K. and Jurgens, G. (2014) Protein delivery to vacuole requires SAND protein-dependent Rab GTPase conversion for MVB-vacuole fusion. *Curr Biol*, **24**, 1383-1389.

Sohn, E.J., Kim, E.S., Zhao, M., Kim, S.J., Kim, H., Kim, Y.-W., Lee, Y.J., Hillmer, S., Sohn, U., Jiang, L. and Hwang, I. (2003) Rha1, an *Arabidopsis* Rab5 Homolog, Plays a Critical Role in the Vacuolar Trafficking of Soluble Cargo Proteins. *The Plant Cell*, **15**, 1057-1070.

Song, K., Jang, M., Kim, S.Y., Lee, G., Lee, G.-J., Kim, D.H., Lee, Y., Cho, W. and Hwang, I. (2012) An A/ENTH Domain-Containing Protein Functions as an Adaptor for Clathrin-Coated Vesicles on the Growing Cell Plate in *Arabidopsis* Root Cells. *Plant Physiology*, **159**, 1013-1025.

Sparkes, I., Tolley, N., Aller, I., Svozil, J., Osterrieder, A., Botchway, S., Mueller, C., Frigerio, L. and Hawes, C. (2010) Five *Arabidopsis* Reticulon Isoforms Share Endoplasmic Reticulum Location, Topology, and Membrane-Shaping Properties. *The Plant Cell*, **22**, 1333-1343.

Stefano, G., Renna, L. and Brandizzi, F. (2014) The endoplasmic reticulum exerts control over organelle streaming during cell expansion. *Journal of Cell Science*, **127**, 947-953.

Stepanenko, O.V., Stepanenko, O.V., Shcherbakova, D.M., Kuznetsova, I.M., Turoverov, K.K. and Verkhusha, V.V. (2011) Modern fluorescent proteins: from

chromophore formation to novel intracellular applications. *BioTechniques*, **51**, 313-323.

Sunilkumar, G., Mohr, L., Lopata-Finch, E., Emani, C. and Rathore, K.S. (2002) Developmental and tissue-specific expression of CaMV 35S promoter in cotton as revealed by GFP. *Plant Molecular Biology*, **50**, 463-479.

Théry, C., Zitvogel, L. and Amigorena, S. (2002) Exosomes: composition, biogenesis and function. *Nature Reviews Immunology*, **2**, 569.

Tong, M., Kotur, T., Liang, W., Vogelmann, K., Kleine, T., Leister, D., Brieske, C., Yang, S., Lüdke, D., Wiermer, M., Zhang, Y., Li, X. and Hoth, S. (2017) E3 ligase SAUL1 serves as a positive regulator of PAMP-triggered immunity and its homeostasis is monitored by immune receptor SOC3. *New Phytologist*, **215**, 1516-1532.

Tse, Y.C., Mo, B., Hillmer, S., Zhao, M., Lo, S.W., Robinson, D.G. and Jiang, L. (2004) Identification of Multivesicular Bodies as Prevacuolar Compartments in *Nicotiana tabacum* BY-2 Cells. *The Plant Cell*, **16**, 672-693.

van IJzendoorn, S.C.D. (2006) Recycling endosomes. *Journal of Cell Science*, **119**, 1679-1681.

Vermeer, J.E., Thole, J.M., Goedhart, J., Nielsen, E., Munnik, T. and Gadella, T.W., Jr. (2009) Imaging phosphatidylinositol 4-phosphate dynamics in living plant cells. *The Plant journal : for cell and molecular biology*, **57**, 356-372.

Vermeer, J.E., van Leeuwen, W., Tobena-Santamaria, R., Laxalt, A.M., Jones, D.R., Divecha, N., Gadella, T.W., Jr. and Munnik, T. (2006) Visualization of PtdIns3P dynamics in living plant cells. *Plant J*, **47**, 687-700.

Viotti, C., Bubeck, J., Stierhof, Y.-D., Krebs, M., Langhans, M., van den Berg, W., van Dongen, W., Richter, S., Geldner, N., Takano, J., Jürgens, G., de Vries, S.C., Robinson, D.G. and Schumacher, K. (2010) Endocytic and Secretory Traffic in *Arabidopsis* Merge in the Trans-Golgi Network/Early Endosome, an Independent and Highly Dynamic Organelle. *The Plant Cell*, **22**, 1344-1357.

Vitko, I., Bidaud, I., Arias, J.M., Mezghrani, A., Lory, P. and Perez-Reyes, E. (2007) The I-II Loop Controls Plasma Membrane Expression and Gating of Ca_v3.2 T-

Type Ca²⁺ Channels: A Paradigm for Childhood Absence Epilepsy Mutations. *The Journal of Neuroscience*, **27**, 322-330.

Vogelmann, K., Subert, C., Danzberger, N., Drechsel, G., Bergler, J., Kotur, T., Burmester, T. and Hoth, S. (2014) Plasma membrane-association of SAUL1-type plant U-box armadillo repeat proteins is conserved in land plants. *Front Plant Sci*, **5**, 37.

Wallroth, A. and Haucke, V. (2017) Phosphoinositide conversion in endocytosis and the endolysosomal system. *Journal of Biological Chemistry*.

Wang, Y.S., Motes, C.M., Mohamalawari, D.R. and Blancaflor, E.B. (2004) Green fluorescent protein fusions to *Arabidopsis* fimbrin 1 for spatio-temporal imaging of F-actin dynamics in roots. *Cell Motility*, **59**, 79-93.

Weigle, B.A., Orchard, R.C., Jimenez, A., Cox, G.W. and Alto, N.M. (2017) A systematic exploration of the interactions between bacterial effector proteins and host cell membranes. *Nature Communications*, **8**, 532.

Wu, B. and Guo, W. (2015) The Exocyst at a Glance. *Journal of Cell Science*, **128**, 2957-2964.

Xu, H. and Ren, D. (2015) Lysosomal Physiology. *Annual Review of Physiology*, **77**, 57-80.

Yamazaki, T., Takata, N., Uemura, M. and Kawamura, Y. (2010) *Arabidopsis* Synaptotagmin SYT1, a Type I Signal-anchor Protein, Requires Tandem C2 Domains for Delivery to the Plasma Membrane. *Journal of Biological Chemistry*, **285**, 23165-23176.

Yoo, S.-D., Cho, Y.-H. and Sheen, J. (2007) *Arabidopsis* mesophyll protoplasts: a versatile cell system for transient gene expression analysis. *Nat. Protocols*, **2**, 1565-1572.

Žárský, V., Kulich, I., Fendrych, M. and Pečenková, T. (2013) Exocyst complexes multiple functions in plant cells secretory pathways. *Current Opinion in Plant Biology*, **16**, 726-733.

Zeigerer, A., Gilleron, J., Bogorad, R.L., Marsico, G., Nonaka, H., Seifert, S., Epstein-Barash, H., Kuchimanchi, S., Peng, C.G., Ruda, V.M., Conte-Zerial, P.D.,

Hengstler, J.G., Kalaidzidis, Y., Kotliansky, V. and Zerial, M. (2012) Rab5 is necessary for the biogenesis of the endolysosomal system in vivo. *Nature*, **485**, 465.

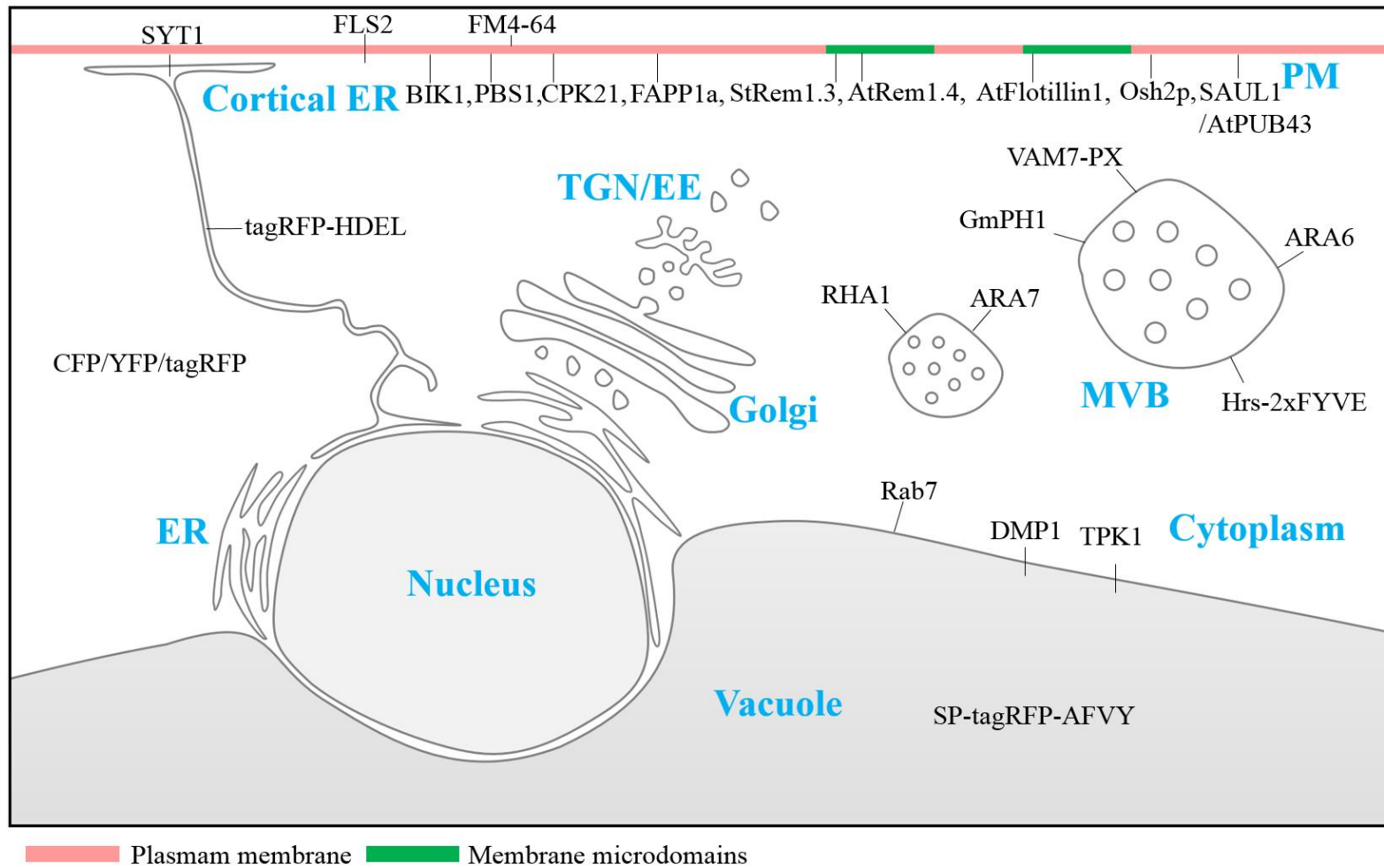
Zhang, C., Hicks, G.R. and Raikhel, N.V. (2015) Molecular Composition of Plant Vacuoles: Important but Less Understood Regulations and Roles of Tonoplast Lipids. *Plants*, **4**, 320-333.

Zhang, D., Vjestica, A. and Oliferenko, S. (2012) Plasma Membrane Tethering of the Cortical ER Necessitates Its Finely Reticulated Architecture. *Current Biology*, **22**, 2048-2052.

Zhu, J.-K. (2001) Plant salt tolerance. *Trends in Plant Science*, **6**, 66-71.

Appendix Figures

Figure 3.1 Subcellular localization of all proteins tested in chapter 3 when transiently expressed in plant cells.



Chapter 4: Fluorescent protein mEOS3.2 shows low self-association in bimolecular fluorescence complementation assays in plants

Fluorescent protein mEOS3.2 shows lower self-association in bimolecular fluorescence complementation assays in plants

Kai Tao^{1,2}, Justin R. Waletich³, Yerim Lee⁴, Felipe Arredondo², Xiaolin Nan⁴, Brett M. Tyler^{1,2,5}.

1. Molecular and Cellular Biology Program, Oregon State University, Corvallis, OR 97331
2. Department of Botany and Plant Pathology, Oregon State University, Corvallis, OR 97331
3. Department of Microbiology, Oregon State University, Corvallis, OR 97331
4. Department of Biomedical Engineering, Knight Cancer Institute, and OHSU Center for Spatial Systems Biomedicine (OCSSB), Oregon Health and Science University, Portland, OR, 97201
5. Center for Genome Research and Biotechnology, Oregon State University, Corvallis, OR 97331

Abstract

A major limitation in current bimolecular fluorescence complementation assays is the non-specific reassociation of two fragments of a fluorescent protein independent of protein-protein interactions, which results in false positive signals. Several strategies have been devised to reduce fragment self-assembly by commonly used fluorescent proteins expressed in mammalian cells, with some success. However, we and others have found that none of those strategies works reliably in plant cells. Therefore, we extensively evaluated a newly reported photoconvertible fluorescent protein mEOS3.2 for its suitability for BiFC experiments. Fragments split at residue 164E showed minimal reassociation, but showed strong reconstituted fluorescence signals in homodimers of the plasma membrane remorin protein, StRem1.3. The reassembled mEOS3.2 retained the capability to be photoconverted from green to red, which aided in distinguishing specific fluorescence from cellular autofluorescence. Furthermore, we could use the reconstituted mEOS3.2 proteins in conjunction with photoactivated localization microscopy (PALM), to examine the distribution patterns of BiFC mEOS3.2-tagged StRem1.3 proteins on the plasma membrane at the nanometer scale.

Introduction

The study of protein-protein interactions (PPIs) is essential to the investigation of the dynamics and mechanisms of biological processes. Numerous strategies have been developed to detect PPIs, including a variety of two-hybrid transcriptional and signaling assays (Brückner et al., 2009), in vitro pull down assays (Brymora et al., 2001), in vivo co-immunoprecipitation assays (Kaboord and Perr, 2008), the fluorescence resonance energy transfer (FRET) assay (Sekar and Periasamy, 2003), and the bimolecular fluorescence complementation (BiFC) assay (Kerppola, 2008). Due to the simplicity of the experimental setup and the ability to provide subcellular

localization information, BiFC has become an increasingly used live-cell imaging approach in various model organisms (Hu et al., 2002, Bracha-Drori et al., 2004, Sung and Huh, 2007, Schütze et al., 2009, Vidi et al., 2010). BiFC is based on the reassembly of two non-fluorescing fragments of a fluorescent protein. The two non-fluorescing fragments are translationally fused with respective proteins of interest; the interaction of the two protein-of-interest could bring the two non-fluorescing fragments into close proximity allowing the reassembly of a functional protein which matures into an irreversible covalent fluorescent complex (Kerppola, 2008). A challenge for this strategy, however, has been the spontaneous reassembly of the two fragments in the absence of associating protein partners. This process produces false-positive fluorescent signals and confounds the identification of valid protein-protein interactions (Shyu et al., 2006, Saka et al., 2007). This problem has been most severe with rapidly maturing fluorescent proteins, such as Venus, which have been favored for their strong fluorescent signals (Kodama and Hu, 2010). To reduce spontaneous self-assembly, several strategies have been explored, such as introducing substitution mutations, combining partially overlapped N-terminal and C-terminal fragments (e.g. 173/155), performing multi-color BiFC, and evaluating alternative split sites (Kodama and Hu, 2010, Lin et al., 2011, Nakagawa et al., 2011, Ohashi et al., 2012). While some of these strategies have shown promise in mammalian cell systems, many of them have been ineffective in plants (Gookin and Assmann, 2014, Horstman et al., 2014). One reported strategy was to use Venus fluorescent protein split at residue 210 (Gookin and Assmann, 2014), but the apparent lack of self-assembly is likely to be an artifact of the instability of the short C-terminal fragment (this report). Therefore, strategies for improving the BiFC assay in plants are still very much needed.

A further need in plant systems is for BiFC assays suitable for super-resolution microscopy. So far in plants, the subcellular localization of BiFC fluorescent complexes has been visualized using conventional confocal microscopy, which could only provide spatial resolution of about 200~300 nm due to the diffraction limits of light (Huang et al., 2009). This resolution is not sufficient to resolve the distribution of protein complexes at the nanometer scale. For example, protein complexes on the plasma membrane (PM) may coalesce into functional domains termed microdomains

or nanodomains which are difficult to resolve by conventional confocal microscopy (Kusumi et al., 2011). Several technologies, collectively known as super-resolution microscopy (SRM), have been developed to enhance the spatial resolution of fluorescent complexes. Two of these technologies are photo-activated localization microscopy (PALM) (Betzig et al., 2006) and stochastic optical reconstruction microscopy (STORM) (Rust et al., 2006). Both can distinguish single fluorescent molecules from nearby molecules at sub-diffraction-limit resolution by stochastically switching on (fluorescent) and off (dark) photo-convertible fluorophores at a particular wavelength. STORM utilizes synthetic dyes, whereas PALM uses genetically encoded photo-convertible fluorescent proteins. Given the physical challenges of assaying live, intact plant tissues, PALM is a promising technology for super-resolution BiFC imaging in plants based on endogenous expression of suitable fragments of fluorescent proteins. Recently, Liu et al. (Liu et al., 2014) successfully performed BiFC assays combined with PALM in *Escherichia coli* cells using a newly developed photo-convertible fluorescent protein mEOS3.2. Of seven available cleavage sites of mEOS3.2, two were shown to generate BiFC fluorescence signals via assembly of fused leucine zipper domains. The residue 164E was identified as the most discriminatory split site, producing minimal non-specific BiFC signals in control experiments.

Here, we first demonstrate that when transiently expressed in *Nicotiana benthamiana* leaf cells, mEOS3.2 fragments split at residue 164E undergo little to no detectable self-assembly when fused to a variety of proteins of interest. Next we evaluated the self-association of remorin protein StRem1.3 (*Solanum tuberosum*) fused with various split mEOS3.2 fragments, confirming the excellent suitability of mEOS3.2 in plant BiFC assays. We also evaluated mEOS3.2 BiFC complexes for suitability for PALM super-resolution microscopy, by observing the spatial distribution and cluster formation of StRem1.3 in PM nanodomains. This is the first time that BiFC combined with PALM has been conducted in plants to visualize membrane proteins at a near-molecular resolution.

Results

Assessment of self-assembly in traditional BiFC systems in *N. benthamiana*

To assess the issue of self-assembly in BiFC assays in plant cells, we initially examined several fluorescent proteins commonly used for BiFC using *Agrobacterium tumefaciens*-mediated transient expression in *N. benthamiana* leaves. All BiFC expression constructs were driven by the constitutively active cauliflower mosaic virus 35S promoter (CaMV35S). Equal amounts of *A. tumefaciens* cells carrying constructs encoding the respective BiFC partners were mixed and infiltrated into leaves. As shown in Figure 4.1a and b, two commonly used BiFC reporter proteins, Yellow Fluorescent Protein (YFP, split at residue 155D) and monomeric Venus (split at residue 155D) showed strong fluorescent signal due to self-assembly without fusion to interacting protein pairs. In the case of mCherry, in contrast to a previous report (Fan et al., 2008), the transient co-expression of two fragments split at 159-160 also yielded strong BiFC signals (Figure 4.1c). Kodama et al (Kodama and Hu, 2010) reported that two mutations in Venus (V150L and I152L) could specifically reduce self-assembly of BiFC complexes. However, in our hands, neither mutation, alone or together, appeared to significantly reduce the non-specific BiFC signal (Figure 4.1d-f). In the case of Venus split at residue 210D, between the 10th and the 11th β -sheets, we observed no BiFC fluorescent signal, similar to the results of Gookin et al (Gookin and Assmann, 2014) (Figure 4.1g). On the other hand, when the C terminus of VenusC²¹⁰ was fused with a short epitope tag, 3xFLAG, linked by a GGGGS linker, a strong BiFC signal was observed (Figure 4.1h), suggesting that the short VenusC²¹⁰ peptide may be unstable, producing false negative results with the VenusN²¹⁰/VenusC²¹⁰ pair. An alternative strategy, employing an overlap pair of fragments (VenusN²¹⁰/VenusC¹⁵⁵), also produced a strong self-assembly signal (Figure 4.1i).

Assessment of photo-convertible fluorescent protein mEOS3.2 for BiFC assays in plants

mEOS3.2 is derived from mEos fluorescent protein from the scleractinian coral *Lobophyllia hemprichii* (Wiedenmann et al., 2004, Zhang et al., 2012). Thus it has an entirely different sequence of amino acids to YFP or Venus which both are derived from *Aequorea* GFP. Also as mEOS3.2 is a photo-convertible fluorescent protein - its emission spectra can be shifted from green to red by irradiation with a 405-nm laser (Mathur et al., 2010). To assess its suitability in plants, we first transiently expressed

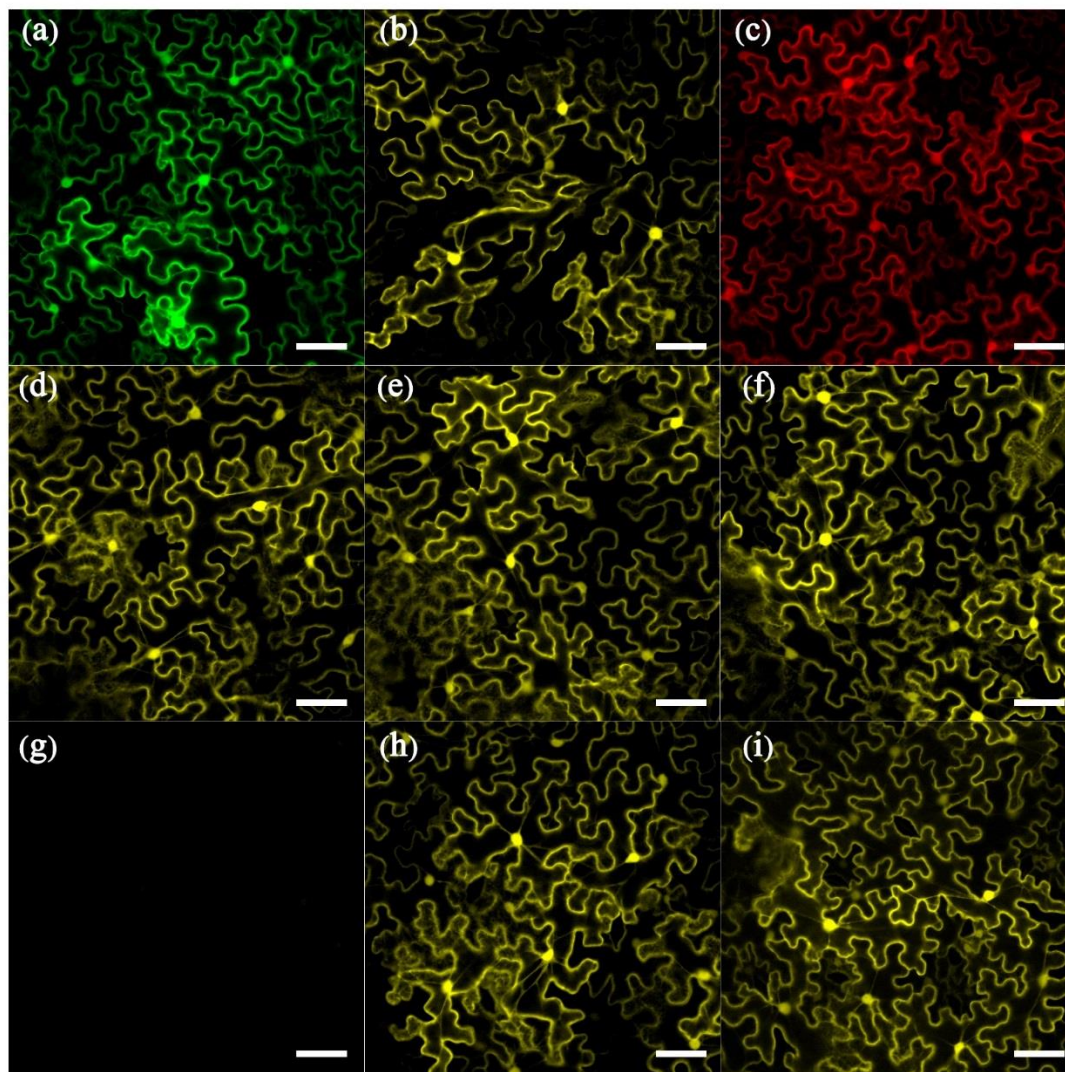


Figure 4.1 Spontaneous assembly of BiFC complexes from free fluorescent protein fragments.

Pairs of fluorescent protein fragments used for BiFC were co-expressed in the *Nicotiana benthamiana* leaf cortical cells. (a) YFP^{N155} and YFP^{C155}; (b) VenusN¹⁵⁵ and VenusC¹⁵⁵; (c) mCherryN¹⁵⁹ and mCherryC¹⁵⁹; (d) VenusN¹⁵⁵(V150L) and VenusC¹⁵⁵; (e) VenusN¹⁵⁵(I152L) and VenusC¹⁵⁵; (f) VenusN¹⁵⁵(V150L, I152L) and VenusC¹⁵⁵; (g) VenusN²¹⁰ and VenusC²¹⁰; (h) VenusN²¹⁰ and 3xFLAG-VenusC²¹⁰; (i) VenusN²¹⁰ paired with VenusC¹⁵⁵. Scale bars represent 50 μ m.

full-length mEOS3.2 unfused to any other protein. Free mEOS3.2 displayed diffuse cytosolic and nuclear localization, indicating that it did not display any unexpected localization in plant cells (Figure 4.2a). Particularly, mEOS3.2 also retained excellent photo-convertibility, in which its fluorescent emission spectra was shifted from green to red by irradiation with a 405-nm laser (Figure 4.2a). Moreover, we confirmed that splitting mEOS3.2 at position 164 (Liu et al., 2014) did not result in observable fluorescence due to the self-assembly of co-expressed mEOS3.2N and mEOS3.2C in the *N. benthamiana* cells (Figure 4.2b).

In order to confirm the complementation of mEOS3.2N and mEOS3.2C in plant cells, we chose fusions with a plant-specific membrane-associated protein StRem1.3 from potato (*Solanum tuberosum*) (Figure S4.1). StRem1.3 has been shown to form homopolymeric filaments through its C terminal alpha-helical coiled-coil structure (Bariola et al., 2004, Perraki et al., 2012). This property allowed us to create four possible constructs with different domain arrangements for evaluating mEOS3.2 in BiFC assays (Figure 4.3a). Independent of its homo-polymerization, StREM1.3 binds to the PM via a C-terminal anchor, which forms a tight hairpin of amphipathic helices in a non-polar environment (Perraki et al., 2012). In order to fuse fluorescent proteins to the C-terminus of StREM1.3 we employed a flexible linker (2xGGGGS) (Figure 4.3a); based on previous experiments with YFP, this linker was needed so that the fused fluorescent protein did not interfere with membrane localization mediated by the C-terminal anchor (Figure S4.1). Thus, placement of StRem1.3 at the N-terminus or C-terminus of the fluorescent protein fusion produced identical PM localization (Figure S4.1). Mutations in the C-terminal anchor abolished PM binding (Figure S4.1) but do not disrupt homo-polymerization (Perraki et al., 2012). Therefore we could rule out potential effects from the orientation of the construct on StREM1.3 localization and dimerization.

As shown in Figure 4.3b, all four pairings of mEOS3.2N and mEOS3.2C, fused to the N- or C-terminus of StRem1.3 yielded strong BiFC signals on the PM in *N. benthamiana* transient co-expression experiments. These results indicated that the mEOS3.2N and mEOS3.2C fragments are suitable for BiFC assays when used as both N-terminal and C-terminal fusions. As negative controls, little BiFC signal was

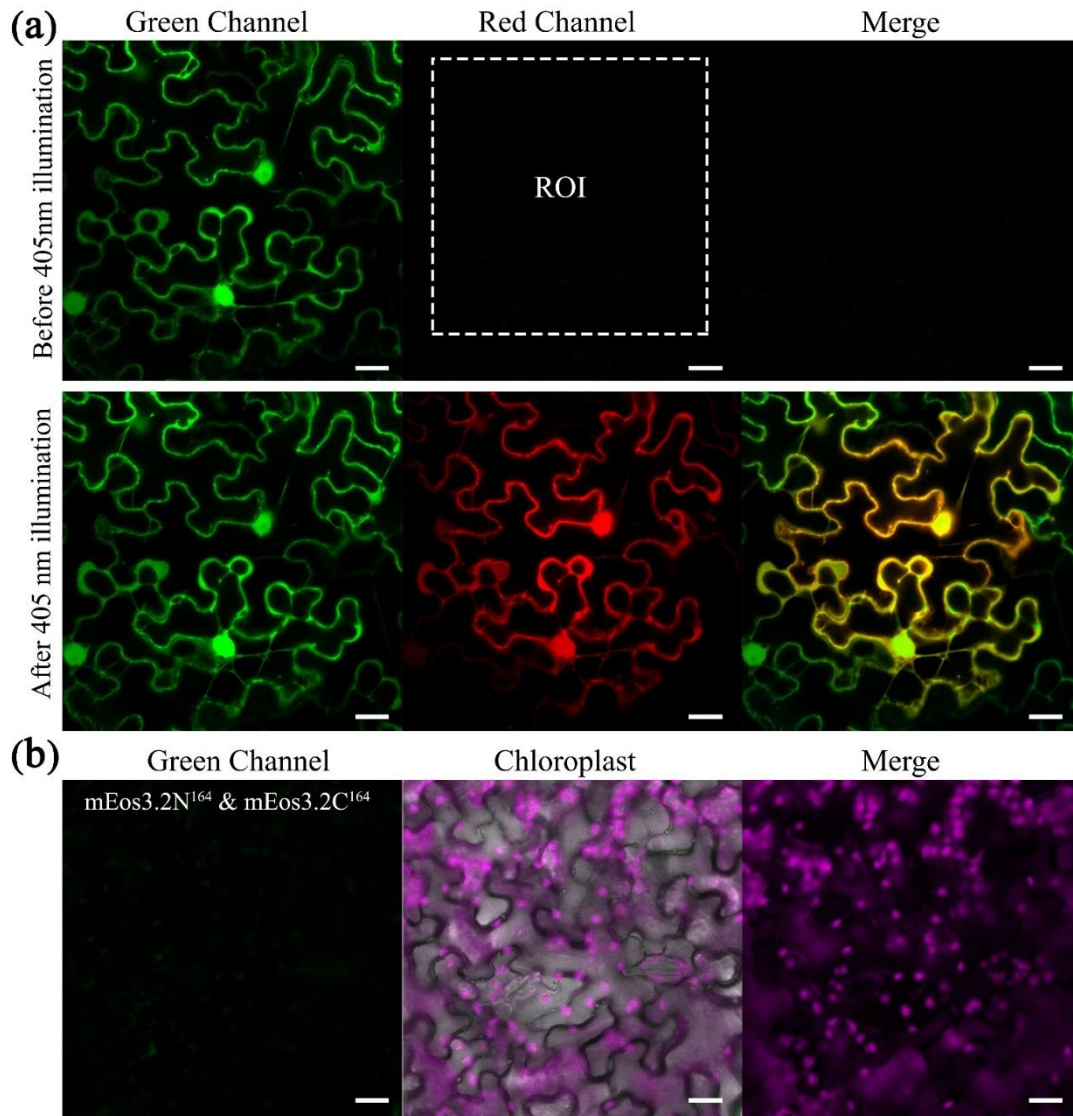


Figure 4.2 Fluorescent protein mEOS3.2 expressed in *N. benthamiana* leaf cortical cells remains photo-convertible and displays minimal BiFC self-assembly.

(a) mEOS3.2 fluorescence before (upper panels) and after (lower panels) photoconversion by illumination with a 405-nm laser. The dotted box labeled “ROI” indicates the Regions of Interest selected for illumination with the 405-nm laser. (b) Lack of fluorescence when mEOS3.2N¹⁶⁴ and mEOS3.2C¹⁶⁴ were co-expressed. Scale bars represent 20 μm .

observed when unfused mEOS3.2N or mEOS3.2C fragments were used, confirming that mEOS3.2N and mEOS3.2C fragments do not spontaneously re-assemble to form functionally fluorescent mEOS3.2 under these conditions.

To examine specific re-assembly of mEOS3.2N and mEOS3.2C in the cytoplasm, we fused the mEOS fragments to StRem1.3*, which carries mutations in the PM-binding domain; these mutations abolish membrane binding, but do not affect dimerization. A strong BiFC signal was observed when mEOS3.2N-StRem1.3* was paired with StRem1.3*-mEOS3.2C or with mEOS3.2C-StRem1.3* (Figure 4.3c), which demonstrates that the suitability of mEOS3.2 BiFC for imaging cytoplasmic protein-protein interactions. In the negative controls, the BiFC signal was not observed in combinations having free mEOS3.2N and/or mEOS3.2C (Figure 4.3c). All transiently expressed BiFC fusion proteins were confirmed by western blot (WB) using anti-FLAG antibody (Figure S4.2).

As with the Venus210 system, in some fusions we did observe evidence of self-assembly by the mEOS fragments. As shown in Figure S4.3, when an FLAG or HA epitope tag was fused to the N-terminus of mEOS3.2N and mEOS3.2C, false positive BiFC interactions could be observed. The false positive signal was strongest when both mEOS3.2 fragments carried N-terminal fusions. However, self-assembly was reduced when the mEOS3.2N fragment carried a C-terminal fusion, and eliminated when both fragments carried a C-terminal fusion.

mEOS3.2 retains photo-convertibility after BiFC complementation

Since full-length mEOS3.2 is photoconvertible from green to red, we tested whether complemented mEOS3.2 BiFC complex still is photoconvertible. As shown in Figure 4.4a and b, both PM- and cytoplasm-targeted mEOS3.2 BiFC complexes retained photoconvertibility. Photoconvertibility provides an effective means to discriminate mEOS3.2 fluorescence from background (Figure 4.4c) and from autofluorescence (Figure 4.4d) which is commonly present in plant cells and caused by phenolic compounds or chlorophyll (Mylle et al., 2013, Du et al., 2014). In order to quantify photoconvertibility, we created a photoconversion index (P.I.) (Figure 4.4e).

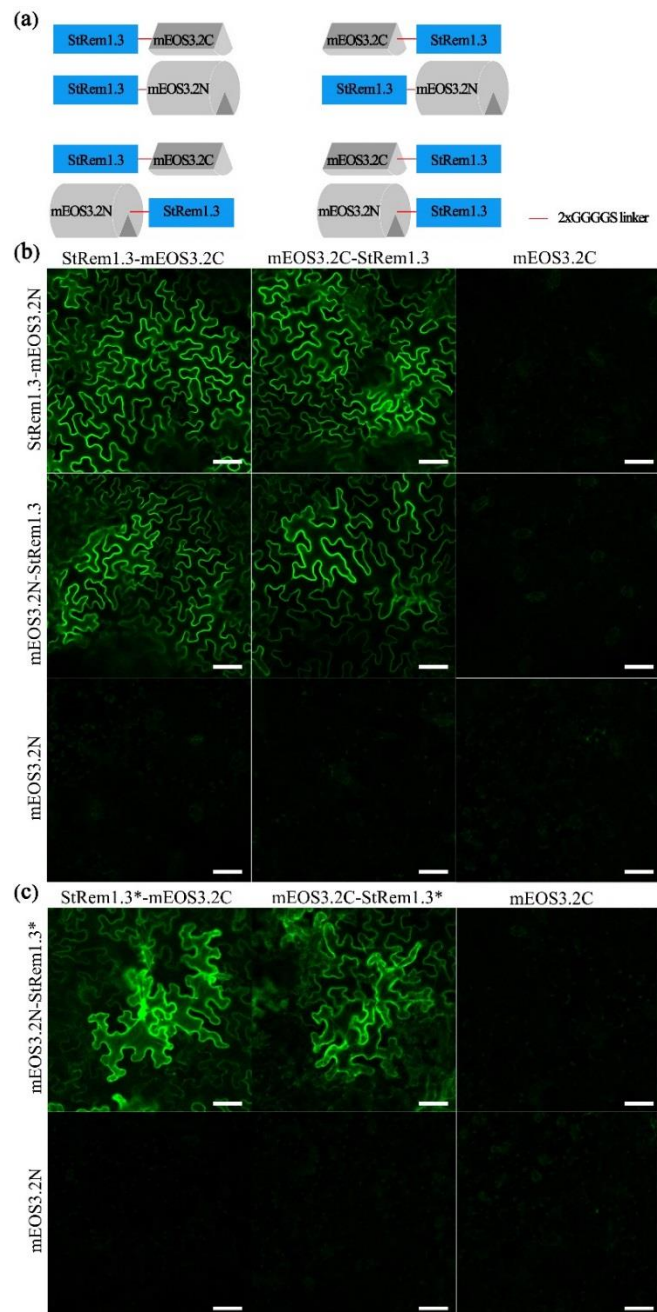


Figure 4.3 Fluorescence of mEOS3.2 BiFC complexes formed with remorin StRem1.3 in *N. benthamiana* leaf cortical cells.

(a) Four possible configurations for mEOS3.2/StRem1.3 fusions constructs for BiFC experiments. Flexible tandem GGGGS linkers (indicated by red lines) were used in all fusions. (b) Confocal fluorescence images produced by co-expression of the indicated mEOS3.2 BiFC fragments with StRem1.3 or control unfused mEOS3.2 BiFC protein fragments (c) Confocal fluorescence images produced by co-expression of the indicated mEOS3.2 BiFC fragments with StRem1.3* or control unfused mEOS3.2 BiFC protein fragments. Mutant StRem1.3* lacks membrane-binding but retains the ability to dimerize. Scale bars represent 50 μ m.

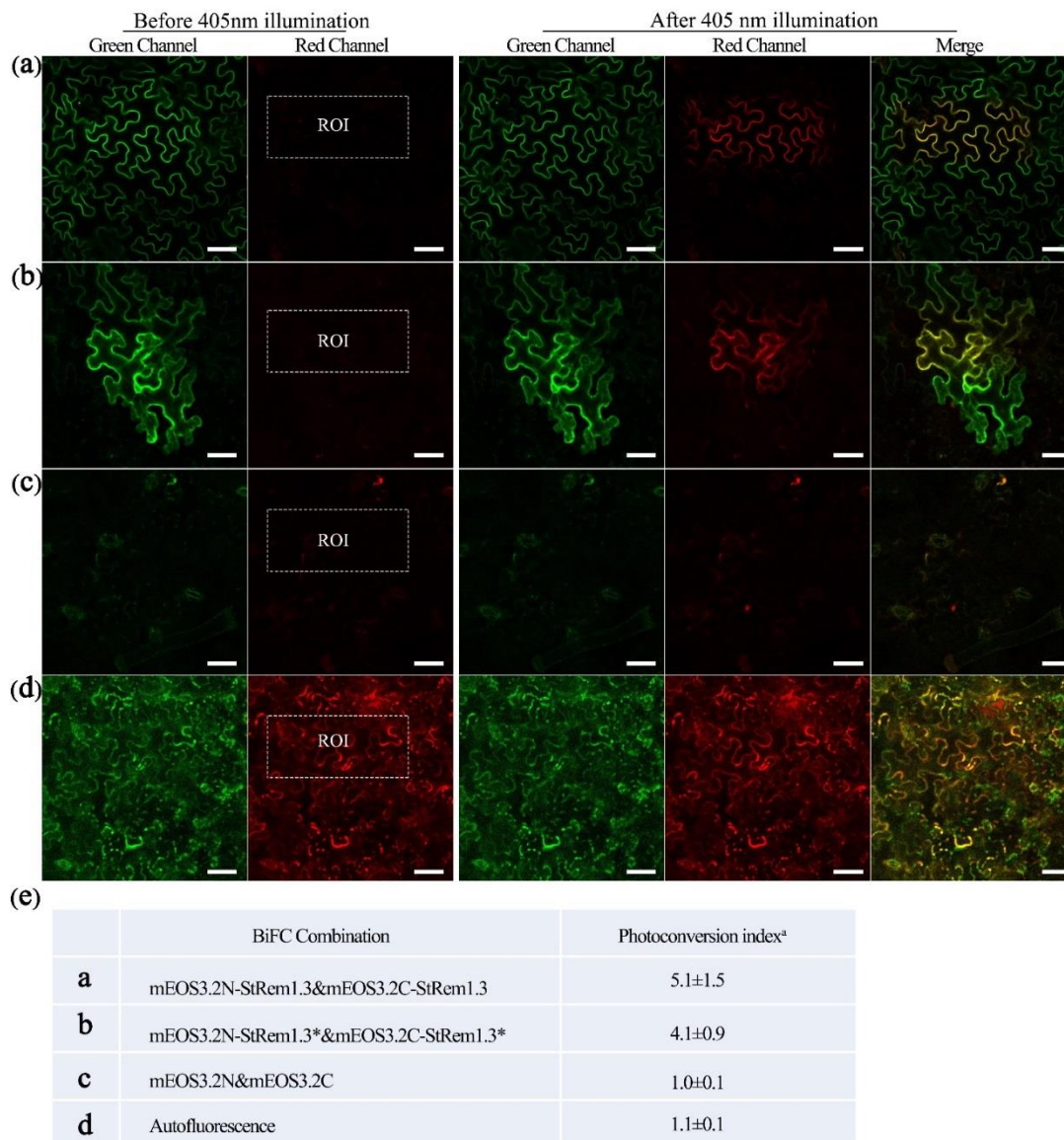


Figure 4.4 Photo-convertibility of mEOS3.2 BiFC complexes in *N. benthamiana* leaf cortical cells.

(a-b) fluorescence of mEOS3.2-StRem1.3 BiFC complexes targeted to the PM (a) or cytoplasm (b) before and after photoconversion using a 405-nm laser. (c-d) Background fluorescence (c) or autofluorescence (d) before and illumination with the 405-nm laser. (e) Photoconversion index (P.I.) of fluorescence from (a) to (d). P.I. = $(R2/R1)/(G2/G1)$ where R2 represents the average intensity of the red channel in the region of interest after photoconversion, R1 represent the average intensity of red channel before photoconversion, G2 represent the average intensity of the green channel after photoconversion, and G1 represent the average intensity of the green channel before photoconversion. The averages were from 6 images randomly taken from 2 different leaves. Scale bars represent 50 μm .

The P.I. was defined as $(R2/R1)/(G2/G1)$ where $R2$ = the average intensity of the red channel in the region of interest after photoconversion, $R1$ = the average intensity of red channel before photoconversion, $G2$ = the average intensity of the green channel after photoconversion, and $G1$ = the average intensity of the green channel before photoconversion. As shown in Figure 4.4e, typical P.I.'s for full length mEOS3.2, and BiFC mEOS3.2 were 5.1 ± 1.5 and 4.1 ± 0.9 , respectively, whereas typical P.I.'s for background and autofluorescence were 1.0 ± 0.1 and 1.1 ± 0.1 , respectively.

BiFC mEOS3.2 provides sub-diffraction resolution of StRem1.3 localization in PALM imaging

To evaluate the suitability of photo-convertible mEOS3.2 BiFC complexes for imaging protein complexes at the nanometer scale using PALM, we examined the localization of StRem1.3 on the PM of *N. benthamiana* leaf cells. Previous studies have suggested StRem1.3 may form metastable trimers in vitro (Bariola et al., 2004, Perraki et al., 2012). In addition, StRem1.3 and its homologs have been found to specifically label PM micro- or nano-domains (Raffaele et al., 2009, Haney et al., 2011, Jarsch et al., 2014). Therefore, StREM1.3 provided an excellent model to evaluate the suitability of mEOS3.2 BiFC complexes in order to quantitatively estimate the distribution and association of membrane proteins on the PM, at nanometer resolution.

To begin with, in live tissue, we found that both mEOS3.2-StRem1.3 and mEOS3.2N-StRem1.3+mEOS3.2C-StRem1.3 BiFC complexes readily provided the brightness and signal-to-background ratio required for single molecule imaging when using a 405-nm laser for photo-conversion and a 561-nm laser for excitation (Figure 4.5a).

Next, we conducted PALM imaging under total internal reflection (TIR) conditions with (Figure 4.5c and d) or without (Figure 4.5b) fixation of the samples using a modified paraformaldehyde method (Brière et al., 2004). In the reconstructed PALM images, the mEOS3.2-StRem1.3 molecules appeared at a higher abundance on the PM than the StRem1.3 BiFC complexes (Figure 4.5b and d). Neither mEOS3.2-StRem1.3 nor co-expressed mEOS3.2N-StRem1.3 and mEOS3.2C-StRem1.3 displayed any evidence of higher-order multimers on the PM; only randomly distributed monomers were observed. At nanometer resolution, it is possible to

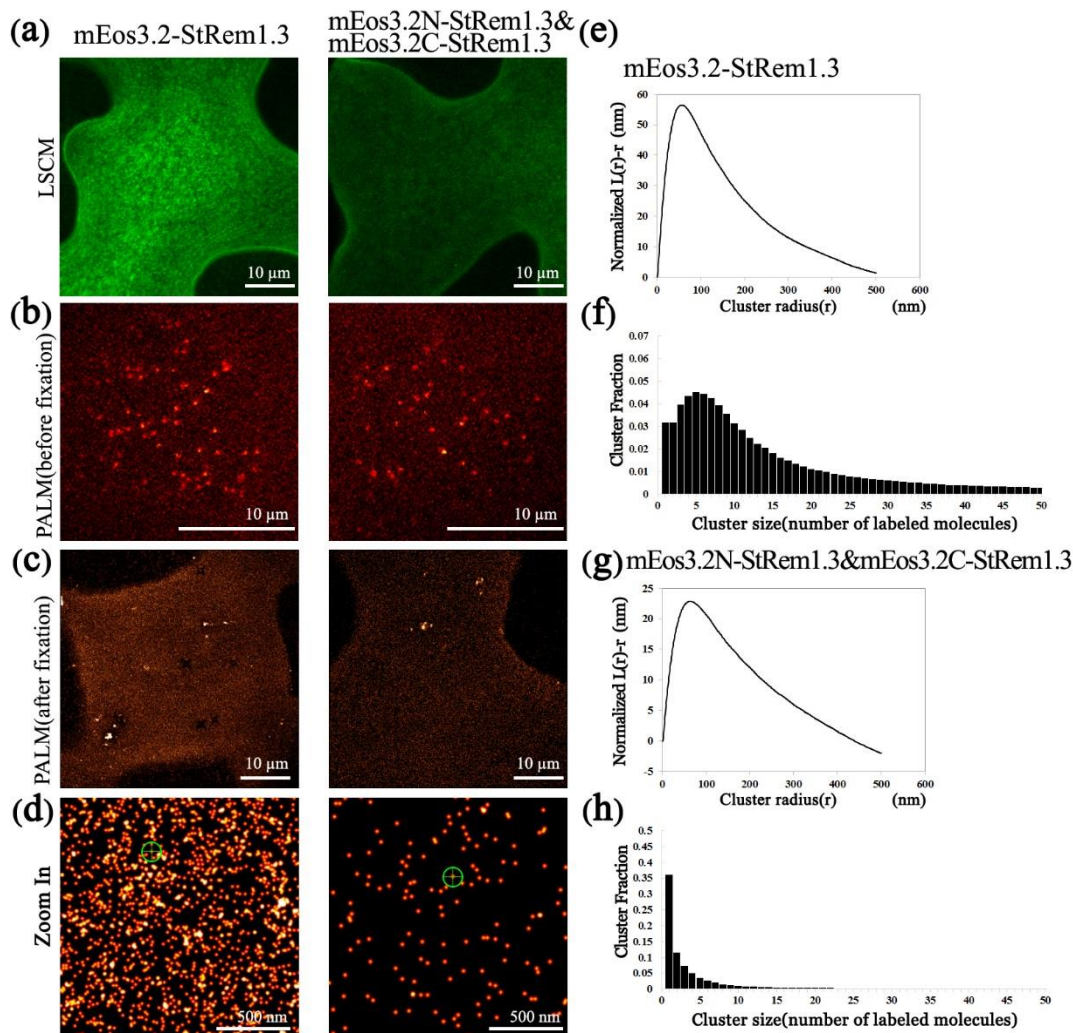


Figure 4.5 Use of mEOS3.2 BiFC complexes for PALM imaging in *N. benthamiana* leaf cortical cells.

PM-targeted mEOS3.2-StRem1.3 or co-expressed mEOS3.2N-StRem1.3 and mEOS3.2C-StRem1.3 were imaged by laser scanning confocal microscopy (LSCM) (a), or PALM (b-d). In (d) the green circles indicate a cluster with the radius of 60 nm centered on a single molecule (e and g), clustering of mEOS3.2 single molecule images assessed using Ripley's K-test analysis, based on three sampled areas from three different cells of either mEOS3.2-StRem1.3 or co-expressed mEOS3.2N-StRem1.3 plus mEos3.2C-StRem1.3. Plotted is $L(r)-r$ versus r , where $L = \sqrt{(K(t)/\pi)}$ and r is any given search radius (see Methods). (f, h) Statistically averaged distribution cluster sizes (numbers of molecules within a radius of 60 nm of a single molecule; count includes the single molecule) within the same three sampled regions.

characterize the clustering of individual molecules, distinct from multimers; clustering may represent locally higher densities of protein molecules, for instance due to the presence of a microdomain. Clusters were more easily detected with mEOS3.2-StRem1.3, due to the higher density of labeled molecules (Figure 4.5d). Using a previously described pairwise clustering algorithm, Ripley's K function (Nickerson et al., 2014), it was revealed that the distributions of clusters in mEOS3.2-StRem1.3 and mEOS3.2N-StRem1.3/mEOS3.2C-StRem1.3 were similar, both resembling a general beta distribution with a peak search radius of ~60 nm, indicating that clusters with diameters centered on 120 nm were most common (Figure 4.5e and g). The similarity of the cluster diameters suggests that the full length and BiFC mEOS3.2 probes were both detecting a similar underlying non-random structure in the membrane distribution of StRem1.3 molecules. Based on analysis by Simulation-Aided-DBSCAN (SAD), the mean numbers of visualized molecules in the StRem1.3 BiFC clusters was significantly smaller than in the mEOS3.2-StRem1.3 clusters (Figure 4.5f and h), due possibly to the need for two differently labeled molecules of StREM1.3 to produce each fluorescent molecule, as well as differences in gene expression levels.

Discussion

The bimolecular fluorescence complementation (BiFC) assay has become an indispensable for examining protein-protein interactions in the context of sub-cellular location. However, this assay has been hampered by the tendency of many fluorescence protein fragments to re-assemble into functional proteins in the absence of fused interaction partners. Here, we evaluated in detail a number of commonly used BiFC FPs for their tendency toward non-specific reassembly when transiently expressed in plant cells, including several mutants reported to exhibit reduced self-assembly. Taking advantage of the self-association of the plant-specific membrane associated protein StRem1.3, we successfully demonstrated that a new genetically engineered FP, mEOS3.2, has excellent performance in BiFC assays with much reduced self-assembly compared to currently used FPs. Importantly, the re-assembled mEOS3.2 BiFC complex retains the capability of photo-conversion from green to red, making it suitable for use in PALM super-resolution microscopy.

Several attempts have been explored to reduce the spontaneous re-assembly of FP fragments used for BiFC assays. The site-directed mutation T153M in the Venus N-terminal fragment, Venus155, was reported significantly reduce self-assembly in *Xenopus* cells (Saka et al., 2007). The site mutations V150L and V150A in Venus155 were also reported to efficiently decrease self-assembly in the BiFC assay (Lin et al., 2010, Nakagawa et al., 2011). In contrast, another study reported that the mutation V150L in Venus completely abolished the authentic BiFC signals in COS-1 cells, while the mutation I152L showed a 4-fold increase in signal-to-noise ratio in the BiFC assay (Kodama and Hu, 2010). However, our data revealed that none of these mutation sites were effective in reducing self-assembly in plant cells, which is in accordance with the results reported by Gookin et al (Gookin and Assmann, 2014). Moreover, although it had been reported that a new split site at residue 210 between the tenth and the eleventh β -sheets of Venus could produce superior signal-to-noise ratios in HeLa cells as well as in *N. benthamiana* leaf cells (Ohashi et al., 2012, Gookin and Assmann, 2014), our results suggest that the apparent low self-assembly of VenusN210/VenusC211 is an artifact of poor stability of the small VenusC211 peptide; we observed considerable false-positive BiFC signal due to self-assembly when VenusC211 was fused to any control peptide such as a 3xFLAG tag.

In contrast with traditional BiFC FPs, the photo-convertible fluorescent protein mEOS3.2 showed strongly reduced self-assembly when split after position 164 between the eighth and ninth β -sheets. Furthermore, self-assembly occurred efficiently and specifically when the mEOS3.2 fragments were fused in all possible configurations with the multimerizing membrane protein StRem1.3. As observed in *E. coli* (Liu et al., 2014), the re-assembled mEOS3.2 BiFC complex also retained the capability of photo-conversion in plant cells, required for PALM imaging. Using BiFC-PALM imaging, we were able to compare, at single-molecule resolution, StRem1.3 tagged with full-length mEOS3.2 with StRem1.3 dimers labeled by reassembled mEOS3.2 BiFC complexes. Notably, both forms of labeled StRem1.3 localized to clusters with a mean diameter of ~120 nm, which is closely similar to a previous report that used immunogold labeling and electron-microscopy (~80 nm) (Raffaele et al., 2009). Although the formation of BiFC complexes did not result in a significant change in

cluster diameter, the frequency of BiFC-labeled complexes was lower than molecules labeled with full length mEOS3.2. This may result from the fact that only dimers could be labeled, and/or that the accumulated protein concentrations of one of both mEOS3.2 fragments was lower than that of the full length protein.

Despite the many positive properties of the mEOS3.2 BiFC system, our data did reveal that even this system could exhibit visible non-specific self-assembly in some conditions, for example severe over-expression or when the fusion partners were placed on the N-termini of the mEOS fragments, especially the C-terminal fragment. This observation may be related to the N-end rule in ubiquitin-mediated protein degradation in which that the stability of a protein is highly related to the nature of its N-terminal amino acid residues (Tasaki et al., 2012). Several studies have shown that addition of different epitope tags, such as FLAG, Myc, or even a GFP fragment to the N-terminus of a protein of interest could variably increase the half-life of the protein (Schnappauf et al., 2003, Trausch-Azar et al., 2004, Alvarez-Castelao et al., 2012). Consistent with these observations, our data revealed that the N-terminal FLAG-tag fused to mEOS3.2 fragments more often resulted in noticeable self-assembly than the N-terminal HA tag. Accordingly, we observed minimal levels of self-assembly with when either mEOS3.2N or mEOS3.2C, or especially both, had a free N-terminus (Figure 4.2). Most likely therefore, minimal self-assembly is observed when the protein expression levels are moderated by degradation. Consistent with this interpretation, we also occasionally observed self-assembly when the protein partners were overexpressed from the strong and constitutive CaMV35 promoter. Presumably, when mEOS3.2 fragments accumulate to high concentrations, there is increased probability of random collisions resulting in self-assembly. We thus recommend that protein partners only be fused to the C-terminus of the mEOS3.2C fragment, and ideally be restricted to the C-terminus of the mEOS3.2N also. With this proviso, mEOS3.2 constitutes an excellent BiFC probe to study the protein-protein interactions in plant cells by both conventional and PALM confocal microscopy.

Materials and Methods

Plant Material

N. benthamiana were grown in soil (Fafard® 4M Mix). *N. benthamiana* plants were grown in a growth chamber with a 14 hr photoperiod at 25°C for 5 weeks before being used for *A. tumefaciens* infiltration assays.

Cloning and Construction

All DNA fragments were amplified using high-fidelity polymerase CloneAmp™ HiFi PCR premix (TaKaRa Bio) using oligonucleotides as listed in Table 4.1. mCherry was cloned from plasmid pSDK2 (Kale et al., 2010). Constructs encoding Venus, YFP, and StRem1.3 (Raffaele et al., 2007) were synthesized by GenScript Corporation. In-Fusion® HD Cloning kits (TaKaRa Bio) were used to insert gel purified PCR fragments into a modified Gateway™ donor vector, pDonR207-GOI, containing a genetically inserted 2xGGGGS linker. Constructs encoding mutant protein StRem1.3*, lacking PM binding, were generated using site-direct mutagenesis according to the In-Fusion® HD Cloning system (TaKaRa Bio). When protein detection experiments were needed, a 1xFLAG epitope tag was inserted between the two GGGGS linkers in the pDonR207-GOI fusion vector. For pDonR207-mEOS3.2N or pDonR207-mEOS3.2C, N-terminal or C-terminal 1xFLAG or 3xFLAG epitope tags were separately inserted using In-Fusion® HD Cloning kits (TaKaRa Bio). Subsequently, using Gateway™ LR reactions (Thermo Fisher scientific Inc.), the resulting fusion constructs were transferred from pDonR207 vectors to the Gateway™ compatible expression vector, pmAEV-35S, derived from the binary vector pCAMBIA (Dou et al., 2008). All constructs were verified by sequencing and propagated using DH10B *E. coli* cells.

Transient expression in *N. benthamiana* leaves

All expression constructs were transformed into *Agrobacterium tumefaciens* strain GV3101 using electroporation (Tasaki et al.). The bacteria were grown on Luria-Bertani (LB) medium (50 µg/ml kanamycin) at 28°C overnight. *A. tumefaciens* cells were collected by centrifugation and re-suspended in pH 5.7 MES buffer (10 mM MgCl₂, 10 mM MES, 100 µM acetosyringone). Cell suspensions for infiltrations were diluted to OD₆₀₀=0.1; equal volumes of the co-localization-partner and BiFC-partner cells with OD₆₀₀ of 0.2 were mixed together. Cell suspensions were incubated in MES

Table 4.1 Primer designed and used in chapter 4.

Oligo Name	Forward primer(5'-3')	Reverse primer(5'-3')	Appliction notes
YFPn	TATATCATGGCCGACTAAGATATCA CCCAGCTTCCTTGTACAAAGTT	GTCGGCCATGATATAGACGTTGTG GC	
YFPc	AAGCAGAAGAACGGCATCAAGG	GCCGTTCTTCTGCTTCATTCGCGA GGAGCCTGCTTTTTTGTACAAACT TG	
VenusN	GGCGGTAGCGCTAGCATGGTGAGCA AGGGCGAGGAGCTGTTC	AAGCTGGGTGATATCTTAGTCGGC GGTGATATAGACGTTG	POI-VenusN
VenusC	AAGCAGGCTCCTCGCGAATGAAGCA GAAGAACGGCATC	CTCCTCCACCTCTAGAGGACTTGT ACAGCTCGTCCATG	POI-VenusC
VenusC stop		CTCCTCCACCTCTAGATTAGGACT TGTACAGCTCGTCCATG	VenusC-stop
mCherryN	GGCGGTAGCGCTAGCATGGTGAGCA AGGGCGAGGAGG	AAGCTGGGTGATATCTTAGTCCTC GGGTACATCCGCTCG	
mCherryC	AGCAGGCTCCTCGCGAATGGGCGCC CTGAAGGGCGAGATCAAG	CTCCTCCACCTCTAGATTAAGATC TGTACAGCTCGTCCATG	
mEOS3.2	GGCGGTAGCGCTAGCATGAGTGCGA TTAAGCCAGACATG	AAGCTGGGTGATATCTTATCGTCT GGCATTGTCAGGC	POI-mEOS3.2
mEOS3.2N 1	AGCAGGCTCCTCGCGAATGAGTGCG ATTAAGCCAGACATG	CTCCTCCACCTCTAGAAAGCTGGG TGATATCTTA	mEOS3.2N-POI
mEOS3.2N 2		AAGCTGGGTGATATCTTATTCAAG CAACAAAGCCATCTC	POI-mEOS3.2N
mEOS3.2C 1	AGCAGGCTCCTCGCGAATGGGAAAT GCCATTACCGATG	CTCCTCCACCTCTAGATCGTCTGG CATTGTCAGGC	mEOS3.2C-POI
mEOS3.2C 2	GGCGGTAGCGCTAGCGGAAATGCC ATTACCGATG	AAGCTGGGTGATATCTTATCGTCT GGCATTGTCAGGC	POI-mEOS3.2C

mEOS3.2C stop		CTCCTCCACCTCTAGATTATCGTC TGGCATTGTCAGGC	mEOS3.2C-stop
VenusN151	CAACCTGTATATCACCGCCG	ATATACAGGTTGTGGCTGTTG	V151L
VenusN153	CTATTTGACCGCCGACTAAGA	GCGGTCAAATAGACGTTGTGG	I153L
VenusN151&153	AACCTGTATTTGACCGCCGACTAAG ATATC	GGTCAAATACAGGTTGTGGCTGTT GTAGTTG	V151L, I153L
StRem1.3-1	GGCGGTAGCGCTAGCGCAGAATTGG AAGCTAAG	AAGCTGGGTGATATCTTAAAATAT TCCAAGGATTTTC	FP-StRem1.3
StRem1.3-2	AGCAGGCTCCTCGCGAATGGCAGAA TTGGAAGCTAAG	CTCCTCCACCTCTAGAAAATATTC CAAGGATTTTC	StRem1.3-FP
StRem1.3*-1	CATCATCATAAATCTCGTTCTACTGT GACTAGTCCA	AGATTTATGATGATGCTCCTCTGC CTTGAGAAGATC	L179H, A180H, A181H, Y184S, A185S, G187V, A189A, L194S, G195Q, I196Q, F197Q
StRem1.3*-2	CAACAGCAATCTAGATGAGATATCA CCCAG	TTGCTGTTGAGAGATTTTCTTTGG ACTAGTC	L179H, A180H, A181H, Y184S, A185S, G187V, A189A, L194S, G195Q, I196Q, F197Q
GGGS- FLAG-GGGS	CAAAGACGATGACGACAAGGGCGG TGGCGGTAGCGCTAGC	CGTCATCGTCTTTGTAGTCGCTGC CTCCTCCACCTCTAGA	
FLAG- mEOS3.2N	CAAAGACGATGACGACAAGGGCGG TGGCGGTAGCGCTAGCATG	TCGTCATCGTCTTTGTAGTCCATC GAGGAGCCTGCTTTTTTGTACAAA GTTG	
mEOS3.2N- FLAG	TAAGCTAGCGATATCACCCAGCTTC CTTGTACAAAGTTGGC	GATATCGCTAGCTTACTTGTCGTC ATCGTCTTTGTAGTCG	
3xFLAG- mEOS3.2C	CCATGACGGTGAATAAAGGATCAC GACATTGACTACAAAGACGATGACG ACAAG	TAGTCACCGTCATGGTCCTTATAA TCCATTCGCGAGGAGCCTGCTTTT TTG	

mEOS3.2C-3xFLAG	GTCATATGGATAGGATCCTGCATAG TCCGGGACGTCATAGGGATAGCCCG CATAGTCAGG	TTATAGTCACCGTCATGGTCCTTA TAATCGCTACCGCCACCGCCTCGT CTGGCATTG	
HA-mEOS3.2N	TACGATGTTCCAGATTACGCTGGCG GTGGCGGTAGCGCTAGCATGAGTGC GATTAAG	ATCTGGAACATCGTATGGGTACAT TCGCGAGGAGCCTGCTTTTTTGTA CAAAGTTG	
mEOS3.2N-HA	TACGATGTTCCAGATTACGCTTAAG CTAGCGACGCCGGCCGAGTTCTCG	ATCTGGAACATCGTATGGGTAGCT GCCTCCTCCACCTCTAGATTCAAG	
3xHA-mEOS3.2C	GCAGGCTCCTCGCGAATGGCGGCCG TTTACCCATACGATGTTC	GCTACCGCCACCGCCGGCGGCCG GAGCGTAATCTGGAAC	Using mEOS3.2C-3xHA as template
mEOS3.2C-3xHA-1	TCCTATCCATATGACGTTCCAGATTA CGCTCCGGCCGCCTAAGATATCACC CAGCTTCCT	GCCCGCATAGTCAGGAACATCGT ATGGGTAAACGGCCGCGCTACCG CCACCGCCTCGTCT	
mEOS3.2C-3xHA-2	CCTGACTATGCGGGCTATCCCTATG ACGTCCCGGACTATGCAGGATCCTA TCCATATGAC	GTCATATGGATAGGATCCTGCATA GTCCGGGACGTCATAGGGATAGC CCGCATAGTCAGG	
YFPn	TATATCATGGCCGACTAAGATATCA CCCAGCTTCCTTGTACAAAGTT	GTCGGCCATGATATAGACGTTGTG GC	
YFPc	AAGCAGAAGAACGGCATCAAGG	GCCGTTCTTCTGCTTCATTCGCGA GGAGCCTGCTTTTTTGTACAAACT TG	
VenusN	GGCGGTAGCGCTAGCATGGTGAGCA AGGGCGAGGAGCTGTTC	AAGCTGGGTGATATCTTAGTCGGC GGTGATATAGACGTTG	POI-VenusN
VenusC	AAGCAGGCTCCTCGCGAATGAAGCA GAAGAACGGCATC	CTCCTCCACCTCTAGAGGACTTGT ACAGCTCGTCCATG	POI-VenusC
VenusC stop		CTCCTCCACCTCTAGATTAGGACT TGTACAGCTCGTCCATG	VenusC-stop
mCherryN	GGCGGTAGCGCTAGCATGGTGAGCA AGGGCGAGGAGG	AAGCTGGGTGATATCTTAGTCCTC GGGTACATCCGCTCG	

mCherryC	AGCAGGCTCCTCGCGAATGGGCGCC CTGAAGGGCGAGATCAAG	CTCCTCCACCTCTAGATTAAGATC TGTACAGCTCGTCCATG	
mEOS3.2	GGCGGTAGCGCTAGCATGAGTGCGA TTAAGCCAGACATG	AAGCTGGGTGATATCTTATCGTCT GGCATTGTCAGGC	POI-mEOS3.2

buffer with 100 μ m acetosyringone at RT for 1 hour with moderate shaking (100 rpm). All infiltrated *N. benthamiana* plants were kept in the growth chamber with same conditions described above until imaging.

Confocal laser scanning microscopy (CLSM) and analysis

Confocal imaging was performed on a ZEISS LSM 780 NLO confocal microscope system using 20x/0.8 air, 40x/1.4 oil-immersion objectives. Argon laser lines 488 nm and 514 nm were respectively used for exciting the green form of mEOS3.2 and YFP. The 561-nm Diode Pumped Solid State (DPSS) laser was used to excite mCherry and the red form of mEOS3.2. For mEOS3.2 photoconversion assays, one image was captured in both the green (491-544 nm) and red (562-640nm) channels prior to photoconversion. Then a selected region of interest (ROI) was subjected to photoconversion using 405-nm diode laser for 20 pulses with a 50% output power. Immediately afterwards, the image was recaptured in the green and red channels.

All microscopy images were processed using ZEN2 software (Blue edition). For quantifying the efficiency of photoconversion of mEOS3.2, including BiFC mEOS3.2, the average intensities of the ROI provided by ZEN2 were used to estimate changes in either the green or red fluorescence channels. The change was quantitatively represented using the equation: Photoconversion index = $(R2/R1)/(G2/G1)$ where R2 = the average intensity of the red channel after photoconversion, R1 = the average intensity of the red channel before photoconversion, G2 = the average intensity of the green channel after photoconversion, and G1 = the average intensity of the green channel before photoconversion.

Protein extraction and western blots

For protein extraction, *N. benthamiana* leaves were harvested at 48 hours after agroinfiltration. Infiltrated fresh leaves were ground into powder using mortar and pestle with liquid nitrogen. About 1g leaf powder was re-suspended with 2 ml of GTEN protein extraction buffer (25 mM Tris-HCl, pH 7.5, 1 mM EDTA, 150 mM NaCl, 10% (V/V) glycerol) to which was freshly added 2% w/v polyvinylpyrrolidone (PVPP), 10 mM dithiothreitol, 10 μ L/ml Halt protease inhibitor single-use cocktail (Thermo Fisher scientific Inc.), 0.1% (V/V) Tween 20 (Sigma), and 0.5% Triton X-100 (Fisher Scientific). FLAG-tagged proteins were collected from the supernatant using ANTI-

FLAG M2 Magnetic Beads (Sigma). After collection, protein samples were added to 4x SDS loading buffer (40% V/V Glycerol, 240 mM Tris-HCl, pH6.8, 8% SDS, 0.04% bromophenol blue, 5% beta-mercaptoethanol) then denatured at 95°C for 10 mins. Protein samples were fractionated by SDS/PAGE (12.5% single-percentage gels) in Tris-Glycine native running buffer (25 mM Tris Base, 192 mM Glycine). Equilibrated gels were transferred to methanol-pretreated Immobilon-P^{SQ} polyvinylidene difluoride membrane (PVDF)(Millipore). Membranes were incubated in TBST (20mM Tris-HCl, pH 7.5, 150 mM NaCl, 0.1%(V/V) Tween 20) containing 3% non-fat dry milk for 1 h, followed by a one time wash with TBST. Subsequently, membranes were incubated for 1.5 h with diluted (V/V=1:4000) mouse monoclonal ANTI-FLAG M2 antibodies (Sigma) in TBST. Membranes were washed for 5 min in TBST with 3 repeats. Then when required, membranes were incubated with goat anti-mouse IgG HRP conjugate(H+L) secondary antibodies (Millipore) at a 1:5000 dilution in TBST for 1 hour. Before chemiluminescent imaging, the membranes were washed three times (5 min for each wash) in TBST. The western signal was visualized on an Azure c600 Imager (Azurebiosystems) using Pierce ECL Plus Western Blotting Substrate (Thermo Fisher scientific Inc.).

Fixation of agroinfiltrated *N. benthamiana* leaves

N. benthamiana leaves for PALM imaging were harvested at 72 hour after agroinfiltration. Leaves were cut into small square pieces (~1 cm²) and transferred into the barrel of a 10 ml syringe. 5 ml freshly prepared 2%(W/V) paraformaldehyde (Sigma) in PHEM (100 mM PIPES, 50 m HEPES, pH 7.2, 20 mM EDTA, 15 mM MgSO₄) was added into barrel making sure all leaf pieces were immersed. Then syringe was held vertically with tip facing up and the plunger was pushed up to expel air out of the barrel. With the tip sealed by its cap, the plunger was pulled back allowing the PHEM/paraformaldehyde solution to enter inside the leaf tissue until only a small volume of air bubble could be observed coming from edge of the leaf pieces (~usually 3-4 cycles of push-pull of the syringe piston). Then the leaf pieces were incubated for 5 mins at room temperature. After incubation, the leaf pieces were rinsed 3 times with PBS (pH7.4) buffer. The leaf pieces then were transferred onto a coverslip with the back (abaxial) side facing up. In order to provide fiducial markers to computationally

correct lateral and axial drift during acquisition, 50 nm gold nanoparticles (BBI solutions) at a dilution of 1: 10(V/V) in DPBS (Thermo Fisher scientific Inc) were added onto the leaf pieces for 5 mins, followed by 3 rinses in PBS. The leaf pieces were mounted into an imaging chamber (ALA Scientific Instruments).

PALM Microscopy

We performed PALM imaging on a Nikon Ti-U inverted microscope with a Nikon 60x APO TIRM objective (NA=1.49) as described previously (Nickerson et al., 2014). A 405-nm laser (CUBE-405; Coherent) was used for photoconversion of mEOS3.2 and a 561-nm laser (MGL-H-561; OptoEngine, UT) was used for excitation. During image acquisition, the 405-nm laser was continuously turned on with the power gradually increased to maintain a convenient density of converted mEOS3.2 within the field of view. Images were recorded with an electron multiplying CCD camera (Andor), and each sequential image had 30,000-50,000 frames.

PALM images were analyzed as described previously (Nan et al., 2013) using custom-written scripts in Matlab. Clustering of mEOS3.2 was assessed using Ripley's K-test analysis, based on three sampled areas from three different cells of either mEOS3.2-StRem1.3 or mEOS3.2N-StRem1.3 plus mEos3.C-StRem1.3. In figure 4.5, $L(r) - r$ is plotted versus r , where $L = \sqrt{(K(t)/\pi)}$ and r is any given search radius. $L(r) - r$ can be interpreted to be the search radius needed to encompass the observed number of molecules on average if the distribution were purely random. Thus if $L(r) - r = 55$ nm when $r = 100$ nm, then on average the numbers of molecules found within a 100 nm search radius (from any single molecule) would be the number expected from a random distribution of the same density with a search radius of 155 nm. The peak value of $L(r) - r$ versus r indicates the search radius where clustering is most evident.

Supplementary Figures:

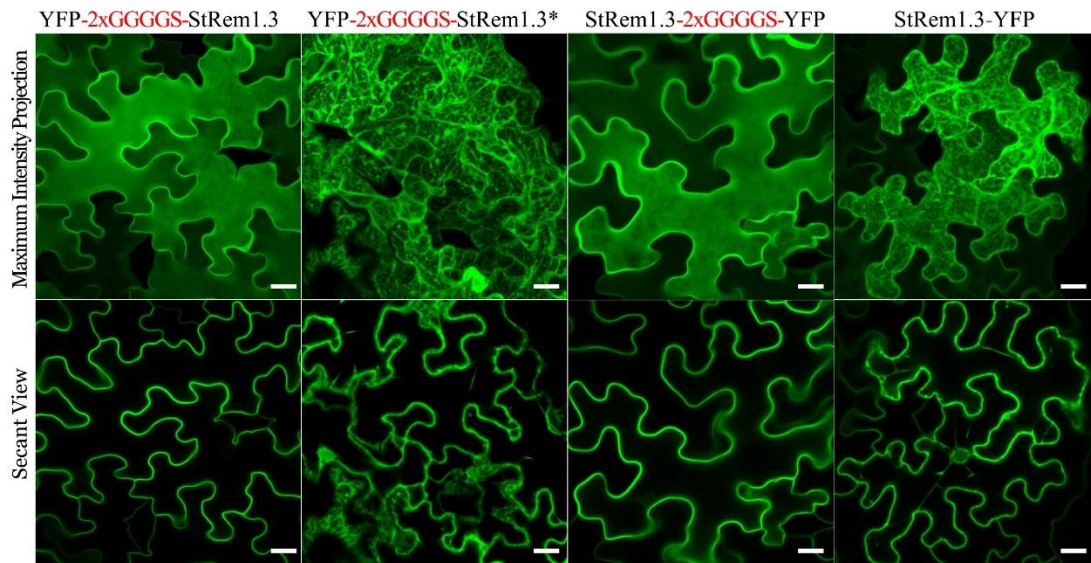


Figure S4.1 Localization of various StRem1.3 with YFP fusions expressed in *N. benthamiana* leaf cortical cells.

Mutations that reduced the hydrophobicity of the C-terminal membrane-insertion domain of StRem1.3, StRem1.3*, result in targeting to the cytoplasm. A flexible linker (2xGGGGS) prevents C-terminal-attached YFP from interfering with the membrane targeting of StREM1.3 by its C-terminal domain. Scale bars represent 20 μm .

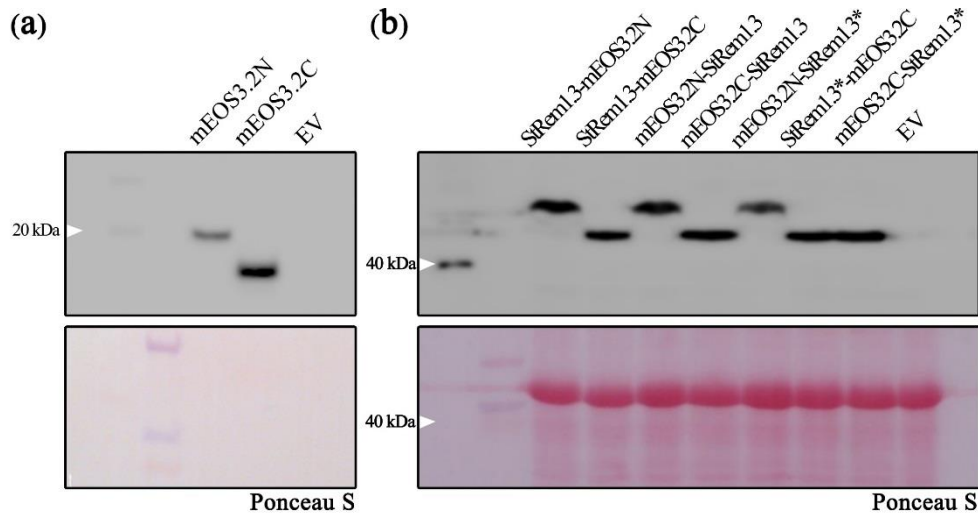


Figure S4.2 Validation of BiFC fusion protein expression in *N. benthamiana* leaves.

(a) Immunoblots of mEOS3.2N-FLAG (21 kD) and mEOS3.2C-3xFLAG (11 kD) in purified protein extracts which were prepared using ANTI-FLAG M2 Magnetic Beads.

(b) Immunoblots of FLAG-tagged StRem1.3-mEOS3.2N (43 kD), StRem1.3-mEOS3.2C (32 kD), mEOS3.2N-StRem1.3 (43 kD), mEOS3.2C-StRem1.3 (32 kD), mEOS3.2N-StRem1.3* (43 kD), StRem1.3*-mEOS3.2C (32 kD), mEOS3.2C-StRem1.3* (32kD) in leaf total protein extracts. The immunoblot analysis was performed using anti-FLAG M2 antibodies. As a control (EV), extracts from leaves cells transfected with expression vector carrying full-length unfused mEOS3.2 were analyzed. Ponceau S staining of Rubisco was used as loading control.

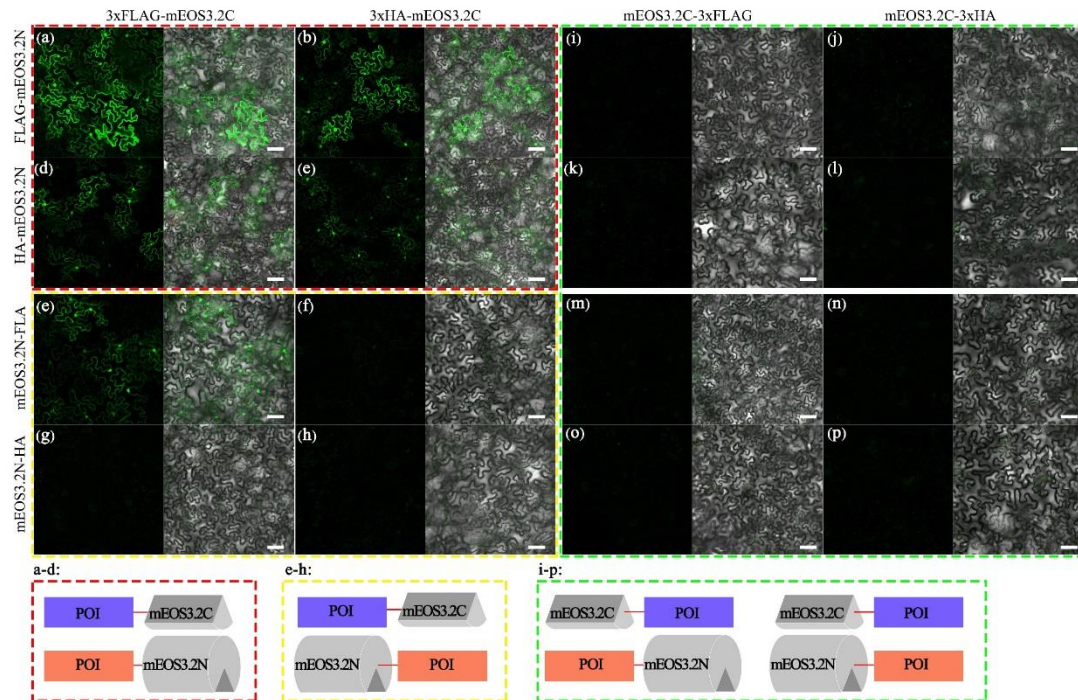


Figure S4.3 Self-assembly of BiFC mEOS3.2 complexes expressed in *N. benthamiana* leaf cortical cells.

(a-d) False positive BiFC signals produced when a FLAG or HA epitope tag was fused to the N-terminus of both mEOS3.2N and mEOS3.2C; highlighted by the red open-dash box. (e-h) Weak false positive BiFC signals produced when the tags were attached to the C-terminus of mEOS3.2N and the N-terminus of mEOS3.2C; highlighted by the yellow open-dash box. (i-p) Minimal to zero false positive BiFC signals produced when the tags were attached to the C-terminus of mEOS3.2N, with tags attached to either terminus of mEOS3.2C; highlighted by the green open-dash box. POI represents the protein of interest. Scale bars represent 50 μm .

Bibliography

Alvarez-Castelao, B., Ruiz-Rivas, C., Castaño, J., and G. (2012) A Critical Appraisal of Quantitative Studies of Protein Degradation in the Framework of Cellular Proteostasis. *Biochemistry Research International*, **2012**, 11.

Bariola, P., Retelska, D., Stasiak, A., Kammerer, R., Fleming, A., Hijri, M., Frank, S. and Farmer, E. (2004) Remorins form a novel family of coiled coil-forming oligomeric and filamentous proteins associated with apical, vascular and embryonic tissues in plants. *Plant Molecular Biology*, **55**, 579-594.

Betzig, E., Patterson, G.H., Sougrat, R., Lindwasser, O.W., Olenych, S., Bonifacio, J.S., Davidson, M.W., Lippincott-Schwartz, J. and Hess, H.F. (2006) Imaging Intracellular Fluorescent Proteins at Nanometer Resolution. *Science*, **313**, 1642-1645.

Bracha-Drori, K., Shichrur, K., Katz, A., Oliva, M., Angelovici, R., Yalovsky, S. and Ohad, N. (2004) Detection of protein-protein interactions in plants using bimolecular fluorescence complementation. *The Plant Journal*, **40**, 419-427.

Brière, C., Barthou, H. and Petitprez, M. (2004) A new tool for plant cell biology: in vivo antibody uptake in plant protoplasts. *Plant Cell Reports*, **22**, 878-884.

Brückner, A., Polge, C., Lentze, N., Auerbach, D. and Schlattner, U. (2009) Yeast Two-Hybrid, a Powerful Tool for Systems Biology. *International Journal of Molecular Sciences*, **10**, 2763-2788.

Brymora, A., Valova, V.A. and Robinson, P.J. (2001) Protein-Protein Interactions Identified by Pull-Down Experiments and Mass Spectrometry. In *Current Protocols in Cell Biology*: John Wiley & Sons, Inc.

Dou, D., Kale, S.D., Wang, X., Jiang, R.H., Bruce, N.A., Arredondo, F.D., Zhang, X. and Tyler, B.M. (2008) RXLR-mediated entry of *Phytophthora sojae* effector Avr1b into soybean cells does not require pathogen-encoded machinery. *Plant Cell*, **20**, 1930-1947.

Du, J., Rietman, H. and Vleeshouwers, V.G.A.A. (2014) Agroinfiltration and PVX Agroinfection in Potato and *Nicotiana benthamiana*. *Journal of Visualized Experiments : JoVE*, 50971.

- Fan, J.-Y., Cui, Z.-Q., Wei, H.-P., Zhang, Z.-P., Zhou, Y.-F., Wang, Y.-P. and Zhang, X.-E.** (2008) Split mCherry as a new red bimolecular fluorescence complementation system for visualizing protein–protein interactions in living cells. *Biochemical and Biophysical Research Communications*, **367**, 47-53.
- Gookin, T.E. and Assmann, S.M.** (2014) Significant reduction of BiFC non-specific assembly facilitates in planta assessment of heterotrimeric G-protein interactors. *The Plant Journal*, **80**, 553-567.
- Haney, C.H., Riely, B.K., Tricoli, D.M., Cook, D.R., Ehrhardt, D.W. and Long, S.R.** (2011) Symbiotic Rhizobia Bacteria Trigger a Change in Localization and Dynamics of the *Medicago truncatula* Receptor Kinase LYK3. *The Plant Cell*, **23**, 2774-2787.
- Horstman, A., Nougalli Tonaco, I.A., Boutilier, K. and Immink, R.G.H.** (2014) A Cautionary Note on the Use of Split-YFP/BiFC in Plant Protein-Protein Interaction Studies. *International Journal of Molecular Sciences*, **15**, 9628-9643.
- Hu, C.-D., Chinenov, Y. and Kerppola, T.K.** (2002) Visualization of Interactions among bZIP and Rel Family Proteins in Living Cells Using Bimolecular Fluorescence Complementation. *Molecular Cell*, **9**, 789-798.
- Huang, B., Bates, M. and Zhuang, X.** (2009) Super-resolution fluorescence microscopy. *Annual review of biochemistry*, **78**, 993-1016.
- Jarsch, I.K., Konrad, S.S.A., Stratil, T.F., Urbanus, S.L., Szymanski, W., Braun, P., Braun, K.-H. and Ott, T.** (2014) Plasma Membranes Are Subcompartmentalized into a Plethora of Coexisting and Diverse Microdomains in *Arabidopsis* and *Nicotiana benthamiana*. *The Plant Cell Online*.
- Kaboord, B. and Perr, M.** (2008) Isolation of Proteins and Protein Complexes by Immunoprecipitation. In *2D PAGE: Sample Preparation and Fractionation* (Posch, A. ed. Totowa, NJ: Humana Press, pp. 349-364.
- Kale, S.D., Gu, B., Capelluto, D.G., Dou, D., Feldman, E., Rumore, A., Arredondo, F.D., Hanlon, R., Fudal, I., Rouxel, T., Lawrence, C.B., Shan, W. and Tyler, B.M.** (2010) External lipid PI3P mediates entry of eukaryotic pathogen effectors into plant and animal host cells. *Cell*, **142**, 284-295.

- Kerppola, T.K.** (2008) Bimolecular Fluorescence Complementation (BiFC) Analysis as a Probe of Protein Interactions in Living Cells. *Annual Review of Biophysics*, **37**, 465-487.
- Kodama, Y. and Hu, C.D.** (2010) An improved bimolecular fluorescence complementation assay with a high signal-to-noise ratio. *Biotechniques*, **49**, 793-805.
- Kusumi, A., Suzuki, K.G.N., Kasai, R.S., Ritchie, K. and Fujiwara, T.K.** (2011) Hierarchical mesoscale domain organization of the plasma membrane. *Trends in Biochemical Sciences*, **36**, 604-615.
- Lin, J., Wang, N., Li, Y., Liu, Z., Tian, S., Zhao, L., Zheng, Y., Liu, S., Li, S., Jin, C. and Xia, B.** (2010) LEC-BiFC: a new method for rapid assay of protein interaction. *Biotechnic & Histochemistry*, **86**, 272-279.
- Lin, J., Wang, N., Li, Y., Liu, Z., Tian, S., Zhao, L., Zheng, Y., Liu, S., Li, S., Jin, C. and Xia, B.** (2011) LEC-BiFC: a new method for rapid assay of protein interaction. *Biotechnic & Histochemistry*, **86**, 272-279.
- Liu, Z., Xing, D., Su, Q.P., Zhu, Y., Zhang, J., Kong, X., Xue, B., Wang, S., Sun, H., Tao, Y. and Sun, Y.** (2014) Super-resolution imaging and tracking of protein-protein interactions in sub-diffraction cellular space. *Nat Commun*, **5**.
- Mathur, J., Radhamony, R., Sinclair, A.M., Donoso, A., Dunn, N., Roach, E., Radford, D., Mohaghegh, P.S., Logan, D.C., Kokolic, K. and Mathur, N.** (2010) mEosFP-based green-to-red photoconvertible subcellular probes for plants. *Plant Physiol*, **154**, 1573-1587.
- Mylle, E., Codreanu, M.-C., Boruc, J. and Russinova, E.** (2013) Emission spectra profiling of fluorescent proteins in living plant cells. *Plant Methods*, **9**, 10.
- Nakagawa, C., Inahata, K., Nishimura, S. and Sugimoto, K.** (2011) Improvement of a Venus-Based Bimolecular Fluorescence Complementation Assay to Visualize bFos-bJun Interaction in Living Cells. *Biosci Biotech Bioch*, **75**, 1399-1401.
- Nan, X., Collisson, E.A., Lewis, S., Huang, J., Tamguney, T.M., Liphardt, J.T., McCormick, F., Gray, J.W. and Chu, S.** (2013) Single-molecule superresolution imaging allows quantitative analysis of RAF multimer formation and signaling. *Proc Natl Acad Sci U S A*, **110**, 18519-18524.

- Nickerson, A., Huang, T., Lin, L.-J. and Nan, X.** (2014) Photoactivated Localization Microscopy with Bimolecular Fluorescence Complementation (BiFC-PALM) for Nanoscale Imaging of Protein-Protein Interactions in Cells. *PLoS ONE*, **9**, e100589.
- Ohashi, K., Kiuchi, T., Shoji, K., Sampei, K. and Mizuno, K.** (2012) Visualization of cofilin-actin and Ras-Raf interactions by bimolecular fluorescence complementation assays using a new pair of split Venus fragments. *Biotechniques*, **52**, 45-50.
- Perraki, A., Cacas, J.L., Crowet, J.M., Lins, L., Castroviejo, M., German-Retana, S., Mongrand, S. and Raffaele, S.** (2012) Plasma membrane localization of *Solanum tuberosum* remorin from group 1, homolog 3 is mediated by conformational changes in a novel C-terminal anchor and required for the restriction of potato virus X movement]. *Plant Physiol*, **160**, 624-637.
- Raffaele, S., Bayer, E., Lafarge, D., Cluzet, S., German Retana, S., Boubekour, T., Leborgne-Castel, N., Carde, J.P., Lherminier, J., Noiro, E., Satiat-Jeunemaitre, B., Laroche-Traineau, J., Moreau, P., Ott, T., Maule, A.J., Reymond, P., Simon-Plas, F., Farmer, E.E., Bessoule, J.J. and Mongrand, S.** (2009) Remorin, a solanaceae protein resident in membrane rafts and plasmodesmata, impairs potato virus X movement. *Plant Cell*, **21**, 1541-1555.
- Raffaele, S., Mongrand, S., Gamas, P., Niebel, A. and Ott, T.** (2007) Genome-wide annotation of remorins, a plant-specific protein family: evolutionary and functional perspectives. *Plant Physiol*, **145**, 593-600.
- Rust, M.J., Bates, M. and Zhuang, X.** (2006) Sub-diffraction-limit imaging by stochastic optical reconstruction microscopy (STORM). *Nature Methods*, **3**, 793.
- Saka, Y., Hagemann, A., Piepenburg, O. and Smith, J.C.** (2007) Nuclear accumulation of Smad complexes occurs only after the midblastula transition in *Xenopus*. *Development (Cambridge, England)*, **134**, 4209-4218.
- Schnappauf, F., Hake, S.B., Carvajal, M.M.C., Bontron, S., Lisowska-Grospierre, B. and Steimle, V.** (2003) N-terminal destruction signals lead to rapid degradation of the major histocompatibility complex class II transactivator CIITA. *European Journal of Immunology*, **33**, 2337-2347.
- Schütze, K., Harter, K. and Chaban, C.** (2009) Bimolecular Fluorescence Complementation (BiFC) to Study Protein-protein Interactions in Living Plant Cells.

In Plant Signal Transduction: Methods and Protocols (Pfannschmidt, T. ed. Totowa, NJ: Humana Press, pp. 189-202.

Sekar, R.B. and Periasamy, A. (2003) Fluorescence resonance energy transfer (FRET) microscopy imaging of live cell protein localizations. *The Journal of Cell Biology*, **160**, 629-633.

Shyu, Y.J., Liu, H., Deng, X. and Hu, C.D. (2006) Identification of new fluorescent protein fragments for bimolecular fluorescence complementation analysis under physiological conditions. *Biotechniques*, **40**, 61-66.

Sung, M.-K. and Huh, W.-K. (2007) Bimolecular fluorescence complementation analysis system for in vivo detection of protein–protein interaction in *Saccharomyces cerevisiae*. *Yeast*, **24**, 767-775.

Tasaki, T., Sriram, S.M., Park, K.S. and Kwon, Y.T. (2012) The N-End Rule Pathway. *Annual review of biochemistry*, **81**, 261-289.

Trausch-Azar, J.S., Lingbeck, J., Ciechanover, A. and Schwartz, A.L. (2004) Ubiquitin-Proteasome-mediated Degradation of Id1 Is Modulated by MyoD. *Journal of Biological Chemistry*, **279**, 32614-32619.

Vidi, P.-A., Przybyla, J.A., Hu, C.-D. and Watts, V.J. (2010) Visualization of G protein-coupled receptor (GPCR) Interactions in Living Cells Using Bimolecular Fluorescence Complementation (BiFC). *Current protocols in neuroscience / editorial board, Jacqueline N. Crawley ... [et al.]*, **CHAPTER**, Unit-5.29.

Wiedenmann, J., Ivanchenko, S., Oswald, F., Schmitt, F., Röcker, C., Salih, A., Spindler, K.-D. and Nienhaus, G.U. (2004) EosFP, a fluorescent marker protein with UV-inducible green-to-red fluorescence conversion. *Proceedings of the National Academy of Sciences of the United States of America*, **101**, 15905-15910.

Zhang, M., Chang, H., Zhang, Y., Yu, J., Wu, L., Ji, W., Chen, J., Liu, B., Lu, J., Liu, Y., Zhang, J., Xu, P. and Xu, T. (2012) Rational design of true monomeric and bright photoactivatable fluorescent proteins. *Nature Methods*, **9**, 727.

Chapter 5: In vivo super-resolution imaging of the dynamics of PtdIns(4)P in the plasma membrane of plant cells.

***In vivo* super-resolution imaging of the dynamics of PtdIns(4)P in the plasma membrane of plant cells.**

Kai Tao^{1,2}, Yerim Lee³, Justin R. Waletich⁴, Felipe Arredondo², Xiaolin Nan⁴, Brett M. Tyler^{1,2,5}.

1. Molecular and Cellular Biology Program, Oregon State University, Corvallis, OR 97331
2. Department of Botany and Plant Pathology, Oregon State University, Corvallis, OR 97331
3. Department of Biomedical Engineering, Knight Cancer Institute, and OHSU Center for Spatial Systems Biomedicine (OCSSB), Oregon Health and Science University, Portland, OR, 97201
4. Department of Microbiology, Oregon State University, Corvallis, OR 97331
5. Center for Genome Research and Biocomputing, Oregon State University, Corvallis, OR 97331

Abstract

The plasma membrane (PM) is an incompletely fluid environment in which phospholipids and proteins are heterogeneously organized and subject to various degrees of lateral diffusion. These properties are central to the function of this key organelle in the regulation of a wide array of cellular functions. Due to the challenging characteristics of plant cells, especially the presence of a cell wall, current imaging techniques, such as Fluorescence Correlation Spectroscopy (FCS) and Fluorescence Recovery After Photobleaching (FRAP) microscopy cannot accurately estimate the dynamics of phospholipids and proteins in the PM. In this work, we have used a newly developed super-resolution microscopy technique called Single Particle Tracking Photo-Activated Localization Microscopy (sptPALM) to characterize the spatial and temporal distribution of proteins bound to phosphatidylinositol 4-phosphate (PtdIns(4)P), the most abundant phosphoinositide species in the plasma membrane (PM) of plant cells. First we used site-directed mutagenesis to produce a refined version (FAPP1a) of the pleckstrin homology (PH) domain of human phosphatidylinositol Four-Phosphate-Adaptor Protein-1 (FAPP1) that has been commonly used to detect PtdIns(4)P in plant cells. The mutations eliminated protein-protein contacts responsible for the binding of FAPP1 to plant Golgi bodies. Using FAPP1a fused with the photoconvertible fluorescent protein mEOS3.2, we successfully demonstrated that sptPALM could be adapted for direct visualization of PtdIns(4)P-binding proteins at the nanometer scale in plants. Our preliminary data also demonstrate the advantages of sptPALM compared to FRAP for studying the molecular dynamics of the plasma membrane.

Introduction

The cellular membrane bilayer has been considered as a two dimensional fluid in which phospholipids and proteins are heterogeneously and asymmetrically organized as mosaic complexes with lateral mobility (Singer and Nicolson, 1972). The lateral diffusion of these mosaic complexes results in the formation of transient substructures in the plasma membrane (PM) which are crucial to regulation of cellular functions, such as signal transduction, membrane trafficking, cell division, and cytoskeletal organization (Murata and Los, 1997, Martin, 2001, Roy and Levine, 2004, Kusumi et al., 2012, Schink et al., 2016). Among the wide diversity of lipids that occur in the PM, the phosphorylated derivatives of inositol-containing phospholipids, namely phosphoinositides (PIs), have been implicated as playing regulatory roles in many kinds of cellular functions. Although PIs comprise less than ~15% of the total phospholipids in cells (Di Paolo and De Camilli, 2006), PIs can determine the spatial identities of subcellular membrane compartments. In particular, different PIs can promote the specific recruitment of cytosolic proteins via direct lipid-protein interactions (Lemmon, 2008). In plant cells, phosphatidylinositol-4-phosphate (PtdIns(4)P) has been identified as the most abundant PI species (Meijer and Munnik, 2003). PtdIns(4)P is predominantly distributed on the inner leaflet of the PM where it establishes the identity of the PM and regulates the PM localization and function of many PM-associated proteins and their associated cellular functions (Vermeer et al., 2009, Simon et al., 2016). For instance, the polarized expansion of root hair cells in *Arabidopsis thaliana* is controlled by the ROOT HAIR DEFECTIVE4 protein whose PM targeting is mediated by binding to PtdIns(4)P (Thole et al., 2008). It was also observed that chloroplast division is negatively correlated with the amount of PtdIns(4)P on the PM (Okazaki et al., 2015). In plant immunity, PtdIns(4)P is involved in salicylic acid (SA)-mediated plant immune signaling pathways through its recruitment of E3 ligase protein PUB13, which in turn modulates homeostasis of the immune receptor FLAGELLIN SENSITIVE 2 (FLS2) (Lu et al., 2011, Antignani et al., 2015, Zhang and Xiao, 2015). Thus, PtdIns(4)P is an attractive target for studying the dynamics of PIs on the plant PM, which could provide insights into mechanisms underlying the spatial and dynamic organization of the PM.

Genetic expression of biosensor proteins consisting of specific PI-binding protein domains fused with fluorescent proteins has proven to be an effective strategy for investigating the subcellular localization and dynamics of PIs in cells (Balla, 2007). In plant cells, the pleckstrin homology (PH) binding domain of human phosphatidylinositol-4-phosphate-adaptor protein-1 (FAPP1) (Vermeer et al., 2009, Simon et al., 2016) has been used to create a PtdIns(4)P biosensor. This biosensor has been detected on the Golgi apparatus and endosomes as well as the PM. Other biosensors have employed the PH domain of human oxysterol binding protein (OSBP) and its yeast homolog (Osh2p) to investigate PtdIns(4)P pools in mammalian and yeast cells (Levine and Munro, 2002, Raychaudhuri and Prinz, 2010). However, these biosensors also have been reported to have binding affinities to PtdIns(4,5)P₂ comparable to that for PtdIns(4)P (Roy and Levine, 2004, Platre and Jaillais, 2016). More recently, a new PtdIns(4)P biosensor based on the P4M domain of the *Legionella pneumophila* effector protein SidM, has been reported to have very high binding specificity for PtdIns(4)P (Hammond et al., 2014). However, since FAPP1 has been widely used and accepted over the years (Lemmon, 2008, Platre and Jaillais, 2016), it is still commonly used for visualization of PtdIns(4)P pools *in vivo* (Dowler et al., 2000, Godi et al., 2004, Vermeer et al., 2009, Vermeer and Munnik, 2010, Simon et al., 2016). More recently, the analysis of the crystal structure of FAPP1 has identified two independent recognition sites in the PH domain of FAPP1, one of which is responsible for PtdIns(4)P binding, and the other of which can interact with the GTPase, ADP-ribosylation Factor 1 (ARF1) (He et al., 2011). This finding highlighted longstanding concerns about the co-incidence binding of lipid biosensors to molecules other than the target lipid (Platre and Jaillais, 2016). It also has raised a question about previous interpretations of PtdIns(4)P pools in plants (Lemmon, 2008, Vermeer et al., 2009).

Fluorescence Correlation Spectroscopy (FCS) (Axelrod et al., 1976) and Fluorescence Recovery After Photobleaching (FRAP) microscopy (Yguerabide et al., 1982) are fluorescence-based optical imaging techniques commonly used for non-invasive visualization of molecular movement in cell membranes (De Los Santos et al., 2015, Li et al., 2016). Both FCS and FRAP have also been applied to living plant cells (Li et al., 2011, Luu et al., 2012, Tanaka et al., 2013, Wang et al., 2015). However, they

still face several challenges. Primarily, the topographic features of plant cells make it difficult to distinguish whether a fluorescent signal is from the plasma membrane or cytoplasm. This can result, for example, in incorrect estimation of diffusion coefficients (D) of membrane molecules. Also, since plant cells readily allow only genetically expressed fluorescent protein labeling, artifacts due to excessive biosensor expression levels can occur. Another challenge is that the major readouts from FCS and FRAP, which are the diffusion time (T_D) and the half-time of recovery ($\tau_{1/2}$), depend highly on experimental parameters such as the confocal observation volume and the bleaching volume, making it difficult to compare measurements across studies (Hink et al., 2008, Kang et al., 2012).

More generically, FCS and FRAP measure ensemble averages of time-resolved imaging of fluorescent intensity over many molecules, thus small changes in the motional characteristics of individual molecules cannot be readily discerned (Sezgin and Schwille, 2011, Li et al., 2016). Furthermore, the spatial resolution available for both FCS and FRAP is still diffraction limited, leaving the nanoscale dynamics of molecules on plasma membranes unresolved. More recently, the development of super-resolution microscopy techniques has provided new opportunities to gain more accurate insights into the molecular dynamics in the PM at nanoscale resolution. Several different approaches for achieving sub-diffraction resolution have been developed. They are STimulated Emission Depletion (STED) microscopy (Eggeling et al., 2008), which has been combined with FCS (Honigmann et al., 2014), Stochastic Optical Reconstruction Microscopy (STORM) (Rust et al., 2006), and Photo-Activated Localization Microscopy (PALM) (Betzig et al., 2006). These techniques have allowed direct visualization of molecular mobility at single molecular resolution. Considering the limitations in the plant cells, PALM, which relies on genetically encoded fluorophores, is the tool of choice to investigate the dynamics of molecules in the plant PM.

In this work, we used a modified FAPP1 PH domain (FAPP1a), from which we removed the ARF1-binding residues, to study the spatiotemporal distribution of PtdIns(4)P in the PM of *Nicotiana benthamiana* epidermal cells. We fused FAPP1a with a photoconvertible fluorescent protein, mEOS3.2, to create a biosensor that could

directly visualize the dynamics of PtdIns(4)P in the PM at single molecule resolution via single particle tracking PALM (sptPALM). Our preliminary data indicate that, even when bound to FAPP1a, PtdIns(4)P has higher lateral freedom than that the PM microdomain protein, remorin StRem1.3. Our results highlight the advantages of sptPALM over FRAP in studying the dynamics of plasma membrane molecules in plant cells. This is the first time that the spatiotemporal dynamics of a PI species have been visualized at nanoscale levels, using a bound biosensor protein.

Results

Different binding locations of FAPP1 are determined by its PtdIns(4)P and ARF1 binding regions.

The PH domain in FAPP1 has been reported to be able to detect the PtdIns(4)P pools on the plasma membrane, Golgi and endosomes in plants (Vermeer et al., 2009, Simon et al., 2016). More recently, the crystal structure of the PH domain of FAPP1 has identified two different sites on its N terminus and C terminus, responsible for PtdIns(4)P binding and ADP-ribosylation factor 1 (ARF1) recognition (He et al., 2011), respectively. A member of the ARF family of GTPases in the Ras superfamily (Kahn et al., 1992), ARF1 has been reported to localize at the Golgi apparatus in plants (Pimpl et al., 2000, Lee et al., 2002, Robinson et al., 2011). In order to clarify the roles of PtdIns(4)P binding and ARF1 recognition in the sub-cellular localization of FAPP1 in plant cells, we created three mutant versions of FAPP1. FAPP1m and FAPP1am contained substitution mutations in two key PtdIns(4)P binding residues (K7E and R18A), whereas FAPP1a and FAPP1am contained substitution mutations in two key ARF1 binding residues (E50A and H54A) (Figure 5.1a). We fused a yellow fluorescent protein (YFP) to the C-termini of the wildtype and mutant FAPP1 PH domains then transiently expressed the fusions under the control of the Cauliflower Mosaic Virus 35S (CaMV35S) promoter in *Nicotiana benthamiana* leaves and in leaf protoplasts of *Arabidopsis thaliana*. As shown in the Figure 5.1b, FAPP1-YFP was enriched on the plasma membrane and numerous irregular dynamic organelles, consistent with previous reports of the localization of FAPP1 in plants (Vermeer et al., 2009, Simon et al., 2016). However, the localization to the irregular organelles was not observed with

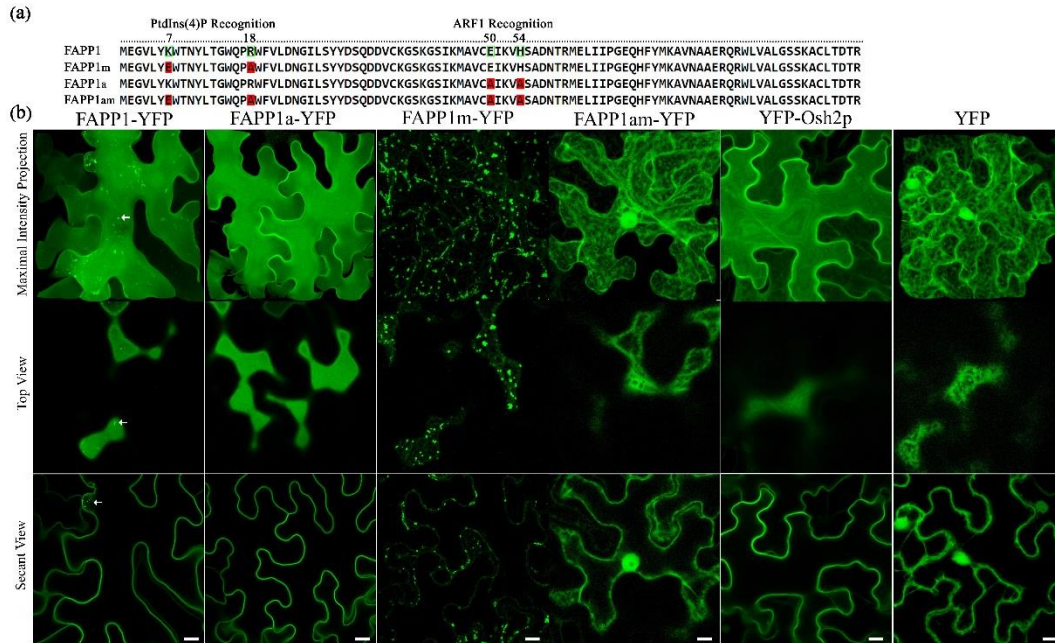


Figure 5.1 Fluorescence distribution of YFP fused to wild-type and mutant FAPP1 PH domains, transiently expressed in *N. benthamiana* leaf cortical cells.

(a) Sequence of FAPP1 PH domain and mutants. Residues highlighted in green boxes are responsible for interactions with PtdIns(4)P and ARF1 GTPase, as indicated. Red highlights substitution mutations designed to abolish either binding to PtdIns(4)P, ARF1, or both. (b) Subcellular localization of FAPP1-YFP fusions, compared to YFP-Osh2 and YFP. Arrows highlight dynamic irregular organelles. White scale bars in all panels represent 10 μ m.

FAPP1a-YFP (Figure 5.1b), that showed exclusively plasma membrane targeting. Conversely, FAPP1m-YFP completely lost its plasma membrane localization, but strongly labeled the irregular organelles instead (Figure 5.1b). Moreover, the double mutant FAPP1am-YFP showed only cytoplasmic and nuclear localization (Figure 5.1b) similar to that of YFP alone (Figure 5.1b). Similar results were also observed in the mesophyll protoplasts of *A. thaliana* (Figure S5.1). For comparison, we expressed a different PtdIns(4)P biosensor comprised of two copies of the PH domain of the yeast oxysterol binding protein Osh2 fused to YFP (Roy and Levine, 2004). Like FAPP1a-YFP, YFP-Osh2p labeled the PM but did not label any internal organelles (Figure 5.1b, and Figure S5.1). Taken together, these results suggest that PtdIns(4)P binding alone is responsible for plasma membrane binding of FAPP1 whereas ARF1 recognition alone is responsible for organellar binding.

Refining the subcellular localization of the three FAPP1 mutants in vivo

To further refine the subcellular localizations of the three FAPP1 mutants, we co-expressed each respective YFP fusion with a variety of well-characterized organelle markers. As shown in Figure 5.2a, FAPP1a-YFP showed complete co-localization with the plasma membrane marker tagRFP-AtRem1.3. AtRem1.3 is a remorin protein family from *A. thaliana* which specifically targets the cytosolic leaflet of the plasma membrane (Raffaele et al., 2007). Since the vacuolar membrane (tonoplast) is often found in close proximity to the plasma membrane in plants (Echeverría, 2000), which can confound sub-cellular localization experiments, we used the tonoplast potassium channel protein AtTPK1 (Maîtrejean et al., 2011) to label the tonoplast. The results (Figure 5.2b) confirmed that FAPP1a-YFP was exclusively targeted to the plasma membrane and was not located on the tonoplast. Since FAPP1 has been reported to bind to Golgi bodies (Godi et al., 2004), we used the trans-Golgi marker STtmd-tagRFP (Boevink et al., 1998) to test whether the dynamic irregular organelles labeled by FAPP1m-YFP corresponded to Golgi bodies. As shown in Figure 5.2c, all of the larger FAPP1m-labeled organelles, comprising approximately two-thirds of all the FAPP1-labeled organelles, were also labeled by STtmd-tagRFP, indicating that they were Golgi bodies. However, the smaller one-third of the FAPP1m-labeled organelles were not

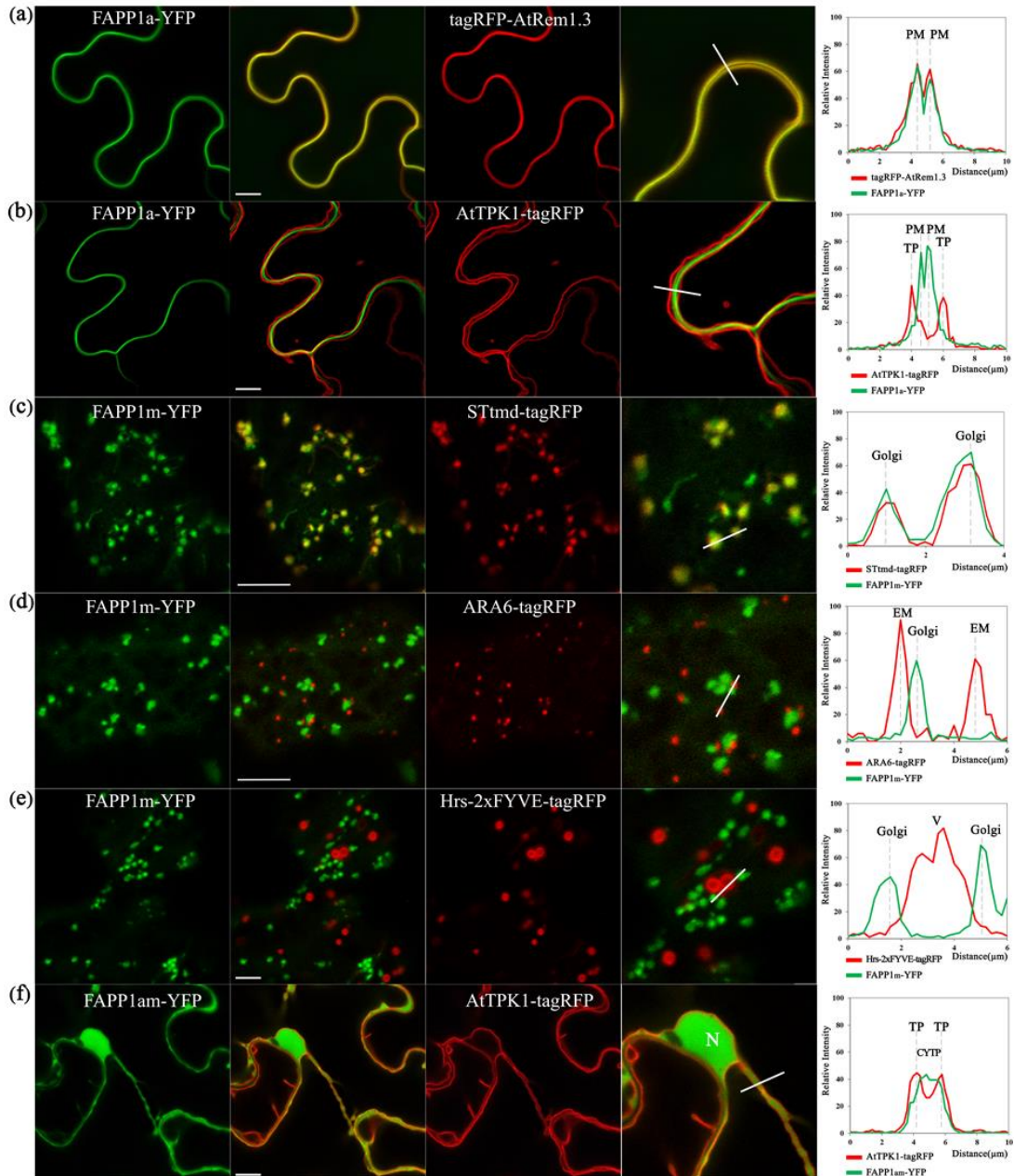


Figure 5.2 Subcellular co-localization analysis of three FAPP1 mutants in *N. benthamiana* leaf cortical cells.

The FAPP1 mutants, fused to YFP, were co-expressed with tagRFP fused to the PM protein StRem1.3 (a), the tonoplast (TP) marker AtTPK1 (b, f), the trans-Golgi marker, STtmd (c), the endosomal markers (EM) ARA6-tagRFP (d), or the PtdIns(3)P-containing vesicle (V) marker, 2xFYVE-tagRFP (e). The fluorescence intensity profiles in the right panels show relative fluorescence levels along the transects marked in white in the right-most enlarged image panels. The lengths of the transects on the images equal the respective distances shown in each histogram. CYTP is an abbreviation for cytoplasm. White scale bars in the left panels represents 10 μ m.

labeled by STmd-tagRFP. To determine if these smaller organelles corresponded to endosomal organelles, we co-expressed FAPP1m-YFP with the two different endosomal membrane markers, a plant-specific Rab5 GTPase ARA6 which mainly locates at the early membrane organelles in the endocytic pathway (Ueda et al., 2001) and a PtdIns(3)P-binding protein Hrs-2xFYVE which specifically targets PtdIns(3)P-containing membrane organelles including late endosomes, multi-vesicular bodies and the prevacuolar membranes (Vermeer et al., 2006). Neither ARA6-tagRFP (Figure 5.2d) nor Hrs-2xFYVE-tagRFP (Figure 5.2e), co-localized with any FAPP1m-YFP-labeled organelles. Others have also noted non-Golgi structures carrying ARF1 in plant cells (Matheson et al., 2007). The cytoplasmic localization of FAPP1am-YFP was confirmed by co-expression with the tonoplast marker AtTPK1 (Figure 5.2f); the strands labeled by FAPP1am-YFP were clearly bounded by the tonoplast, ruling any vacuolar localization of FAPP1am-YFP. Similar co-localization assays performed on mesophyll protoplasts of *A. thaliana* were consistent with the results above (Figure S5.2). Together, all the data above indicate that the subcellular localization of FAPP1 is determined by the PtdIns(4)P binding and ARF1 recognition sites independently, and it would be more accurate to use the mutant derivative FAPP1a for the purpose of detecting the PtdIns(4)P pool in plant cells.

PALM single-particle tracking of FAPP1a on the PM in vivo

Next, we took advantage of the super-resolution imaging technique sptPALM to characterize the spatiotemporal dynamics of PtdIns(4)P on the plasma membrane at nanometer resolution, as detected by a biosensor protein. To begin with, we chose a newly reported photoconvertible fluorescent protein mEOS3.2, which is a derivative of mEosFP from the scleractinian coral *Lobophyllia hemprichii*. mEOS3.2 has excellent characteristics for sub-cellular imaging including being truly monomeric and bright, and having a fast maturation rate and a high photon budget (Wiedenmann et al., 2004, Zhang et al., 2012). We fused FAPP1a with mEOS3.2 via a flexible 2xGGGGS linker. Consistently, the FAPP1a-mEOS3.2 fusion specifically targeted the PM where it was homogeneously distributed (Figure 5.3a). Importantly, the mEOS3.2 in this fusion construct could still be photoconverted from green to red emission after illumination

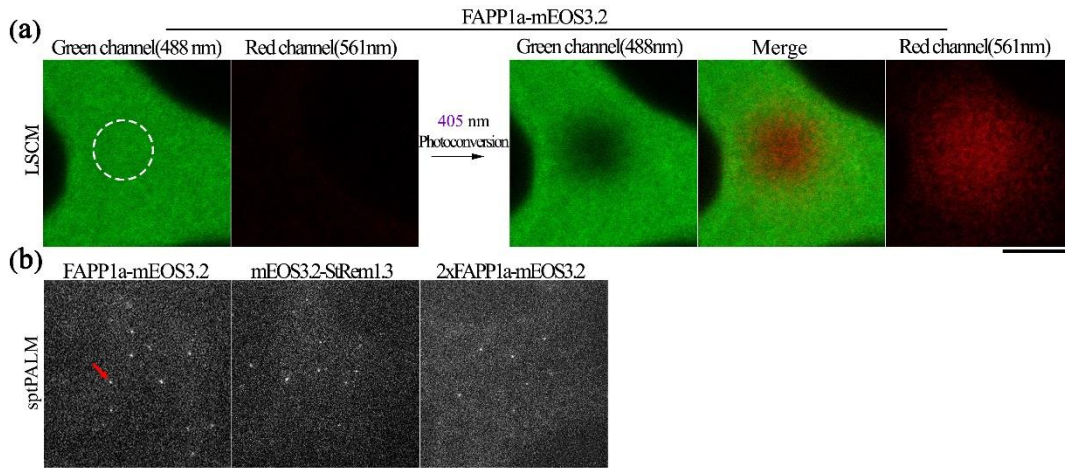


Figure 5.3 Confocal and PALM single-particle tracking imaging of mEOS3.2 fusions in the PM of *N. benthamiana* leaf cortical cells.

(a) 405-nm irradiation applied to photoconvert FAPP1a-mEOS3.2 from green to red emission under laser scanning confocal microscopy (LSCM). (b) PALM imaging under total internal reflection (TIR) conditions of FAPP1a-mEOS3.2, mEOS3.2-StRem1.3, and 2xFAPP1a-mEOS3.2. The brightly fluorescent spot indicated by the red arrow represents a red photoconverted FAPP1a-mEOS3.2 single molecule. Black scale bars represent 10 μm .

with a 405 nm UV laser (Figure 5.3a). FAPP1a-mEOS3.2 also displayed excellent single-molecule photophysical properties with a high signal to background ratio under the conditions of sptPALM imaging (Figure 5.3b).

We compared the lateral mobility of FAPP1a-bound PtdIns(4)P with that of mEOS3.2-labeled StRem1.3. Remorins are a marker of plant membrane microdomains (Jarsch et al., 2014), so we expected the mobility of StRem1.3 to be reflective of mobility within a microdomain (Kenworthy et al., 2004, Lingwood and Simons, 2010, Kusumi et al., 2012). As is evident from Supplementary Video 5.1 and 5.2, the mobility of the FAPP1a-mEOS3.2 bound to PtdIns(4)P was noticeably higher than that of mEOS3.2-StRem1.3.

Since several membrane receptor proteins have been reported to show significantly different membrane dynamics corresponding to different oligomerization states (Caiolfa et al., 2007, Chung et al., 2010, Pryor et al., 2013), we tested whether dimerization of FAPP1a would reduce its lateral mobility compared to monomeric FAPP1a, using a construct with two FAPP1a PH domains. In addition, to ensure both PH domains in 2xFAPP1a could bind PtdIns(4)P molecules simultaneously, we split the mEOS3.2 into two non-fluorescing fragments (mEOS3.2N¹⁻¹⁶⁴, mEOS3.2C¹⁶⁵⁻²²⁶) suitable for a bimolecular fluorescence complementation (BiFC) assay (Liu et al., 2014) (Chapter 4). Each mEOS3.2 fragment (mEOS3.2N and mEOS3.2C) was fused with one FAPP1a PH domain each and then the two were co-expressed in the *N. benthamiana* cells. Colocalization of mEOS3.2N-FAPP1a and mEOS3.2C-FAPP1a to the PM was sufficient to produce a strong BiFC signal (Supplementary Figure S5.3). In contrast, mutations in the PtdIns(4)P binding site of either one of the protein fusions (i.e. the FAPP1am mutant) greatly diminished the BiFC signal. Similarly, if the FAPP1a domain was omitted from either fusion, no BiFC signal was observed.

As is evident from Supplementary Video 5.1-5.3, the mobility of the 2xFAPP1a-mEOS3.2 bound to PtdIns(4)P was noticeably slower than monomeric FAPP1a-mEOS3.2 bound to PtdIns(4)P and comparable to that of mEOS3.2-StRem1.3. To confirm the difference in lateral mobility between 1xFAPP1a and 2xFAPP1a, we carried out a FRAP assay. Regions of the plant PM displaying mEOS3.2 fluorescence as a result of binding FAPP1a-mEOS3.2 or 2xFAPP1a-mEOS3.2, were bleached by

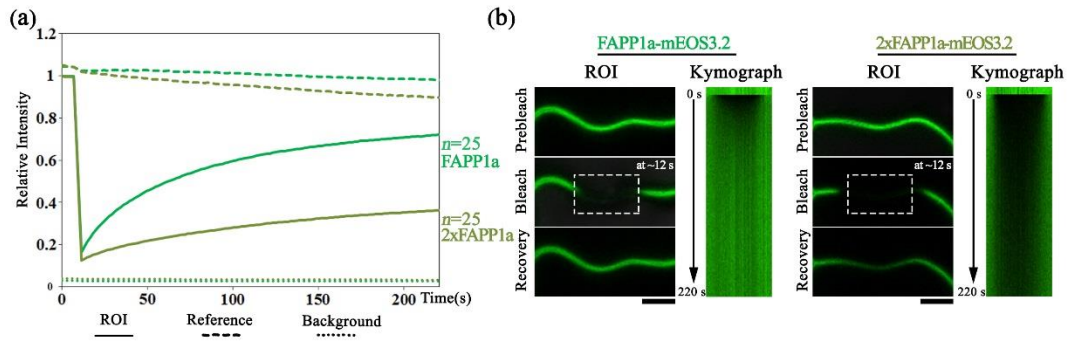


Figure 5.4 FRAP analysis of the mobility of FAPP1a and 2xFAPP1a in the PM of *N. benthamiana* leaf cortical cells.

(a) average normalized recovery curves of fluorescent intensity for FAPP1a-mEOS3.2 (n= 25, bright green) and 2xFAPP1a-mEOS3.2 (n=25, olive green). Dashed lines represent reference intensity from a fluorescent neighboring cell, and dotted lines represent background regions. (b) Secant images and kymographs of mEOS3.2 fluorescence on the PM during the FRAP procedure. Dashed box indicates the ROIs subjected to FRAP. Scale bars represents 10 μ m.

exposure to 488nm laser. The recovery of the signal as a result of lateral diffusion of unbleached molecules into the bleached zone was then followed over a period of 200 seconds. As shown in Figure 5.4, recovery of the fluorescence conferred by 2xFAPP1a-mEOS3.2 was much slower than for FAPP1a-mEOS3.2. After 200 seconds, around 70% of the FAPP1a-mEOS3.2 fluorescence had been recovered whereas only about 30% of the 2xFAPP1a-mEOS3.2 fluorescence had been recovered. Thus the FRAP assay results aligned well with the sptPALM observations of mobility.

Discussion

To determine the subcellular localization of phosphoinositides in specific membrane compartments of cells, a convenient and effective approach has been to use specific phosphoinositide-binding proteins fused with fluorescent proteins (referred to as biosensors) and ectopically expressed in living cells (Balla, 2007, Hammond and Balla, 2015, Simon et al., 2016). A challenge with this approach however is that the specificity of such binding proteins for particular phosphoinositides varies considerably. Furthermore, many phospholipid-binding proteins, especially those in the PH domain family, may contain more than one binding site for different membrane components such as other lipids or proteins (Lemmon, 2008). This is the case for the PH domain of FAPP1, the PtdIns(4)P-specific binding protein most commonly used in mammals, yeasts, and plants as a PtdIns(4)P biosensor (Godi et al., 2004, Roy and Levine, 2004, Vermeer et al., 2009). The PH domain of FAPP1 contains two binding sites, one for recognition of PtdIns(4)P and one for binding to the GTPase ARF1; each binding site was shown to be independent to the other *in vitro* (He et al., 2011).

Here, using site-directed mutagenesis, we have been able to show that, in plant cells, plasma membrane localization of FAPP1 is determined exclusively by its PtdIns(4)P-binding site, while its Golgi localization is determined exclusively by its ARF1-binding site. We observed that fluorescently labeled wild type FAPP1 displayed two subcellular localizations, namely the plasma membrane and a variety of irregular organelles, including the Golgi apparatus, which confirms a previous observation (Vermeer et al., 2009). In line with those subcellular localizations, mutant FAPP1am

lacking both PtdIns(4)P and ARF1 binding sites exclusively showed cytoplasmic and nuclear localization.

We observed that the irregular organelles were detected by the PtdIns(4)P-non-binding mutant biosensor, FAPP1m, but not by the PtdIns(4)-non-binding mutant, FAPP1a. One subset of the organelles, larger in size and about two-thirds of the total, co-localized with the TGN marker STtmd-tagRFP, and thus to correspond to the trans-Golgi. A second subset, smaller in size and about one third of the total, were labeled with FAPP1m but not STtmd-tagRFP. None of the organelles labeled with FAPP1m colocalized with the plant-specific Rab5 GTPase ARA6 or with the PtdIns(3)P biosensor, Hrs-2xFYVE, which label distinct endosome compartments. Matheson et al (2007) identified non-Golgi organelles labeled by ARF1, and suggested that they may be endosomal compartments where the endocytic and secretory pathways meet. It is likely that the smaller subset of organelles we observed to be labeled by FAPP1m but not STtmd-tagRFP correspond to the organelles described by Matheson et al. (2007). Simon et al. (2014) reported that FAPP1 labeled a similar subset of endosomes that partially co-localized with the FM4-64 dye (Simon et al., 2014). However, they did not use an ARF1-non-binding mutant of FAPP1, and so their conclusion that PtdIns(4)P is located on these endosomes (and the Golgi) is likely incorrect.

We observed that FAPP1a localized predominantly to the plasma membrane, and no signal was observed on the tonoplast. We observed that the independent PtdIns(4)P biosensor, YFP-Osh2p also localized to the PM, with no organellar signal, indicating that PtdIns(4)P was confined to the PM. Simon et al (Simon et al., 2016) also observed that mutation of the ARF1 binding sites of FAPP1 resulted in FAPP1 being localized predominantly to the PM. Furthermore, they observed that biosensors based on Osh2 and on the PtdIns(4)P-binding bacterial effector, SidM, also bound predominantly to the PM. Together these results confirm that, in plants, PtdIns(4)P is located predominantly on the PM, and that PtdIns(4)P is not a significant component of the Golgi membranes. These results contrast markedly with the situation in animal cells where PtdIns(4)P plays a key role in establishing the identity of the Golgi membrane, and the PM is marked by a high level of PtdIns(4,5)P₂ (Godi et al., 2004, Roy and Levine, 2004, D'Angelo et al., 2008, Hammond et al., 2012). In mammalian

cells, FAPP1 regulates vesicle trafficking from the trans-Golgi networks to the plasma membrane via the binding of its PH domain to PtdIns(4)P and ARF1 on the Golgi membrane (Godi et al., 2004). ARF1 can also interact with PI4-kinase III β resulting in increased generation of PtdIns(4) on the Golgi which in turn stimulates the rapid accumulation of FAPP1 (Godi et al., 1999).

Having defined FAPP1a as a clean, specific biosensor for PtdIns(4)P, we were able to use sptPALM imaging to directly visualize the dynamics of PtdIns(4)P-bound FAPP1a on the plasma membrane at single molecule resolution. Our preliminary data revealed that the PtdIns(4)P-bound FAPP1a had a higher rate of diffusion compared to the membrane micro-domain marker protein StRem1.3. This observation suggests that the PtdIns(4)P molecules targeted by the FAPP1a biosensor were not located in the same liquid-ordered phase as StRem1.3 (Lingwood and Simons, 2010, Kusumi et al., 2012). We also observed different degrees of mobility between biosensors carrying one FAPP1a domain versus one carrying two FAPP1a domains suggesting that the avidity of the lipid-protein interaction could influence the kinetics of the bound biosensor. This observation is consistent with a previous report that the diffusion constants of biosensors carrying GRP1 PH domains were inversely proportional to the number of bound phosphatidylinositol-3,4,5-trisphosphate (PIP3) molecules (Knight et al., 2010). Since it has been common practice to duplicate lipid-binding domains in lipid biosensors to increase the strength of the signal, e.g. the commonly used PtdIns(3)P biosensor Hrs-2xFYVE, our observations suggest that biosensors intended for use in measuring membrane dynamics should be designed with care.

The sptPALM super-resolution imaging used in this study opens a new way to study molecular components of the plasma membrane of plant cells at single molecule level, which previously required electron microscopy. For example, the FAPP1a biosensor we have characterized here could be used to learn how the dynamics of PtdIns(4)P respond to receptor signaling. Use of sptPALM requires comparatively low physiological perturbation, and offers high versatility and specificity for fluorescence labeling because of the usage of genetically encoded fluorescent tags fused to the proteins of interest. For live-cell imaging, the challenging characteristics of plant cells make fluorescence labeling using chemical dyes difficult (Komis et al., 2015). In

addition to providing sub-diffraction spatial resolution, sptPALM can provide more specific information than traditional methods such as FRAP, such as quantitatively estimating the diffusion coefficient of each molecule and defining populations of molecules with different diffusive states. Therefore, sptPALM will facilitate research on the spatial and dynamic properties of protein-protein, lipid-lipid, and protein-lipid interactions within the PM of plant cells.

Materials and Methods

Plant Material

Both *N. benthamiana* and *A. thaliana* plants were grown in soil (Fafard® 4M Mix). *N. benthamiana* plants were grown in a growth chamber with a 14 hr photoperiod at 25°C for 5 weeks before being used for *A. tumefaciens* infiltration assays. Cold stratification (3 days at 4°C) was applied to *A. thaliana* seeds prior to planting. *A. thaliana* seedlings were grown in a growth chamber with a 12 hr photoperiod at 20°C for 4 weeks before harvesting of leaves for protoplast isolation.

Cloning and Construction

The FAPP1 and Hrs-2xFYVE constructs in this study were described previously (Kale et al., 2010). Genes encoding Osh2 (Roy and Levine, 2004) and the Golgi marker STtmd (Boevink et al., 1998) were synthesized by GenScript Corporation. DNA encoding AtRem1.3 (AT2G45820), AtTPK1 (AT5G55630.1), and ARA6 (AT3G54840.1) was amplified from Col-0 cDNA. The mEOS3.2 sequence was cloned from pENTR-D-TOPO-mEOS3.2 provided by Xiaolin Nan (Department of Biomedical Engineering, Oregon Health and Science University). The split site for mEOS3.2 was chosen at residue 164 as reported previously (Liu et al., 2014). All DNA fragments were amplified using high-fidelity polymerase CloneAmp™ HiFi PCR premix (TaKaRa Bio) using primers as listed in Table 5.1. In Fusion® HD Cloning strategies (TaKaRa Bio) were used to insert all gel-purified PCR fragments into the modified Gateway donor vectors based on pDONR207. The vectors contain a genetically inserted 2xGGGGS linker connecting the protein of interest to either the N-terminus or C-terminus of YFP, tagRFP, mEOS3.2, mEOS3.2N, or mEOS3.2C. FAPP1m (K7E, R18A), FAPP1a (E50A, H54A), and FAPP1am (K7E, R18A, E50A,

Table 5.1 Primer designed and used in chapter 5.

Oligo Name	Forward primer(5'-3')	Reverse primer(5'-3')	Application notes
FAPP1	AGCAGGCTCCTCGCGAATGGAA GGTGTCTGTAT	CTCCTCCACCTCTAGAGCGAGTA TCGGTCAGACACG	FAPP1-FP
FAPP1m-1	GTATGAATGGACAAATTAC	TCCATTCATACAGAACACCTTC	K7E
FAPP1m-2	CCAGCTTGGTTTGTCTGGATA AC	AAACCAAGCTGGCTGCCAGCCG GTCAG	R18A
FAPP1a	GCTATCAAGGTGGCATCTGCAG ATAATACCCGTATG	TGCCACCTTGATAGCGCAAACA GCCATCTTGATAC	E50A, H54A
Osh2	GGCGGTAGCGCTAGCCCAAGTA ATAACGTGACACCCGAAATC	AAGCTGGGTGATATCTCATGGG AGGCTACCTTGGGTTTTGCTGTG	FP-Osh2
STtmd	AGCAGGCTCCTCGCGAATGATT CATACCAACTTGAAG	CTCCTCCACCTCTAGAGGCCACT TTCTCCTGGCTCTTG	STtmd-FP
Hrs-2xFYVE-2	AGCAGGCTCCTCGCGAATGGAA ATTTGAAAGCGATGCGATGTTT G	CTCCTCCACCTCTAGACTTCGGT TGCAGGTCCACGGCC	Hrs-2xFYVE-FP
StRem1.3	GGCGGTAGCGCTAGCGCAGAA TTGGAAGCTAAG	AAGCTGGGTGATATCTTAAAAT ATTCCAAGGATTTTC	FP-StRem1.3
AtTPK1	AGCAGGCTCCTCGCGAATGTCG AGTGATGCAGCTCGTACGCCAT TG	CTGCCTCCTCCACCTCTAGACCT TTGAATCTGAGACGTGGTCTGA GC	AtTPK1-FP
ARA6	AGCAGGCTCCTCGCGAATGGGA TGTGCTTCTTCTTCCAGATAG	CTCCTCCACCTCTAGATGACGAA GGAGCAGGACGAGGTAG	ARA6-FP
mEOS3.2	GGCGGTAGCGCTAGCATGAGTG CGATTAAGCCAGACATG	AAGCTGGGTGATATCTTATCGTC TGGCATTGTCAGGC	POI-mEOS3.2
mEOS3.2N 1	AGCAGGCTCCTCGCGAATGAGT GCGATTAAGCCAGACATG	CTCCTCCACCTCTAGAAAGCTGG GTGATATCTTA	mEOS3.2N-POI

mEOS3.2N 2		AAGCTGGGTGATATCTTATTCAA GCAACAAAGCCATCTC	POI-mEOS3.2N
mEOS3.2C 1	AGCAGGCTCCTCGCGAATGGGA AATGCCATTACCGATG	CTCCTCCACCTCTAGATCGTCTG GCATTGTCAGGC	mEOS3.2C-POI
mEOS3.2C stop		CTCCTCCACCTCTAGATTATCGT CTGGCATTGTCAGGC	mEOS3.2C-stop

H54A) were constructed similarly. Subsequently, all inserts carried on pDonR207 vectors were transferred to the Gateway™ compatible expression vector pmAEV-35S, which is derived from the binary vector pCAMBIA (Eggeling et al., 2008), via Gateway™ LR reactions (Thermo Fisher scientific Inc.). All constructs were verified by Sanger sequencing and were propagated using DH10B *E.coli* cells.

Transient expression in *N. benthamiana* leaves and *A. thaliana* protoplasts

All expression constructs were introduced into *A. tumefaciens* strain GV3101 by transformation using electroporation (Xiong et al., 2014). The bacteria were grown on Luria-Bertani (LB) medium (plus 50 µg/ml kanamycin) at 28°C overnight. *A. tumefaciens* cells were collected by centrifugation and re-suspended in MES buffer (10 mM MgCl₂, 10mM MES pH 5.7, 100 µM acetosyringone). Cell suspensions for infiltrations were diluted to a concentration of OD₆₀₀=0.1; for co-infiltrations, equal volumes of the appropriate cells with OD₆₀₀ of 0.2 were mixed together. Cell suspensions were incubated at RT for 1 hour with moderate shaking (100 rpm). All infiltrated *N. benthamiana* seedlings were maintained in the growth chamber with same conditions as described above until imaging. *A. thaliana* mesophyll protoplasts were prepared from well-expanded leaves on 4-week-old seedlings. Procedures for protoplast isolation and transfection were performed according to the polyethylene glycol method (Yoo et al., 2007). 10 µg of expression vector DNA were used in each transfection or, for co-localization assays equal amounts (7.5 ug) of each expression vector were mixed for transfection. Transfected protoplasts were incubated in W5 buffer at 25°C overnight before observation.

Laser confocal scanning microscopy (LCSM) and image analysis

Confocal imaging was performed on a ZEISS LSM 780 NLO confocal microscope system using 20x/0.8 air, 40x/1.4 and 63x/1.4 oil-immersion objectives. Excitation lasers for mEOS3.2 and YFP/Venus were provided by the Argon lines 488 and 514 nm respectively. tagRFP was excited by a 561-nm diode-pumped solid-state (DPSS) laser when in combination with YFP/Venus. Using acousto-optic tunable filters (AOTF), emission wavelengths were specifically selected as 491-544 nm for GFP, 518-553 nm for YFP/Venus and 562-640 nm for tagRFP. For FRAP quantitative imaging, 10 images were firstly captured, then a selected region of interest (ROI) in a

secant view of the fluorescent PM was bleached by using the 514-nm laser for 10 iterations at highest intensity (100%). Subsequently, 120 frames were recorded for fluorescence recovery with a combined scanning speed 1.6 s/frame with a low power (1%) of the 514-nm laser. For mEOS3.2 photoconversion, one image was captured in both the green (491-544 nm) and red (562-640nm) channels prior to photoconversion. Then a selected region of interest (ROI) was subjected to photoconversion using 405-nm diode laser for 20 pulses with a 50% output power. Immediately afterwards, the image was recaptured in the green and red channels.

Maximal intensity projection(MIP) in 3D module of ZEN2 (Blue edition) was chosen to generate a comprehensive view for Z-axis scanning images. For all FRAP data collected, fluorescence intensity was measured for 130 frames images recorded before and after bleaching using a rectangular region-of-interest (ROI), together with an identical background region (used for data correction), and non-bleached region (used to correct data for unintentional bleaching at each time point). The mono-exponential model in ZEN2 (Blue edition) was selected for fitting the FRAP data. Each normalized FRAP curve plotted in Figure 4 corresponds to a total of 25 ROIs from at least three imaged leaves.

sptPALM imaging

We performed PALM imaging on a Nikon Ti-U inverted microscope with a Nikon 60x APO TIRM objective (NA=1.49) as described previously (Nickerson et al., 2014). *N. benthamiana* leaves prepared for imaging were cut as small as possible and at least must be smaller than 0.5 cm square. The small cut leaf piece was mounted with PBS buffer (pH 7.4) in a recording and imaging chamber (MS-502 DW, ALA Scientific Instruments). Imaging was performed at room temperature. A 405-nm laser (CUBE-405; Coherent) was used for photoconversion of mEOS3.2 and a 561-nm laser (MGL-H-561; OptoEngine, UT) was used for excitation. During image acquisition, the 405-nm laser was continuously turned on with the power gradually increased to maintain a convenient density of converted mEOS3.2 within the field of view. A ROI set to 256 x 256 pixels was recorded with an electron multiplying CCD camera (Andor) at 10 ms exposure time. PALM images were analyzed as described previously (Hammond et al., 2014) using custom-written scripts in Matlab.

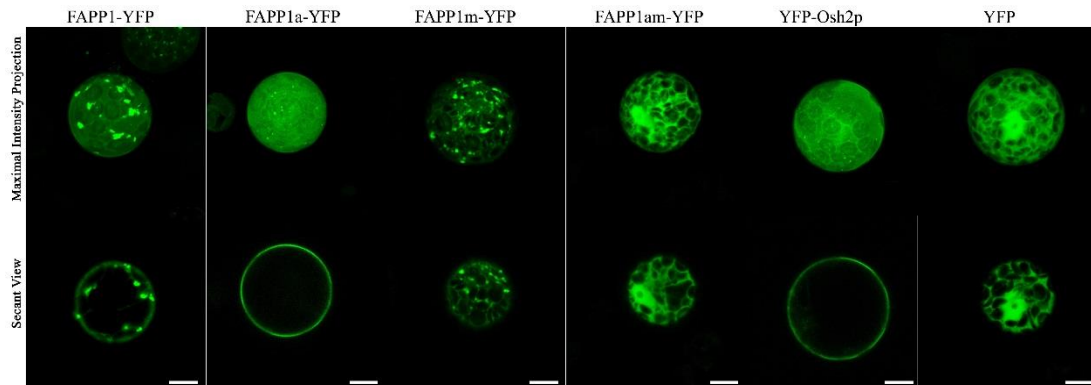
Supplementary Figures

Figure S5.1 YFP tagged PtdIns(4)P-bound biosensors and mutants transiently expressed in *A. thaliana* mesophyll protoplasts.

White bars in all panels represents 10 μm .

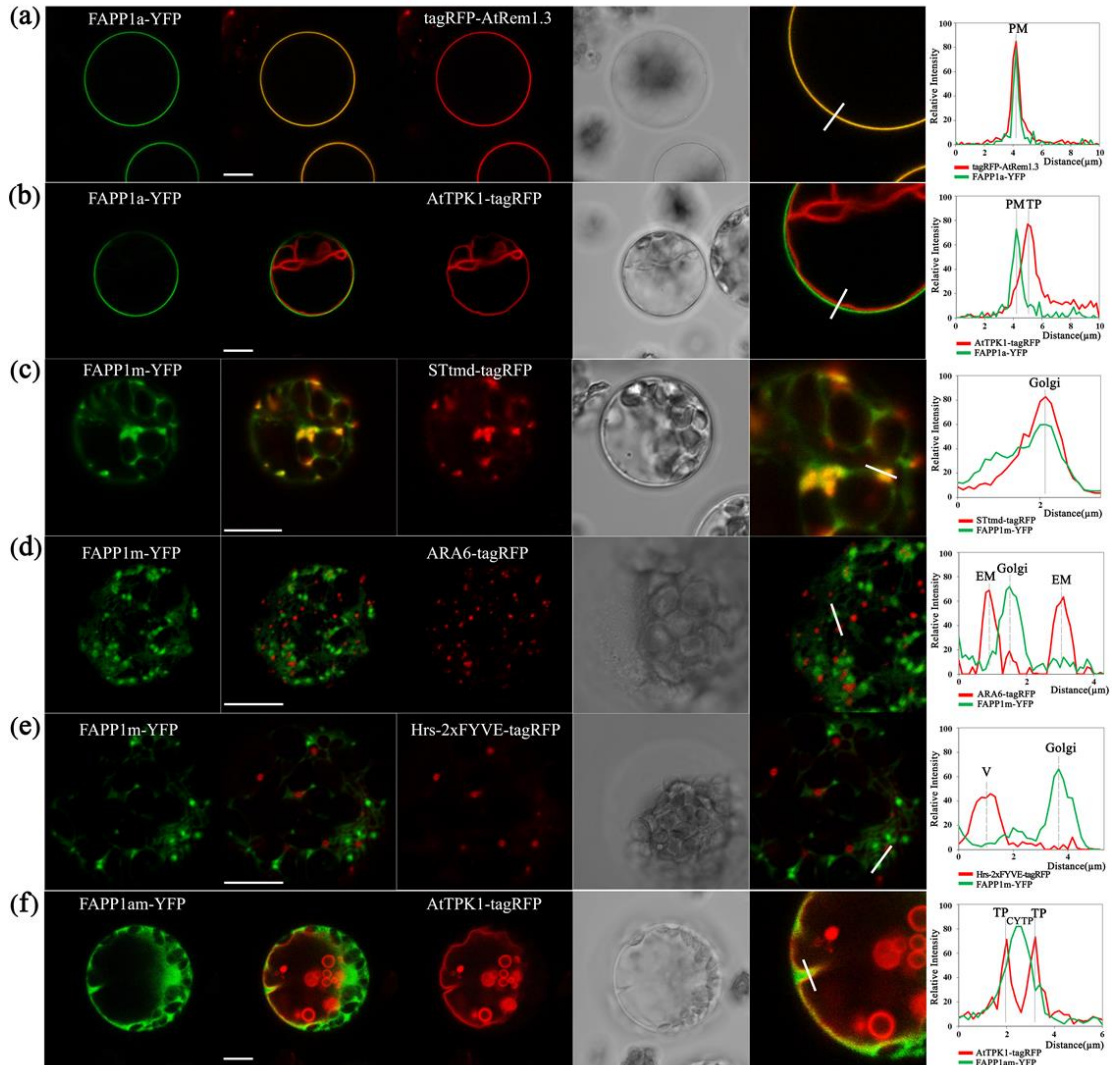


Figure S5.2 Subcellular co-localization analysis of three FAPP1 mutants in *A. thaliana* mesophyll protoplasts.

The FAPP1 mutants, fused to YFP, were co-expressed with tagRFP fused to the PM protein StRem1.3 (a), the tonoplast marker AtTPK1 (b, f), the trans-Golgi marker, STtmd (c), the endosomal markers ARA6-tagRFP (d), or the PtdIns(3)P-containing vesicle marker, 2xFYVE-tagRFP (e). The fluorescence intensity profiles in the right panels show relative fluorescence levels along the transects marked in white in the right-most enlarged image panels. The lengths of the transects on the images equal the respective distances shown in each histogram. CYTP is an abbreviation for cytoplasm. White scale bars in the left panels represents 10 μm .

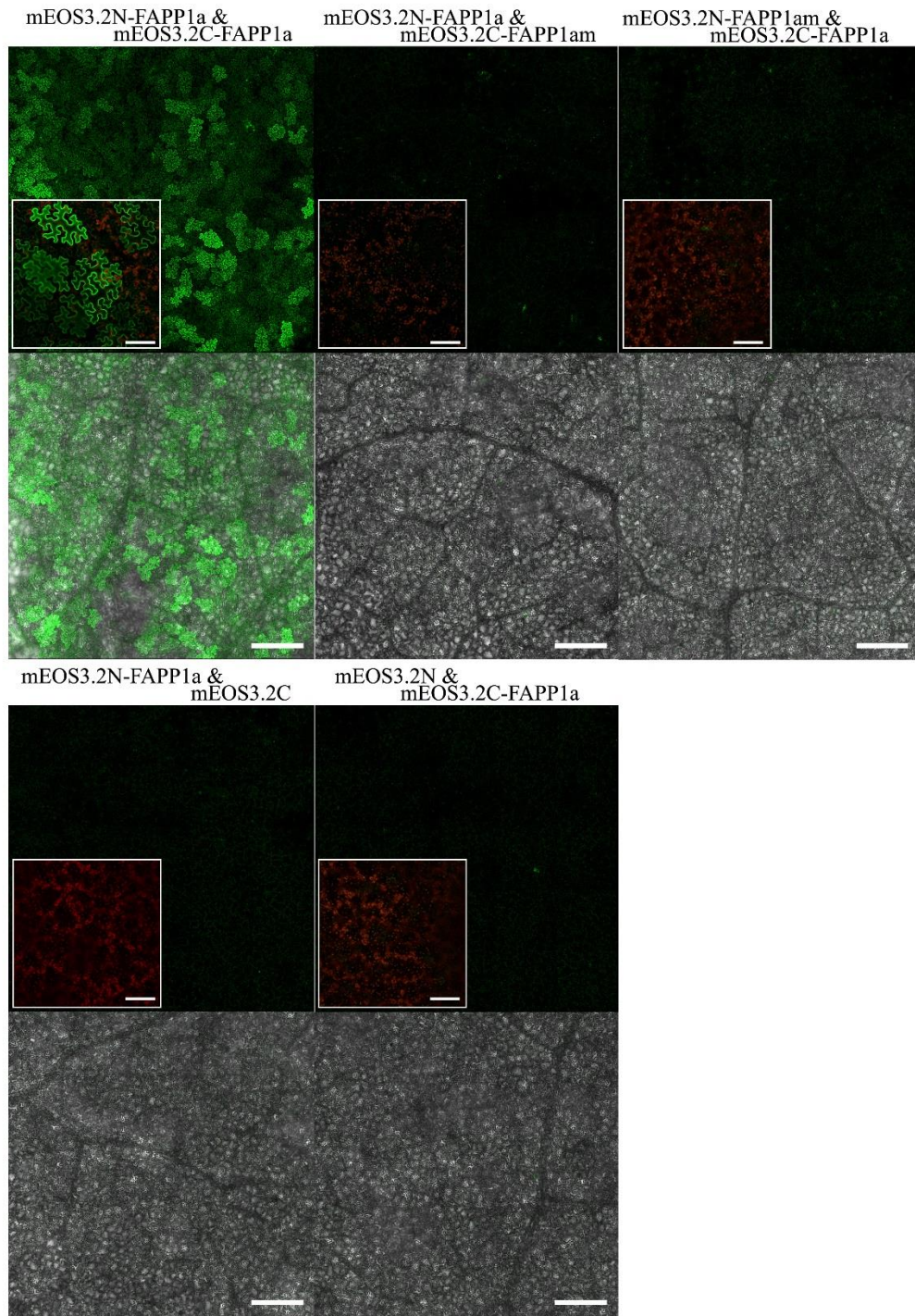


Figure S5.3 Specific formation of mEOS3.2 BiFC complexes on the PM through binding of FAPP1a biosensors, compared to controls.

Indicated constructs were transiently co-expressed in *N. benthamiana* leaf cortical cells and imaged by tile scanning. White scale bars in zoomed-in images represent 50 μm .

Thick scale bars represent 500 μm .

Bibliography

Antignani, V., Klocko, A.L., Bak, G., Chandrasekaran, S.D., Dunivin, T. and Nielsen, E. (2015) Recruitment of PLANT U-BOX13 and the PI4K β 1/ β 2 Phosphatidylinositol-4 Kinases by the Small GTPase RabA4B Plays Important Roles during Salicylic Acid-Mediated Plant Defense Signaling in *Arabidopsis*. The Plant Cell Online.

Axelrod, D., Koppel, D.E., Schlessinger, J., Elson, E. and Webb, W.W. (1976) Mobility measurement by analysis of fluorescence photobleaching recovery kinetics. Biophysical Journal, **16**, 1055-1069.

Balla, T. (2007) Imaging and manipulating phosphoinositides in living cells. The Journal of physiology, **582**, 927-937.

Betzig, E., Patterson, G.H., Sougrat, R., Lindwasser, O.W., Olenych, S., Bonifacio, J.S., Davidson, M.W., Lippincott-Schwartz, J. and Hess, H.F. (2006) Imaging Intracellular Fluorescent Proteins at Nanometer Resolution. Science, **313**, 1642-1645.

Boevink, P., Oparka, K., Cruz, S.S., Martin, B., Betteridge, A. and Hawes, C. (1998) Stacks on tracks: the plant Golgi apparatus traffics on an actin/ER network. The Plant Journal, **15**, 441-447.

Caiolfa, V.R., Zamai, M., Malengo, G., Andolfo, A., Madsen, C.D., Sutin, J., Digman, M.A., Gratton, E., Blasi, F. and Sidenius, N. (2007) Monomer–dimer dynamics and distribution of GPI-anchored uPAR are determined by cell surface protein assemblies. The Journal of Cell Biology, **179**, 1067-1082.

Chung, I., Akita, R., Vandlen, R., Toomre, D., Schlessinger, J. and Mellman, I. (2010) Spatial control of EGF receptor activation by reversible dimerization on living cells. Nature, **464**, 783.

D'Angelo, G., Vicinanza, M., Di Campli, A. and De Matteis, M.A. (2008) The multiple roles of PtdIns(4)P – not just the precursor of PtdIns(4,5)P₂. Journal of Cell Science, **121**, 1955-1963.

- De Los Santos, C., Chang, C.-W., Mycek, M.-A. and Cardullo, R.A.** (2015) FRAP, FLIM, and FRET: Detection and analysis of cellular dynamics on a molecular scale using fluorescence microscopy. *Molecular reproduction and development*, **82**, 587-604.
- Di Paolo, G. and De Camilli, P.** (2006) Phosphoinositides in cell regulation and membrane dynamics. *Nature*, **443**, 651-657.
- Dowler, S., Currie, R.A., Campbell, D.G., Deak, M., Kular, G., Downes, C.P. and Alessi, D.R.** (2000) Identification of pleckstrin-homology-domain-containing proteins with novel phosphoinositide-binding specificities. *The Biochemical journal*, **351**, 19-31.
- Echeverría, E.** (2000) Vesicle-Mediated Solute Transport between the Vacuole and the Plasma Membrane. *Plant Physiology*, **123**, 1217-1226.
- Eggeling, C., Ringemann, C., Medda, R., Schwarzmann, G., Sandhoff, K., Polyakova, S., Belov, V.N., Hein, B., von Middendorff, C., Schönle, A. and Hell, S.W.** (2008) Direct observation of the nanoscale dynamics of membrane lipids in a living cell. *Nature*, **457**, 1159.
- Godi, A., Di Campli, A., Konstantakopoulos, A., Di Tullio, G., Alessi, D.R., Kular, G.S., Daniele, T., Marra, P., Lucocq, J.M. and De Matteis, M.A.** (2004) FAPPs control Golgi-to-cell-surface membrane traffic by binding to ARF and PtdIns(4)P. *Nature cell biology*, **6**, 393-404.
- Godi, A., Pertile, P., Meyers, R., Marra, P., Di Tullio, G., Iurisci, C., Luini, A., Corda, D. and De Matteis, M.A.** (1999) ARF mediates recruitment of PtdIns-4-OH kinase- β and stimulates synthesis of PtdIns(4,5)P₂ on the Golgi complex. *Nature cell biology*, **1**, 280.
- Hammond, G.R.V. and Balla, T.** (2015) Polyphosphoinositide binding domains: key to inositol lipid biology. *Biochimica et biophysica acta*, **1851**, 746-758.
- Hammond, G.R.V., Fischer, M.J., Anderson, K.E., Holdich, J., Koteci, A., Balla, T. and Irvine, R.F.** (2012) PI4P and PI(4,5)P Are Essential But Independent Lipid Determinants of Membrane Identity. *Science*, **337**, 727-730.
- Hammond, G.R.V., Machner, M.P. and Balla, T.** (2014) A novel probe for phosphatidylinositol 4-phosphate reveals multiple pools beyond the Golgi. *The Journal of Cell Biology*, **205**, 113-126.

- He, J., Scott, J.L., Heroux, A., Roy, S., Lenoir, M., Overduin, M., Stahelin, R.V. and Kutateladze, T.G.** (2011) Molecular Basis of Phosphatidylinositol 4-Phosphate and ARF1 GTPase Recognition by the FAPP1 Pleckstrin Homology (PH) Domain. *Journal of Biological Chemistry*, **286**, 18650-18657.
- Hink, M.A., Shah, K., Russinova, E., de Vries, S.C. and Visser, A.J.W.G.** (2008) Fluorescence Fluctuation Analysis of *Arabidopsis thaliana* Somatic Embryogenesis Receptor-Like Kinase and Brassinosteroid Insensitive 1 Receptor Oligomerization. *Biophysical Journal*, **94**, 1052-1062.
- Honigmann, A., Mueller, V., Ta, H., Schoenle, A., Sezgin, E., Hell, S.W. and Eggeling, C.** (2014) Scanning STED-FCS reveals spatiotemporal heterogeneity of lipid interaction in the plasma membrane of living cells. *Nature Communications*, **5**, 5412.
- Jarsch, I.K., Konrad, S.S.A., Stratil, T.F., Urbanus, S.L., Szymanski, W., Braun, P., Braun, K.-H. and Ott, T.** (2014) Plasma Membranes Are Subcompartmentalized into a Plethora of Coexisting and Diverse Microdomains in *Arabidopsis* and *Nicotiana benthamiana*. *The Plant Cell Online*.
- Kahn, R.A., Der, C.J. and Bokoch, G.M.** (1992) The ras superfamily of GTP-binding proteins: guidelines on nomenclature. *The FASEB Journal*, **6**, 2512-2513.
- Kale, S.D., Gu, B., Capelluto, D.G., Dou, D., Feldman, E., Rumore, A., Arredondo, F.D., Hanlon, R., Fudal, I., Rouxel, T., Lawrence, C.B., Shan, W. and Tyler, B.M.** (2010) External lipid PI3P mediates entry of eukaryotic pathogen effectors into plant and animal host cells. *Cell*, **142**, 284-295.
- Kang, M., Day, C.A., Kenworthy, A.K. and DiBenedetto, E.** (2012) Simplified equation to extract diffusion coefficients from confocal FRAP data. *Traffic (Copenhagen, Denmark)*, **13**, 1589-1600.
- Kenworthy, A.K., Nichols, B.J., Remmert, C.L., Hendrix, G.M., Kumar, M., Zimmerberg, J. and Lippincott-Schwartz, J.** (2004) Dynamics of putative raft-associated proteins at the cell surface. *The Journal of Cell Biology*, **165**, 735-746.
- Knight, J.D., Lerner, M.G., Marcano-Velázquez, J.G., Pastor, R.W. and Falke, Joseph J.** (2010) Single Molecule Diffusion of Membrane-Bound Proteins: Window into Lipid Contacts and Bilayer Dynamics. *Biophysical Journal*, **99**, 2879-2887.

- Komis, G., Šamajová, O., Ovečka, M. and Šamaj, J.** (2015) Super-resolution Microscopy in Plant Cell Imaging. *Trends in Plant Science*, **20**, 834-843.
- Kusumi, A., Fujiwara, T.K., Chadda, R., Xie, M., Tsunoyama, T.A., Kalay, Z., Kasai, R.S. and Suzuki, K.G.** (2012) Dynamic organizing principles of the plasma membrane that regulate signal transduction: commemorating the fortieth anniversary of Singer and Nicolson's fluid-mosaic model. *Annu Rev Cell Dev Biol*, **28**, 215-250.
- Lee, M.H., Min, M.K., Lee, Y.J., Jin, J.B., Shin, D.H., Kim, D.H., Lee, K.-H. and Hwang, I.** (2002) ADP-Ribosylation Factor 1 of *Arabidopsis* Plays a Critical Role in Intracellular Trafficking and Maintenance of Endoplasmic Reticulum Morphology in *Arabidopsis*. *Plant Physiology*, **129**, 1507-1520.
- Lemmon, M.A.** (2008) Membrane recognition by phospholipid-binding domains. *Nat Rev Mol Cell Biol*, **9**, 99-111.
- Levine, T.P. and Munro, S.** (2002) Targeting of Golgi-Specific Pleckstrin Homology Domains Involves Both PtdIns 4-Kinase-Dependent and -Independent Components. *Current Biology*, **12**, 695-704.
- Li, X., Wang, X., Yang, Y., Li, R., He, Q., Fang, X., Luu, D.-T., Maurel, C. and Lin, J.** (2011) Single-Molecule Analysis of PIP₂;1 Dynamics and Partitioning Reveals Multiple Modes of *Arabidopsis* Plasma Membrane Aquaporin Regulation. *The Plant Cell*, **23**, 3780-3797.
- Li, X., Xing, J., Qiu, Z., He, Q. and Lin, J.** (2016) Quantification of Membrane Protein Dynamics and Interactions in Plant Cells by Fluorescence Correlation Spectroscopy. *Molecular Plant*, **9**, 1229-1239.
- Lingwood, D. and Simons, K.** (2010) Lipid rafts as a membrane-organizing principle. *Science*, **327**, 46-50.
- Liu, Z., Xing, D., Su, Q.P., Zhu, Y., Zhang, J., Kong, X., Xue, B., Wang, S., Sun, H., Tao, Y. and Sun, Y.** (2014) Super-resolution imaging and tracking of protein-protein interactions in sub-diffraction cellular space. *Nat Commun*, **5**.
- Lu, D., Lin, W., Gao, X., Wu, S., Cheng, C., Avila, J., Heese, A., Devarenne, T.P., He, P. and Shan, L.** (2011) Direct Ubiquitination of Pattern Recognition Receptor FLS2 Attenuates Plant Innate Immunity. *Science*, **332**, 1439-1442.

- Luu, D.T., Martinière, A., Sorieul, M., Runions, J. and Maurel, C.** (2012) Fluorescence recovery after photobleaching reveals high cycling dynamics of plasma membrane aquaporins in *Arabidopsis* roots under salt stress. *The Plant Journal*, **69**, 894-905.
- Maîtrejean, M., Wudick, M.M., Voelker, C., Prinsi, B., Mueller-Roeber, B., Czempinski, K., Pedrazzini, E. and Vitale, A.** (2011) Assembly and Sorting of the Tonoplast Potassium Channel AtTPK1 and Its Turnover by Internalization into the Vacuole. *Plant Physiology*, **156**, 1783-1796.
- Martin, T.F.J.** (2001) PI(4,5)P₂ regulation of surface membrane traffic. *Current Opinion in Cell Biology*, **13**, 493-499.
- Matheson, L.A., Hanton, S.L., Rossi, M., Latijnhouwers, M., Stefano, G., Renna, L. and Brandizzi, F.** (2007) Multiple Roles of ADP-Ribosylation Factor 1 in Plant Cells Include Spatially Regulated Recruitment of Coatamer and Elements of the Golgi Matrix. *Plant Physiology*, **143**, 1615-1627.
- Meijer, H.J.G. and Munnik, T.** (2003) PHOSPHOLIPID-BASED SIGNALING IN PLANTS. *Annual Review of Plant Biology*, **54**, 265-306.
- Murata, N. and Los, D.A.** (1997) Membrane Fluidity and Temperature Perception. *Plant Physiology*, **115**, 875-879.
- Nickerson, A., Huang, T., Lin, L.-J. and Nan, X.** (2014) Photoactivated Localization Microscopy with Bimolecular Fluorescence Complementation (BiFC-PALM) for Nanoscale Imaging of Protein-Protein Interactions in Cells. *PLoS ONE*, **9**, e100589.
- Okazaki, K., Miyagishima, S.-y. and Wada, H.** (2015) Phosphatidylinositol 4-Phosphate Negatively Regulates Chloroplast Division in *Arabidopsis*. *The Plant Cell*, **27**, 663-674.
- Pimpl, P., Movafeghi, A., Coughlan, S., Denecke, J., Hillmer, S. and Robinson, D.G.** (2000) In Situ Localization and in Vitro Induction of Plant COPI-Coated Vesicles. *The Plant Cell*, **12**, 2219-2235.
- Platre, M.P. and Jaillais, Y.** (2016) Guidelines for the use of protein domains in acidic phospholipid imaging. *Methods in molecular biology (Clifton, N.J.)*, **1376**, 175-194.
- Pryor, Meghan M., Low-Nam, Shalini T., Halász, Ádám M., Lidke, Diane S., Wilson, Bridget S. and Edwards, Jeremy S.** (2013) Dynamic Transition States of

ErbB1 Phosphorylation Predicted by Spatial Stochastic Modeling. *Biophysical Journal*, **105**, 1533-1543.

Raffaele, S., Mongrand, S., Gamas, P., Niebel, A. and Ott, T. (2007) Genome-wide annotation of remorins, a plant-specific protein family: evolutionary and functional perspectives. *Plant Physiol*, **145**, 593-600.

Raychaudhuri, S. and Prinz, W.A. (2010) The Diverse Functions of Oxysterol-Binding Proteins. *Annual review of cell and developmental biology*, **26**, 157-177.

Robinson, D.G., Scheuring, D., Naramoto, S. and Friml, J. (2011) ARF1 Localizes to the Golgi and the Trans-Golgi Network. *The Plant Cell*, **23**, 846-849.

Roy, A. and Levine, T.P. (2004) Multiple Pools of Phosphatidylinositol 4-Phosphate Detected Using the Pleckstrin Homology Domain of Osh2p. *Journal of Biological Chemistry*, **279**, 44683-44689.

Rust, M.J., Bates, M. and Zhuang, X. (2006) Sub-diffraction-limit imaging by stochastic optical reconstruction microscopy (STORM). *Nat Meth*, **3**, 793-796.

Schink, K.O., Tan, K.-W. and Stenmark, H. (2016) Phosphoinositides in Control of Membrane Dynamics. *Annual Review of Cell and Developmental Biology*, **32**, 143-171.

Sezgin, E. and Schwille, P. (2011) Fluorescence Techniques to Study Lipid Dynamics. *Cold Spring Harbor Perspectives in Biology*, **3**, a009803.

Simon, M.L.A., Platre, M.P., Assil, S., van Wijk, R., Chen, W.Y., Chory, J., Dreux, M., Munnik, T. and Jaillais, Y. (2014) A multi-colour/multi-affinity marker set to visualize phosphoinositide dynamics in *Arabidopsis*. *The Plant journal : for cell and molecular biology*, **77**, 322-337.

Simon, M.L.A., Platre, M.P., Marquès-Bueno, M.M., Armengot, L., Stanislas, T., Bayle, V., Caillaud, M.-C. and Jaillais, Y. (2016) A PtdIns(4)P-driven electrostatic field controls cell membrane identity and signalling in plants. *Nature Plants*, **2**, 16089.

Singer, S.J. and Nicolson, G.L. (1972) The Fluid Mosaic Model of the Structure of Cell Membranes. *Science*, **175**, 720-731.

Tanaka, H., Kitakura, S., Rakusová, H., Uemura, T., Feraru, M.I., De Rycke, R., Robert, S., Kakimoto, T. and Friml, J. (2013) Cell Polarity and Patterning by PIN

Trafficking through Early Endosomal Compartments in *Arabidopsis thaliana*. PLOS Genetics, **9**, e1003540.

Thole, J.M., Vermeer, J.E.M., Zhang, Y., Gadella, T.W.J. and Nielsen, E. (2008) ROOT HAIR DEFECTIVE4 Encodes a Phosphatidylinositol-4-Phosphate Phosphatase Required for Proper Root Hair Development in *Arabidopsis thaliana*. The Plant Cell, **20**, 381-395.

Ueda, T., Yamaguchi, M., Uchimiya, H. and Nakano, A. (2001) Ara6, a plant-unique novel type Rab GTPase, functions in the endocytic pathway of *Arabidopsis thaliana*. The EMBO Journal, **20**, 4730-4741.

Vermeer, J.E., Thole, J.M., Goedhart, J., Nielsen, E., Munnik, T. and Gadella, T.W., Jr. (2009) Imaging phosphatidylinositol 4-phosphate dynamics in living plant cells. The Plant journal : for cell and molecular biology, **57**, 356-372.

Vermeer, J.E., van Leeuwen, W., Tobena-Santamaria, R., Laxalt, A.M., Jones, D.R., Divecha, N., Gadella, T.W., Jr. and Munnik, T. (2006) Visualization of PtdIns3P dynamics in living plant cells. The Plant journal : for cell and molecular biology, **47**, 687-700.

Vermeer, J.M. and Munnik, T. (2010) Imaging Lipids in Living Plants. In Lipid Signaling in Plants (Munnik, T. ed: Springer Berlin Heidelberg, pp. 185-199.

Wang, L., Li, H., Lv, X., Chen, T., Li, R., Xue, Y., Jiang, J., Jin, B., Baluška, F., Šamaj, J., Wang, X. and Lin, J. (2015) Spatiotemporal Dynamics of the BRI1 Receptor and its Regulation by Membrane Microdomains in Living *Arabidopsis* Cells. Molecular Plant, **8**, 1334-1349.

Wiedenmann, J., Ivanchenko, S., Oswald, F., Schmitt, F., Röcker, C., Salih, A., Spindler, K.-D. and Nienhaus, G.U. (2004) EosFP, a fluorescent marker protein with UV-inducible green-to-red fluorescence conversion. Proceedings of the National Academy of Sciences of the United States of America, **101**, 15905-15910.

Xiong, Q., Ye, W., Choi, D., Wong, J., Qiao, Y., Tao, K., Wang, Y. and Ma, W. (2014) Phytophthora Suppressor of RNA Silencing 2 Is a Conserved RxLR Effector that Promotes Infection in Soybean and *Arabidopsis thaliana*. Molecular Plant-Microbe Interactions, **27**, 1379-1389.

Yguerabide, J., Schmidt, J.A. and Yguerabide, E.E. (1982) Lateral mobility in membranes as detected by fluorescence recovery after photobleaching. *Biophysical Journal*, **40**, 69-75.

Yoo, S.-D., Cho, Y.-H. and Sheen, J. (2007) *Arabidopsis* mesophyll protoplasts: a versatile cell system for transient gene expression analysis. *Nat. Protocols*, **2**, 1565-1572.

Zhang, M., Chang, H., Zhang, Y., Yu, J., Wu, L., Ji, W., Chen, J., Liu, B., Lu, J., Liu, Y., Zhang, J., Xu, P. and Xu, T. (2012) Rational design of true monomeric and bright photoactivatable fluorescent proteins. *Nat Methods*, **9**, 727-729.

Zhang, Q. and Xiao, S. (2015) Lipids in salicylic acid-mediated defense in plants: focusing on the roles of phosphatidic acid and phosphatidylinositol 4-phosphate. *Frontiers in Plant Science*, **6**, 387.